



VCU

Virginia Commonwealth University
VCU Scholars Compass

Theses and Dissertations

Graduate School

2019

DETERMINATION OF OPTIMAL PARAMETER ESTIMATES FOR MEDICAL INTERVENTIONS IN HUMAN METABOLISM AND INFLAMMATION

Marcella Torres
Virginia Commonwealth University

Follow this and additional works at: <https://scholarscompass.vcu.edu/etd>



Part of the [Other Applied Mathematics Commons](#), and the [Systems Biology Commons](#)

© The Author

Downloaded from

<https://scholarscompass.vcu.edu/etd/5890>

This Dissertation is brought to you for free and open access by the Graduate School at VCU Scholars Compass. It has been accepted for inclusion in Theses and Dissertations by an authorized administrator of VCU Scholars Compass. For more information, please contact libcompass@vcu.edu.

©Marcella Maria Torres, May 2019

All Rights Reserved.

DETERMINATION OF OPTIMAL PARAMETER ESTIMATES FOR MEDICAL
INTERVENTIONS IN HUMAN METABOLISM AND INFLAMMATION

A Dissertation submitted in partial fulfillment of the requirements for the degree of
Doctor of Philosophy at Virginia Commonwealth University.

by

MARCELLA MARIA TORRES

M.S. Applied Mathematics, Virginia Commonwealth University, 2015

B.S. Mathematical Sciences, Minor in Physics, Virginia Commonwealth University, 2007

Director: Angela Reynolds,

Associate Professor, Department of Mathematics and Applied Mathematics

Virginia Commonwealth University

Richmond, Virginia

May, 2019

Acknowledgements

I am extremely grateful to my advisor, Dr. Angela Reynolds. Thank you for supporting my random walk over the applied mathematics landscape. Also, thank you - from one mother to another - for understanding my at times high level of distraction. Especially for missing the start of that one meeting that one time.

I am also deeply indebted to Dr. Rebecca Segal for being a great collaborator and mentor. Your career advice has been instrumental.

I would also like to thank Dr. Shobha Ghosh, committee member and collaborator on two of my research projects. Thank you for your expertise that made it possible for me really explore parameter estimation with good data.

I also wish to thank my committee members Dr. David Edwards and Dr. Ihsan Topaloglu for bringing your knowledge of statistics and mathematics and for fitting this work into spring final exams week.

Special thanks to advisor Terry Green at Pierce College in Steilacoom, WA, for helping me navigate the TRIO summer bridge program in mathematics for first generation minority students. If you hadn't opened that door for me 17 years ago I would not be here today.

Finally, thank you to my husband Derek for co-parenting two small children with me over the course of this journey. Miles and Maxine, thank you for simply existing and for reminding me every day of my purpose.

TABLE OF CONTENTS

Chapter	Page
Acknowledgements	iii
Table of Contents	iv
List of Tables	vi
List of Figures	viii
Abstract	xvii
1 Introduction	1
2 Resistance Exercise Induced Muscle Hypertrophy	3
2.1 Introduction	3
2.2 Methods	5
2.2.1 Model background	5
2.2.1.1 Glycogen Storage	5
2.2.1.2 Extracellular Fluid	7
2.2.1.3 Adaptive Thermogenesis	7
2.2.1.4 Energy Partitioning	7
2.2.2 Model development	9
2.3 Results	16
2.3.1 Case study	17
2.3.2 Simulated cohort	20
2.3.3 Parameter estimation	24
2.3.4 Sensitivity analysis	28
2.3.5 Discussion	32
2.3.6 Conclusion	34
3 Optimal Control of Body Mass Change	35
3.1 Introduction	35
3.2 Methods	36
3.2.1 The Basic Problem in Optimal Control	36
3.2.2 Statement of the Optimal Control Problem	37

3.2.3	Existence and Uniqueness of an Optimal Control	38
3.2.4	Characterization of the Optimal Control Problem	41
3.3	Results	44
3.4	Discussion	46
4	Qualitative Analysis of Model Behavior with Decision Trees	49
4.1	Introduction	49
4.2	Methods	50
4.2.1	Simulation of data for training and testing	50
4.2.2	Definitions and notation	50
4.2.3	Building a tree	51
4.2.3.1	Splitting	52
4.2.3.2	Decision to terminate splitting	53
4.2.3.3	Assignment of terminal node to a class	53
4.2.4	Error rate	54
4.2.5	Cross-validation	54
4.3	Results	55
4.3.1	Classifying parameter sets in a model of resistance exercise induced muscle hypertrophy	57
4.4	Discussion	59
5	Macrophage polarization in peritonitis	62
5.1	Introduction	62
5.2	Methods	65
5.2.1	Model Development	66
5.2.2	Identification and analysis of equilibrium points	75
5.2.3	Analysis of equilibria	77
5.2.4	Numerical simulations	79
5.2.5	Parameter Estimation Background	81
5.2.6	Parameter Estimation	82
5.2.7	Goodness-of-fit measures	84
5.3	Results	84
5.3.1	Determination of an identifiable subset of model parameters	84
5.3.2	Goodness-of-fit	93
5.3.3	Sensitivity Analysis	96
5.3.4	Simulations	100
5.3.5	Discussion	103
6	Macrophage polarization in atherosclerosis	115

6.1	Introduction	115
6.2	The Inflammatory Process in Early Atherosclerosis	115
6.2.1	The Blood	115
6.2.2	The Gut	116
6.2.3	The Endothelium	117
6.2.4	Foam cells	117
6.2.5	The Role of Neutrophils	118
6.2.6	Treatments	119
6.3	A Selection of ODE and PDE Models	119
6.4	Model Development	122
6.5	Discussion	137
7	Conclusion	138
7.1	Summary	138
7.2	Future directions	142
	Appendix A Code for the resistance exercise model	144
A.1	SBML model file	144
A.2	Matlab code for Latin Hypercube Sampling	163
A.2.1	ODE_LHS_NHANESmale.m (ODEs)	163
A.2.2	Parameter_settings_LHS_NHANESmale.m (parameter baseline values and initial conditions)	165
A.2.3	Model_LHS_NHANESmale.m (main file)	166
A.2.4	LHS_Call.m (LHS algorithm file)	167
	Appendix B Matlab code for the optimal control problem	170
	Appendix C Peritonitis model	183
C.1	Experimental data	183
C.2	Code for the PottersWheel Matlab toolbox (model definition file)	183
C.3	XPP files	186
C.3.1	Simplified model used for numerical analysis of equilibria	186
C.3.2	Full model	187
	Appendix D SBML code for the atherosclerosis model	189
	References	222
	Vita	248

LIST OF TABLES

Table		Page
1	Variables, parameters, and constants in the model of Hall et al. [1].	6
2	Comparison of initial conditions and parameter values for an average US male versus female aged 20-39 years [41].	13
3	Model inputs for experiment comparing the effects of a hypocaloric diet only to diet with CE or RE. Initial conditions are specific to a hypothetical individual weighing 100 kg with 27.2% body fat. Parameters appear in Eqn. 2.1 and were chosen such that a modest LM gain in response to RE was simulated.	18
4	Parameter set data. LHS was restricted to these parameter ranges to ensure that physiologically reasonable simulations were generated given initial conditions. Sample means are close to the midpoints we expect for a uniform distribution, so a sample size of $n = 100$ was deemed sufficient.	22
5	Cohort statistics. Mean and standard deviation calculated for absolute change in LM and FM after 12 weeks and 24 weeks of RE.	22
6	Initial conditions and parameter estimates for group data.	25
7	PRCC. Time point $t = 730$ days. *Significant ($p < 0.10$).	31
8	Description of parameters and estimates for the full model.	71
9	Pairwise collinearity indices. Pairs of parameters were considered collinear (highly correlated) if $CI > 20$	91
10	All identifiable parameter subsets of size 6.	91
11	Parameter values and 95% pointwise confidence intervals for identifiable model. Remaining parameters were fixed at values given in Table 8.	94

12	Goodness-of-fit statistics. In the full model, 24 parameters were estimated. After identifiability analysis, estimated parameters were reduced to 6 and the remaining parameters were fixed prior to fitting. The reduction in estimated parameters improved the weighted least squares merit function value (χ^2), increased p-value on a χ^2 test indicating that the identifiable model sufficiently explains the data, and lowered the estimated amount of information lost between the model and the data by the Aikake Information Criterion (AIC) measure.	97
13	Description of model variables.	124
14	Description of parameters and values.	129
15	Experimental data from mouse model of peritonitis. At each time point, cells were harvested from a sample of n mice. Average cell counts for neutrophils (\bar{N}), M1 macrophages ($\bar{M1}$), and M2 macrophages ($\bar{M2}$) are given in units of (10^7) cells. Standard error of the mean for each cell type x is calculated as $\sigma_{\bar{x}} = \sigma_x/\sqrt{n}$	183

LIST OF FIGURES

Figure		Page
1	<p>Model behavior and predictions for initial body measurements corresponding to the average US male [41] performing RE with varying parameter values and energy intakes (A) Daily change in LM in response to RE is plotted against total LM. As LM accumulates the rate of increase slows and approaches zero. (B) Predicted time course of accumulation of LM in response to RE is plotted for different sets of parameter values shown in the legend. Physical activity level, PAL, was set to 1.6 for each simulation in order to compare the effects of varying parameters in the muscle hypertrophy term in Eqn. 2.1.</p>	10
2	<p>Effect of an 800 kcal/day decrease in energy intake on total lean body mass.</p>	12
3	<p>Effects of initial conditions on model predictions. Initial conditions and parameters used to generate simulations in (A)-(D) are shown in Table 2. (A) A comparison of predicted LM in response to RE for the same parameter set and varying energy intakes: maintenance, a hypocaloric diet, and a hypercaloric diet. Initial body measurements used to generate simulations correspond to those of an average US male aged 20-39 years from NHANES 1999-2004 [41]. (B) Predicted FM is compared for the same conditions as in (A). (C) Predicted LM in response to RE for the average US male on a maintenance energy intake (shown in (A)). (D) Predicted LM in response to RE for an average US female aged 20-39 years from NHANES 1999-2004 [41].</p>	14
4	<p>Comparison of predicted change in LM using predictive equation $RMR = 21.6 \times LM + 370$ [46] versus Mifflin-St.Jeor equation $RMR = 9.99 \times Weight + 6.25 \times Height - 4.92 \times Age + 166 \times Sex$ ($Male = 1, Female = 0$) - 161. Initial conditions and parameters used to generate these simulations are the male values given in Table 2.</p>	15

5	Change in LM over time in response to RE for a 100 kg individual with 27.2% body fat and a maintenance energy intake of 3024 kcal/day, with a hypocaloric diet consisting of an 800 kcal/day deficit was begun on Day 1 and maintained for 12 weeks followed by a gradual return to 3024 kcal/day over 8 weeks. Parameter values: $PAL=1.5$, $r = 0.25$, $\alpha = 9$, $\beta = 77$, $H_1 = 66$, $H_2 = 74$	19
6	A comparison of diet and exercise interventions for a 100 kg hypothetical individual with 27.2% body fat and a maintenance energy intake of 3024 kcal/day. In each scenario, a hypocaloric diet consisting of an 800 kcal/day deficit was begun on Day 1 and maintained for 12 weeks followed by a gradual return to 3024 kcal/day over 8 weeks. Diet Only has $PAL = 1.5$, appropriate for a sedentary individual. Cardiovascular exercise was modeled with an increase in PAL to 1.6, approximating light activity such as several short duration jogs per week. RE was modeled with parameter values $PAL=1.5$, $r = 0.25$, $\alpha = 9$, $\beta = 77$, $H_1 = 66$, $H_2 = 74$	20
7	Change in LM over time in response to RE for a simulated cohort of 100, 100 kg individuals with 27.2% body fat. RE was modeled with parameter values sampled from a uniform distribution with ranges restricted to the values given in Table 4.	23
8	Mean of the transients for LM and FM of the full cohort.	24
9	Predicted and measured body mass during a trial comparing the effects of a moderate volume RE program on elderly men and women [2]. (A) Predicted and measured average LM with SEM for 29 elderly men. (B) Predicted and measured average FM with SEM for 29 elderly men. (C) Predicted and measured average LM with SEM for 24 elderly women. (D) Predicted and measured average FM with SEM for 24 elderly women.	26

10	Model predictions of long-term change in LM and FM following 24 weeks of RE. Parameter estimates obtained in fitting the model to mean data from elderly subjects completing a RE program for 24 weeks [2] were then used to simulate a long-term scenario: cessation of RE after 24 weeks. (A) Predicted average LM for the male group. (B) Predicted average FM for the male group. (C) Predicted average LM for the female group. (D) Predicted average FM for the female group	27
11	Linear-linear plot of the residuals of the linear regressions of each parameter versus all other parameters of the model (horizontal axis) and the residuals of the linear regression of the output versus each parameter (vertical axis).	29
12	PRCC results. The magnitude of the dummy parameter value is used as a significance measure for the parameters; a PRCC parameter value less than the PRCC dummy value indicates insignificance.	30
13	Comparison of effects of different priorities on state and control variables.	47
14	Example of a binary tree with two measurements and two classifiers.	52
15	Illustration of how proportions of observations are split between nodes.	54
16	Dependence of misclassification rate on maximum number of splits in tree.	56
17	A classification tree trained using a data set containing 1000 parameter sets and an associated response variable defined as total lean mass gained after 180 days. Each of the 1000 parameter sets was classified as being likely to produce a High or Low response to resistance training in simulations according to parameter splitting rules marked on each branch of the tree. Terminal nodes are outlined in red if observations within are in the High class and blue if they are assigned to the Low class.	56
18	Predictor importance estimates.	58

19	Experimental details. Gating strategy and representative dot plots and histograms used to identify individual cell populations	67
20	Model schematic. Model schematic for the inflammatory response with components defined in key. Arrows represent up-regulation and bars represent destruction or inhibition. Parameters in the schematic that are included in the final subset of identifiable parameters appear in bold; additional non-interaction parameters that do not appear in the schematic are given with the full subset in Table 11.	70
21	Bifurcation diagram for M1 as k_{m1m1} varies. Stable steady states are plotted as solid lines and unstable steady states as thin lines. For small values of k_{m1m1} , the system has one stable steady state at health. For intermediate values, the system is bistable between health and a sustained M1 and M2 response before health loses stability via a transcritical bifurcation. For high values of k_{m1m1} , the system is monostable with a sustained M1 response.	80
22	Two parameter plot of cusp.	81
23	Plot of changes in M1 dynamics as k_{m1m1} varies through limit points. . .	82
24	Steps to estimate an identifiable subset of parameters. Step 1 (gray): estimate all parameters and generate a discretized sensitivity matrix from the fitted model. Step 2 (pink): Fix parameters that fall below a determined sensitivity threshold. Step 3 (blue): Select one group of low collinearity (identifiable) parameters. Step 4 (green): Estimate the chosen identifiable subset and fix all other parameters. . . .	86
25	Parameter importance ranking (RMS) for full and identifiable model. We ranked the impact of each parameter on all three observable model outputs (N , $M1$, and $M2$) by calculating a root mean square sensitivity measure, as defined in Brun et al. [104]. The sensitivity threshold was set at 5% of the maximum RMS value calculated over all parameters. Eight parameters in the full model were thus deemed insensitive and fixed in step 2 of our identifiability analysis. The inset plot shows RMS values for the identifiable model.	89

26	Correlation matrix plot for the full model. An approximate correlation matrix was obtained from the Fisher Information Matrix for the sensitive subset of parameters and used to visualize correlations. There are many significant linear correlations (greater than 0.7) between sensitive parameters that appear as black or white squares on the off diagonal.	90
27	Correlation matrix plot for the identifiable model. An approximate correlation matrix was obtained from the Fisher Information Matrix of the identifiable model and used to visualize correlations between model parameters. There is one significant correlation (greater than 0.7) between parameters k_{m1m2} and k_{m2m2}	95
28	Model response variable predictions versus observations for the identifiable model. Model predictions for M1 macrophage ($M1$), M2 macrophage ($M2$), and neutrophil (N) counts are plotted versus mean observed values and standard errors.	96
29	Model state variable predictions for the identifiable model. Model predictions for levels of pathogen (P) and nutrient (B) and apoptotic neutrophil (AN) counts.	97
30	Predictions versus observations. Model predictions versus observations are plotted for M1 macrophages ($M1$), M2 macrophages ($M2$), and neutrophils (N). Data points are labeled with time (in days).	98
31	Profile likelihood plots. The six parameters in the identifiable subset are plotted versus the estimated parameters on a logarithmic scale. Only estimated parameters that change significantly are plotted. These changes can indicate dependencies between parameters.	99
32	Baseline characteristics for M1 and sensitivity of characteristics to parameter variations. The M1 transient curve and its characteristics are plotted for the baseline parameter values given in Tables 8 and 11. Parameter sensitivity plots show the effects on M1 characteristics of varying model parameters one-at-a-time by a factor of 1.001 of its baseline value while holding all other parameters at their baseline values. Insensitive parameters, which have zero sensitivity for all characteristics, are not shown.	107

33	<p>Baseline characteristics for M2 and sensitivity of characteristics to parameter variations. The M2 transient curve and its characteristics are plotted for baseline parameter values given in Tables 8 and 11. Parameter sensitivity plots show the effects on M2 characteristics of varying model parameters one-at-a-time by a factor of 1.001 of its baseline value while holding all other parameters at their baseline values. Insensitive parameters, which have zero sensitivity for all characteristics, are not shown.</p>	108
34	<p>Extreme trajectories corresponding to pointwise 95% confidence interval. The six identifiable parameters given in Table 11 were set one-at-a-time to values at either extreme of their 95% confidence intervals to explore variations in behavior within physiologically reasonable bounds given experimental data.</p>	109
35	<p>Results of perturbations in parameter k_{m1m2}. Parameter k_{m1m2}, which models the transition rate of M1 to M2 macrophages, was varied within a factor of 1.3 of its baseline value of $k_{m1m2} = 8.62$. The effects of variations on M1, M2, and on the maximum values of each phenotype are shown. An increase in k_{m1m2} shortens the time course for both M1 and M2 and diminishes M1 peak magnitude slightly relative to the increasing in M2 peak magnitude. A decrease in k_{m1m2} extends the span of M1 and M2 activity and increases M1 peak magnitude slightly while decreasing M2 peak magnitude.</p>	110
36	<p>Results of perturbations in parameter k_{an}. Parameter k_{an}, which models the rate of neutrophil apoptosis, was varied around its baseline value of $k_{an} = 7.108$. The effects of variations on M1, M2, and neutrophils are shown. If there is no neutrophil apoptosis, there is no M2 response. Values lower than baseline lead to a sustained inflammatory response from all immune cells while higher values shorten the time course of each.</p>	111

37	<p>Sensitivity of M1 and M2 characteristics to parameter variations in the case of delayed neutrophil apoptosis (unhealthy response) versus a healthy response. Predictions and sensitivities for a healthy response are plotted in blue, while predictions and sensitivities for an unhealthy response are plotted in red. A healthy M1 and M2 response that resolves, with all parameters at baseline values given in Tables 8 and 11 (including $k_{an} = 7.108$), is plotted versus an unhealthy, sustained M1 and M2 response resulting from reducing the value of parameter k_{an} to 5.56 while holding all other parameters constant. The bar charts compare the associated sensitivity of M1 and M2 characteristics to parameter variations in the healthy case versus the unhealthy case. Insensitive parameters, which have zero sensitivity for all characteristics, are not shown.</p>	112
38	<p>Parameter variations that resolve inflammation in the case of delayed neutrophil apoptosis. Reducing the value of parameter k_{an} from baseline while holding all other parameters constant leads to sustained inflammation. We resolved inflammation in this case by varying each of three parameters separately: μ_{m2}, u_{nr}, or s_{nr}. All immune cells return to low levels if resting neutrophil influx or decay is modulated, while a population of M2 macrophages persists if M2s are directly targeted to resolve the inflammation.</p>	113
39	<p>Predicted effects of reducing source of monocytes s_{mr}. The effects of the baseline case of a constant influx of resting monocytes (that will differentiate into macrophages) is compared to the effects of reducing influx of monocytes at an early timepoint (16 hours) versus a late timepoint (5 days). Early intervention leads to sustained inflammation while late intervention leads to an increase in neutrophils.</p>	114
40	<p>Diagram showing plan for model development. Currently the model is built from the viewpoint of the plaque, with influxing macrophage and neutrophil precursors and cholesterol transported via high and low density lipoproteins. Reverse cholesterol transport occurs within the foam cells, modeled with variables C_f (free cholesterol) and C_e (cholesterol ester). For now we consider HDL-C influx constant.</p>	123

- 41 **Predicted effects of removing dietary cholesterol on cells in the basic model.** (a) Parameters are set at the nominal values given in Table 14. (b) For $t < 50$, there is some level of circulating LDL-C in the blood (i.e. $L_b = 1$) that is dependent on dietary cholesterol. For $t > 50$, we set the parameter $L_b=0.001$ to simulate a drastic reduction in circulating LDL-C that would result from the removal of cholesterol in the diet. Immune cell levels decrease except for M1- and M2-derived foam cells due to reduced foam cell apoptosis. 135
- 42 **Predicted effects of removing dietary cholesterol on cholesterol in the basic model.** (a) Parameters are set at the nominal values given in Table 14. (b) For $t < 50$, there is some level of circulating LDL-C in the blood (i.e. $L_b = 1$) that is dependent on dietary cholesterol. For $t > 50$, we set the parameter $L_b=0.001$ to simulate a drastic reduction in circulating LDL-C that would result from the removal of cholesterol in the diet. Both free and esterified cholesterol per foam cell are substantially decreased, although esterified cholesterol is still increasing over time. 136

Abstract

DETERMINATION OF OPTIMAL PARAMETER ESTIMATES FOR MEDICAL INTERVENTIONS IN HUMAN METABOLISM AND INFLAMMATION

By Marcella Maria Torres

A Dissertation submitted in partial fulfillment of the requirements for the degree of
Doctor of Philosophy at Virginia Commonwealth University.

Virginia Commonwealth University, 2019.

Director: Angela Reynolds,

Associate Professor, Department of Mathematics and Applied Mathematics

In this work we have developed three ordinary differential equation models of biological systems: body mass change in response to exercise, immune system response to a general inflammatory stimulus, and the immune system response in atherosclerosis. The purpose of developing such computational tools is to test hypotheses about the underlying biological processes that drive system outcomes as well as possible real medical interventions. Therefore, we focus our analysis on understanding key interactions between model parameters and outcomes to deepen our understanding of these complex processes as a means to developing effective treatments in obesity, sarcopenia, and inflammatory diseases.

We develop a model of the dynamics of muscle hypertrophy in response to resistance exercise and have shown that the parameters controlling response vary between male and female group means in an elderly population. We further explore this individual variability by fitting to data from a clinical obesity study. We then apply logistic regression and classification tree methods to the analysis of between- and within-group

differences in underlying physiology that lead to different long-term body composition outcomes following a diet or exercise program. Finally, we explore dieting strategies using optimal control methods.

Next, we extend an existing model of inflammation to include different macrophage phenotypes. Complications with this phenotype switch can result in the accumulation of too many of either type and lead to chronic wounds or disease. With this model we are able to reproduce the expected timing of sequential influx of immune cells and mediators in a general inflammatory setting. We then calibrate this base model for the sequential response of immune cells with peritoneal cavity data from mice. Next, we develop a model for plaque formation in atherosclerosis by adapting the current inflammation model to capture the progression of macrophages to inflammatory foam cells in response to cholesterol consumption. The purpose of this work is ultimately to explore points of intervention that can lead to homeostasis.

CHAPTER 1

INTRODUCTION

Deterministic ordinary differential equation models are often applied to biological systems when knowledge or data is limited but a qualitative and/or quantitative understanding of the system is desired. Simulated experiments can then be conducted to guide experimental design, aid in the selection of time points for future data collection, and predict treatment efficacy. In this work, this approach is employed to explore interventions for obesity and atherosclerosis with the development of three ordinary differential equation models of biological systems: body mass change in response to exercise, immune system response to a general inflammatory stimulus, and the immune system response in atherosclerosis in the following chapters.

In chapter 2, we present a model of muscle hypertrophy in response to resistance training. We model this with the addition of a muscle hypertrophy term to a model of human metabolic processes developed by Hall et al. [1]. We then use this model to compare the effects of different interventions and explore individual variation in response by varying parameters controlling response and by fitting to experimental data from an elderly population undertaking a resistance exercise program [2].

In chapter 3, we frame the problem of body mass change as an optimal control problem in order to investigate optimal diet strategies to maintain or increase lean mass under different priorities: fat loss, lean mass gain, or equal prioritization. This requires proof of existence and uniqueness of an optimal control for a simplified version of the model developed in chapter 2. For this simplified case, we solve the optimal control problem in a variety of scenarios and compare results.

In chapter 4, we apply machine learning methods to the problem of parameter estimation in a mechanistic model. We use classification and regression tree methods to find parameter subsets leading to different outcomes in measurement variables using simulated data. This could be considered a novel method for identifiability and sensitivity analysis, as collinearities between model parameters can be revealed during the tree building process and only influential parameters are selected. In addition, results are more easily visualized with a tree diagram than with traditional methods.

In chapter 5, we present a model of immune cell response to an inflammatory stimulus. This model builds on previous work [3, 4, 5] to include macrophage polarization: the transition between extreme macrophage phenotypes M1 and M2. Model parameters are calibrated with experimental data from a mouse model of peritonitis and model identifiability and sensitivity are analyzed. We identify neutrophil apoptosis as a key driver of population-level macrophage phenotype shift in addition to testing a selection of treatment strategies *in silico*. This model is extended to the inflammatory setting in atherosclerosis in chapter 6 as a first step in the development of a multi-compartmental spatio-temporal model for the formation of plaques in the heart.

Finally, chapter 7 contains a summary of results presented in this work as well as an outline of future directions. Code for all of the models presented is included in the appendices.

CHAPTER 2

RESISTANCE EXERCISE INDUCED MUSCLE HYPERTROPHY

Abbreviations

CE Cardiovascular exercise

LHS Latin Hypercube Sampling

LM Lean mass

PAL Physical activity level

RE Resistance exercise

2.1 Introduction

Health complications such as obesity, cardiovascular disease, stroke, and diabetes are in part attributable to the disproportionate allocation of body mass to adipose tissue versus lean body mass. The focus, however, is often on how to reduce body fat rather than on how to increase the lean component of body mass. Obesity interventions in particular tend to focus on reducing overall body weight by reducing energy intake or by increasing energy expenditure through CE. A typical response to these interventions is an initial loss of both FM and LM, with free-living research subjects typically failing to maintain the predicted maximum of weight loss achieved after 6-8 months, gradually regaining weight [1, 6, 7, 8]. While physical activity has been shown to aid in long-term weight maintenance [9], type of activity could be an important consideration, especially for sarcopenic populations. Sarcopenia, the loss of muscle mass and strength that can occur with aging, is implicated in a variety

of health issues among the elderly from fractures to increased risk of cardiovascular disease and prediabetes [10, 11]. Since RE has been shown to preserve LM [12, 13, 14, 15, 16, 17, 18] while CE is associated with loss of LM [12, 13, 14, 15], it deserves consideration as an ideal type of exercise to improve body composition, especially when combined with a hypocaloric diet or CE.

Here we extend a mathematical model of human metabolism to include the effects of RE in order to investigate the impact of this activity on long-term body composition, both alone and when combined with a hypocaloric diet. Many energy balance models of body mass change have evolved over the preceding decades [19, 20, 21, 22, 23, 24, 25, 26, 27, 28, 29, 30, 31, 1, 32, 33, 34, 35]; and some of these specifically investigate the effects of modulating physical activity level [32, 34, 27, 31]. However, in each of these models physical activity is defined as a body weight or BMI dependent source of additional energy expenditure that is solely a component of total energy expenditure. The production of significant additional LM is unique to RE type physical activity, and the effects of this have not yet been investigated with mathematical modeling. Our simulations support what has been shown clinically, that additional LM generated via RE may shift the body composition set point to a healthier state.

We first use this model to conduct a simulated case study comparing the long-term outcomes of a hypocaloric diet alone, dieting with CE, and dieting with RE for a hypothetical individual. We then simulate a cohort of individuals with varying responses to RE. Finally, to further validate the model and its general applicability, we use parameter estimation methods to fit data from an RE study in elderly subjects and perform statistical analyses to evaluate biological feasibility of model results.

2.2 Methods

2.2.1 Model background

The regulation of human metabolism and body weight involve a myriad of complex biological processes, but the whole-body system is ultimately governed by the laws of thermodynamics, making mathematical modeling possible. The law of conservation of energy requires that changes in the body’s energy content are due to an imbalance in energy intake and energy expenditure and, since energy is stored in the body as either FM or LM, it is possible to predict changes in body mass given an energy surplus or deficit [36]. Such an energy-balance model, developed by Hall et al. [30, 1], consists of five differential equations that describe the storage of glycogen from ingested carbohydrate (Eqn. 1), extracellular fluid retention (Eqn. 2), adaptive thermogenesis (Eqn. 3), and the partitioning of energy stored in the body into FM (Eqn. 4) or LM (Eqn. 5). These differential equations depend on energy expenditure (Eqn. 6) and energy expenditure due to physical activity (Eqn. ??). A description of the terms in each equation appears in Table 1.

2.2.1.1 Glycogen Storage

$$\rho_G \frac{dG}{dt} = CI - k_G G^2 \quad (1)$$

Carbohydrate consumed in food is stored in the body as glycogen, primarily in the liver and in muscle tissue. Although glycogen dynamics are a complex function of many metabolic processes, glycogen content in the body primarily depends on dietary carbohydrate intake CI , the first term in Eqn. (1). The glycogen term is quadratic so that carbohydrate intake must be increased three-fold to increase glycogen by a factor of 1.8 [1]. The parameter $\rho_G=0.004$ kcal/kg, the energy density of carbohydrate, and

Table 1. **Variables, parameters, and constants in the model of Hall et al. [1].**

G	stored glycogen	$G(0) = 0.5$ kg
ρ_G	energy density of carbohydrate	0.004 kcal/kg
CI	carbohydrate intake	$CI(t) = 0.6E(t)$ kcal
k_G	calculated constant	$k_G = \frac{CI(0)}{G_{init}^2}$
CI_b	carbohydrate intake at baseline	kcal
G_{init}	glycogen stored at baseline	500 g
$[Na]$	extracellular sodium concentration	3.22 mg/ml
$\Delta[Na]_{diet}$	change in dietary sodium	mg/d
ξ_{Na}	renal sodium excretion	3000 mg/L/d
ξ_{CI}	renal sodium excretion	4000 mg/d
ECF_{init}	extracellular fluid at baseline	kg
AT	adaptive thermogenesis	kcal
τ_{AT}	AT time constant	14 days
β_{AT}	AT parameter	0.14
EI	energy intake	kcal
ΔEI	change in EI from initial input	$\delta = EI(t) - EI(0)$
F	fat mass	kg
L	lean mass	kg
ρ_F	energy density per unit change of fat	9440.7 kcal
ρ_L	energy density per unit change of lean mass	9440.7 kcal
p	energy partitioning function	$p = \frac{C}{C+F}$, $C = 10.4$ kg $\cdot \frac{\rho_L}{\rho_F}$
TEF	thermic effect of feeding	kcal
δ	energy cost of physical activity	kcal
PAL	physical activity level	dimensionless parameter

$k_G = CI_b/G_{init}^2$, where $G_{init}=500$ g and CI_b is carbohydrate intake at the start of the diet [1].

2.2.1.2 Extracellular Fluid

$$\frac{ECF}{dt} = \frac{1}{[Na]} \left(\Delta[Na]_{diet} - \xi_{[Na]}(ECF - ECF_{init}) - \xi_{CI}(1 - \frac{CI}{CI_b}) \right) \quad (2)$$

Extracellular fluid (ECF), or water retained in the body, changes according to dietary sodium intake in Eqn. (2) where $[Na]$ is the extracellular sodium concentration, $\Delta[Na]_{diet}$ is the change in dietary sodium, and $\xi_{[Na]}$ and ξ_{CI} describe the effect of dietary carbohydrate intake on renal sodium excretion [1].

2.2.1.3 Adaptive Thermogenesis

$$\tau_{AT} \frac{dAT}{dt} = \beta_{AT} \Delta EI - AT \quad (3)$$

Like friction opposes the movement of a pendulum, adaptive thermogenesis acts in opposition to weight change, bringing energy expenditure into equilibrium with energy intake. In this model, adaptive thermogenesis changes according to perturbations of EI and persists until energy expenditure is equal to energy intake [30], where $\beta_{AT} = 0.14$ and $\tau_{AT} = 14$ days, the estimated time constant for the onset of adaptive thermogenesis, is equal to 14 days.

2.2.1.4 Energy Partitioning

Energy stored in the body is compartmentalized into either lean tissue or fat. Changes in body fat (F) and lean mass (L) depend on energy intake (EI) and energy

expenditure (EE) and are modeled in Eqns. (4) and (5) [1].

$$\rho_F \frac{dF}{dt} = (1 - p)(EI - EE - \rho_G \frac{dG}{dt}) \quad (4)$$

$$\rho_L \frac{dL}{dt} = p(EI - EE - \rho_G \frac{dG}{dt}) \quad (5)$$

In these equations ρ_F and ρ_L are the energy content per unit change in body fat or lean tissue, respectively, and p is a dimensionless energy partitioning function $p = \frac{C}{C+F}$ with C a constant [1]. Energy expenditure EE is given by Eqn. (6) where K is a calculated constant, γ_F and γ_L are regression coefficients from models describing the contribution of fat mass and lean mass, respectively, to resting metabolic rate (RMR) [37], and η_F and η_L are the energy expended to change body fat and lean mass.

$$EE = \frac{K + \gamma_F F + \gamma_L L + \delta BW + TEF + AT + (EI - \rho_G \frac{dG}{dt})[p \frac{\eta_L}{\rho_L} + (1 - p) \frac{\eta_F}{\rho_F}]}{1 + p \frac{\eta_L}{\rho_L} + (1 - p) \frac{\eta_F}{\rho_F}} \quad (6)$$

Changes in energy intake result in an immediate change in the energy expended during digestion, with $TEF = \beta_{TEF} \Delta EI$, where $\beta_{TEF} = 0.1$ [1].

Energy expenditure due to physical activity is modeled by Eqn. (??) with PAL the physical activity level of the individual, BW current bodyweight, and RMR resting metabolic rate [1].

$$\delta = \frac{[(1 - \beta_{TEF})PAL - 1]RMR}{BW} \quad (7)$$

Weight-loss trajectory output from this model, which closely matches clinical outcomes, predicts an initial steep drop in both FM and LM, variables F and L , in response to dieting that gradually approaches equilibrium, or weight maintenance, due to the effect of adaptive thermogenesis (AT) which is modeled by Eqn. 3 [1].

2.2.2 Model development

In order to model RE-mediated muscle hypertrophy, we have added a term to Eqn. 5 resulting in the new differential equation to model change in LM, less extra-cellular fluid, given by Eqn. 2.1.

$$\frac{dL}{dt} = p(EI - EE - \rho_G \frac{dG}{dt})/\rho_L + r \frac{L^\alpha}{L^\alpha + H_1^\alpha} \frac{1}{1 + \left(\frac{L}{H_2}\right)^\beta} \quad (2.1)$$

This term consists of a Hill-type factor for the growth dynamics, which is inhibited by amount of LM accumulated. The inhibition multiplier was used to capture the later decay in growth rate as the body adapts to the training program.

While the time course of muscle growth varies among different modes of training and total LM gained varies widely among individuals [38, 39], studies suggest that for less damaging modes of RE, the rate of muscle hypertrophy is most rapid for the initial 6-15 week period following the start of a new RE program, followed by a long, slow decline as the body adapts to the exercise [40]. The functional form of Eqn. 2.1 captures these dynamics, as shown in Figure 1 with the rate of LM gain slowing and eventually decreasing towards zero as it accumulates for a hypothetical individual who has 58 kg of LM before beginning a simulated RE program.

By subtracting the muscle hypertrophy term from the fat equation

$$\frac{dF}{dt} = (1 - p)(EI - EE - \rho_G \frac{dG}{dt})/\rho_F - \frac{r\rho_L}{\rho_F} \frac{L^\alpha}{L^\alpha + H_1^\alpha} \frac{1}{1 + \left(\frac{L}{H_2}\right)^\beta} \quad (2.2)$$

the model can be made energy balanced. Adding this term makes the simplifying biological assumption that the gain in lean mass corresponds to a loss in adipose tissue to achieve energy balance. We acknowledge that this process is significantly more complicated and that stored adipose tissue is not used to generate lean tissue. Future models can be developed to more accurately model this process.

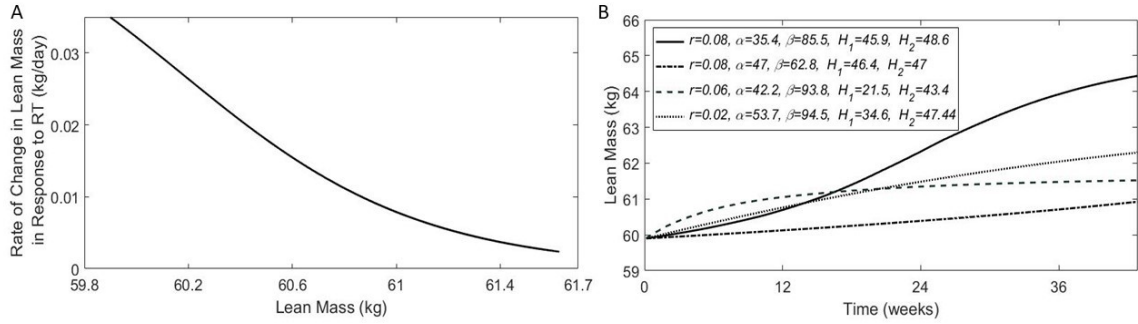


Fig. 1. **Model behavior and predictions for initial body measurements corresponding to the average US male [41] performing RE with varying parameter values and energy intakes** (A) Daily change in LM in response to RE is plotted against total LM. As LM accumulates the rate of increase slows and approaches zero. (B) Predicted time course of accumulation of LM in response to RE is plotted for different sets of parameter values shown in the legend. Physical activity level, PAL, was set to 1.6 for each simulation in order to compare the effects of varying parameters in the muscle hypertrophy term in Eqn. 2.1.

The parameters in the muscle hypertrophy term are not directly measurable, but can be interpreted both mathematically and physiologically. Since r is a scaling parameter, it can be considered the response to dose of RE, where higher frequency, intensity, or volume of training are reflected in higher values of r . The exponent α controls the steepness of the ascent of the curve shown in Figure 1, or the speed of response to training. Parameter H_1 is defined as the level of LM at which the Hill-type factor is $1/2$ and also controls speed of initial response; thus parameters α and H_1 can be modulated to simulate fast or slow responders. Parameter H_2 is defined as the level of LM at which the multiplicative inhibition factor is $1/2$. This parameter plays a large role in magnitude of response and can be considered representative of genetic potential for hypertrophy in response to training. The exponent β controls the steepness of the descent of the curve shown in Figure 1A, and can be thought

of as controlling speed of adaptation to training. By varying these parameters, the predicted time course and magnitude of muscle hypertrophy in response to RE can be modulated to fit data or otherwise conform to physiological expectations. A comparison of model predictions achieved by varying parameters for the same hypothetical individual, with initial conditions corresponding to those of the average US male aged 20-39 years from NHANES 1999-2004 [41], is shown in Figure 1B. Further modulating the effectiveness of RE is the level of LM as shown in Figure 1A for the same individual.

To explicitly model changes in total lean body mass including extracellular fluid fluctuations due to changes in dietary sodium and carbohydrate intake we have added an additional variable, LBM , given by Eqn. 2.3.

$$\frac{dLBM}{dt} = \frac{dL}{dt} + \frac{dECF}{dt} \quad (2.3)$$

In the absence of dietary changes, $dECF/dt = 0$ and Eqn. 2.3 reduces to Eqn. 2.1. Changes in energy intake or dietary sodium will result in a rapid change in extracellular fluid storage that will shift the predictive curve for LBM up or down slightly as shown in Figure 2. When dietary changes are modeled here, it is total lean body mass that is shown.

Energy intake will also influence predicted changes in body mass, as shown in the upper panel of Figure 3 which compares the effects of varying energy intake for the same hypothetical individual and the same model parameters. A hypercaloric diet is predicted to allow for energy storage in both the lean and fat compartments of body mass. Under a hypocaloric diet muscle hypertrophy is predicted to be inhibited, which is consistent with experimental results [42, 43, 44], and FM is predicted to decrease. Continued maintenance energy intake is predicted to allow for a modest

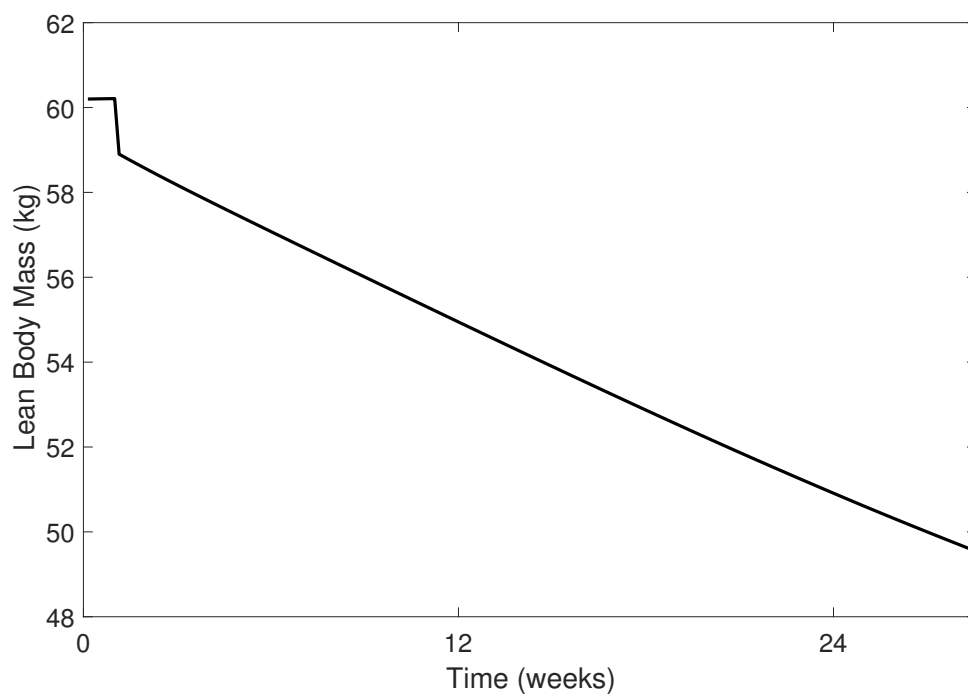


Fig. 2. **Effect of an 800 kcal/day decrease in energy intake on total lean body mass.**

Table 2. **Comparison of initial conditions and parameter values for an average US male versus female aged 20-39 years [41].**

	LM (kg)	FM (kg)	Fat %	PAL	r	α	β	H_1	H_2
Male	59.9	23.4	28.1	1.6	0.06	42.2	93.8	21.5	43.4
Female	42.3	28.9	40.6	1.6	0.02	32.1	86.2	25.2	28

increase in LM at a slight expense of FM. Since energy intake may be an important determinant of muscle hypertrophy in response to RE [42, 43, 44], any uncertainty in the estimation of initial energy intake will influence model predictions.

At this stage of development, the model does not explicitly account for differences in gender or age; however, differences in initial conditions between these groups are accounted for and may lead to different parameter sets that are group-specific. For example, women tend to have lower body mass and a higher percentage of body fat than males, therefore, parameters that produce physiologically reasonable behavior for these relative body measurements will not be the same as for males. Figure 3 (C) and (D) compare model predictions for an average US male versus an average US female aged 20-39 and the parameter values that generated these predictions are compared in Table 2.

The effect of cardiovascular exercise on energy expenditure was modeled by varying the value of parameter PAL (physical activity level) in Eqn. ?? as in Hall et al. [1]. LM has consistently been shown to be the best single predictor of RMR [45, 46, 47] and, given that LM is likely to change with RE, we chose to model the resting metabolic rate (RMR) with LM-dependent predictive equation $RMR = 21.6LM + 370$ [46] versus the Mifflin-St.Jeor equations used in Hall et al. [1] which depend on age, sex, and height. If RMR is known, it can be treated as a model input, otherwise its estimation will effect model predictions and associated uncertainty can be considered

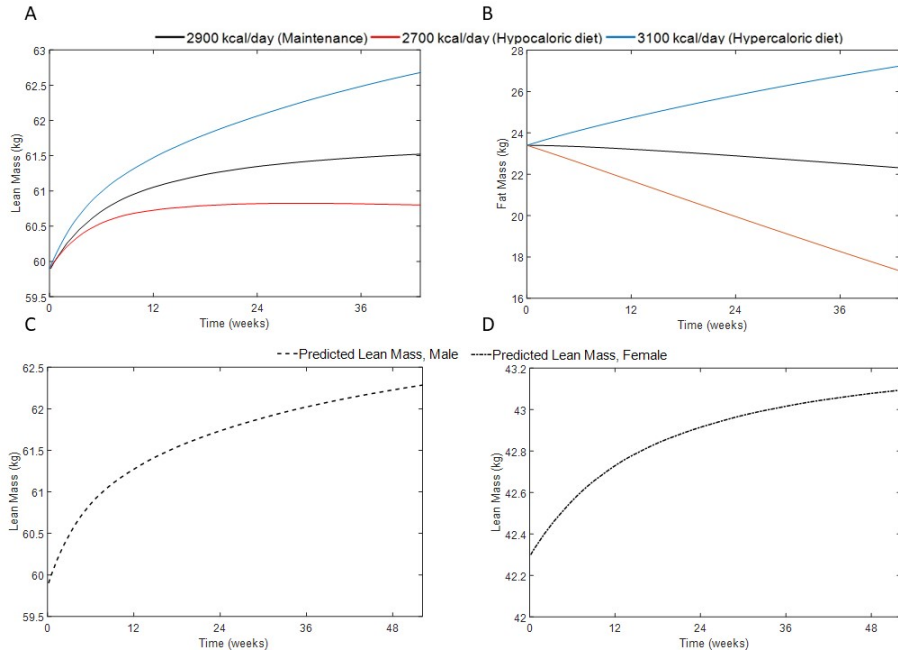


Fig. 3. **Effects of initial conditions on model predictions.** Initial conditions and parameters used to generate simulations in (A)-(D) are shown in Table 2. (A) A comparison of predicted LM in response to RE for the same parameter set and varying energy intakes: maintenance, a hypocaloric diet, and a hypercaloric diet. Initial body measurements used to generate simulations correspond to those of an average US male aged 20-39 years from NHANES 1999-2004 [41]. (B) Predicted FM is compared for the same conditions as in (A). (C) Predicted LM in response to RE for the average US male on a maintenance energy intake (shown in (A)). (D) Predicted LM in response to RE for an average US female aged 20-39 years from NHANES 1999-2004 [41].

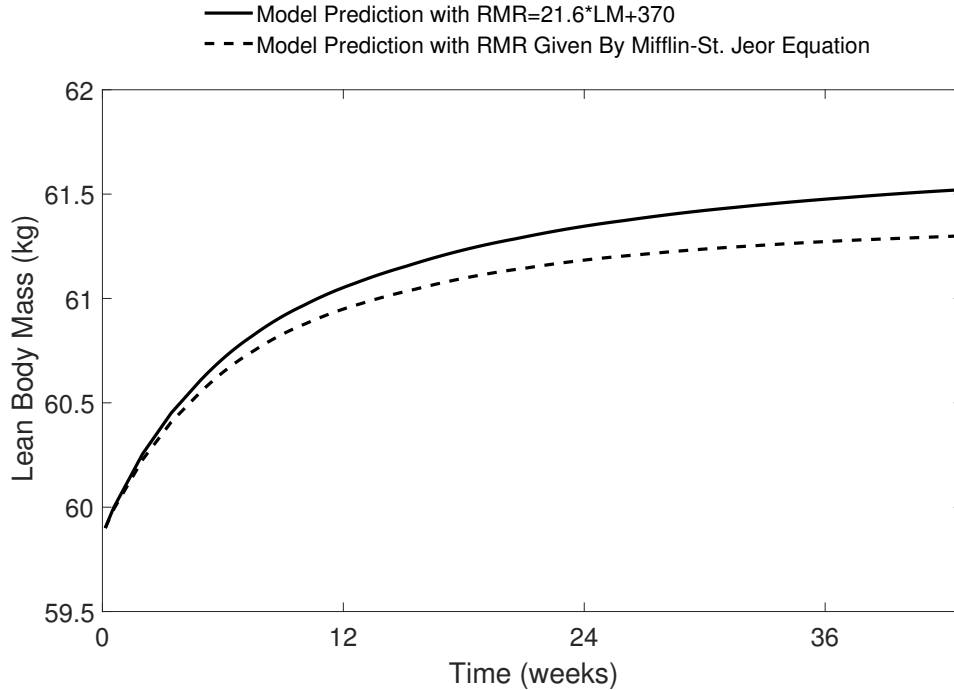


Fig. 4. Comparison of predicted change in LM using predictive equation $RMR = 21.6 \times LM + 370$ [46] versus Mifflin-St.Jeor equation $RMR = 9.99 \times Weight + 6.25 \times Height - 4.92 \times Age + 166 \times Sex (Male = 1, Female = 0) - 161$. Initial conditions and parameters used to generate these simulations are the male values given in Table 2.

a model limitation. A comparison of predicted change in LM for two different RMR estimations is shown in Figure 4 for an average US male with initial conditions and parameters given in Table 2.

Mathematical models of biological phenomena such as this also need to be evaluated for robustness. To do this we need to determine sensitivity of outcomes to perturbations in these parameters, which parameters are most responsible for which outcomes, whether outcomes for a given range of parameter values can be deemed biologically feasible, and if variation of parameters produces expected results. To answer these questions we combined the uncertainty analysis (sampling using LHS)

employed in Section 2.3.2 first with sensitivity analysis and then with classification and regression tree methods (CART). Partial rank correlation coefficient results from our sensitivity analysis showed that each parameter in the model has a significant effect on predicted LM, and that correlations between each parameter and predicted LM are consistent with our expectations. A full description of our methodology and results appears in Section 2.3.4. CART methods provide some further insight into how different combinations of parameter values can lead to similar outcomes, which can both guide parameter selection for experiments and also allow us to evaluate biological feasibility.

2.3 Results

We first fit parameters to an individual in a case study to view results for a simulated RE program and determine whether model dynamics capture expected behavior. We then explore the role of the muscle hypertrophy term in Eqn. 2.1 by varying the parameters controlling it using LHS as seen in [48, 49]. LHS is a stratified sampling without replacement method in which each parameter is independently sampled from a statistical distribution in order to create a collection of parameter sets that can each be used to generate model output, thus simulating a variety of responses. This was done both to simulate how an RE program might effect a cohort of individuals and to simulate the variability in response to RE that is seen clinically. Parameter ranges shown in Table 4 were divided into 100 subintervals of a uniform distribution with each subinterval sampled exactly once so that the entire parameter range, including extreme values, was explored. Each combination of six independently sampled parameters is then grouped into a parameter set that is used to generate model output, creating 100 simulated responses to RE for the same initial conditions.

2.3.1 Case study

A hypothetical individual is considered, weighing 100 kg with 27.2% body fat and with a maintenance energy intake level of 3024 kcal/day. Initial conditions and model constants specific to this individual are shown in Table 3 and, while gender is not explicitly modeled, these initial conditions of 100 kg body weight and 72.8 kg LM are more representative of male characteristics. Parameters were selected that produced a moderate response in LM to RE for this individual of about 3 kg gained in one year while in energy balance, consistent with the projected average gain seen in clinical studies with shorter time periods [50, 51, 14, 12, 52, 53, 54]. Parameter values are listed in Table 3 and the resulting predicted time course of change in LM in response to RE is shown in Figure 5.

For this hypothetical individual, we simulated a hypocaloric diet consisting of an 800 kcal/day deficit maintained for 12 weeks followed by a gradual return to a pre-diet level of 3024 kcal/day over an 8-week period. This scenario was chosen because it has been shown in clinical studies that subjects on a hypocaloric diet will eventually return to pre-diet energy intake levels [6, 55, 7, 8].

We then compared the effects of a hypocaloric diet with no exercise to the effects of this diet when combined with an ongoing healthy lifestyle change of either CE or RE. The addition of CE was modeled as an increase in *PAL* that remained constant for the entire time period, simulating light activity such as jogging performed several times per week on an ongoing basis. The addition of RE was modeled with the parameter values shown in Table 3 that produced the accumulation of LM over time shown in Figure 5. Predicted long-term, three-year body composition outcomes for each of the three scenarios are shown in Figure 6.

Table 3. **Model inputs for experiment comparing the effects of a hypocaloric diet only to diet with CE or RE.** Initial conditions are specific to a hypothetical individual weighing 100 kg with 27.2% body fat. Parameters appear in Eqn. 2.1 and were chosen such that a modest LM gain in response to RE was simulated.

Name	Description	Value
LM_0	Initial LM	72.8
FM_0	Initial FM	27.2
K	Energy balance constant in Eqn. 6	658.8224
k_G	Glycogen constant in Eqn. 1	7257.6
PAL	Parameter	1.5
r	Parameter	0.25
α	Parameter	9
β	Parameter	77
H_1	Parameter	66
H_2	Parameter	74

This simulation predicts that a temporary hypocaloric diet will result in an eventual return to the pre-diet body composition, as was predicted in Hall et al. [1] and which is supported by clinical study outcomes. The boost in physical activity level that results from continued CE appears to result in maintenance of a lower body composition. The greatest predicted change results from continued RE and its accompanying increase in LM, with a body composition trajectory that continues to decrease. These predictions depend on clamped energy intake after 20 weeks.

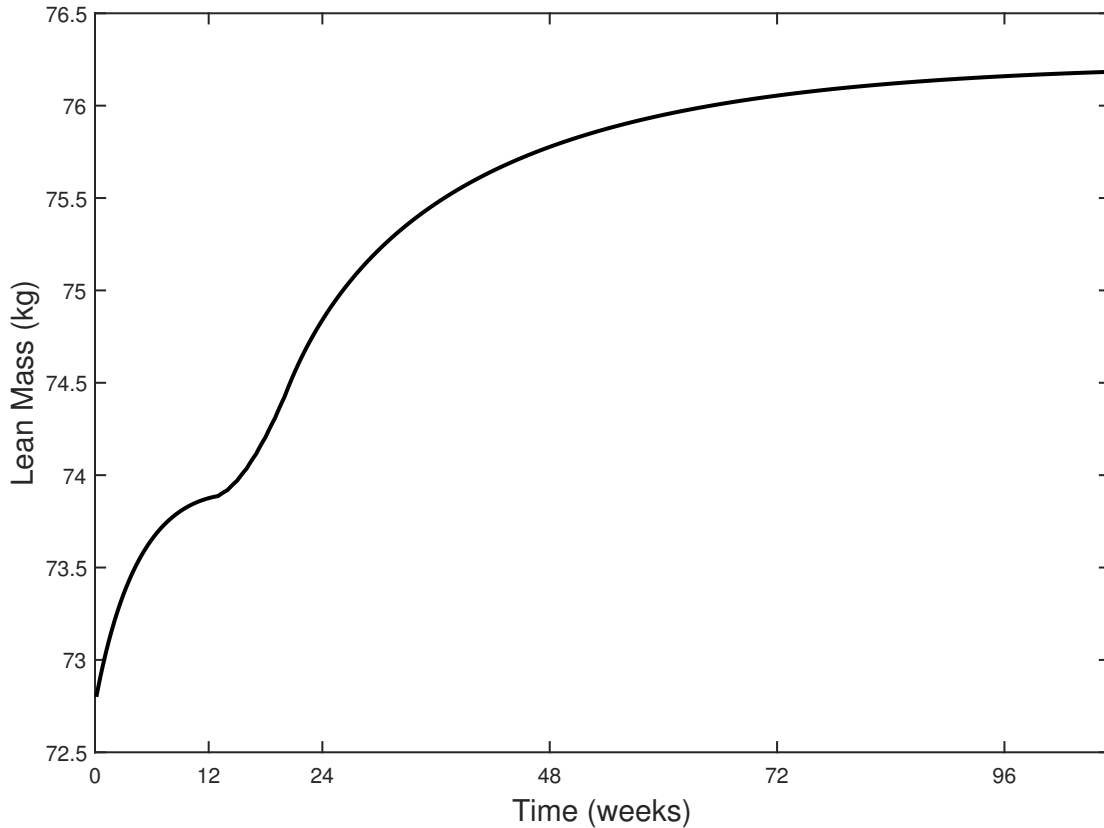


Fig. 5. Change in LM over time in response to RE for a 100 kg individual with 27.2% body fat and a maintenance energy intake of 3024 kcal/day, with a hypocaloric diet consisting of an 800 kcal/day deficit was begun on Day 1 and maintained for 12 weeks followed by a gradual return to 3024 kcal/day over 8 weeks. Parameter values: $PAL=1.5$, $r = 0.25$, $\alpha = 9$, $\beta = 77$, $H_1 = 66$, $H_2 = 74$.

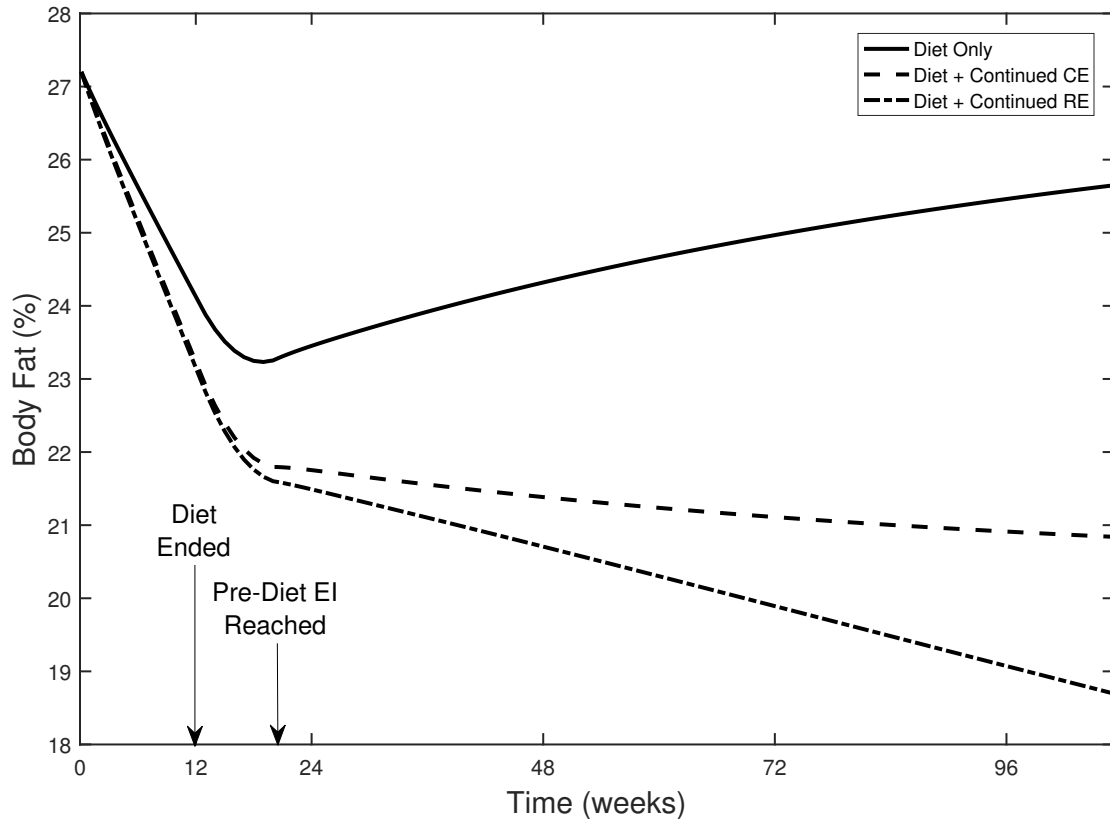


Fig. 6. A comparison of diet and exercise interventions for a 100 kg hypothetical individual with 27.2% body fat and a maintenance energy intake of 3024 kcal/day. In each scenario, a hypocaloric diet consisting of an 800 kcal/day deficit was begun on Day 1 and maintained for 12 weeks followed by a gradual return to 3024 kcal/day over 8 weeks. Diet Only has $PAL = 1.5$, appropriate for a sedentary individual. Cardiovascular exercise was modeled with an increase in PAL to 1.6, approximating light activity such as several short duration jogs per week. RE was modeled with parameter values $PAL=1.5$, $r = 0.25$, $\alpha = 9$, $\beta = 77$, $H_1 = 66$, $H_2 = 74$.

2.3.2 Simulated cohort

Individual response to RE is known to vary widely among individuals [2, 39], with high, low, slow, or fast response to training stimulus possible. In order to cap-

ture physiologically reasonable variation in response to RE, we simulated a cohort of 100 hypothetical individuals with the same initial conditions given in Table 3, yet different responses to RE that were simulated by allowing parameters to vary. This was done using LHS. Parameter ranges sampled from, shown in Table 4, were restricted to ranges that produced physiologically reasonable results for these initial conditions. Statistics calculated on results for the full cohort are shown in Table 5.

A typical clinical study differs from this simulated cohort in that both responses *and* initial conditions vary between individuals. However, it is still possible to evaluate reasonableness of the statistics and mean behavior for this simulated cohort by comparing results to clinical study results for a variety of populations. For example, the mean values for absolute gain in LM and loss of FM seen for our simulated cohort in Table 5 are comparable to results from studies of the effects of RE on young, elderly, or obese individuals [50, 51, 14, 12]. More significantly, a key aspect of the physiology of LM gain that was described in Section 2.2.2 is reproduced: a rapid initial increase that occurs over approximately the first 12 weeks followed by a greatly reduced response over the following 12 weeks as the simulated cohort adapts to the RE program. Statistics calculated on our simulated cohort shown in Table 5 highlight this qualitative behavior, since mean gain of LM over the second twelve week period versus the first twelve week period decreased by 66.4%, a similar decrease to what is seen clinically over a period of 24 weeks [2, 54]. The mean of the transients for over time of the full cohort was calculated by averaging the values for LM and FM, respectively, at each time point. Figure 7 shows the time course of LM change for all 100 simulated individuals in the cohort, while Figure 8 displays the mean of the transients of the full cohort to give an idea of average behavior.

Table 4. **Parameter set data.** LHS was restricted to these parameter ranges to ensure that physiologically reasonable simulations were generated given initial conditions. Sample means are close to the midpoints we expect for a uniform distribution, so a sample size of $n = 100$ was deemed sufficient.

Parameter name	Range	Mean
PAL	1.5 - 1.6	1.55
r	0 - 0.5	0.2505
α	2 - 80	9.001
β	20 - 80	49.974
H_1	60 - 74	67.001
H_2	65 - 75	70

Table 5. **Cohort statistics.** Mean and standard deviation calculated for absolute change in LM and FM after 12 weeks and 24 weeks of RE.

Change in Response Variable	12 Wk Mean	12 Wk SD	24 Wk Mean	24 Wk SD
Δ LM (kg)	1.6905	1.8756	2.2114	2.3990
Δ FM (kg)	-0.9463	0.5007	-2.0934	1.1194

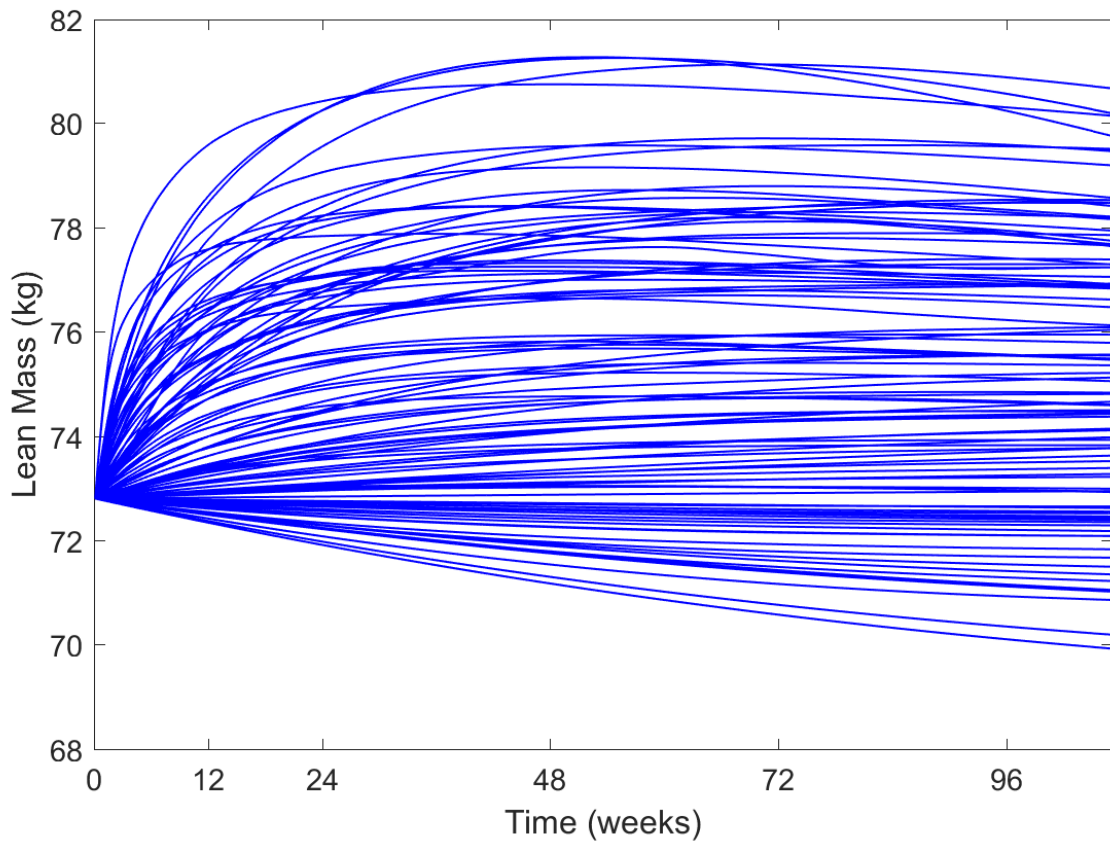


Fig. 7. Change in LM over time in response to RE for a simulated cohort of 100, 100 kg individuals with 27.2% body fat. RE was modeled with parameter values sampled from a uniform distribution with ranges restricted to the values given in Table 4.

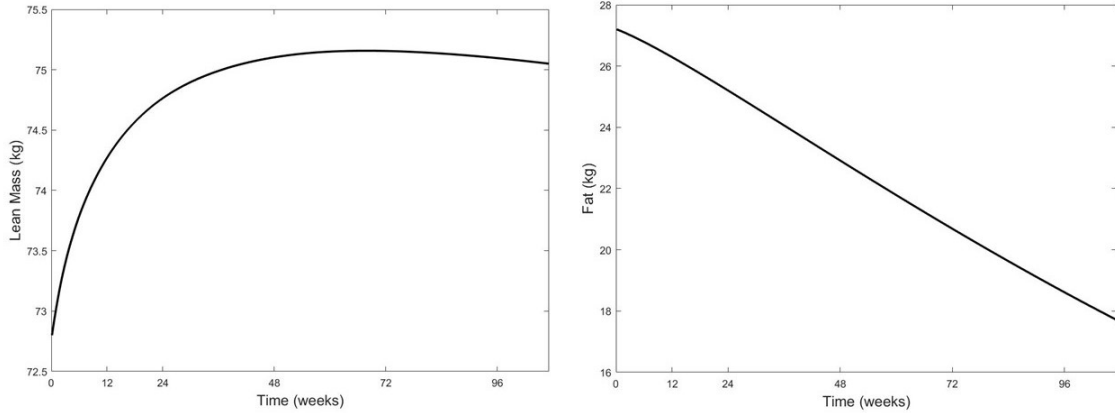


Fig. 8. Mean of the transients for LM and FM of the full cohort.

2.3.3 Parameter estimation

The ability to select parameters such that experimental results are closely matched can provide model validation. Here we validate the model’s ability to fit data from a study comparing the effects of RE between elderly women and men. RE is known to effectively combat sarcopenia. One meta-analysis of 49 studies and a total of 1328 participants showed an increase of about 1 kg of LM annually after RE versus the decline usually observed for sedentary individuals over 50 [56].

In this study, 60 subjects performed a moderate volume of RE three times per week for 24 weeks with assessments at 0, 12, and 24 weeks [2]. To fit mean time course data for the male and female groups in this study, we sought to separately simulate a mean elderly male response and a mean elderly female response. This was done by creating male and female variants of the model using the mean initial LM and FM for each group given in Table 5 as initial conditions and with initial energy intake for each estimated such that a male or female individual with mean values for each characteristic (age, height, weight, body composition) would be in energy balance. The fitting procedure was then performed via ordinary nonlinear least squares using

Table 6. **Initial conditions and parameter estimates for group data.**

Group	LM (kg)	FM (kg)	Fat %	PAL	r	α	β	H_1	H_2
Men	62.2	19.3	22.6	1.6	0.5	18.14	100	8.07	60.79
Women	42.5	21.2	32.1	1.6	0.21	2.37	99.94	13.48	42.16

the Matlab `lsqnonlin` routine with bound constraints, with bounds placed on the parameter value search that were appropriate for the given initial conditions. This local optimization routine seeks parameters within given bounds that minimize the sum of squared errors between the data and model predictions using a trust region algorithm. Data for both FM and LM were fit simultaneously and the resulting parameter estimates for each group are shown in Table 6. Model output versus mean data for both the male and female groups is shown in Figure 9.

For the male group, the difference between predicted and observed LM at 12 and 24 weeks was 0.087 kg and 0.27 kg, respectively, and the difference between predicted and observed FM at 12 and 24 weeks was 0.5 kg and 0.68 kg, respectively. For the female group, the difference between predicted and observed LM at 12 and 24 weeks was 0.14 kg and 0.15 kg, respectively, and the difference between predicted and observed FM at 12 and 24 weeks was 0.3 kg and 0.3956 kg, respectively. Each of these predicted values is within the standard error of measurement of the experimental data.

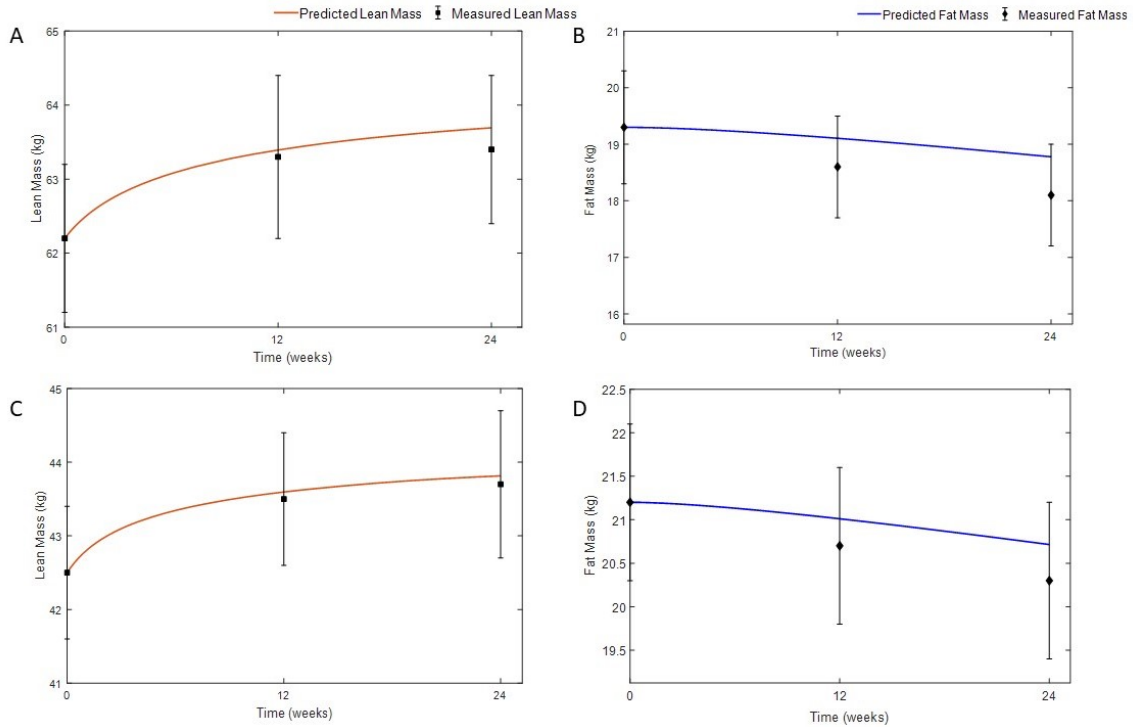


Fig. 9. **Predicted and measured body mass during a trial comparing the effects of a moderate volume RE program on elderly men and women [2].** (A) Predicted and measured average LM with SEM for 29 elderly men. (B) Predicted and measured average FM with SEM for 29 elderly men. (C) Predicted and measured average LM with SEM for 24 elderly women. (D) Predicted and measured average FM with SEM for 24 elderly women.

We then used the parameter estimates that were obtained in fitting mean data for each group in the study [2], shown in Table 6, combined with the associated mean initial conditions to simulate a longer-term scenario in which hypothetical “average” male and female elderly subjects in the study cease RE completely following the 24-week supervised training period. The projected results are shown in Figure 10. For the hypothetical male, following the cessation of training there is a slight loss of LM until the level of energy intake is sufficiently above that of energy expenditure to cause a second increase. Although initial dynamics are different for the hypothetical

female, predicted LM and FM for both hypothetical subjects appear to eventually reach a stable steady state at a new, healthier body composition. These scenarios are only two of many possible outcomes that could be investigated for a variety of hypothetical individuals using this model.

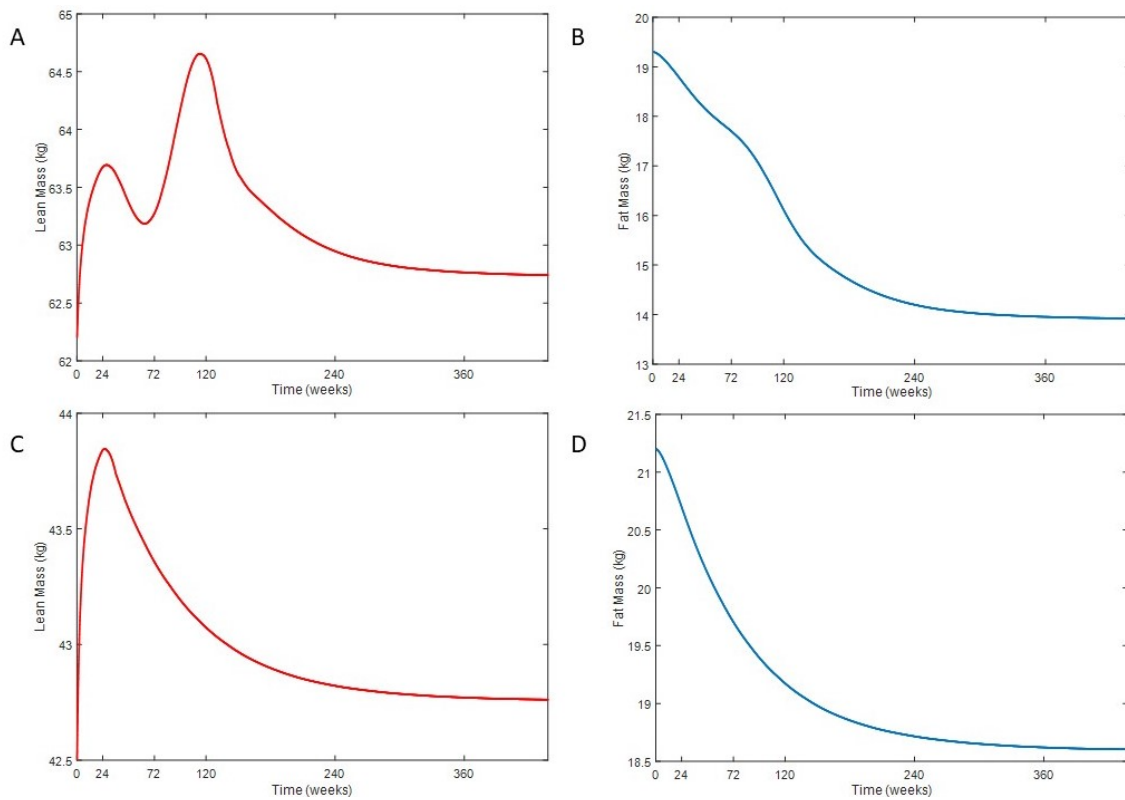


Fig. 10. **Model predictions of long-term change in LM and FM following 24 weeks of RE.** Parameter estimates obtained in fitting the model to mean data from elderly subjects completing a RE program for 24 weeks [2] were then used to simulate a long-term scenario: cessation of RE after 24 weeks. (A) Predicted average LM for the male group. (B) Predicted average FM for the male group. (C) Predicted average LM for the female group. (D) Predicted average FM for the female group

2.3.4 Sensitivity analysis

Latin Hypercube Sampling (LHS) was used to generate 1000 samples with each parameter sampled from ranges given in Table 4. Since the relationship between parameters and output (LM) was assumed to be nonlinear and monotonic, PRCCs (Partial Rank Correlation Coefficients) were calculated for each parameter at time point $t = 730$ days (2 years) when the system is approaching steady state for each sample. We then tested for significance of each parameter in the model at an α -level of 0.10 to determine whether it impacted model output. Insignificant parameters can indicate that there are problems with the model or that parameters should be eliminated, combined, or set to constant values. This method uses partial rank correlation to first rank transform the vectors containing sample parameters and associated outputs, and then calculates the correlation between each parameter and output after discounting the effects of the remaining parameters [49]. Thus this global method apportions variability in model output to variability in parameters, allowing us to determine how each parameter effects model output and evaluate biological feasibility of these effects. Results are shown in Figures 11 and 12.

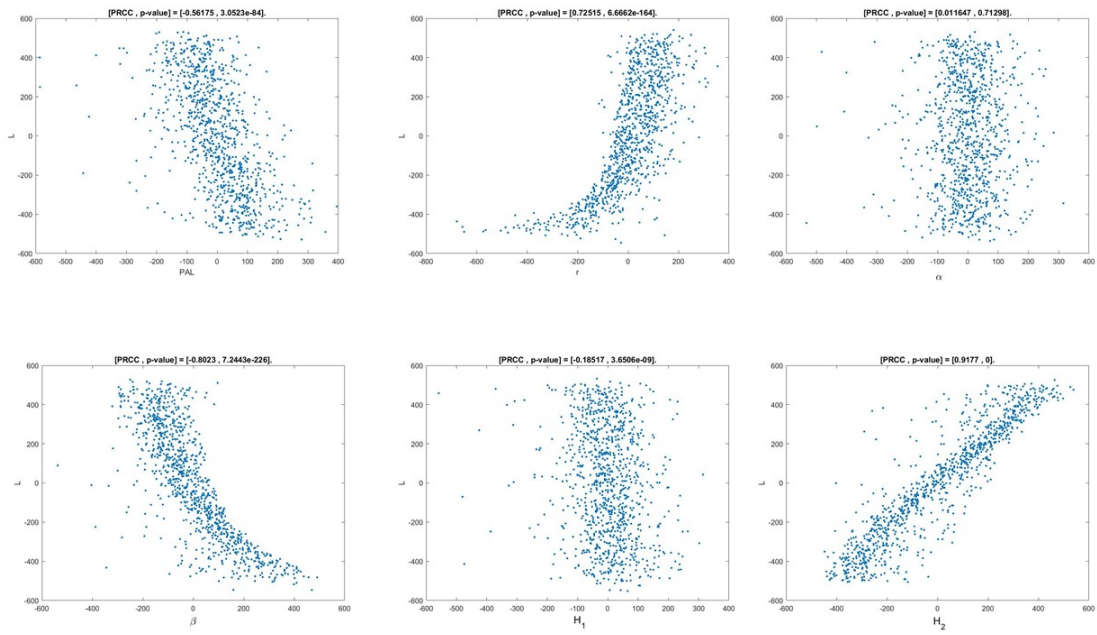


Fig. 11. Linear-linear plot of the residuals of the linear regressions of each parameter versus all other parameters of the model (horizontal axis) and the residuals of the linear regression of the output versus each parameter (vertical axis).

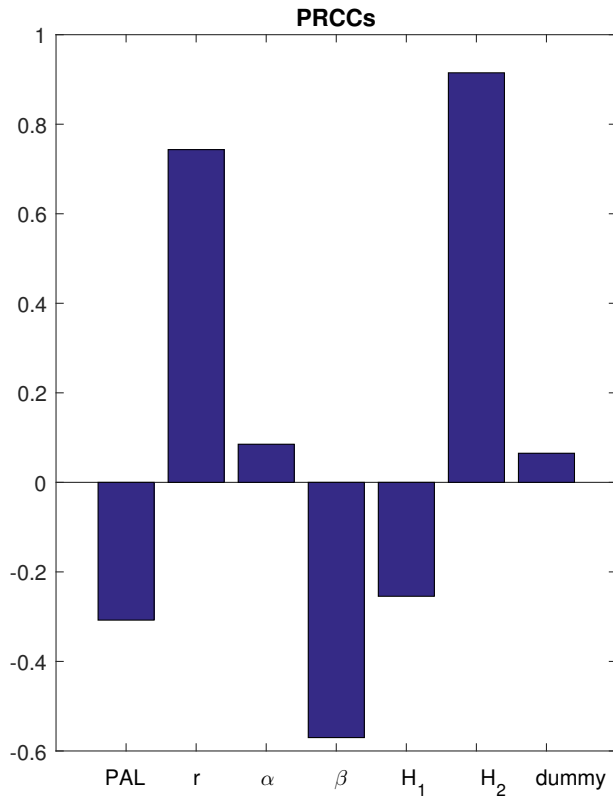


Fig. 12. PRCC results. The magnitude of the dummy parameter value is used as a significance measure for the parameters; a PRCC parameter value less than the PRCC dummy value indicates insignificance.

The plots in Figure 11 confirm that there are some nonlinearities in relationships between the parameters and output and that the assumption of monotonicity is valid. PRCCs and p-values are also given in Table 5; every parameter has a significant effect on LM although α , the exponent on the Hill term, is only weakly influential as its PRCC value is close to that of the random dummy variable included in the analysis for comparison, shown in Figure 12. Positive PRCC values indicate a positive correlation between the parameter and LM and negative PRCC values indicate a negative correlation between the parameter and *LM*. Thus an increase in parameter *PAL*

Parameter	$LM(t)$
PAL	-0.2730*
r	0.7278*
α	0.0242
β	-0.4779*
H_1	-0.2197*
H_2	0.9023*

Table 7. **PRCC**. Time point $t = 730$ days. *Significant ($p < 0.10$).

(energy expended through physical activity) is predicted to decrease LM, which is expected as LM is consumed along with FM when energy expenditure exceeds energy intake. Increases in β , the exponent on the multiplicative inhibition term, and H_1 , the half max of the Hill term, are also predicted to decrease LM. This is physiologically reasonable as increases in these parameters can be interpreted as increased speed of adaptation to RE and delayed onset of response to RE, respectively.

An increase in parameter r is predicted to increase LM; given that r scales the lean mass gain term this is expected. Parameter H_2 , the half max of the inhibition multiplier, is also positively correlated with LM. This parameter can be thought of as being related to an individual's genetic potential as it is the amount of LM at which the rate of lean mass gain is half of the maximum achieved. Parameter α is also weakly positively correlated with LM; an increase in this parameter is related to a faster rate of lean mass gain.

2.3.5 Discussion

We have extended the Hall et al. energy balance model [1] of human metabolism to include muscle hypertrophy in response to RE with the addition of the muscle hypertrophy term in Eqn. 2.1. Statistical analyses was performed that provides support for the biological interpretation of the parameters given in Section 2.2.2. We also determined that, for selected parameters, the model is able to reproduce a key aspect of the physiology of RE: a fast initial rate of response over the first 12 weeks of a training program that slows over the following 12 weeks as the body adapts.

A simulated case study comparing the effects of a hypocaloric diet alone versus combined with CE or RE followed by a resumption of pre-diet energy intake levels showed that the increased energy expenditure from LM gained in response to RE could lead to better long-term body composition outcomes. The modest gain in LM from RE leads to an energy expenditure of 3084 kcal/day. This is sufficiently above energy intake to produce continued fat loss. Higher energy expenditure from moderate CE gives an energy expenditure of 3030 kcal/day, barely above pre-diet energy intake levels. A hypocaloric diet alone with no exercise results in a new, lower energy expenditure of 3003 kcal/day due to the energetically expensive LM lost during the period of reduced energy intake, and an eventual FM regain. Additionally, the boost in energy expenditure that results from increased LM due to RE or increased calories burned due to CE offsets the effect of adaptive thermogenesis, which works in opposition to the maintenance of a new, lower body weight [57]. It is known that a majority of individuals on a weight loss diet eventually return to higher energy intake levels leading to a regain of weight lost [6, 55, 7, 8]. A way to combat this could be the addition of a RE program with the support and education necessary to make it an ongoing lifestyle change.

We also simulated a cohort of individuals with varying responses to RE by sampling parameters from a uniform distribution using LHS to capture known variation in individual response. This demonstrates how the model presented here could be used to simulate clinical studies for hypothesis testing or experimental design.

To further validate the model, we used parameter estimation methods to fit data from an RE study and performed statistical analyses to evaluate biological feasibility of model results. The parameter estimates shown in Table 6, when considered along with the sensitivity analysis results in Section 2.3.4, seem to be reasonable in the context of known biology. Versus the male group, the female group has a lower r value (corresponding to a lower overall gain), a lower α value (corresponding to slower overall response), a higher H_1 value (corresponding to a somewhat delayed response), and a lower H_2 value (corresponding to a lower potential for gain given lower initial LM). Both groups have a high β value corresponding to quick adaptation to RE that could result in a lower level of gain over time which would not be unexpected for elderly trainees.

Our predictions for LM and FM at 12 and 24 weeks were within the standard error of measurement for the data, yet it would be ideal to have more than three longitudinal data points. Additionally, we have had to make assumptions regarding energy intake given the free-living status of the research subjects. It is possible that better fits could be achieved with more knowledge about energy intake of subjects over the course of the study. However, given the relative closeness of fit for both LM and FM achieved with these limitations, one can see how group and patient-specific parameters could be estimated and then used to simulate different diet and exercise strategies. It is not currently established that there are inherent differences in response to RE between groups such as young or old, or male and female; fitting this model to data from different groups and comparing parameter estimates could

provide some intuition in this area.

2.3.6 Conclusion

Stability analysis performed on this model could provide insight into how the addition of LM from RE affects body weight set point. This model could also be further refined to include additional physiological responses to varying energy intake and exercise such as hormonal effects and even the response to specific styles of training such as high intensity interval training, a type of CE which is also known to have a positive effect on metabolism and increase LM. Submodels that are specific to populations could also be developed; for example, the addition of a muscle loss term to account for sarcopenia could produce an elderly-specific model. Since this model is unique in its inclusion of response to resistance-type exercise, it can now be used to perform *in silico* testing of this type of exercise as part of a simulated obesity or sarcopenia intervention.

CHAPTER 3

OPTIMAL CONTROL OF BODY MASS CHANGE

3.1 Introduction

Optimal control theory seeks to determine how to control an element of the system such that the "best" outcome is achieved, subject to physical constraints. By applying optimal control to the problem of body mass change during diet and exercise interventions, we first seek to find a dietary control that produces a balancing effect between the competing goals of fat loss and lean mass retention in a reduced model that considers variables fat mass (F), lean mass (L), and energy intake (EI). A hypocaloric diet (below weight maintenance levels) results in a reduction of both adipose tissue and lean tissue. Retention of lean mass while dieting may improve weight loss outcomes and prevent muscle wasting in individuals over 60, as described in detail in Section 2.1.

Optimal control techniques have been applied to many problems in medicine where interventions may have undesirable side effects, such as chemotherapy and immunotherapy for cancer [58, 59, 60], drug therapy for infection [61, 62], and vaccination and quarantine in epidemics [63, 64]. Optimal control has also been applied to models focusing on the social and psychological aspects of obesity [65, 66], but to our knowledge this is the first application that considers exercise and body mass partitioning.

First, we describe the basic optimal control problem and the steps required to find an optimal control. Next, we prove the existence and uniqueness of an optimal control for the specific problem and then characterize it in terms of the necessary conditions.

Finally, we compute the optimal control numerically and investigate dependence of the optimal control on parameters via simulations.

3.2 Methods

3.2.1 The Basic Problem in Optimal Control

The basic problem with one state variable $x(t)$ and one control variable $u(t)$ is formulated as

$$\begin{aligned} \max_u \quad & \int_{t_0}^{t_f} f(t, x(t), u(t)) dt \\ \text{subject to} \quad & x'(t) = g(t, x(t), u(t)) \\ & x(t_0) = x_0 \text{ and } x(t_1) \text{ free} \end{aligned} \tag{3.1}$$

where f is the objective functional and g is the differential equation satisfied by $x(t)$. To find the solution we must solve a set of necessary conditions that are satisfied by an optimal control $u^*(t)$ and its corresponding state $x^*(t)$. With the application of Pontryagin's Maximum Principle [67], necessary conditions can be written in terms of the Hamiltonian H which is defined as

$$H(t, x, u, \lambda) = f(t, x, u) + \lambda g(t, x, u)$$

where λ is an adjoint function. Our problem is then to maximize H with respect to the control u at u^* and the necessary conditions we must satisfy can be expressed as

$$\begin{aligned} \frac{\partial H}{\partial u} = 0 \text{ at } u^* &\Rightarrow f_u + \lambda g_u = 0 \text{ optimality condition,} \\ \lambda' = -\frac{\partial H}{\partial x} &\Rightarrow \lambda' = -(f_x + \lambda g_x) \text{ adjoint equation,} \\ \lambda(t_1) &= 0 \text{ transversality condition.} \end{aligned}$$

The dynamics of the state equation are given as

$$x' = g(t, x, u) = \frac{\partial H}{\partial \lambda}, \quad x(t_0) = x_0.$$

If, instead of maximizing (minimizing) a function over the entire time course, we prefer to maximize (minimize) it's value at the final time, we can append a payoff term to the objective functional

$$J(u) = \int_{t_0}^{t_f} f(t, x(t), u(t))dt + \phi(x(t_f)) \quad (3.2)$$

Only the transversality condition changes as a result: we now require that $\lambda(t_f) = \phi'(x^*(t_f))$.

The one-dimensional problem can be extended to include multiple states and controls with \vec{u}^* maximizing $H(t, \vec{x}^*, \vec{u}, \vec{\lambda})$ with respect to \vec{u} over $[t_0, t_f]$ and satisfying the same necessary conditions for each vector component.

3.2.2 Statement of the Optimal Control Problem

Our purpose in applying optimal control to the problem of body mass change is to determine how diet and exercise controls balance competing goals such as fat loss and muscle retention. The goal is to minimize fat mass over a finite time period such that lean mass is maximized at the final time. In an optimal control framework, the problem is

$$\min_u J(u) = \int_{t_0}^{t_f} \left[F(t) + \frac{\epsilon}{2} u^2 \right] dt - L(t)$$

$$\text{subject to } \rho_F F'(t) = (1-p)(EI(t) - EE(F, L) - u(t)) - RT, F(t_0) = F_0 \quad (3.3)$$

$$\rho_L L'(t) = p(EI(t) - EE(F, L) - u(t)) - RT, L(t_0) = L_0$$

$$EI'(t) = -u(t), EI(t_0) = EI_0$$

where $RT = rL^\alpha / (L^\alpha + H_1^\alpha) * 1 / (1 + (L/H_2)^\beta)$. We seek optimal control u^* such that $J(u^*) = \min_u \{J(u) | u \in U\}$, where U is the set of admissible controls $U = \{u | a \leq u \leq b\}$ where a and b are constants specific to the initial conditions and u is Lebesgue measurable.

We have defined a quadratic control for its convex property so that convergence can be achieved; however, there is no biological rationalization for such a choice. In a practical context, the control u is daily dietary change in kilocalories from the previous day, and the state variable EI , which is the solution to $EI'(t) = -u(t)$, gives total kilocalories that should be consumed daily.

3.2.3 Existence and Uniqueness of an Optimal Control

We first prove the existence of an optimal control that minimizes the objective functional.

Due to physiological constraints, $\tilde{F}(t) = \tilde{L}(t) = \tilde{EI}(t) = 0$ is a lower solution to the system. To find an upper solution, it is first convenient to define the initial value problem associated with optimal control problem 3.3 as

$$\begin{cases} F' = f_1(F, L, EI), F'(0) = F_0 \\ L' = f_2(F, L, EI), L'(0) = L_0 \\ EI' = f_3, EI'(0) = EI_0. \end{cases}$$

An upper solution to the IVP is then given by the solutions of

$$\begin{cases} \tilde{F} = \sup\{f_1(F, \theta_1, \theta_2) | 0 \leq \theta_1 \leq L, 0 \leq \theta_2 \leq EI\} = EE(F)(p-1) \\ \tilde{L} = \sup\{f_2(L, \theta_1, \theta_2) | 0 \leq \theta_1 \leq F, 0 \leq \theta_2 \leq EI\} = EI - EE(L) + RT \\ \tilde{EI} = \sup\{f_3(EI, \theta_1, \theta_2) | 0 \leq \theta_1 \leq F, 0 \leq \theta_2 \leq L\} = -u(t). \end{cases}$$

Further, since the set U of admissible controls is bounded with $\vec{x}(t), u(t), t, t_0 \leq t \leq t_f$ any admissible pair, then the RHS of $\vec{x}' = f(t, \vec{x}(t), u(t)) = (f_1, \dots, f_3)$ is bounded and therefore $x(t)$ satisfies a Lipschitz condition [68, p. 167]. We can then apply a comparison result to conclude that the system is bounded [69].

We can now apply a result from Fleming and Rishel [70, p. 68].

Theorem 3.2.1. *Given objective functional $J(u) = \int_{t_0}^{t_f} [F(t) + u^2] dt - L(t)$, where $U = \{u \text{ Lebesgue integrable} \mid a \leq u \leq b \forall a, b \in \mathbb{R}, t \in [t_0, t_f]\}$ subject to states and initial conditions given in system 3.3, there exists an optimal control $u^*(t)$ such that $\min_{u(t) \in [a, b]} J(u) = J(u^*)$ if the following conditions are met:*

- (a) *The class of all feasible pairs (\vec{x}_0, u) such that $u \in U$ is Lebesgue integrable on $[t_0, t_f]$ with values in U is non-empty;*
- (b) *U is closed;*
- (c) *The set S is compact and ϕ is continuous on S , where $e \in S$ with $e = (t_0, t_f, \vec{x}(t_0), \vec{x}(t_f))$ and S is a given subset of $E^{2n+2} = E^6$ (solutions at the boundary);*
- (d) *U is convex, $f(t, \vec{x}, u) = \alpha(t, \vec{x}) + \beta(t, \vec{x})u$ and the integrand of $J(u)$ is convex on U*
- (e) *The integrand of $J(u)$ is greater than $c_1 u^2 - c_2$, $c_1 > 0$*

Proof.

- (a) Since the parameters of the system are non-negative and bounded above by physiological constraints and since the solutions of the system and $u(t)$ are bounded on a finite time interval we obtain the existence of a solution [68, p. 167];
- (b) U is closed by definition;
- (c) Since the set of solutions is closed and bounded the set S is compact, and $\phi = -L(t)$ (the payoff term) is continuous;

(d) U is convex by definition. We can write $f(t, \vec{x}, u)$ as

$$f(t, \vec{x}, u) = \vec{\alpha}(t, \vec{x}) + \begin{bmatrix} 0 \\ 0 \\ -u \end{bmatrix},$$

where

$$\vec{x} = \begin{bmatrix} F \\ L \\ EI \end{bmatrix}$$

and $\vec{\alpha}(t, \vec{x})$ is the RHS of the system without control u .

To show the integrand of $J(u)$ is convex on u , we need to show

$$J(t, F, au_1 + (1-a)u_2) \leq aJ(t, F, u_1) + (1-a)J(t, F, u_2), \quad 0 \leq a \leq 1$$

$$J(t, F, au_1 + (1-a)u_2) - aJ(t, F, u_1) + (1-a)J(t, F, u_2) \leq 0$$

$$\begin{aligned} J(t, F, au_1 + (1-a)u_2) - aJ(t, F, u_1) + (1-a)J(t, F, u_2) &= \\ F + (au_1 + (1-a)u_2)^2 - (F + au_1^2 + u_2^2 - au_2^2) &= \\ a^2u_1^2 + 2a(1-a)u_1u_2 + (1-a)^2u_2^2 - au_1^2 - u_2^2 - au_2^2 &= \\ a^2u_1^2 + 2au_1u_2 - 2a^2u_1u_2 + (1-2a+a^2)u_2^2 - au_1^2 - u_2^2 + au_2^2 &= \\ a^2u_1^2 + 2au_1u_2 - 2a^2u_1u_2 + u_2^2 - 2au_2^2 + a^2u_2^2 - au_1^2 - u_2^2 + au_2^2 &= \\ a(u_1 - u_2)^2 * (a - 1) &= \\ (a^2 - a)(u_1 - u_2)^2 \end{aligned}$$

Since $0 \leq a \leq 1$, then $(a^2 - a) < 0$, and $(u_1 - u_2)^2 > 0$ so $(a^2 - a)(u_1 - u_2)^2 < 0$ and therefore $J(t, F, au_1 + (1-a)u_2) \leq aJ(t, F, u_1) + (1-a)J(t, F, u_2)$.

(e) We need to show the integrand $J(u)$ is bounded below by $c_1u^2 - c_2$ with $c_1 > 0$.

We can choose $c_1 = \frac{\epsilon}{2}$. Then

$$J(u) = F + \frac{\epsilon}{2}u^2(t) \geq \frac{\epsilon}{2}u^2(t) \geq \frac{\epsilon}{2}u^2(t) - c_2.$$

So $J(u)$ is bounded below by $\frac{\epsilon}{2}u^2(t) - c_2$.

□

3.2.4 Characterization of the Optimal Control Problem

Theorem 3.2.2. *Given that there exists an optimal control $u^* \in U$ and corresponding solution F^* , L^* , and EI^* that minimizes $J(u)$ over U , there exists adjoint functions λ_F , λ_L , λ_{EI} satisfying*

$$\begin{aligned}
\lambda'_F = & -1 - \frac{\lambda_F C}{\rho_F (C+F)^2} (EI - 1(K + \gamma_F F + \gamma_L L + ((1 - \beta_{TEF}) PAL - 1)) \\
& (21.6 L + 370) + \beta_{TEF} (EI0 - EI) + EI \left(\frac{C\eta_L}{(C+F)\rho_L} + \frac{\eta_F}{\rho_F} \left(1 - \frac{C}{C+F} \right) \right) \\
& \left(1 + \frac{C\eta_L}{(C+F)\rho_L} + \frac{\eta_F}{\rho_F} \left(1 - \frac{C}{C+F} \right) \right)^{-1} - \frac{\lambda_F}{\rho_F} \left(1 - \frac{C}{C+F} \right) \\
& \left(-1 \left(\gamma_F + EI \left(-\frac{C\eta_L}{(C+F)^2\rho_L} + \frac{C\eta_F}{\rho_F (C+F)^2} \right) \right) \right) \\
& \left(1 + \frac{C\eta_L}{(C+F)\rho_L} + \frac{\eta_F}{\rho_F} \left(1 - \frac{C}{C+F} \right) \right)^{-1} + 1(K + \gamma_F F + \gamma_L L \\
& + ((1 - \beta_{TEF}) PAL - 1) (21.6 L + 370) + \beta_{TEF} (EI0 - EI) + EI \left(\frac{C\eta_L}{(C+F)\rho_L} \right. \\
& \left. + \frac{\eta_F}{\rho_F} \left(1 - \frac{C}{C+F} \right) \right) \left(-\frac{C\eta_L}{(C+F)^2\rho_L} + \frac{C\eta_F}{\rho_F (C+F)^2} \right) \left(1 + \frac{C\eta_L}{(C+F)\rho_L} + \frac{\eta_F}{\rho_F} \right. \\
& \left. \left(1 - \frac{C}{C+F} \right) \right)^{-2} + \frac{\lambda_L C}{(C+F)^2\rho_L} (EI - 1(K + \gamma_F F + \gamma_L L + ((1 - \beta_{TEF}) PAL - 1)) \\
& (21.6 L + 370) + \beta_{TEF} (EI0 - EI) + EI \left(\frac{C\eta_L}{(C+F)\rho_L} + \frac{\eta_F}{\rho_F} \left(1 - \frac{C}{C+F} \right) \right) \\
& \left(1 + \frac{C\eta_L}{(C+F)\rho_L} + \frac{\eta_F}{\rho_F} \left(1 - \frac{C}{C+F} \right) \right)^{-1} - \frac{\lambda_L C}{(C+F)\rho_L} (-1(\gamma_F + EI \\
& \left(-\frac{C\eta_L}{(C+F)^2\rho_L} + \frac{C\eta_F}{\rho_F (C+F)^2} \right) \left(1 + \frac{C\eta_L}{(C+F)\rho_L} + \frac{\eta_F}{\rho_F} \left(1 - \frac{C}{C+F} \right) \right)^{-1} \\
& + 1(K + \gamma_F F + \gamma_L L + ((1 - \beta_{TEF}) PAL - 1) (21.6 L + 370) + \beta_{TEF} (EI0 - EI) \\
& + EI \left(\frac{C\eta_L}{(C+F)\rho_L} + \frac{\eta_F}{\rho_F} \left(1 - \frac{C}{C+F} \right) \right) \\
& \left(-\frac{C\eta_L}{(C+F)^2\rho_L} + \frac{C\eta_F}{\rho_F (C+F)^2} \right) \left(1 + \frac{C\eta_L}{(C+F)\rho_L} + \frac{\eta_F}{\rho_F} \left(1 - \frac{C}{C+F} \right) \right)^{-2}
\end{aligned}$$

$$\begin{aligned}
\lambda'_L = & 1 + \frac{\lambda_F (\gamma_L + 21.6 (1 - \beta_T EF) PAL - 21.6)}{\rho_F} \left(1 - \frac{C}{C+F}\right) \left(1 + \frac{C\eta_L}{(C+F)\rho_L}\right) \\
& + \frac{\eta_F}{\rho_F} \left(1 - \frac{C}{C+F}\right)^{-1} + \frac{\lambda_F}{\rho_F} D \left(\frac{rL^\alpha}{L^\alpha + H_1^\alpha} \left(1 + \left(\frac{L}{H_2}\right)^\beta\right)^{-1} \right) \\
& \left(\frac{rL^\alpha \alpha}{L(L^\alpha + H_1^\alpha)} \left(1 + \left(\frac{L}{H_2}\right)^\beta\right)^{-1} - \frac{r(L^\alpha)^2 \alpha}{(L^\alpha + H_1^\alpha)^2 L} \left(1 + \left(\frac{L}{H_2}\right)^\beta\right)^{-1} \right) \\
& - \frac{rL^\alpha \beta}{L(L^\alpha + H_1^\alpha)} \left(\frac{L}{H_2}\right)^\beta \left(1 + \left(\frac{L}{H_2}\right)^\beta\right)^{-2} \\
& + \frac{\lambda_2 C (\gamma_L + 21.6 (1 - \beta_T EF) PAL - 21.6)}{(C+F)\rho_L} \left(1 + \frac{C\eta_L}{(C+F)\rho_L}\right) \\
& + \frac{\eta_F}{\rho_F} \left(1 - \frac{C}{C+F}\right)^{-1} - \frac{\lambda_2 rL^\alpha \alpha}{\rho_L L(L^\alpha + H_1^\alpha)} \left(1 + \left(\frac{L}{H_2}\right)^\beta\right)^{-1} \\
& + \frac{\lambda_2 r(L^\alpha)^2 \alpha}{\rho_L (L^\alpha + H_1^\alpha)^2 L} \left(1 + \left(\frac{L}{H_2}\right)^\beta\right)^{-1} + \frac{\lambda_2 rL^\alpha \beta}{\rho_L L(L^\alpha + H_1^\alpha)} \left(\frac{L}{H_2}\right)^\beta \\
& \left(1 + \left(\frac{L}{H_2}\right)^\beta\right)^{-2}
\end{aligned}$$

$$\begin{aligned}
\lambda'_{EI} = & -\frac{\lambda_F}{\rho_F} \left(1 - \frac{C}{C+F}\right) \left(1 - 1 \left(-\beta_T EF + \frac{C\eta_L}{(C+F)\rho_L} + \frac{\eta_F}{\rho_F} \left(1 - \frac{C}{C+F}\right)\right)\right) \\
& \left(1 + \frac{C\eta_L}{(C+F)\rho_L} + \frac{\eta_F}{\rho_F} \left(1 - \frac{C}{C+F}\right)\right)^{-1} - \frac{\lambda_2 C}{(C+F)\rho_L} (1 - 1(-\beta_{TEF} \\
& + \frac{C\eta_L}{(C+F)\rho_L} + \frac{\eta_F}{\rho_F} \left(1 - \frac{C}{C+F}\right) \left(1 + \frac{C\eta_L}{(C+F)\rho_L} + \frac{\eta_F}{\rho_F} \left(1 - \frac{C}{C+F}\right)\right)^{-1}
\end{aligned}$$

with transversality conditions $\lambda_F(t_f) = \lambda_L(t_f) = 0$ and $\lambda_{EI} = C$ for some constant C . In addition, $u^*(t)$ is given by

$$u^* = \min(b, \max(a, \frac{\lambda_{EI}}{\epsilon})).$$

Proof. The adjoint equations and transversality conditions can be found using Pon-

tryagin's Maximum Principle such that

$$\begin{aligned}\lambda'_F &= -\frac{\partial H}{\partial F}, \quad \lambda_F(t_f) = 0 \\ \lambda'_L &= -\frac{\partial H}{\partial L}, \quad \lambda_L(t_f) = 0 \\ \lambda'_{EI} &= -\frac{\partial H}{\partial EI}, \quad \lambda_{EI}(t_f) = C.\end{aligned}$$

The optimal control u^* can be found using the optimality condition $\frac{\partial H}{\partial u} = 0$. We obtain u^* in the form of Theorem 3.2.2 using the bounds on U ($a \leq u \leq b$). \square

3.3 Results

Since the optimality system given in Theorem 3.2.2 contains initial conditions on the state variables and terminal conditions on the adjoints, it is a two-point boundary value problem that can be solved numerically with the Forward-Backward Sweep method. A brief description of this algorithm based on [71] is given below:

1. Discretize the time interval $[t_0, t_f]$ with time step h so that $t_i = t_0 + ih$.
2. Guess initial \vec{u}^* .
3. Solve for \vec{x} forward in time with initial conditions and \vec{u} values.
4. Solve adjoint equations $\vec{\lambda}$ backward in time using transversality conditions and values for \vec{u} and \vec{x} .
5. Update \vec{u} .
6. Check for convergence and stop if the variables of the current iteration have values sufficiently close to values for the previous iteration. Otherwise, return to step 3.

Code to implement this algorithm using a Runge-Kutta routine was written in Matlab [72] and is included in Appendix B.

We first compare the effects on the control and states of different priorities when implementing a change in diet during a resistance training program:

- Prioritize fat loss
- Equal emphasis on fat loss and muscle retention
- Maximize lean mass at the final time.

To do this, we apply weighting constants A and B to $F(t)$ and $-L(t)$ in the objective functional of the optimality system (3.3) so that it becomes

$$\min_u J(u) = \int_{t_0}^{t_f} \left[AF(t) + \frac{\epsilon}{2} u^2 \right] dt - BL(t).$$

To prioritize fat loss, we set $A = 10, B = 1$; to prioritize lean mass gain, we set $A = 1, B = 10$; under equal emphasis for each goal, $A = 1, B = 1$. The same hypothetical individual is considered here as in the simulated case study in Section 2.3.1, weighing 100 kg with 27.2% body fat and with a maintenance energy intake level of 3024 kcal/day. Initial conditions and model constants specific to this individual are shown in Table 3 along with parameters used. Parameters were selected that produced a moderate increase in lean mass in response to resistance exercise that is consistent with the projected average gain seen in clinical studies [50, 51, 14, 12, 52, 53, 54]. The control u is daily decrease in calories from the previous day and EI gives total kilocalories that should be consumed daily.

Results of numerical experiments for an 8 week diet under different priorities are shown in Fig 13. The optimal daily change in calories is largest at the beginning of

the time period (84 days) and slowly reaches zero over time. This strategy results in an energy intake that very gradually increases/decreases over the first 3/4 of the time course before saturating. Placing a priority on maximizing lean mass at the final time has the effect of drastically moderating the severity of the diet control. Even under prioritization of fat loss, the diet control is moderate enough to allow for an increase in lean mass for this hypothetical individual undergoing a resistance training program (for different parameters, the negative impact on lean mass of a hypocaloric diet may be greater). Fat loss is reduced when the dietary strategy prioritizes lean mass retention. Control u is negative when the priority is to maximize lean mass at the final time because the optimal strategy is to increase energy intake.

3.4 Discussion

We have framed body mass partitioning during a diet and exercise program as an optimal control problem and explicitly characterized an optimal quadratic control using Pontryagin's Maximum Principle. We also numerically simulated and compared optimal controls and their associated state variables under different goals: fat loss prioritization, equal weight given to fat loss and lean mass retention, and prioritization of maximum lean mass at the final time. The resulting optimal quadratic controls, shown in Fig 13, require precise manipulation of daily calories consumed and would therefore be difficult to implement. However, this model can provide some strategic insight for how to approach dieting while minimizing muscle loss. Overall, the model shows that diets should be moderate if there is a muscle retention goal and that even a moderate, gradual diet can successfully reach a fat loss goal. The long-term implications of greater lean mass retention for successful weight maintenance also remain to be explored.

In future work, controls for exercise could be added as well (cardiovascular and

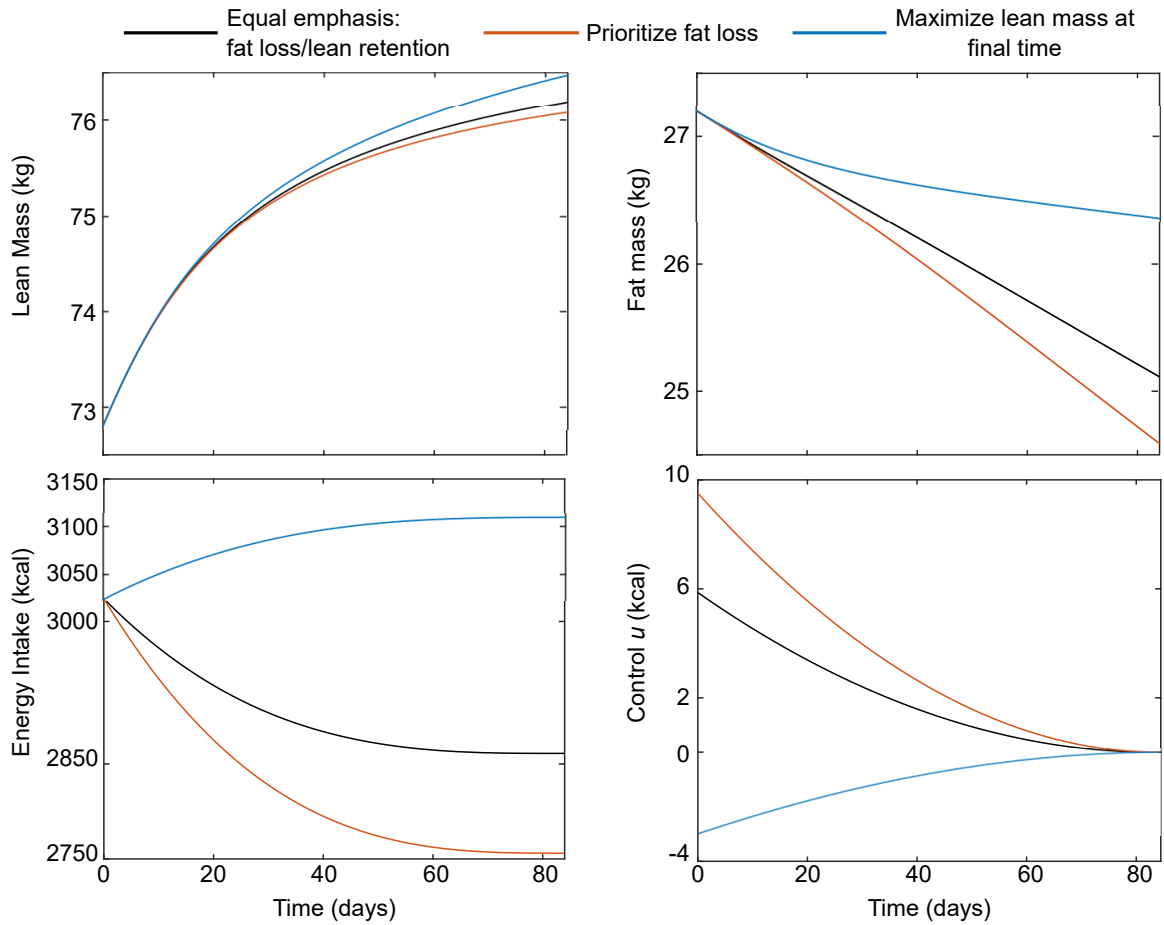


Fig. 13. Comparison of effects of different priorities on state and control variables.

resistance training), since often weight loss interventions combine diet and exercise strategies. A more intuitive linear control for diet in the objective functional could also be characterized, with appropriate constraints. Here we have imposed a fixed end time with state variables at the final time free. Alternatively, we could fix a state variable at the final time, for example a fat mass target, and allow a free end time, thus solving for goal time frame. Further, effects of parameters on control could be compared. The long-term outcomes of different short-term strategies can also be compared.

CHAPTER 4

QUALITATIVE ANALYSIS OF MODEL BEHAVIOR WITH DECISION TREES

4.1 Introduction

Machine learning, a subfield of artificial intelligence, is most commonly used to produce an accurate classifier given data; for example, one biological application is to use clinical data for medical diagnosis and prognosis. However, it can also be used to uncover the predictive structure of a problem. In systems biology modeling it could be used to gain an understanding of which system components or interactions drive the phenomenon or best characterize the conditions that determine outcomes or phenotype.

Machine learning uses pattern recognition methods to construct classifiers for data sets. When we know the class of each observation in the data set, we can use supervised learning to build a classifier based on the current data to classify future observations. Decision trees methods, developed by Breiman [73], are an example of supervised learning. If we do not know the classes associated with our observations, or even how many classes exist, we can use unsupervised learning methods. Clustering is an example of this approach.

Here we use classification trees, a supervised learning method, because it can provide complex decision boundaries and can help visualize decision rules in an easily digested format. We have made a first exploration of applying classification tree algorithms to perform qualitative analysis on our model of response to resistance training. We also use the method for validation of concept: does the classifier sort by

parameters in the way that we expect given our hypotheses?

4.2 Methods


4.2.1 Simulation of data for training and testing


A data set containing 1000 parameter sets with an associated response variable defined as total lean mass gained after 180 days was created from 1000 simulations.


4.2.2 Definitions and notation

A simplified table showing the representation of data is given in Table 4.2.2.

Simulation	$\vec{\theta}_1$	\cdots	$\vec{\theta}_{m-1}$	$\vec{L}(180)$	Class label
1	$\theta_1^{(1)}$	\cdots	$\theta_{m-1}^{(1)}$	$L(180)^{(1)}$	High
2	$\theta_1^{(2)}$	\cdots	$\theta_{m-1}^{(2)}$	$L(180)^{(2)}$	Low
\vdots					\vdots
n	$\theta_1^{(n)}$	\cdots	$\theta_{m-1}^{(n)}$	$L(180)^{(n)}$	High


 observations


 measurements


 classes

Measurements are made on an observation. In this case, as shown in Table 4.2.2, the measurements are the parameter sets used to generate a predicted response together with the response. We want to predict which class the observation is in based on the measurements (parameters).

The data set contains n observations $\{\vec{x}^{(1)}, \dots, \vec{x}^{(n)}\}$. Each observation is a vector of m measurements $\vec{x}^{(i)} = [x_1^{(i)}, x_2^{(i)}, \dots, x_m^{(i)}]$ and \mathcal{X} is the measurement space of all possible measurement vectors.

Assume observations fall into j classes and let C be the set of classes $C = \{1, \dots, j\}$. Define A_j as the subset of X for which the $C = j$: $A_j = \{\vec{x} | C = j\}$. The

sets A_1, \dots, A_j are disjoint and $\mathcal{X} = \bigcup_j A_j$ so that the A_j form a partition of \mathcal{X} . Then a classifier is defined as a partition of \mathcal{X} into j disjoint subsets A_1, \dots, A_j with $\mathcal{X} = \bigcup_j A_j$ such that for each $\vec{x} \in A_j$ the predicted class is j .

Classifiers for new data are constructed from prior knowledge of the system in the form of a learning set \mathcal{L} made up of n observed measurement vectors with their class labels as shown in Table 4.2.2.

Let n_j be the number of observations in class j in \mathcal{L} . Prior knowledge used in the construction of the classifier appears as a prior class probability $\pi(j) = \frac{n_j}{n}$. The joint probability that an observation will be in node t and belong to class j is given by

$$p(j, t) = \frac{\pi(j)n_j(t)}{n_j}.$$

The probability that an observation is in node t is given by

$$p(t) = \sum_1^j p(j, t)$$

and the probability that an observation is in class j given it is in node t is calculated as

$$p(j|t) = \frac{p(j, t)}{p(t)}.$$

4.2.3 Building a tree

Binary tree classifiers repeatedly split subsets of \mathcal{X} into two descendant subsets at each node t . Subsets not split are terminal nodes. For example, if we have two measurements x_1 and x_2 and two classes then an example tree is shown in Fig 14. Fig 14 illustrates that splits can occur on either measurement variable, with observation values that are less than the assigned splitting value going to the left node and the rest to the right. When an observation reaches a terminal node it is assigned a class.

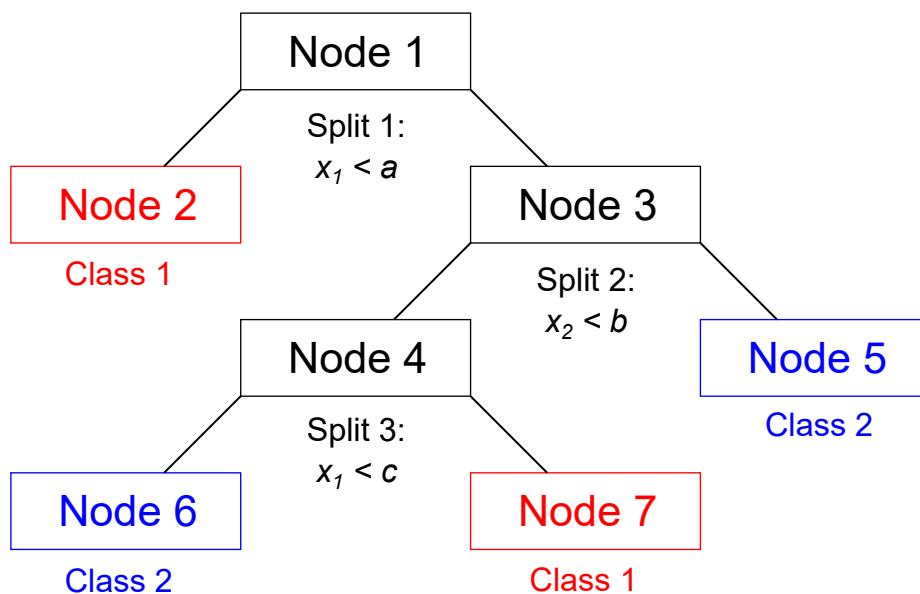


Fig. 14. **Example of a binary tree with two measurements and two classifiers.**

The partition corresponding to the classifier is found by combining all terminal nodes with the same class. For example, in Fig, A_1 =node 2 + node 7 and A_2 =node 5 + node 6.

Constructing a tree has three parts:

1. Selection of the splits.
2. Decision to terminate or keep splitting.
3. Assignment of each terminal node to a class.

4.2.3.1 Splitting

Learning set \mathcal{L} is used to find binary splits of \mathcal{X} so that each split reduces the “impurity” of the descendant subsets, i.e. the number of different classes in the subset.

- Define a measure of impurity $i(t)$ where t is the node. We use the Gini diversity

index

$$i(t) = 1 - \sum_1^j [p(j|t)]^2.$$

- Determine all splits s on each measurement by proposing splits halfway between consecutive values for that measurement
- Pick the best split on each measurement as the one which yields the largest decrease in impurity

$$\Delta i(s, t) = i(t) - p_R i(t_R) - p_L i(t_L)$$

where p_R is the proportion of observations in t that go to the right node t_R . Similarly for p_L as shown in Fig 15.

- Pick the measurement variable on which to split at each node as the one with the greatest overall decrease in impurity $\Delta i(s, t)$.

4.2.3.2 Decision to terminate splitting

A variety of stopping rules are possible. We declare a node to be terminal if all observations are from one class or if a a pre-defined criterion is met. The criterion used here is a set maximum on the number of splits.

4.2.3.3 Assignment of terminal node to a class

For class j_0 , if

$$p(j_0|t) = \max_j p(j|t)$$

then t is a class j_0 terminal node. In other words, we assign class label j_0 to a node if the probability over all classes is maximized for class j_0 given that it is in node t .

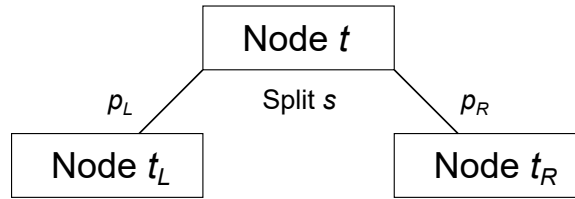


Fig. 15. **Illustration of how proportions of observations are split between nodes.**

4.2.4 Error rate

The error rate of the tree tells us the rate at which observations in the learning set \mathcal{L} have been misclassified. The error at each node t is the fraction of misclassified observations at each node and is given by

$$r(t) = 1 - \max_j p(j|t)$$

and the overall error rate for the entire tree is calculated using the error at each terminal node

$$R(t) = \sum_T r(t)p(t)$$

where T is the set of all nodes.

4.2.5 Cross-validation

Overfitting of a tree classifier to the learning data set can give an incorrect estimate of the misclassification error rate for new data. There are a variety of methods for increasing accuracy of the error estimate given limited data. Here we use k-fold cross-validation, which shuffles the learning set and then divides it into k groups. Each group takes a turn as the holdout set while all other groups combine to form the learning set. A tree is trained on the learning set and tested on the holdout set at each step. For every fold, this method computes the fraction of misclassified data

for in-fold (learning set) observations using a model trained on out-of-fold (holdout set) observations.

4.3 Results

A learning sample consisting of 1000 parameter sets together with lean mass predictions and our assigned class labels was generated using Latin Hypercube Sampling as described in Section 2.2. Parameter sets that generated a predicted lean mass gain of less than 2 kg/year after 180 days were labeled Low response while those with predicted lean mass gain of greater than 2 kg/year were labeled High response. In this way the continuous variable L (lean mass) was converted to a binary value for classification. While it is possible to grow a *regression* tree on a continuous variable, this requires a linear dependence of the response variable on the parameters which does not apply here. Classification trees were generated using 10-fold cross-validation to calculate an error rate at different pruning levels to select the best size tree. Using this method, \mathcal{L} was divided into several training and testing sets.

The `fitctree` function in Matlab was used to generate decision trees. This algorithm grows complex decision trees with many branches by default. The default average number of splits for this data was around 23, which is far too large for meaningful interpretation. To determine the best tree depth (i.e. when to stop splitting), we look at the error rate as a function of the maximum number of splits allowed in Fig 16. An increase above eight splits does not reduce error significantly, so we set the maximum number of splits to eight.

A classification tree trained on the learning set is shown in Fig 17. Decision rules used to generate the tree as returned from Matlab (see code 4.1) can also be used to code rules on parameter splits in other languages and for other contexts such as setting bounds on random sampling or parameter estimation.

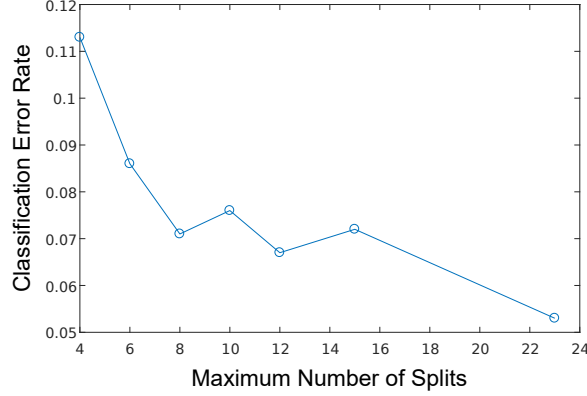


Fig. 16. Dependence of misclassification rate on maximum number of splits in tree.

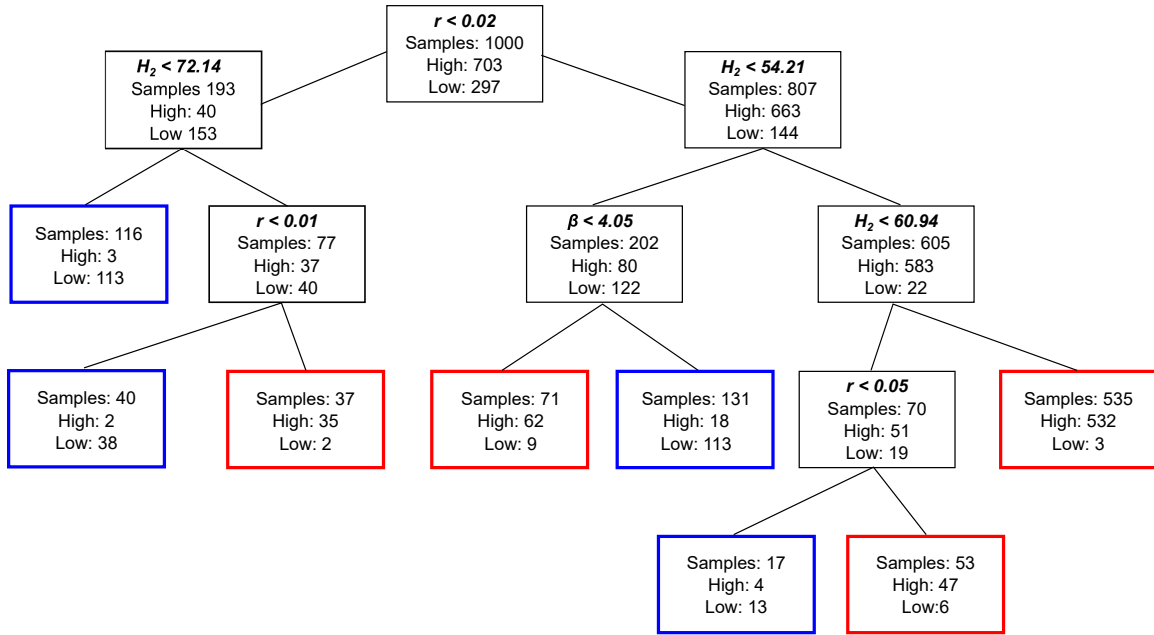


Fig. 17. A classification tree trained using a data set containing 1000 parameter sets and an associated response variable defined as total lean mass gained after 180 days. Each of the 1000 parameter sets was classified as being likely to produce a High or Low response to resistance training in simulations according to parameter splitting rules marked on each branch of the tree. Terminal nodes are outlined in red if observations within are in the High class and blue if they are assigned to the Low class.

Listing 4.1 Matlab output of decision rules used to fit a binary classification tree with a maximum of 8 splits

```

1 Decision tree for classification
2 1  if x1<0.0201011 then node 2 elseif x1≥0.0201011 then ...
   node 3 else 0
3 2  if x5<72.1374 then node 4 elseif x5≥72.1374 then node ...
   5 else 1
4 3  if x5<55.4891 then node 6 elseif x5≥55.4891 then node ...
   7 else 0
5 4  class = 1
6 5  if x1<0.0105772 then node 8 elseif x1≥0.0105772 then ...
   node 9 else 1
7 6  if x3<4.0457 then node 10 elseif x3≥4.0457 then node ...
   11 else 1
8 7  if x5<60.9438 then node 12 elseif x5≥60.9438 then node ...
   13 else 0
9 8  class = 1
10 9  class = 0
11 10 class = 0
12 11 class = 1
13 12 if x1<0.0395436 then node 14 elseif x1≥0.0395436 then ...
   node 15 else 0
14 13 class = 0
15 14 class = 1
16 15 class = 0

```

These rules on parameters can be used to guide simulation and parameter fitting

4.3.1 Classifying parameter sets in a model of resistance exercise induced muscle hypertrophy

A tree generated from the full data set misclassified only 4.7% of observations and a second tree generated using a holdout data set with equally apportioned classes misclassified 5.5%. This accuracy in prediction of lean mass outcomes given only the parameter sets that generated them indicates that there is a well-defined relationship between parameter sets and associated predicted changes in lean mass. Further, only parameters r , H_2 , and β were found significant in predicting total lean mass gained

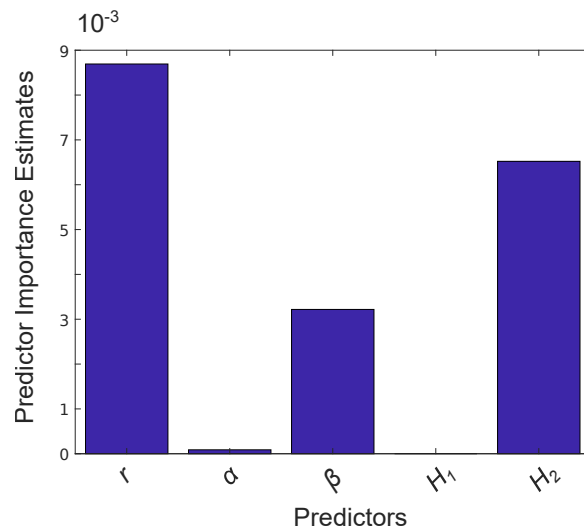


Fig. 18. **Predictor importance estimates.**

after 180 days (see Fig 18). This is consistent with the sensitivity analysis results in Section 2.3.4.

The splitting rules for each parameter shown in the tree diagram in Figure 17, and the paths that lead to a predicted High or Low response to resistance exercise, bear closer examination. This information can guide parameter selection for case studies in the future and can also allow us to evaluate biological feasibility of the model outcomes. At the uppermost level of the tree diagram we begin with 1000 samples (observations) that are then partitioned into the High and Low classes at each subsequent level by the given splitting rule. Terminal nodes are red if the observations within are classified as High and blue if they are classified as Low.

For example, if we view the leftmost main branch of the diagram in Figure 17 we see that for the 193 parameter sets with r -value less than .02, the likelihood of being a Low responder is greater because 153 of them are classified as producing a low response. However, this can be overcome if $H_2 > 72.14$ and if r is at least above a

threshold value of .01, and this applies to only 37 of the parameter sets.

This could be interpreted biologically as well: if frequency, intensity, and volume of exercise (total effort) as defined by r are low, it is unlikely to result in a high response unless the genetic potential for hypertrophy, as defined by H_2 , is high and if total effort is above a certain threshold. The other available pathways off the left main branch show that when effort is low and genetic potential is low, or when genetic potential is high yet effort is below a certain threshold, the result is a low response.

Other paths yield similar insights. The tree diagram provides an illustration of how very different paths, which can be viewed both as different combinations of parameters and different combinations of physiological tendencies, can ultimately lead to the same outcomes.

4.4 Discussion

We have used our model of response to resistance exercise to demonstrate the qualitative analysis of biological model behavior using decision trees. Using this relatively simple method, intuition can be gained about how partitions in parameter space produce different model behaviors - intuition that cannot usually be gained from limited experimentation. In this way we can learn what other behaviors the model is capable of producing. This preliminary exploration can also serve several practical purposes:

- **Visual communication of the significance of model parameters to non-mathematicians.** The tree format allows interactions between multiple parameters and the associated output to be represented simultaneously. In this way it can be made clear that the same behavior can result from different combinations of parameters. Most other statistical methods of parameter exploration are not easily visualized or are restricted to pairwise parameter plots.

- **Sensitivity analysis.** Unbiased predictor importance estimates can be calculated by summing changes in the misclassification risk due to splits on every predictor and dividing the sum by the number of branch nodes. More informally, we can simply look at the parameters used in pruned decision trees to identify the important parameters. In general, this a much quicker way of getting a first look at the key parameters that drive model behavior. We can change class definitions dependant on the behavior for which we want to identify these important parameters; for example, instead of High and Low responders, we could have defined Fast and Slow responders if we wanted to identify which parameters drive adaptation to training.

- **Decision rules can be used to find representative sets for simulation.**

To do this, we can sample parameter sets from value ranges restricted to those suggested by a decision tree. For example, given the tree in Fig 17, we can choose parameters that satisfy:

- $0.01 < r < 0.02, H_2 < 72.14$
- $r \geq 0.02, H_2 < 54.21, \beta < 4.05$
- $r \geq 0.05, H_2 \geq 60.94$

to select parameter sets representative of a hypothetical High responder or a cohort of hypothetical High responders.

- **Decision rules can be used to set bounds on parameter space for fitting.** Given experimental data, we know the ultimate class of the observation. Setting bounds on the parameter space and choosing initial parameter values for data fitting is nontrivial and can be time consuming. Generation of a decision tree from simulated data is relatively fast and straightforward. We can then refer

to the decision rules on parameters that result in the same class the observation is in to initiate parameter estimation.

There are many ways of improving the likelihood that decision trees will accurately classify new data. For a more complex model, using an ensemble of classifiers such as random forests, bagging, or boosting may be more appropriate. There are many variations of tree-based classification methods; the choice of which to use will depend on whether prediction or exploration is the goal, and whether classes are discrete or continuous.

Effects of initial conditions will also need to be investigated before decision rules could be considered to apply to any biologically reasonable sample. One possible way to do this is to include different initial conditions as parameters in an expanded learning data set when training decision trees.

CHAPTER 5

MACROPHAGE POLARIZATION IN PERITONITIS

5.1 Introduction

Macrophages play an essential role in both the progression and the resolution of inflammation. These contradictory roles may be explained by the idea of a spectrum of macrophage phenotypes, ranging from the inflammatory M1 phenotype to the anti-inflammatory M2 phenotype at either extreme, with diverse subpopulations of macrophages in between [74, 75, 76, 77]. Another possible explanation is that macrophages exhibit typically M1 or M2 type functions to varying degrees at various points in time, or there are portions of each type present at each of the different phases of inflammation [78]. While this duality of purpose is not fully understood, it is known that an imbalance between pro- and anti-inflammatory macrophage activities has been linked to disordered healing and implicated in many inflammatory diseases. For example, overpopulation of M1 macrophages can induce tissue injury [74], and the accumulation of M1s in adipose tissue which secrete pro-inflammatory cytokines can lead to insulin resistance, diabetes, and atherosclerosis [79, 80]. Even M2 macrophages, which are thought of as resolving inflammation, can cause disorders such as allergies, asthma, fibrosis, and excessive scarring when present in large numbers [77]. There is also an increased association of M2 polarized macrophages with solid tumor formation [81, 82].

All macrophages begin life as monocytes circulating in the bloodstream and, upon settling into tissues and organs in the body, will adapt to their local environment. At an inflamed site, monocytes are triggered to differentiate into macrophages in re-

sponse to stimuli such as chemokines and cytokines in the extracellular environment, phagocytosis of apoptotic cells or debris, or the presence of pathogen [74, 80, 83, 77, 84]. These first invading macrophages primarily activate to a more M1 phenotype but, under normal conditions, M2 macrophages producing anti-inflammatory cytokines will eventually dominate, suppressing the inflammatory and Th1 adaptive immune response, while promoting a Th2 response [77]. In response to infection or presence of pathogens, neutrophils are the first immune cell to appear to facilitate removal. Subsequent macrophage infiltration is essential for the removal of apoptotic neutrophils and continued secretion of cytokines to further limit the effects of the invading pathogens [85].

This timely recruitment and egress of immune cells is central to the mounting of an appropriate immune response that resolves to restore tissue homeostasis. Dysfunction or disruption of this response is the cause of essentially all chronic inflammatory diseases. Appropriate switching of phenotype of the overall macrophage population from initial M1 to M2 phenotype is critical for a balanced response. Knowledge of which subpopulations of macrophages to modulate is therefore necessary for the development of interventions that can aid in the resolution of inflammation.

Mathematical modeling has been extensively applied to the problem of inflammation in a variety of contexts such as wound healing [86, 3, 87, 88, 5, 89, 90, 4, 91, 92, 93, 94] and atherosclerosis [95, 96, 97, 98, 99, 100, 101, 102]. Deterministic ordinary differential equations (ODEs) in particular have been used when the primary interest is capturing time course and/or qualitative behavior at the cellular level. Reynolds et al. in 2006 [3] modeled the innate immune response to pathogen including activated phagocytes, level of pathogen, tissue damage, and anti-inflammatory mediators and this model was modified to apply to a local wound with the inclusion of fibroblast activity and the effect of tissue oxygen levels in Menke et al. [5]. The work was

further extended by Segal et al. in 2012 [4], adding collagen accumulation as a means of tracking the healing progress. Cooper et al. [93] next tracked macrophages and neutrophils specifically rather than a single variable representing immune response. Phagocytosis of apoptotic neutrophils was considered a key driver of the resolution of inflammation in models developed by Dunster et al. [92]. In a study analyzing macrophage polarization following myocardial infarction, Wang et al. [91] tracked both M1 and M2 macrophages as well as pro- and anti-inflammatory mediators. Recent work by Lee et al. [103] models M1 and M2 macrophage response to respiratory viral infection along with epithelial cells, cytokines, and enzymes.

Here we draw on the work done in these previous models to develop a new computational model of inflammation that seeks, in part, to explain the relationship between macrophage polarization and neutrophils. To our knowledge, our model is the first to include both inflammatory M1s and resolving M2s that is fit to *in vivo* experimental data.

We first use ODEs to develop a computational model of the sequential influx of immune cells in response to an external trigger to permit a system-level analyses of the processes. We then parametrize the model by fitting to cell count data for neutrophils, M1 macrophages, and M2 macrophages obtained from a mouse model of peritonitis, a well-accepted model to assess inflammatory responses *in vivo* that is also widely used to evaluate the efficacy of targeted anti-inflammatory interventions. This step entails finding a subset of identifiable parameters to estimate and fixing those that were unidentifiable, a process that has many approaches across a wide application area [104, 105, 106, 107, 108, 109]. Once a final parameter set is estimated, we conduct a local sensitivity analysis of the fitted model in order to gain an understanding of the primary controls of the system. The results support the dependence of macrophage polarization on neutrophils that has been hypothesized in the literature

[110, 74, 111, 112, 76]. Finally, we use the model to test several macrophage-targeted treatment scenarios that are hypothesized to dampen inflammation. The resulting predictions could have implications in the development of treatment strategies for chronic inflammation.

5.2 Methods

Experimental details

Induction of peritonitis by intraperitoneal injection of thioglycollate broth, which will facilitate the rapid growth of bacteria in the peritoneal cavity, is a well-suited platform to monitor the influx of immune cells and also permits easy characterization of the infiltrating cells in a time dependent manner. Peritoneal exudates were harvested from mice at 10 different time-points over 7 days after a single intraperitoneal injection of 3% thioglycollate broth. The peritoneal cavity was flushed with serum free RPMI medium. The cells were collected by brief centrifugation, re-suspended, and then stained with fluorescently conjugated antibodies to CD45, CD11b, Ly6G (Gr-1), F4/80 and Ly6C and analyzed by flow cytometry to determine the distribution of neutrophils, macrophages and Ly6CHi (M1) or Ly6CLo (M2) polarization [113]. While all leukocytes are CD45+, neutrophils and macrophages can be distinguished by the presence of specific markers, namely Ly6G or Gr1 and CD11b or F4/80 on neutrophils and macrophages, respectively. The macrophages in the peritoneal exudates can further be differentiated into resident (CD11bHi and F4/80Hi), inflammatory M1 (CD11b+Ly6CHi) and anti-inflammatory M2 (CD11b+Ly6CLo) phenotypes. The gating strategy and representative dot plots and histograms used to identify individual cell populations are shown in Figure 19. Flow cytometry data was analyzed using the FlowJo software and percent distribution of individual cell type

determined as described earlier [113]. The data collected from these experiments is used to calibrate the model parameters (see C.1).

5.2.1 Model Development

This model tracks the signaling and resulting immune response within the peritoneal cavity. We do not explicitly model the blood component and all variables represent local levels. To create this model, previous models of immune response to a wound [3, 4, 93] have been adapted to include polarization of macrophages between phenotypes M1 and M2, transition of neutrophils to the apoptotic state, and the injection of nutrient broth to induce growth of pathogen and stimulate immune response. System variables include cell populations given by $M1$ (M1 macrophages), $M2$ (M2 macrophages), N (neutrophils), and AN (apoptotic neutrophils) as well as P (pathogen) and B (inflammatory stimulus). We track the total cells for each population with units of 10^7 cells. Model parameters for rates of activation, transition, decay, and interactions are specified in Table 8. Units for many of the model parameters are given in terms of their associated variable, since they are representative of immune functions such as cell signaling and mediators for which units cannot be determined. The model is summarized in Fig 20 and described by Eqs 5.1-5.6.

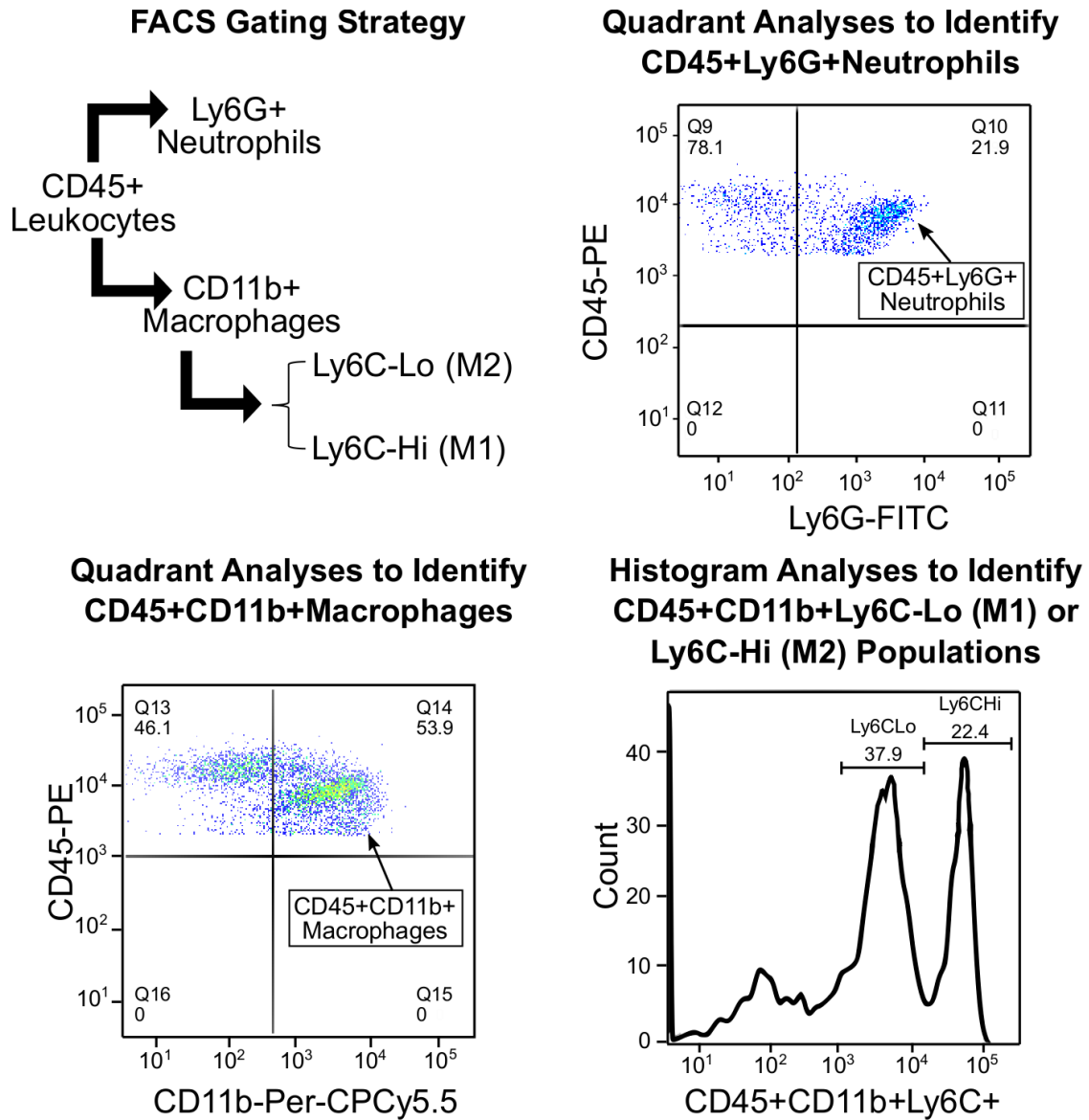


Fig. 19. **Experimental details.** Gating strategy and representative dot plots and histograms used to identify individual cell populations

Macrophages:

$$\frac{dM1}{dt} = \frac{\overbrace{s_{mr}R_{M1}(P, N, M1, AN)}^{\text{activation/influx rate}}}{\mu_{mr} + R_{M1}(P, N, M1, AN) + R_{M2}(M2)} - \overbrace{k_{m1m2}k_{anm1}AN f_i(M1, N)}^{\text{switch to M2 from M1 per phagocytized AN}} \quad (5.1)$$

$$+ \overbrace{k_{m2m1}M2}^{\text{switch to M1 from M2}} - \overbrace{\mu_{m1}M1}^{\text{decay}}$$

$$\frac{dM2}{dt} = \frac{\overbrace{s_{mr}R_{M2}(M2)}^{\text{activation/influx rate}}}{\mu_{mr} + R_{M1}(P, N, M1, AN) + R_{M2}(M2)} + \overbrace{k_{m1m2}k_{anm1}AN f_i(M1, N)}^{\text{switch rate from M1 per phagocytized AN}} \quad (5.2)$$

$$- \overbrace{k_{m2m1}M2}^{\text{switch from M2 to M1}} - \overbrace{\mu_{m2}M2}^{\text{decay}}$$

where the activation/influx rates for M1 and M2 are given by

$$R_{M1} = \overbrace{k_{m1p}P}^{\text{activation by } P} + \overbrace{k_{m1n}N}^{\text{activation by byproducts of } N} + \overbrace{k_{m1m1}M1}^{\text{activation by M1s and their cytokines}}$$

$$+ \overbrace{k_{m1an}\mu_{an}AN}^{\text{activation by necrotic AN}}$$

$$R_{M2} = \overbrace{k_{m2m2}M2}^{\text{activation by M2s and their cytokines}} + \overbrace{k_c}^{\text{background anti-inflammatory cytokines}}$$

Neutrophils:

$$\frac{dN}{dt} = \frac{\overbrace{s_{nr}R_N(P, AN)}^{\text{activation rate}}}{\mu_{nr} + R_N(P, AN)} - \overbrace{k_{an}N}^{\text{apoptosis}} \quad (5.3)$$

$$\frac{dAN}{dt} = \overbrace{k_{an}N}^{\text{apoptosis of } N} - \overbrace{k_{anm1}AN f_i(M1, N)}^{\text{removal by M1}} - \overbrace{k_{anm2}AN f_i(M2, N)}^{\text{removal by M2}} - \overbrace{k_{ann}N}^{\text{removal by } N}$$

$$- \overbrace{\mu_{an}AN}^{\text{secondary necrosis}}$$

where the activation rate for neutrophils is

$$R_N = \overbrace{k_{np}P}^{\text{activation by } P} + \overbrace{k_{nan}\mu_{an}AN}^{\text{activation by necrotic AN}}$$

Inflammatory Stimulus:

$$\frac{dP}{dt} = \overbrace{k_{pg}P \left(1 - \frac{P}{P_\infty + B}\right)}^{\text{logistic broth-dependent growth}} - \overbrace{k_{pn}PN}^{\text{removal by N}} - \overbrace{k_{pm}P f_i(M1, N)}^{\text{removal by M1}} \quad (5.5)$$

$$\frac{dB}{dt} = \overbrace{-k_{pm}P f_i(M2, N)}^{\text{removal by M2}} - \overbrace{k_bBP}^{\text{consumption by P}} \quad (5.6)$$

Inhibition function:

$$f_i(x, N) = \frac{x}{1 + \left(\frac{N}{n_\infty}\right)^2}$$

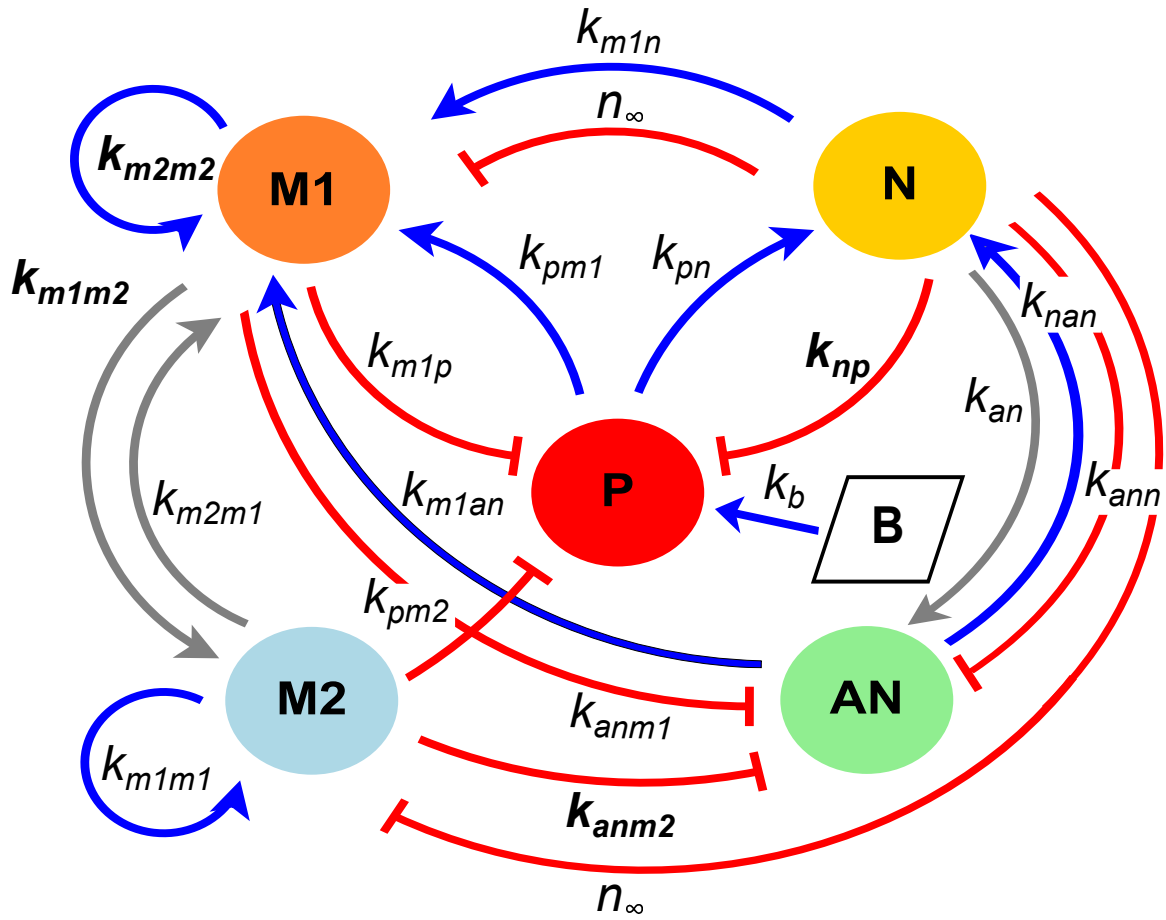


Fig. 20. **Model schematic.** Model schematic for the inflammatory response with components defined in key. Arrows represent up-regulation and bars represent destruction or inhibition. Parameters in the schematic that are included in the final subset of identifiable parameters appear in bold; additional non-interaction parameters that do not appear in the schematic are given with the full subset in Table 11.

Table 8.: **Description of parameters and estimates for the full model.** The value for k_c was set to the value for s_c , source of anti-inflammatory mediator, in Reynolds et al. [3]. To set bounds for parameter fitting, Latin Hypercube Sampling was used to find parameter sets that resulted in a physiologically reasonable range of responses. This process is described in detail in Cooper et al. [93]. Parameters included in the final subset of identifiable parameters, with all other parameters fixed, are marked with *, with final estimates given in Table 11.

Parameter	Description	Initial Estimate	Bounds
P_0	initial concentration of pathogen	$3 \times 10^3 / \text{cm}^3$	(fixed)
B_0	initial concentration of nutrient broth	$1 \times 10^3 / \text{cm}^3$	(fixed)
k_b	destruction rate of B by P	10/day	(fixed)
p_∞	pathogen carrying capacity	$3 \times 10^3 / \text{cm}^3$	(set equal to P_0)
k_{pg}	growth rate of pathogen	35/day	(10, 35)
k_{pn}	destruction rate of pathogen by N	0.295/ N -units/day	(0.11, 5)
k_{pm}	destruction rate of pathogen by macrophages	6.11/ M -units/day	(1, 10)
s_{mr}	source of resting monocytes	21.440/ M -units/day	(8, 100)

Continued on next page

Table 8 – Continued from previous page

Parameter	Description	Initial Estimate	Bounds
μ_{nr}	decay of resting monocytes	5.156/day	(5,80)
k_{m1p}	activation rate of M1 by P	1.00/ M -units/day	(1, 5)
k_{m1n}	activation rate of M1 by N byproducts	0.025/ M -units/day	(0.01, 5)
k_{m1an}	activation rate of M1 by AN	0.997/ M -units/day	(1×10^3 , 5)
k_{m1m1}	activation rate of M1 by M1s and their cytokines	0.001/ M -units/day	(1×10^4 , 5)
k_{m2m1}	transition rate of M2 to M1	0.117/ M -units/day	(0.01, 1)
μ_{m1}^*	decay of M1 macrophages	6.956/day	(1, 20)
k_{m1m2}^*	transition rate of M1 to M2	8.281/ M -units/day	(0.1, 100)
k_{m2m2}^*	activation rate of M2 by M2s and their cytokines	1.624/ M -units/day	(1×10^3 , 5)
k_c	concentration of background anti-inflammatory	0.0125/ M -units/day	(fixed [3])
μ_{m2}	decay of M2 macrophages	8.271/day	(1, 20)
s_{nr}^*	source of resting N	15.889/ N -units/day	(10, 100)
u_{nr}	decay of resting N	3.978/day	(1, 10)
k_{np}^*	activation rate of N by P	3.703/ N -units/day	(1×10^3 , 50)
k_{nan}	activation rate of N by AN	0.607/ N -units/day	(0.0001, 5)

Continued on next page

Table 8 – Continued from previous page

Parameter	Description	Initial Estimate	Bounds
n_∞	level of N for 50% inhibition of M activity	$0.156/N$ -units	$(0.01, 5)$
k_{an}	transition rate of N to AN	$7.108/N$ -units/day	$(1, 30)$
k_{ann}	destruction rate of AN by N	$0.001/N$ -units/day	$(1 \times 10^6, 0.01)$
k_{annm1}	destruction rate of AN by $M1$	$2.898/N$ -units/day	$(0.1, 1 \times 10^3)$
k_{annm2*}	destruction rate of AN by $M1$	$87.080/N$ -units/day	$(5, 1 \times 10^3)$
μ_{an}	secondary necrosis of AN	$1.309/\text{day}$	$(1, 15)$

The healthy peritoneal cavity is impermeable and is assumed to be nearly sterile prior to inflammatory stimulus, with very low levels of pathogen, and so contains only a very small number of “surveying” macrophages. Therefore, all of our immune cell variables have an initial condition of zero. The injection of nutrient broth is assumed to stimulate a very rapid increase in pathogen growth that quickly subsides as broth is consumed and pathogen is removed by macrophages and neutrophils. Timely removal of pathogens is dependent on appropriate influx and egress of inflammatory cells. Therefore, development and/or resolution of peritonitis report on an individual’s ability to mount or resolve inflammation. The initial spike in pathogen modeled by Eqs 5.5-5.6 initiates the subsequent immune cell response.

As in Cooper et al. [93], immune cells are assumed to activate and influx into the local environment rapidly compared to other dynamics, so the quasi-steady state assumption is used. This gives rise to Michaelis-Menten type activation and influx terms in Eqs 5.1-5.3. In addition, we do not explicitly model cytokines but instead allow the presence of immune cells to act as an indicator of associated cytokine level.

Resting neutrophils are the first immune cells to arrive at the site of infection, rapidly becoming activated by pathogen and the debris formed by apoptotic neutrophils at the rate $R_N(P, AN)$. As neutrophils become laden with bacteria, they undergo apoptosis at rate k_{an} . Apoptotic neutrophils are then removed by M1s at rate k_{anm1} , M2s at rate k_{anm2} , and by active neutrophils at rate k_{ann} . We have chosen k_{ann} to be much smaller than both k_{anm1} and k_{anm2} as appropriate for the case when both macrophages and neutrophils are present, but in the absence of macrophages, the clearance of apoptotic cells by neutrophils may take on greater importance [114, 115]. Apoptotic neutrophils that are not cleared undergo secondary necrosis at rate μ_{an} , contributing to the positive feedback described in the neutrophil activation term R_N . Resting monocytes (M_R) are next to arrive. The majority of these first monocytes

differentiate to an inflammatory M1 phenotype in response to pathogen, byproducts of neutrophils, M1s and their cytokines, and cytokines spilled by necrotic apoptotic neutrophils at rate $R_{M1}(P, N, M1, AN)$. Background levels of anti-inflammatory cytokines, k_c (related to the anti-inflammatory source term in Reynolds et al. [3]), cause a small portion of monocytes to differentiate to an M2 phenotype. Intrinsic decay is assumed to occur at rate μ_{m1} in M1s and at rate μ_{m2} in M2s. M1s are assumed to be able to switch to M2s at rate k_{m1m2} , and this switch is assumed to be promoted by the phagocytosis of apoptotic cells [116, 112, 76, 74]. Plasticity of macrophage phenotype is not fully understood, therefore, we allow for the possibility of a transition from M2 to M1 in Eq 5.1 at rate k_{m2m1} as well. Late arriving monocytes are assumed to be able to activate to the M2 phenotype in response to anti-inflammatory cytokines produced by M2s at rate $R_{M2}(M2)$.

The inhibition term $f_i(x, N)$ models the inhibition of macrophage activity by neutrophils due to oxidation of the environment, in which parameter n_∞ controls the level of neutrophils at which inhibition reduces macrophage activity by 50% [93].

5.2.2 Identification and analysis of equilibrium points

We assume the initial inflammatory stimulus (nutrient broth and pathogen) is removed in the determination of steady state solutions. This reduces the system to M1, M2, AN, and N and removes all terms associated with the stimulus:

$$\frac{dM1}{dt} = \frac{\overbrace{s_{mr} R_{M1}(N, M1, AN)}^{\text{activation/influx rate from } M_R}}{u_{mr} + R_{M1}(N, M1, AN) + R_{M2}(M2)} - \frac{\overbrace{k_{m1m2} k_{anm1} AN f_i(M1, N)}^{\text{switch to M2 from M1 per phagocytosed AN}}}{+ \underbrace{k_{m2m1} M2}_{\text{switch to M1 from M2}} - \underbrace{\mu_{m1} M1}_{\text{decay}}} \quad (5.7)$$

$$\frac{dM2}{dt} = \frac{\overbrace{s_{mr}R_{M2}(M2)}^{\text{activation/influx rate from } M_R}}{u_{mr} + R_{M1}(N, M1, AN) + R_{M2}(M2)} + \frac{\overbrace{k_{m1m2}k_{anm1}AN f_i(M1, N)}^{\text{switch rate from M1 per phagocytosed AN}}}{\underbrace{k_{m2m1}M2}_{\text{switch from M2 to M1}} - \underbrace{\mu_{m2}M2}_{\text{decay}}} \quad (5.8)$$

where the activation/influx rates for M1 and M2 are given by

$$R_{M1} = \underbrace{k_{m1n}N}_{\text{activation by byproducts of N}} + \underbrace{k_{m1m1}M1}_{\text{activation by M1s and their cytokines}} + \underbrace{k_{m1an}\mu_{an}AN}_{\text{activation by necrotic AN}}$$

$$R_{M2} = \underbrace{k_{m2m2}M2}_{\text{activation by M2s and their cytokines}} + \underbrace{k_c}_{\text{background anti-inflammatory cytokines}}$$

Neutrophils:

$$\frac{dN}{dt} = \frac{\overbrace{s_{nr}R_N(AN)}^{\text{activation rate}}}{\mu_{nr} + R_N(AN)} - \underbrace{k_{an}N}_{\text{apoptosis}} \quad (5.9)$$

$$\frac{dAN}{dt} = \underbrace{k_{an}N}_{\text{apoptosis of N}} - \underbrace{k_{anm1}AN f_i(M1, N)}_{\text{removal by M1}} - \underbrace{k_{anm2}AN f_i(M2, N)}_{\text{removal by M2}} - \underbrace{k_{ann}N}_{\text{removal by N}} - \underbrace{\mu_{an}AN}_{\text{secondary necrosis}} \quad (5.10)$$

where the activation rate for neutrophils is

$$R_N = \underbrace{k_{nan}\mu_{an}AN}_{\text{activation by necrotic AN}}$$

Inhibition function:

$$f_i(x, N) = \frac{x}{1 + \left(\frac{N}{N_\infty}\right)^2}$$

We set each of the 4 time derivatives equal to zero. Since there is no dependence on N in the first term of Eq 5.11, we can solve for N in terms of AN which results in a reduction of the system to three equations. In order for all three time derivatives to equal zero, AN must equal zero (as solved using Maple 2018), and so we are left with the following two equations determining steady states:

$$\frac{s_{mr}k_{m1m1}M1}{u_{mr} + k_{m1m1}M1 + k_{m2m2}M2 + k_c} + k_{m2m1}M2 - \mu_{m1}M1 = 0$$

$$\frac{s_{mr}(k_{m2m2}M2 + k_c)}{u_{mr} + k_{m1m1}M1 + k_{m2m2}M2 + k_c} - k_{m2m1}M2 - \mu_{m2}M2 = 0.$$

5.2.3 Analysis of equilibria

If we do not consider the influence of background levels of anti-inflammatory mediator (k_c), which have been shown with numerical simulations to have slight impact on dynamics, then we obtain the following result.

1. If $\frac{s_{mr}}{\mu_{mr}} < \frac{\mu_{m1}}{k_{m1m1}}$, then the system has one biologically possible equilibrium at health: $E_1(0, 0, 0)$;
2. If $\frac{s_{mr}}{\mu_{mr}} > \frac{\mu_{m1}}{k_{m1m1}}$ and $\frac{\mu_{m1}}{k_{m1m1}} < \frac{k_{m2m1} + \mu_{m2}}{k_{m2m2}}$, then the system has two biologically possible equilibria: health $E_1(0, 0, 0)$ and a sustained M1 population $E_2(\frac{s_{mr}}{\mu_{m1}} - \frac{\mu_{mr}}{k_{m1m1}}, 0, 0)$;
3. If $\frac{s_{mr}}{\mu_{mr}} > \frac{\mu_{m1}}{k_{m1m1}} > \frac{k_{m2m1} + \mu_{m2}}{k_{m2m2}}$, then the system has three biologically possible equilibria: health $E_1(0, 0, 0)$, a sustained M1 population $E_2(\frac{s_{mr}}{\mu_{m1}} - \frac{\mu_{mr}}{k_{m1m1}}, 0, 0)$, and sustained M1 and M2 populations $E_3(-\frac{k_{m2m1}P}{Q}, \frac{(k_{m1m1}(k_{m2m1} + \mu_{m2}) - k_{m2m2}\mu_{m1})P}{k_{m2m2}Q}, 0)$;

where $P = s_{mr}k_{m2m2} - \mu_{mr}k_{m2m1} - \mu_{mr}\mu_{m2}$ and $Q = (k_{m2m1} + \mu_{m2})(k_{m1m1}\mu_{m2} -$

$k_{m2m2}\mu_{m1}$).

Stability of these equilibria can be analyzed by linearization and calculation of the Jacobian matrix at each point. The trivial steady state E_1 is analogous to the resolution of inflammation, and biological feasibility of this equilibrium is independent of parameter values. The Jacobian matrix at E_1 is

$$J(E_1) = \begin{bmatrix} \frac{s_{mr}k_{m1m1}}{\mu_{mr}} - \mu_{m1} & k_{m2m1} & 0 \\ 0 & \frac{s_{mr}k_{m2m2}}{\mu_{mr}} - k_{m2m1} - \mu_{m2} & 0 \\ 0 & 0 & \frac{s_{nr}k_{nan}\mu_{an}}{\mu_{nr}} - \frac{s_{nr}k_{nan}k_{ann}\mu_{an}}{k_{an}\mu_{nr}} - \mu_{an} \end{bmatrix}.$$

Since $J(E_1)$ is upper triangular, the eigenvalues appear on the main diagonal, with all three real-valued. The trivial steady state is therefore locally stable when the following conditions on the parameters are met:

1. $\frac{s_{mr}}{\mu_{mr}} < \frac{\mu_{m1}}{k_{m1m1}}$
2. $\frac{s_{mr}}{\mu_{mr}} < \frac{k_{m2m1} + \mu_{m2}}{k_{m2m2}}$
3. $\frac{s_{nr}}{\mu_{nr}}(k_{an} - k_{ann}) < \frac{k_{an}}{k_{nan}}$

Evaluating stability of E_1 in the context of the current parameter set, we find that condition 3 simplifies to $\frac{s_{nr}}{\mu_{nr}} < \frac{1}{k_{nan}}$ due to the very small value of parameter k_{ann} .

1. $\frac{s_{mr}}{\mu_{mr}} \approx 4 \times 10^0 < \frac{\mu_{m1}}{k_{m1m1}} \approx 7 \times 10^4$
2. $\frac{s_{mr}}{\mu_{mr}} \approx 4 \times 10^0 < \frac{k_{m2m1} + \mu_{m2}}{k_{m2m2}} \approx 5 \times 10^0$
3. $\frac{s_{nr}}{\mu_{nr}} \approx 4 \times 10^1 < \frac{1}{k_{nan}} \approx 2 \times 10^1$

Only the first two conditions are satisfied, although the third condition is close to being met. Increasing decay of resting neutrophils (u_{nr}) or decreasing positive feedback from neutrophils (k_{ann}) will lead to stability. Parameters were fit to real data with inflammatory stimulus, however, and we will see in the following numerical simulations that in this more realistic scenario E_1 is stable even for this simplified model.

5.2.4 Numerical simulations

The M1 and M2 macrophage populations exert positive feedback on themselves via pro- and anti-inflammatory cytokines, respectively. Rate of activation of M1s by M1 cytokines is modeled with parameter k_{m1m1} and similarly, k_{m2m2} models positive feedback of M2s. In our analysis of equilibria, we found existence criteria (1) and (2) that identify k_{m1m1} and k_{m2m2} as bifurcation parameters. In this section, we employ numerical simulations to give bifurcation diagrams of the system for parameter k_{m1m1} and coupled variations in k_{m1m1} and k_{m2m2} that can investigate our theoretical analysis. All figures in this section were created using XPPAUT [117].

Initial conditions for the system were set to $(M1, M2, AN) = (0, 0, 0.5)$, so that we are essentially starting the system at the point after the initial inflammatory stimulus has triggered neutrophil response before subsiding. Changes in stability and existence of equilibria with variation of parameter k_{m1m1} are shown in Fig 21, which demonstrates that the system features both monostable and bistable regimes. For a low level of positive feedback from M1s (k_{m1m1}), the system has one stable steady state at health (E_1). For intermediate values, the system is bistable between E_1 and E_3 before health loses stability via a transcritical bifurcation at $k_{m1m1} = 2.15$. For high levels of positive feedback from M1s, the system is bistable between E_2 and E_3 .

A two parameter bifurcation diagram in Fig 22 shows the division of the k_{m1m1} and k_{m2m2} parameter space between a region with one steady state (E_1) and a region with three steady states (E_1 , E_2 , and E_3). Finally, Fig 23 shows the effects on M1 of varying k_{m1m1} through the limit points shown in Fig 21. As we increase the value of k_{m1m1} through 2.75, we can see the jump to E_3 .

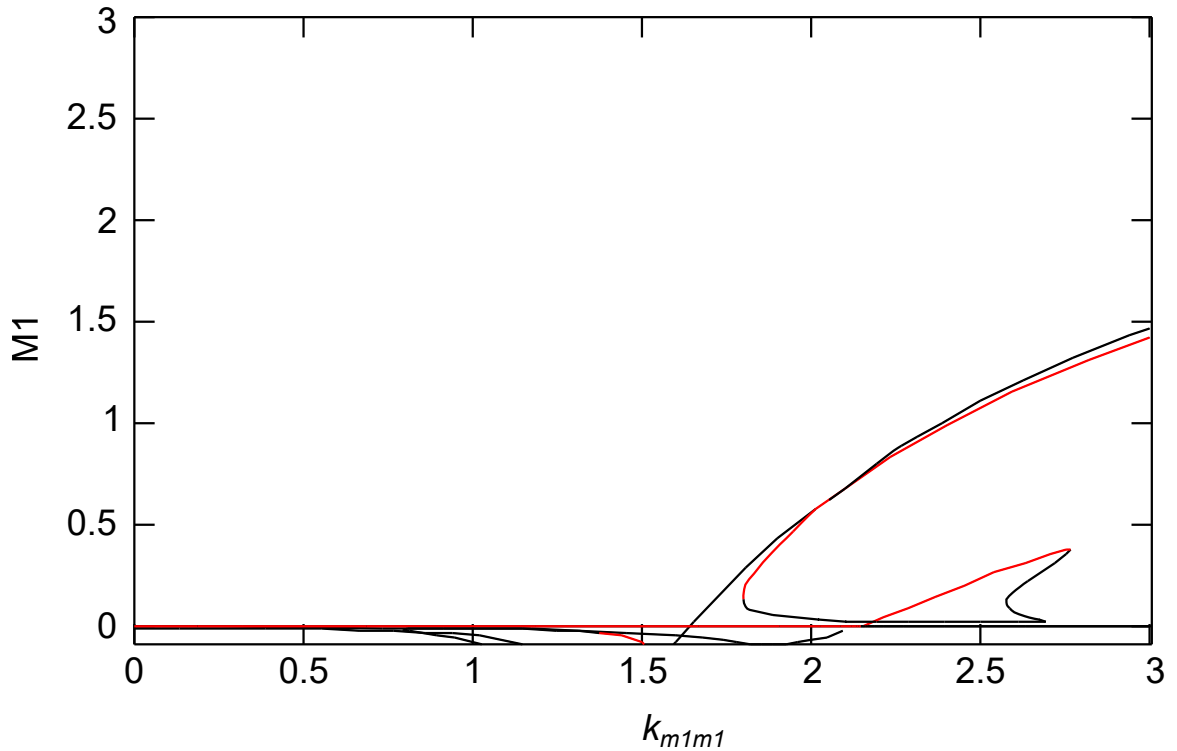


Fig. 21. **Bifurcation diagram for M1 as k_{m1m1} varies.** Stable steady states are plotted as solid lines and unstable steady states as thin lines. For small values of k_{m1m1} , the system has one stable steady state at health. For intermediate values, the system is bistable between health and a sustained M1 and M2 response before health loses stability via a transcritical bifurcation. For high values of k_{m1m1} , the system is monostable with a sustained M1 response.

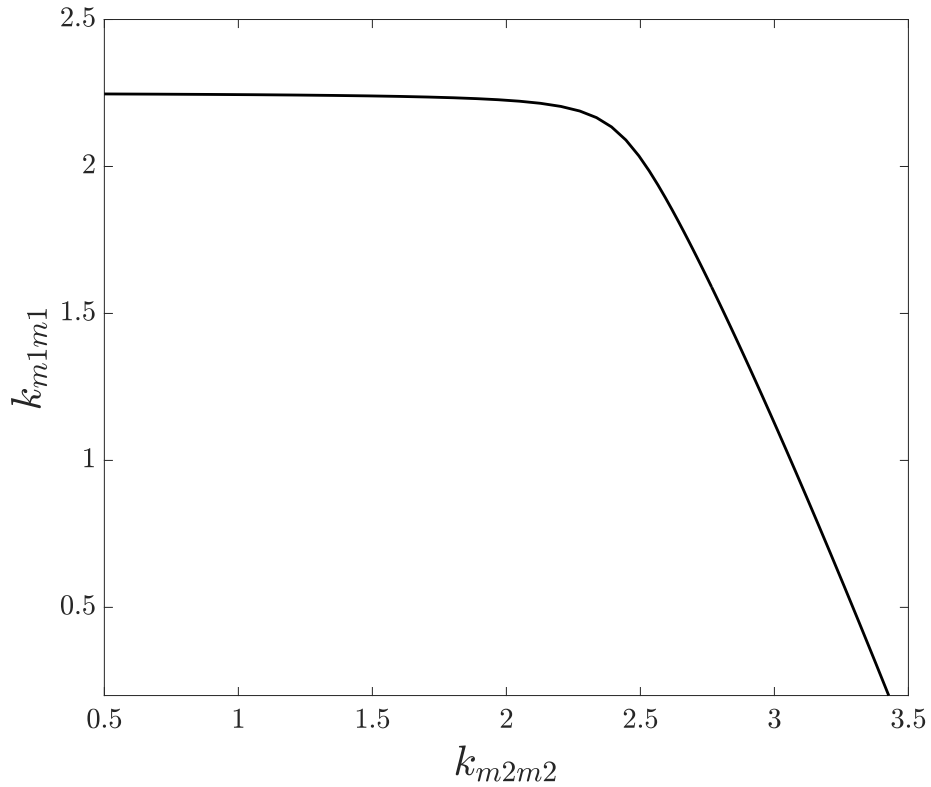


Fig. 22. **Two parameter plot of cusp.**

5.2.5 Parameter Estimation Background

Determining which parameters can be uniquely determined, or at least limited to a finite range of possible values, is a critical step in informing further experimentation. Ideally only parameters that significantly influence measurable model outputs will be targeted for manipulation, either clinically or *in silico*. Therefore, using the nominal parameter values obtained from data fitting, we will then explore structural and numerical identifiability of the proposed model *a posteriori* via the Fisher Information Matrix obtained from the discretized sensitivity matrix.

Given k state variables x , i outputs y , and j parameters p , the sensitivity of the i th model output to the j th parameter is

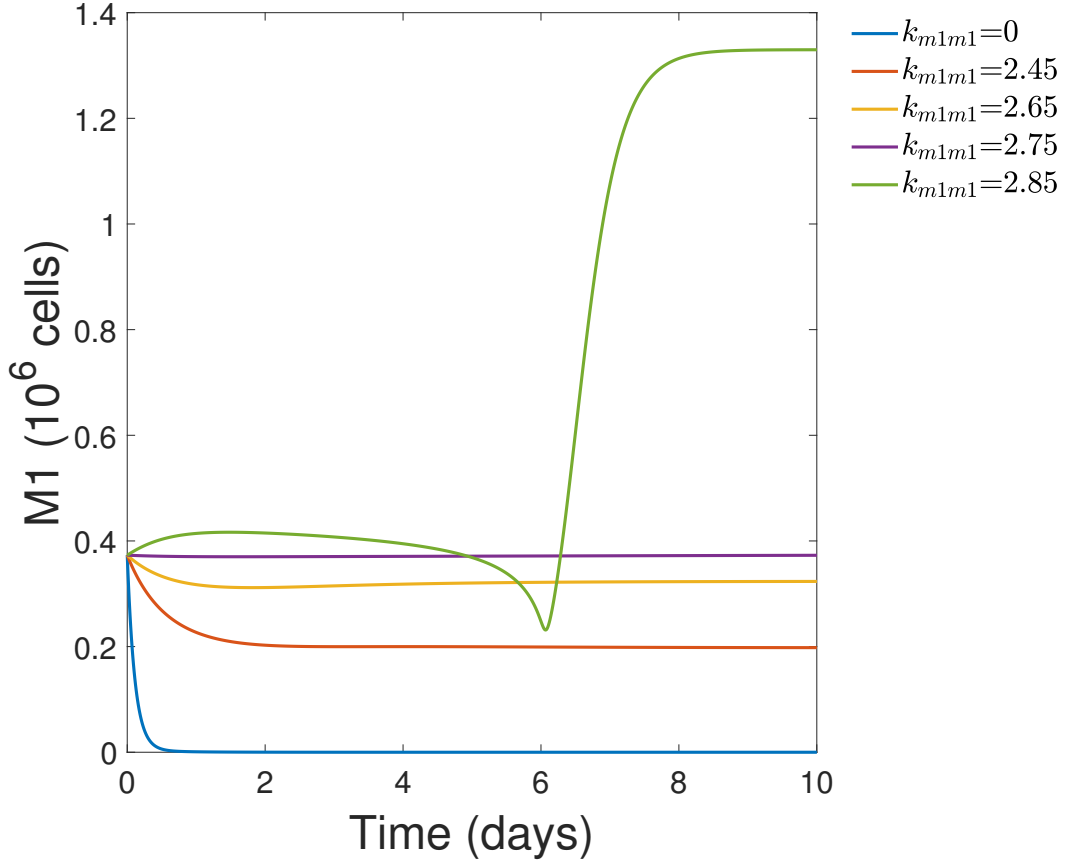


Fig. 23. Plot of changes in M1 dynamics as k_{m1m1} varies through limit points.

$$\frac{\partial y_i}{\partial p_j} = \sum_{k=1}^n \frac{\partial f_i}{\partial x_k} v_{kj} + \frac{\partial f_i}{\partial p_j}$$

where f_i is the RHS of the i th state variable x_i and $v_{kj} = \frac{\partial x_k}{\partial p_j}$. The discretized sensitivity matrix is then formed by numerically solving the state equations and sensitivity equations simultaneously at discrete time points.

5.2.6 Parameter Estimation

Cell count data is given in units of 10^7 cells. The model given by Eqs 5.1-5.6 was fit to experimental data using the trust region method within PottersWheel, a

Matlab toolbox for parameter estimation [118]. The trust region approach uses the *lsqnonlin* algorithm of Matlab’s optimization toolbox, which allows for the specification of bounds on the parameter space to be searched. Bounds for each parameter are given in Table 8.

The fitting procedure was then performed iteratively via weighted least squares with merit function

$$\chi^2(\vec{p}) = \sum_{i=1}^n \left(\frac{y_i - y(t_i; \vec{p})}{\sigma_i} \right)^2 \quad (5.11)$$

with \vec{p} the vector of estimated parameters, y_i the observations, $y(t_i; \vec{p})$ the model predictions given the parameter estimates, σ_i the standard errors, and n equal to the total number of observations over all response variables. Minimizing $\chi^2(\vec{p})/2$ is equivalent to maximizing the log-likelihood

$$\log \mathcal{L}(\vec{p} | y_{data}) = - \sum_i \frac{(y_i^{data} - y_i^{model})^2}{2\sigma_i^2} - N \log \sqrt{2\pi} - \sum_i \log \sigma_i$$

since only the first term is parameter-dependant [118].

Fitting was performed in logarithmic parameter space since some parameter bounds span several orders of magnitude. This local optimization routine seeks parameters that minimize the sum of squared errors between the data and model predictions while accounting for variance. Since each observable N , $M1$, and $M2$ has high standard deviations for measurements taken at time points near the maximum, weighting by these standard deviations would result in compliance with many models. We chose instead to use error model $\sigma_i = 0.05y_i + 0.1\max(y)$, assuming 5% uncertainty at each time point and 10% overall uncertainty relative to the maximum of each observable. At each step of the fitting process, parameter estimations were performed iteratively to ensure minimization of the merit function. Results at each step were analyzed to determine free and fixed parameters and to narrow the search for an identifiable

subset of parameters as described in the Results section.

5.2.7 Goodness-of-fit measures

Under the assumption that residuals between the data and model predictions are Gaussian distributed, the log-likelihood is distributed like a χ^2 distribution with $N - M$ degrees of freedom, with N data points and M parameters being estimated [118]. PottersWheel calculates a χ^2 p-value after each fit for the null hypothesis that (1) the model sufficiently explains the data, (2) true standard deviations do not exceed standard deviation estimates, and (3) the residuals are normally distributed [118].

PottersWheel also calculates the Akaike Information Criterion $AIC = -2 \log \mathcal{L} + 2p$ for a model with p parameters [119]. Given two models under consideration, the one with the lowest AIC value is preferred.

5.3 Results

With the general model developed, we next estimate model parameters, analyze sensitivity of model characteristics to perturbations in the parameters and, finally, predict changes in neutrophil and macrophage behavior in response to parameter variations.

5.3.1 Determination of an identifiable subset of model parameters

Structural identifiability (SI) is a prerequisite for model prediction [120], while numerical or practical identifiability is required to determine confidence intervals around parameter estimates and ensure that the connection between the dynamic

model and the data model is sufficiently strong for prediction. Determining which parameters can be uniquely determined, or at least limited to a finite range of possible values, is also a critical step in informing further experimentation. This process includes selecting parameters that significantly impact model outputs as well as defining interactions between parameters that can influence parameter estimates obtained during fitting. In this section, we analyze local parameter identifiability as outlined in the steps below and in Fig 24 :

1. Estimate all parameters.
 - Use the fitted model to generate the discretized sensitivity matrix S .
2. Fix insensitive parameters.
 - Use S to rank parameters by sensitivity.
 - Set a threshold such that parameters with sensitivity below the threshold (insensitive) are fixed and parameters with sensitivity above the threshold (sensitive) are analyzed in Step 3.
3. Select low collinearity group of parameters as identifiable (ID) subset.
 - Check for pairwise correlations between parameters by deriving an approximate correlation matrix from S .
 - Check for collinearity between groups of parameters with a collinearity index (CI) measure. Set a threshold such that groups of parameters with CI above the threshold are considered collinear. Groups of parameters with CI below the threshold are considered identifiable subsets.
4. Estimate identifiable (ID) subset of parameters.

- One identifiable subset of parameters is selected to be estimated.
- The remaining parameters are fixed.

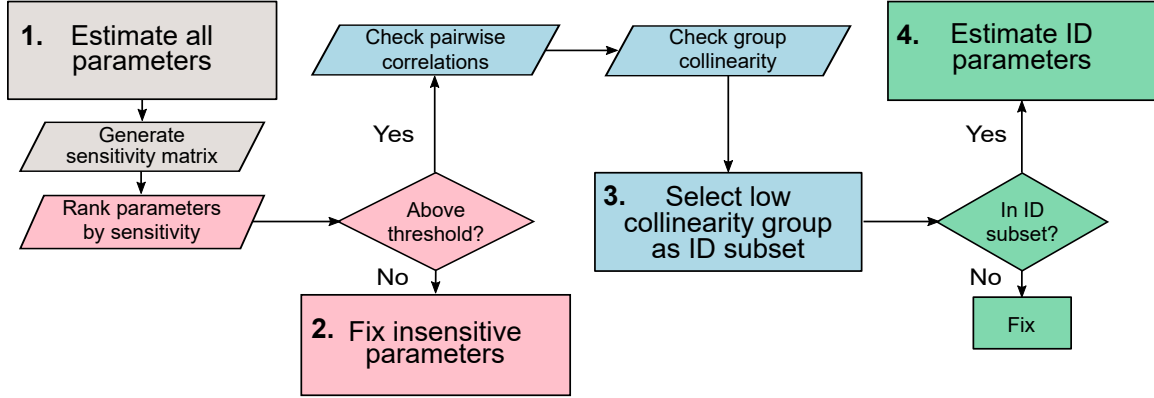


Fig. 24. **Steps to estimate an identifiable subset of parameters.** Step 1 (gray): estimate all parameters and generate a discretized sensitivity matrix from the fitted model. Step 2 (pink): Fix parameters that fall below a determined sensitivity threshold. Step 3 (blue): Select one group of low collinearity (identifiable) parameters. Step 4 (green): Estimate the chosen identifiable subset and fix all other parameters.

Model parameters were estimated using a maximum likelihood equivalent criterion and trust region search algorithm as described (see Materials and Methods). Since reducing parameters to be estimated can be considered a form of model reduction [121], we refer to our final model with 6 estimated parameters as the “identifiable” model versus the “full” model with all 24 parameters estimated in the comparisons below.

First, we performed parameter estimation on the full model. For all three observable model outputs (N , $M1$, and $M2$) sampled at 10 time points with 24 model parameters, a 30×24 discretized sensitivity matrix S is produced. To test structural identifiability of the model *a posteriori*, we generated these matrices at a variety of

locations in parameter space within the bounds given in Table 8 and found the rank and the singular values for each. Since each of these matrices was determined to have full column rank and no zero singular values, we concluded that the model is locally SI [122] within the bounds we had set for parameter estimation.

Next, we ranked the impact of each parameter on all three observable model outputs (N , $M1$, and $M2$) by calculating a root mean square sensitivity measure, as defined in Brun et al. [104], for each column j of the normalized sensitivity matrix as

$$RMS_j = \sqrt{\frac{1}{n} \sum_{i=1}^n \left(\frac{p_j}{y_i} \frac{\partial y_i}{\partial p_j} \right)^2}.$$

Parameter j is deemed insensitive if RMS_j is less than 5% of the value of the maximum RMS value calculated over all parameters. By this measure, 8 parameters were deemed insensitive, as shown in Figure 25, and fixed at their nominal values.

We had determined that all singular values were greater than zero, indicating SI, but only 6 of the 24 singular values obtained had values with order of magnitude greater than zero. If we consider the very small singular values essentially zero for the purpose of rank calculation (in order to reduce problems with numerical identifiability) this gives $\text{rank}(S)=6$, and since $\text{rank}(S)$ can be used to identify the number of parameters that can be included in an identifiable subset [121, 106], a subset of size 6 is suggested. The parameter estimation problem was therefore reduced to finding identifiable subsets of size 6 out of the 16 sensitive parameters.

The estimated correlation matrix for the sensitive subset of parameters, shown in Figure 26, shows a large number of dependencies between pairs of parameters. Effects of nearly linearly dependent parameters on output are pairwise indistinguishable and cannot be reliably estimated, due to compensating effects by changes in other parameters in the group. In addition to discovering pairwise parameter relationships,

we sought a minimally correlated group of 6 parameters. A measure that applies to parameter subsets of any size is the collinearity index defined by Brun et al. [104] as

$$CI = \frac{1}{\sqrt{\lambda_k}}$$

where λ_k is the smallest eigenvalue of $\bar{S}_k^T \bar{S}_k$ and \bar{S} is a submatrix of S containing the sensitivity vectors for parameters in subset K . In practical terms, changes in model output caused by a change in parameter p_j can be compensated for by other parameters by up to $\frac{1}{CI}$ (e.g., for $CI=20$ a change in output caused by a change in p_j can be compensated for up to 5% by other parameters in subset K) [104]. A cutoff of $CI = 20$ was used to select subsets of parameters with low collinearity.

Collinearity indices were calculated for parameter subsets of increasing size as described in Brun et al. [104], using code in the VisId Matlab toolbox [105]. Thirteen parameter pairs that were found highly correlated by this measure are shown in Table 9; others are not shown due to the large number of collinear groups (for example, there were 68 highly collinear parameter subsets of size 3). No subsets of size greater than 6 met our criteria for low collinearity between parameters. In all, 25 parameter subsets of size 6 met our criteria, involving 10 different parameters (shown in Table 10).

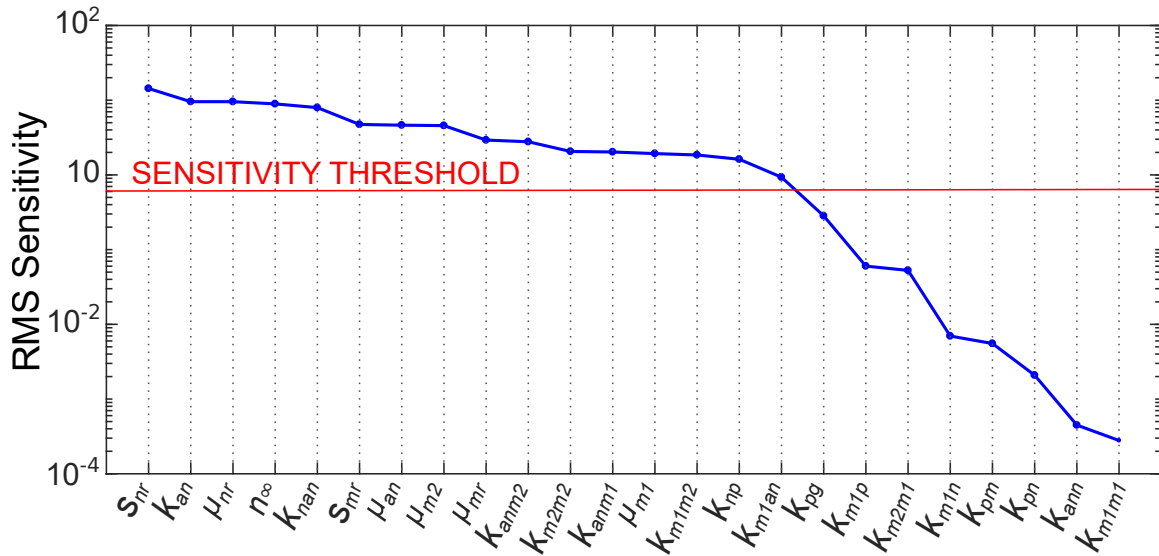


Fig. 25. **Parameter importance ranking (*RMS*) for full and identifiable model.** We ranked the impact of each parameter on all three observable model outputs (N , $M1$, and $M2$) by calculating a root mean square sensitivity measure, as defined in Brun et al. [104]. The sensitivity threshold was set at 5% of the maximum *RMS* value calculated over all parameters. Eight parameters in the full model were thus deemed insensitive and fixed in step 2 of our identifiability analysis. The inset plot shows *RMS* values for the identifiable model.

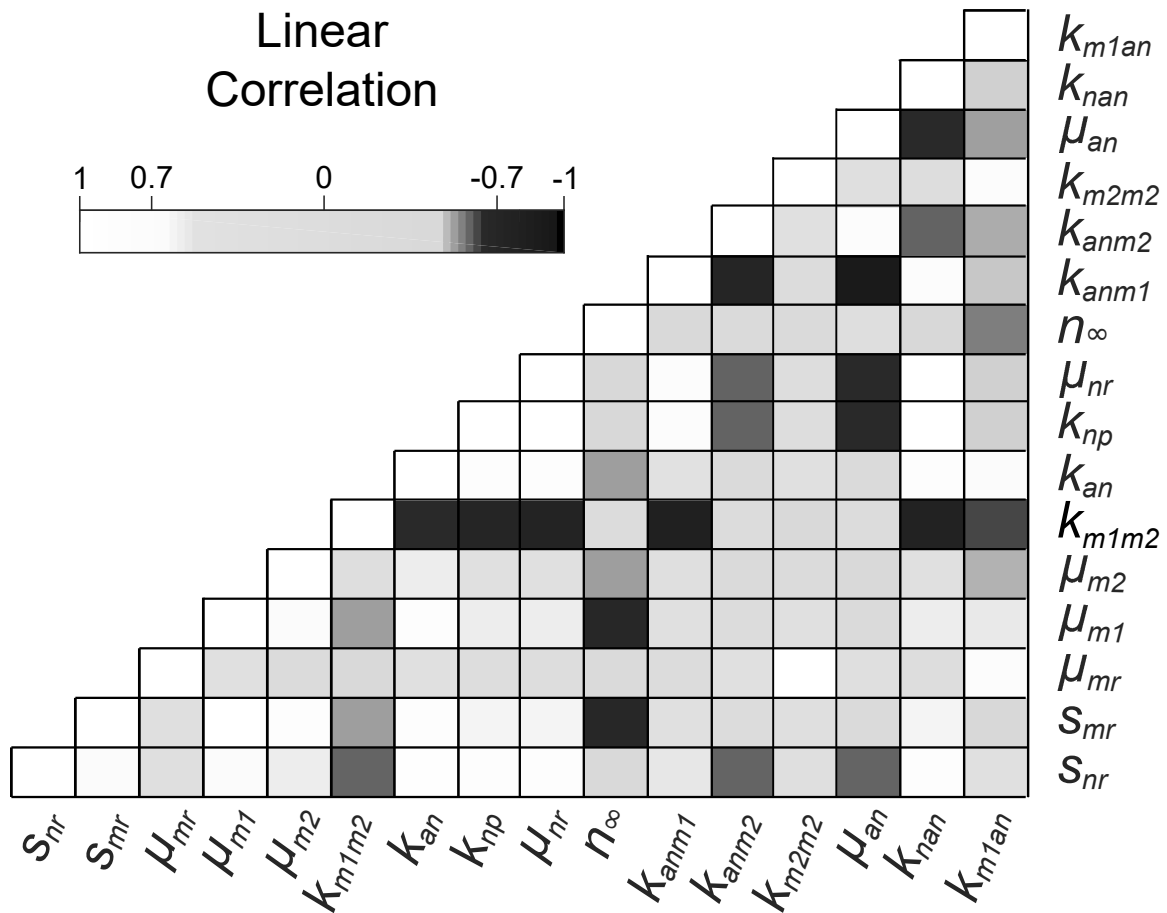


Fig. 26. **Correlation matrix plot for the full model.** An approximate correlation matrix was obtained from the Fisher Information Matrix for the sensitive subset of parameters and used to visualize correlations. There are many significant linear correlations (greater than 0.7) between sensitive parameters that appear as black or white squares on the off diagonal.

Table 9. **Pairwise collinearity indices.** Pairs of parameters were considered collinear (highly correlated) if $CI > 20$.

Parameter Pair	CI
k_{m1m2}, k_{anm1}	67.98
s_{nr}, u_{nr}	47.04
s_{nr}, k_{nan}	46.16
u_{nr}, k_{nan}	43.50
k_{an}, k_{nan}	28.28
s_{nr}, k_{an}	26.79
k_{an}, u_{nr}	25.79
u_{nr}, u_{an}	25.13
n_{∞}, k_{nan}	24.84
k_{an}, n_{∞}	24.20
s_{nr}, u_{an}	24.14
u_{an}, k_{nan}	20.77
s_{nr}, n_{∞}	20.16

Table 10.: **All identifiable parameter subsets of size 6.** A subset of sensitive parameters was considered identifiable if its collinearity index was below 20. Of these twenty-five identifiable subsets of size 6 (generated from 10 parameters), we chose one subset to estimate given in Table 11. With our choice, we sought to both minimize the CI and maximize the sum of the RMS sensitivity measures over all of the parameters in a subset containing parameters that may be reasonably estimated from currently available data and that we hope to vary in future simulated experiments.

Parameter group	Collinearity Index
$s_{nr}, s_{mr}, \mu_{m1}, k_{m1m2}, k_{np}, k_{anm2}$	18.492

Table 10 – *Continued from previous page*

Parameter group	Collinearity Index
$s_{nr}, s_{mr}, \mu_{m1}, k_{np}, k_{anm1}, k_{anm2}$	18.915
$s_{nr}, s_{mr}, \mu_{m2}, k_{m1m2}, k_{np}, k_{anm2}$	18.726
$s_{nr}, s_{mr}, \mu_{m2}, k_{np}, k_{anm1}, k_{anm2}$	19.281
$s_{nr}, s_{mr}, k_{m1m2}, k_{np}, k_{anm2}, k_{m2m2}$	18.197
$s_{nr}, s_{mr}, k_{m1m2}, k_{np}, k_{anm2}, k_{m1an}$	19.170
$s_{nr}, s_{mr}, k_{np}, k_{anm1}, k_{anm2}, k_{m2m2}$	18.562
$s_{nr}, s_{mr}, k_{np}, k_{anm1}, k_{anm2}, k_{m1an}$	19.815
$s_{nr}, \mu_{mr}, \mu_{m1}, k_{m1m2}, k_{np}, k_{anm2}$	18.009
$s_{nr}, \mu_{mr}, \mu_{m1}, k_{np}, k_{anm1}, k_{anm2}$	18.311
$s_{nr}, \mu_{mr}, \mu_{m1}, k_{np}, k_{anm2}, k_{m1an}$	19.060
$s_{nr}, \mu_{mr}, k_{m1m2}, k_{np}, k_{anm2}, k_{m2m2}$	18.606
$s_{nr}, \mu_{mr}, k_{m1m2}, k_{np}, k_{anm2}, k_{m1an}$	18.323
$s_{nr}, \mu_{mr}, k_{np}, k_{anm1}, k_{anm2}, k_{m2m2}$	19.032
$s_{nr}, \mu_{mr}, k_{np}, k_{anm1}, k_{anm2}, k_{m1an}$	18.741
$s_{nr}, \mu_{m1}, \mu_{m2}, k_{m1m2}, k_{np}, k_{anm2}$	18.370
$s_{nr}, \mu_{m1}, \mu_{m2}, k_{np}, k_{anm1}, k_{anm2}$	18.800
$s_{nr}, \mu_{m1}, \mu_{m2}, k_{np}, k_{anm2}, k_{m1an}$	19.984
$s_{nr}, \mu_{m1}, k_{m1m2}, k_{np}, k_{anm2}, k_{m2m2}$	18.207
$s_{nr}, \mu_{m1}, k_{np}, k_{anm1}, k_{anm2}, k_{m2m2}$	18.567
$s_{nr}, \mu_{m1}, k_{np}, k_{anm2}, k_{m2m2}, k_{m1an}$	19.251
$s_{nr}, \mu_{m2}, k_{m1m2}, k_{np}, k_{anm2}, k_{m1an}$	18.610
$s_{nr}, \mu_{m2}, k_{np}, k_{anm1}, k_{anm2}, k_{m1an}$	19.121

Continued on next page

Table 10 – *Continued from previous page*

Parameter group	Collinearity Index
$s_{nr}, k_{m1m2}, k_{np}, k_{anm2}, k_{m2m2}, k_{m1an}$	18.364
$s_{nr}, k_{np}, k_{anm1}, k_{anm2}, k_{m2m2}, k_{m1an}$	18.771

In selecting one of these parameter subsets to be estimated in an identifiable model, we considered several factors. First, from a practical standpoint, it was desirable to choose parameters that may be reasonably estimated from currently available data and also that we hope to vary in future simulated experiments. Next, we sought to both minimize the *CI* and maximize the sum of the *RMS* sensitivity measures over all of the parameters in the subset. Minimizing the *CI* reduces the likelihood of parameter dependencies interfering with optimization, while choosing the subset with the most sensitive parameters should require the smallest adjustment to their values [121].

The chosen identifiable subset of 6 parameters is shown in Table 11 along with point-wise 95% confidence intervals calculated based on the approximate Hessian matrix of the objective function given in Eq 5.11, as described in Maiwald et al. [118]. The correlation matrix for the identifiable model, shown in Fig 27, shows less correlation between estimated parameters than in the full model. The fit of the identifiable model to M1, M2, and neutrophil data is shown in Fig 28. State variable predictions for pathogen, nutrient broth, and apoptotic neutrophils are shown in Fig 29. Differences between model predictions and observations are also shown in Fig 30.

5.3.2 Goodness-of-fit

The full model, with 24 parameters estimated, and the identifiable model, with 6 parameters estimated, are compared with respect to goodness-of-fit using the Akaike

Table 11. **Parameter values and 95% pointwise confidence intervals for identifiable model.** Remaining parameters were fixed at values given in Table 8.

Parameter	Estimate	95% CI
μ_{m1}	6.83	(5.45, 8.54)
k_{m1m2}	8.62	(5.56, 13.4)
k_{m2m2}	1.59	(0.86, 1.96)
s_{nr}	16.4	(16.0, 16.8)
k_{np}	3.10	(1.68, 5.65)
k_{anm2}	91.0	(66.4, 125)

information criterion (AIC) and χ^2 test (see Methods) in Table 12. By these measures, the data is best explained by the identifiable model even though the difference in χ^2 metric value between models is small. There is close agreement between model predictions and observations achieved with our obtained parameters, however, we remark that there is some dependency between fixed and estimated parameters and that there are inherent limitations in estimating parameters with limited experimental data. Therefore, these estimates should be taken as conditional, and we can determine which fixed parameters they may be conditioned on by viewing the profile likelihood [107, 123, 124].

The profile likelihood approach for analyzing identifiability fixes a parameter p_i at values over a specified range, re-estimating all other parameters at each point [123]:

$$\chi_{PL}^2(p_i) = \min_{p_j \neq i} [\chi^2(p)] .$$

Using the profile likelihood, it is possible to trace out the functional form of identifiable combinations of parameters, and this information can be used in re-parametrization

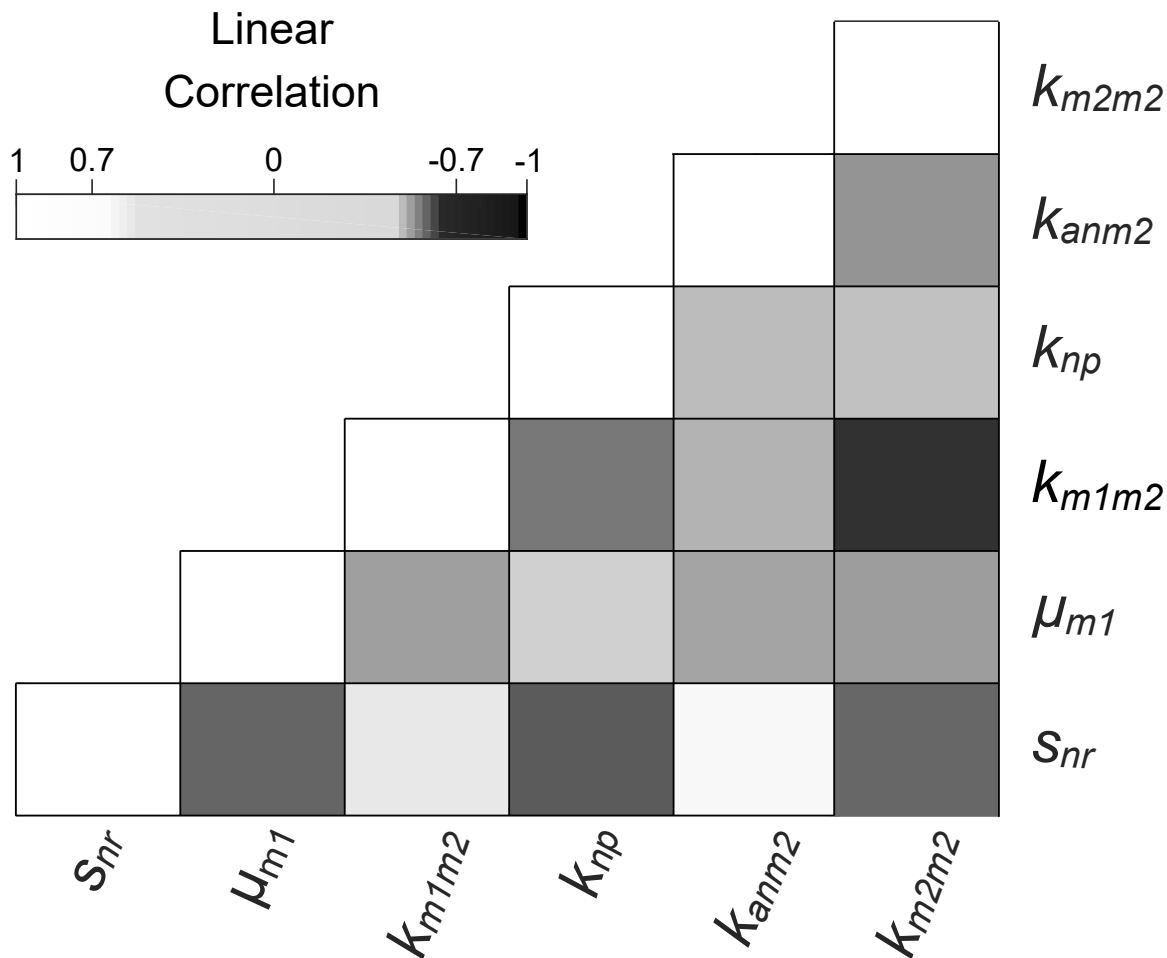


Fig. 27. **Correlation matrix plot for the identifiable model.** An approximate correlation matrix was obtained from the Fisher Information Matrix of the identifiable model and used to visualize correlations between model parameters. There is one significant correlation (greater than 0.7) between parameters k_{m1m2} and k_{m2m2} .

[107, 106]. However, this requires reducing extra degrees of freedom in the estimated parameters in order to avoid compensation effects. [107]. Even with collinearities present, it is possible to get an idea of compensation effects between parameters during fitting by observing how estimated parameters change over the profiled parameter. This can be important in determining whether estimated parameters are conditional on parameters that were fixed prior to fitting [104]. We have plotted the profile like-

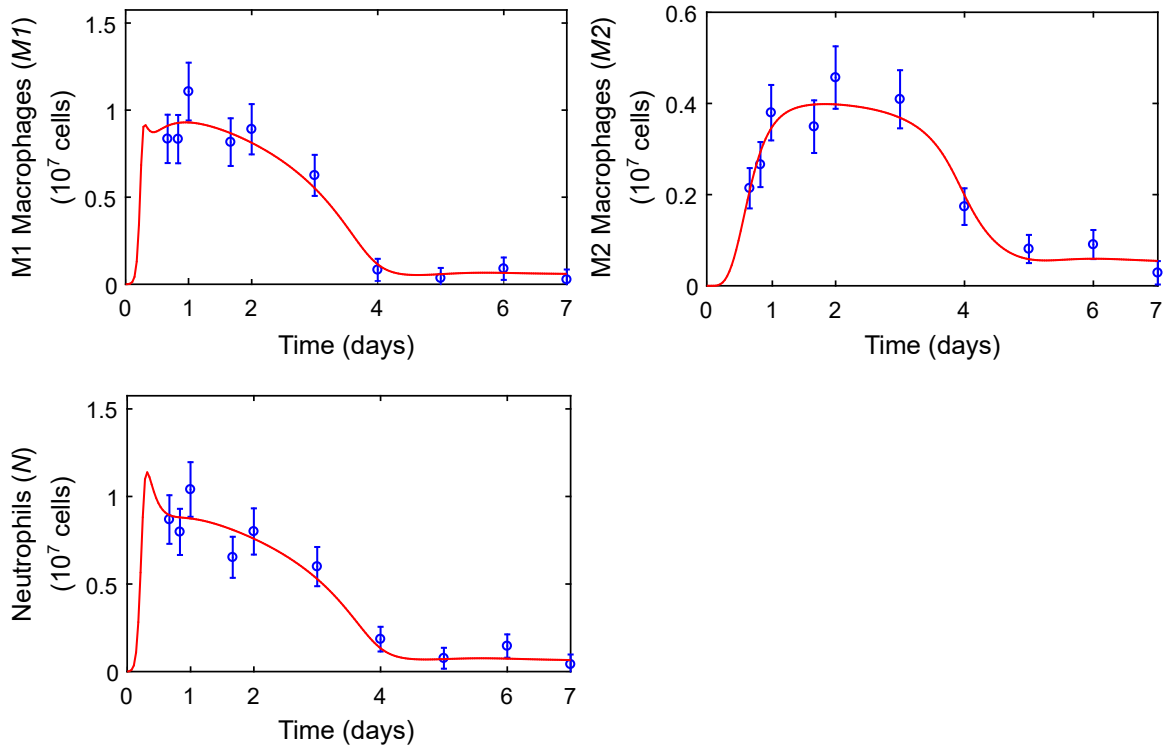


Fig. 28. **Model response variable predictions versus observations for the identifiable model.** Model predictions for M1 macrophage ($M1$), M2 macrophage ($M2$), and neutrophil (N) counts are plotted versus mean observed values and standard errors.

likelihoods of parameters in the identifiable subset versus other parameters that change significantly over the profile likelihood in Fig 31.

5.3.3 Sensitivity Analysis

The impact that both fixed and estimated parameters have on predictions for $M1$ and $M2$ macrophages was analyzed with one-at-a-time sensitivity analysis. We focused our analysis on these two observable outputs since our goal is to identify drivers of population level phenotype switch in macrophages. In applying this method, we increased each parameter by a factor of 1.001 of its baseline value while holding all other parameters at their baseline values to determine the effects on the $M1$ and

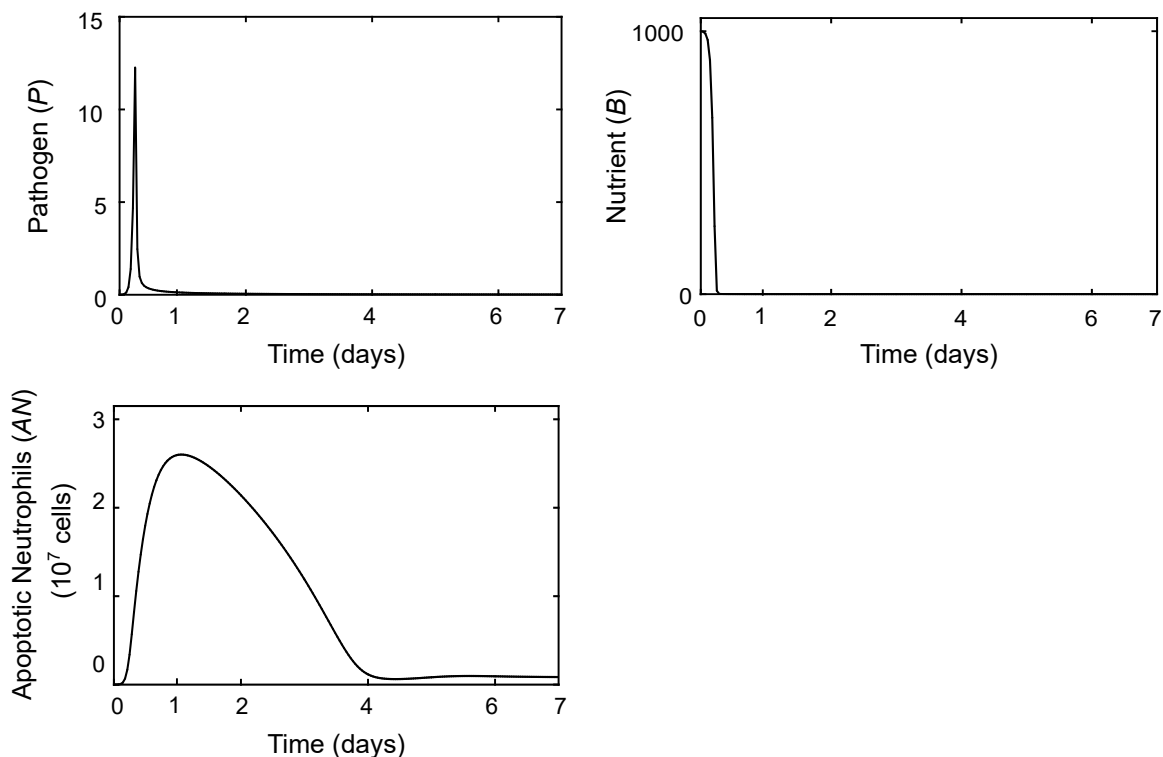


Fig. 29. **Model state variable predictions for the identifiable model.** Model predictions for levels of pathogen (P) and nutrient (B) and apoptotic neutrophil (AN) counts.

Table 12. **Goodness-of-fit statistics.** In the full model, 24 parameters were estimated. After identifiability analysis, estimated parameters were reduced to 6 and the remaining parameters were fixed prior to fitting. The reduction in estimated parameters improved the weighted least squares merit function value (χ^2), increased p-value on a χ^2 test indicating that the identifiable model sufficiently explains the data, and lowered the estimated amount of information lost between the model and the data by the Aikake Information Criterion (AIC) measure.

	n_p	χ^2	p-value	AIC
Full model	24	19.325	0.003	122.462
Identifiable model	6	15.473	0.906	82.61

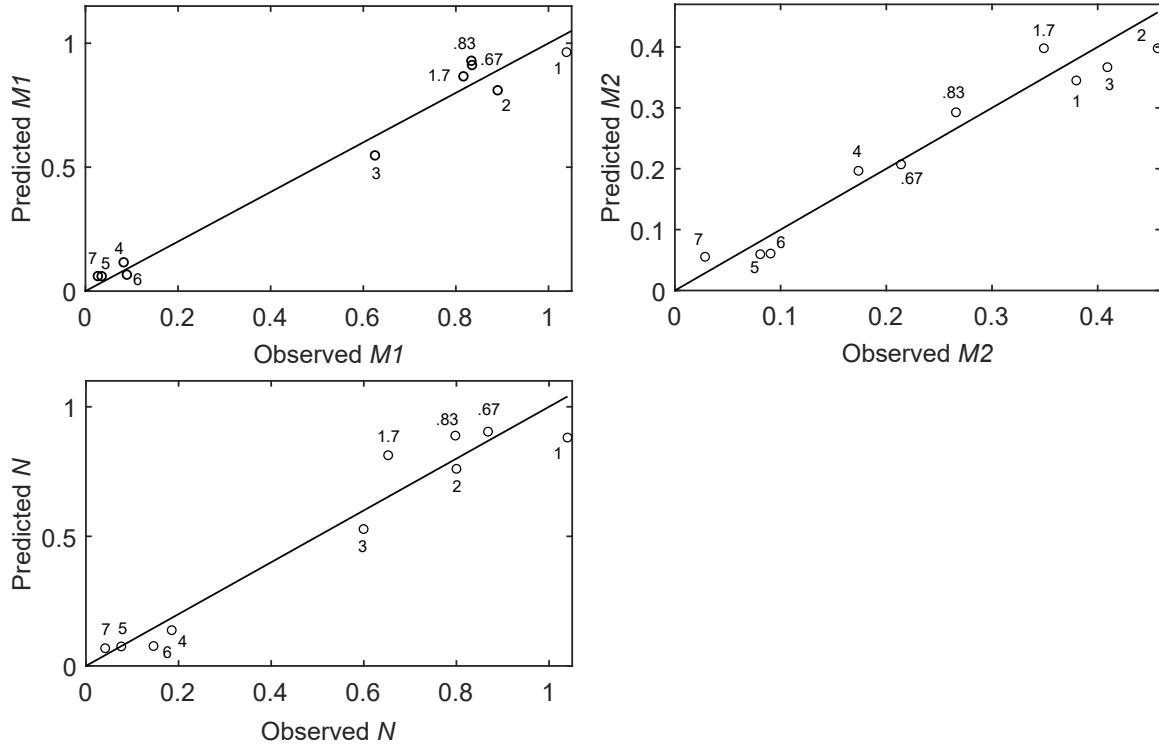


Fig. 30. **Predictions versus observations.** Model predictions versus observations are plotted for M1 macrophages ($M1$), M2 macrophages ($M2$), and neutrophils (N). Data points are labeled with time (in days).

M2 characteristics shown in Figs 32 and 33. The sensitivity of characteristic f with respect to parameter p is then estimated as $s = (f(1.001*p) - f(p)) / ((1.001*p - p) * p / f)$ using the PottersWheel Matlab toolbox [118]. The parameter is then reset to its baseline value and the process is repeated for the next parameter, until sensitivity of all parameters is analyzed. Baseline values for parameters that were fixed during fitting are given in Table 8 and baseline estimated parameter values are given in Table 11. Baseline characteristics of each cell type are shown in Figs 32 and 33, along with sensitivities of each characteristic to variations in each parameter. Since parameters are varied individually, this analysis does not take into account interactions between variables that may influence model results in unexpected ways if more than one

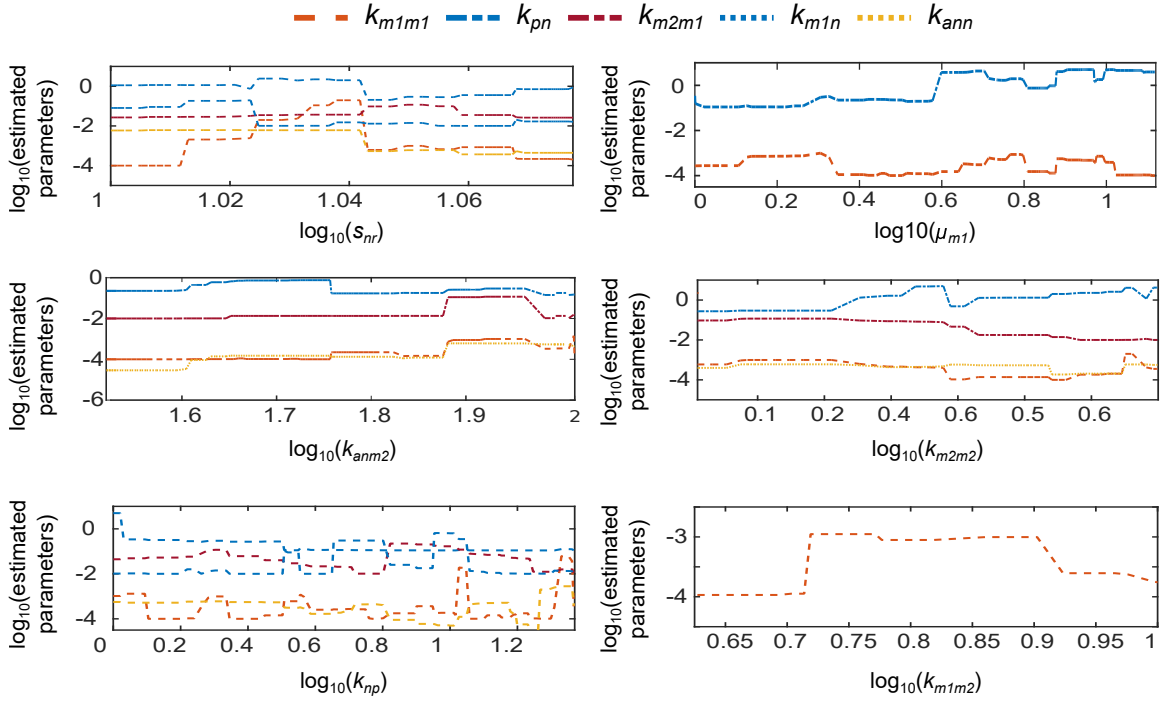


Fig. 31. **Profile likelihood plots.** The six parameters in the identifiable subset are plotted versus the estimated parameters on a logarithmic scale. Only estimated parameters that change significantly are plotted. These changes can indicate dependencies between parameters.

parameter is varied simultaneously. Taken with the above caution, however, we can gain some insight into which factors may drive macrophage phenotype balance.

The most influential parameters on M1 behavior are s_{nr} and s_{mr} (availability of resting neutrophils and monocytes), k_{pg} (behavior of inflammatory stimulus), k_{m1p} and k_{np} (response of M1s and neutrophils to inflammatory stimulus), and u_{an} (rate of secondary necrosis of neutrophils). In the present context, M1s are primarily activated by initial inflammatory stimulus and necrosis of apoptotic neutrophils that have not been phagocytosed. This supports the hypothesis that effective clearance of apoptotic cells is important in the resolution of inflammation [125, 126, 127, 128, 110, 129, 130, 116, 74]. If our parameter estimates had been obtained by fitting to data from chronic

inflammation, feedback from existing M1s and the pro-inflammatory byproducts of existing neutrophils would likely be greater contributors to M1 response. Negatively related to magnitude of M1 response are parameters μ_{m1} (decay or efflux rate of M1s) and n_∞ (the level of neutrophils required to inhibit macrophage activity by 50%). As the threshold for inhibition of M1s increases, the magnitude of the M1 population decreases because less M1s are required to mount an adequate response.

The importance of neutrophils and neutrophil apoptosis in mounting a timely and sufficient M2 response is evidenced by the high sensitivity of M2 peak timing and amplitude to neutrophil-associated parameters s_{nr} , u_{an} , k_{an} , k_{np} , u_{nr} , n_∞ , k_{anm1} , k_{anm2} , and k_{nan} . The magnitude of the M2 population peak is also strongly positively associated with k_{m1m2} (switch rate from M1s) and k_{m2m2} (feedback from existing M2s). Increasing rates of decay or efflux for resting monocytes (μ_{mr}) and resting neutrophils (u_{nr}) diminishes M2 population magnitude, as does reduced M1 activation by pathogen (k_{m1p}), indicating M2 dependence on the population size of other immune cells.

5.3.4 Simulations

Our objective in this work is to identify key drivers of macrophage phenotype balance during the inflammatory response, in order to identify potential clinical targets. Therefore we now perturb parameters from fitted values in order to view effects on model behavior and simulate therapeutic targeting of macrophages for intervention in the early inflammatory process critical to disease progression, as has been proposed [131, 132, 133].

Even varying the identifiable subset of parameters (μ_{m1} , k_{m1m2} , k_{m2m2} , s_{nr} , k_{np} , k_{anm2}) within confidence interval bounds determined during fitting can significantly alter the time course of response variables N , $M1$, and $M2$ as shown in Fig 34. One proposed

strategy to dampen inflammation is to directly polarize M1 macrophages to an M2 phenotype [131]. To evaluate the effects of varying the transition rate of M1 to M2, we varied parameter k_{m1m2} over 10 linearly spaced values within a factor of $1 \pm .3$ of its baseline value, with resulting dynamics shown in Fig 35. The model predicts that increasing k_{m1m2} has a small effect on M1 magnitude of response while increasing the magnitude of M2 response, which is expected. However, the time course of both macrophage populations is predicted to be shortened due to a higher transition rate; whether this results in faster resolution of inflammation or an insufficient M2 population for a subsequent proliferation or repair phase may depend on the nature and magnitude of the inflammatory stimulus.

Next, we simulated a change in the apoptosis rate of neutrophils, k_{an} , based on our hypothesis that efferocytosis (phagocytic removal of apoptotic and necrotic cells) is a key driver of macrophage phenotype change and that this requires a sufficiently sized population of apoptotic cells [110, 74, 111, 112, 76]. Dysregulation of neutrophil population level and turnover is known to be a direct contributor to human inflammatory and autoimmune diseases such as coronary artery disease, rheumatoid arthritis, acute arterial occlusions, gout, asthma, and many others [134, 135]. Macrophages themselves are known to modulate neutrophil lifespan by releasing cytokines that can delay apoptosis [136] and some microbial pathogens delay or accelerate neutrophil apoptosis to promote their own growth [134]. From the results in Fig 36, we note that modulating the size k_{an} has some interesting effects. In the biologically unlikely case where $k_{an} = 0$ and there is no population of apoptotic neutrophils available for efferocytosis, neutrophils remain the dominant immune cell. For low values of k_{an} , sustained inflammation appears to be the result of too many inflammatory neutrophil byproducts and the low M2 population levels. Midrange k_{an} values were determined

during fitting to produce a normal response, while higher k_{an} levels seem to produce faster resolution similar to increasing the transition rate k_{m1m2} . This is unsurprising given the dependency of the second term of Eq 5.1 on k_{m1m2} , k_{anm1} , and AN , which tracks the size of the apoptotic neutrophil population. Yet the magnitude of the effects of modulating k_{an} versus acting on transition directly via k_{m1m2} are predicted to diverge for lower values, with the former providing more dramatic changes.

To explore points of intervention in the case of delayed neutrophil apoptosis, we set $k_{an} = 5.56$. This results in sustained inflammation as shown in Fig 36, and changes in sensitivity to parameters across this bistability is also shown in Fig 37. For example, with delayed neutrophil apoptosis (unhealthy case), the number of M1s remaining at day 7 becomes strongly positively associated with parameter s_{nr} (influx rate of resting neutrophils) and the number of M2s remaining at day 7 becomes negatively associated with increased μ_{m2} .

By changing these as shown in Fig 38 we are able to resolve inflammation in spite of impaired neutrophil apoptosis. Modulating resting neutrophils by either reducing influx (simulated by lowering the value of s_{nr}) or increasing decay or efflux (simulated by increasing the value of u_{nr}) returns all immune cell populations to homeostasis. However, reducing decay or efflux of M2s (by lowering the value of μ_{m2}) led to a resolution of inflammation but a sustained M2 population that could potentially be problematic.

Finally, we simulated reducing availability of monocytes for recruitment by reducing monocyte source parameter, s_{mr} , by 1/2 at early versus late time points (16 hours or 5 days) to compare effects as shown in Fig 39. Resulting predictions support what has been demonstrated experimentally: that intervening at early timepoints

to block or reduce monocyte recruitment and their subsequent differentiation to inflammatory macrophages can actually impair resolution of inflammation [131, 137, 138].

5.3.5 Discussion

Modulating macrophage subpopulations has been proposed as a strategy to resolve inflammation [131, 132, 133, 139], but the mechanisms driving macrophage phenotypic switch are not well understood. In this work we have developed a model that includes macrophage polarization during inflammation. To our knowledge, it is the first model of its kind to be fit to *in vivo* experimental data. Our model allows some insight into key drivers of macrophage population shift over the time course of inflammation and allows us to predict the effects of therapies targeting macrophages.

The experimental data used to fit this mathematical model was obtained from the widely studied peritonitis model of inflammation. In addition to recapitulating the influx and egress of inflammatory cells in response to stimulus-induced inflammation, this model is also extensively used to assess the involvement of endogenous processes in mounting as well resolving the inflammatory processes. In recent studies, the pro-inflammatory role of human proteinase 3 (PR3) during acute inflammatory responses by modulating neutrophil accumulation and the underlying mechanisms were almost entirely determined using a zymosan-induced peritonitis model [140]. Extending the investigations into endogenously produced pro-resolving lipid mediators, Ramon et al. not only identified PCTR1, a member of the protectin family as a potent monocyte/macrophage agonist but also established the therapeutic potential of PCTR1 supplementation in resolving inflammation using microbial-induced peritonitis in mice [141]. Similarly, Juhas et al. confirmed the ability of RX-207 to reduce

neutrophil migration using thioglycollate-induced peritonitis [142]. These examples not only underscore the importance of developing a mathematical model based on experimental data from mouse peritonitis, but also provide the rationale and future application of such a model for evaluating and predicting outcomes to be validated by subsequent experimentation.

The process of parameter selection is fully elucidated (see Results). Parameter estimation was carefully conducted such that unidentifiable parameters were fixed and the confounding effects of parameter interactions were reduced in order to obtain an identifiable subset of parameters of interest for estimation. We also stipulate that other, equally viable, identifiable subsets could have been estimated (see Table 10) and that estimated parameters may be conditional on parameters that were previously fixed. It is important to acknowledge that parameters chosen for estimation will depend on the experimental context and available measurements. To this end we also display variations of parameters within their confidence intervals to give an idea of different, yet physiologically reasonable, behaviors (see Fig 34).

It is hypothesized that efferocytosis of apoptotic cells is an important determinant of macrophage phenotype [110, 74, 111, 112, 76], and our sensitivity analysis supports the dependence of macrophage behavior on neutrophils. Our analysis indicates that timing and magnitude of the M2 response in particular is closely related to neutrophil dynamics.

We simulated several treatment scenarios targeting macrophages both directly and indirectly. We compared the effects of targeting macrophage transition rate directly (in the model via parameter k_{m1m2}) versus varying neutrophil apoptosis rate, k_{an} , in order to increase the population of apoptotic cells available for macrophage efferocytosis. A shorter time course of both M1 and M2 response is predicted in both cases;

whether this indicates fast resolution or introduces the possibility of an insufficient M2 population given a sustained pathogen insult or injury requires further examination.

Our model predicts that timing may be critical in blocking or reducing availability of monocytes in order to reduce the inflammatory M1 response, as has been proposed, and that this could lead to chronic inflammation. These effects have been observed in an experimental setting as well [131, 137, 138].

Since pro- and anti-inflammatory mediators could not be measured experimentally, we instead used cellular feedback loops to describe their contribution to inflammatory processes. The future addition of parameters such as local production/levels of pro- or anti-inflammatory mediators that likely influence the function of infiltrated immune cells will further fine-tune this model. It is noteworthy that using the mouse model of peritonitis, Dequine et al. demonstrated that local TNFR1 signaling modulated neutrophils for increased cytokine production with implications on neutrophil recruitment and egress [143]. Further experimentation is also likely to allow a larger identifiable subset of parameters, especially if cytokines associated with the various cell types are explicitly measured, giving a stronger connection between available data and feedback loop components in the model.

In future work, this peritonitis model will be extended to the case of early atherosclerosis. In addition to the routinely monitored changes in serum lipid profiles, changes in monocytes as well as increased circulation of pro-inflammatory mediators are also causally related to atherogenesis and chronic unresolved inflammation is recognized as an underlying cause of multiple metabolic diseases. It is noteworthy that Angsana et al. reported a positive correlation between delayed clearance of macrophages from the peritoneal cavity and atherosclerotic plaque burden [144]

and Feige et al. showed that a small molecule lecinoxoid (VB-201) which reduced monocyte migration in a peritonitis model, also reduced atheroma development [145]. These studies underscore the predictive value of computational models based on cellular influx/egress from the peritoneal cavity.

Chronic inflammatory diseases in general require timely peaks and ebbs in immune cell response in order for homeostasis to be restored; particularly in macrophages, which include subpopulations that either contribute to or resolve inflammation. In the case of atherosclerosis, this phenotype switching is believed to be critical to a balanced response to hyperlipidemia. Our extended model will be able to provide hypothesis testing for points of intervention in atherosclerosis that target macrophage phenotype. Jacinto et al. have recently demonstrated the importance of extra-arterial contributors such as functionality of monocytes in aggravation of atherosclerosis under normocholesterolemic conditions emphasizing the need for the inclusion of such measures into predictive models [146]. This work could also be extended to other disease systems that feature chronic inflammation, and the modeling of variables pathogen and nutrient broth could be replaced by an inflammatory stimulus input function $f(t)$ that is more general and applicable to pathogen insult or injury.

In conclusion, data presented herein describes the development of a computational model of the sequential influx of immune cells in response to an external trigger and fitting this model to experimental data obtained from a well-established *in vivo* model of inflammatory response namely peritonitis. Fine tuning this model with inclusion of other systemic parameters related to inflammation will permit the future application to chronic inflammatory diseases with dysfunctional resolution of inflammation.

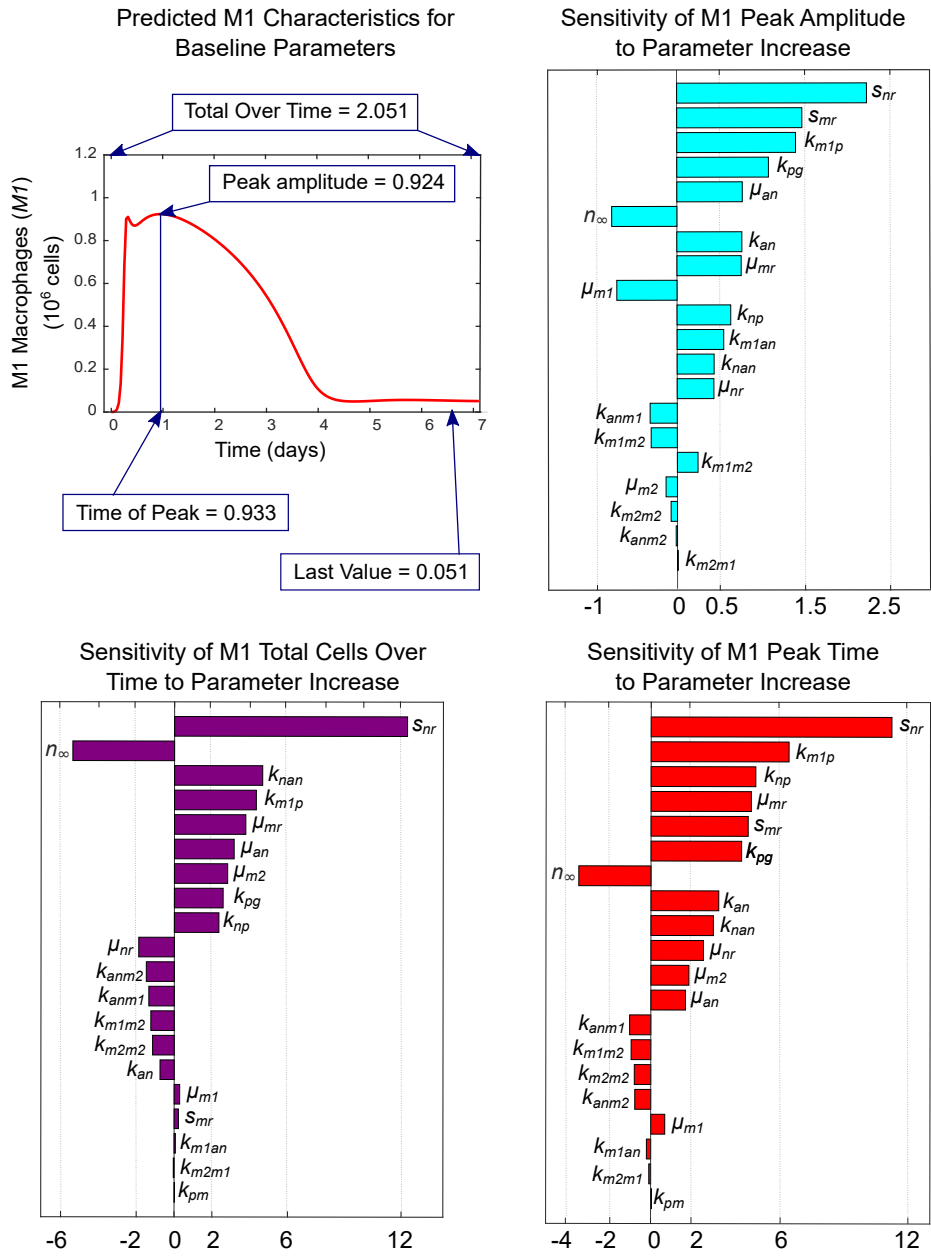


Fig. 32. **Baseline characteristics for M1 and sensitivity of characteristics to parameter variations.** The M1 transient curve and its characteristics are plotted for the baseline parameter values given in Tables 8 and 11. Parameter sensitivity plots show the effects on M1 characteristics of varying model parameters one-at-a-time by a factor of 1.001 of its baseline value while holding all other parameters at their baseline values. Insensitive parameters, which have zero sensitivity for all characteristics, are not shown.

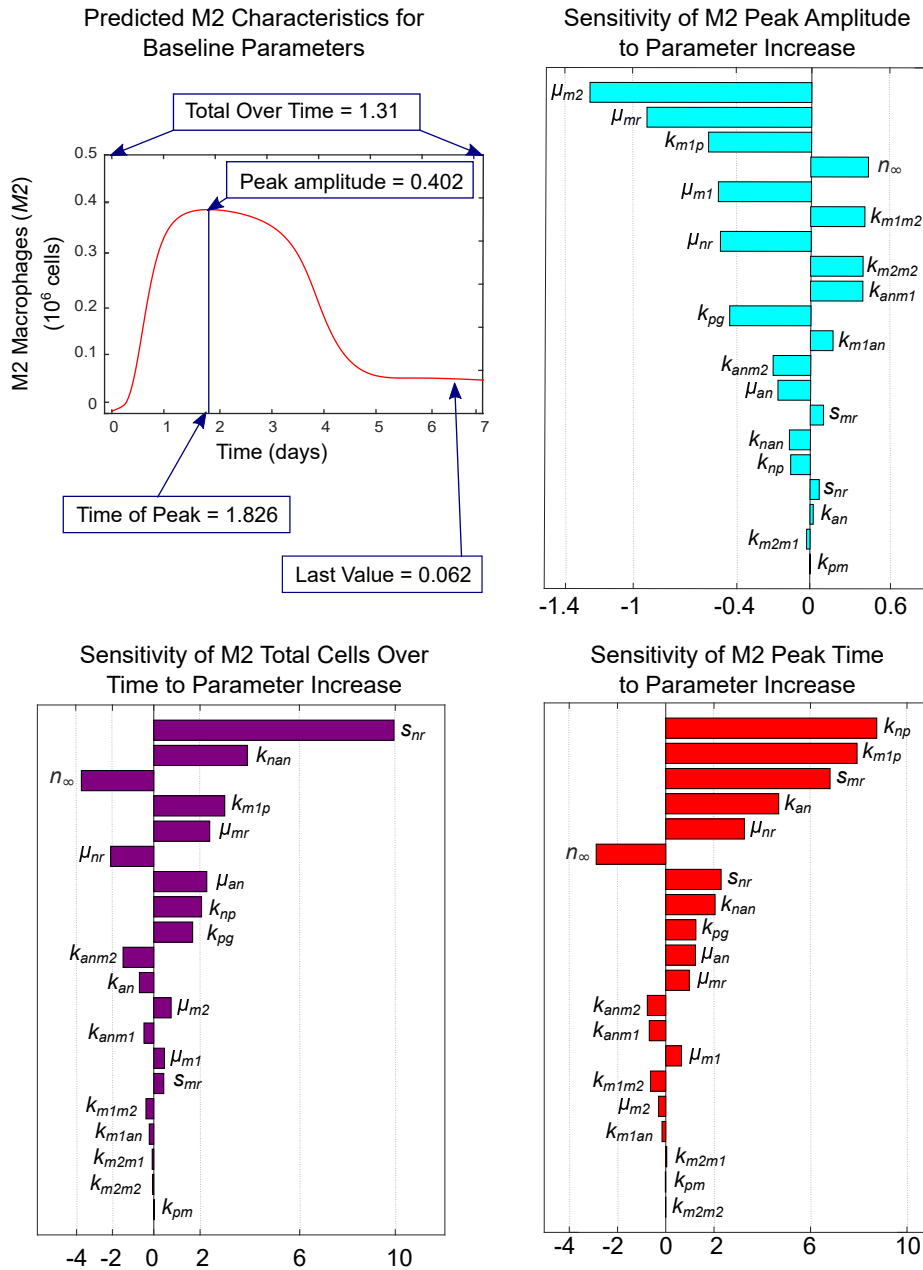


Fig. 33. **Baseline characteristics for M2 and sensitivity of characteristics to parameter variations.** The M2 transient curve and its characteristics are plotted for baseline parameter values given in Tables 8 and 11. Parameter sensitivity plots show the effects on M2 characteristics of varying model parameters one-at-a-time by a factor of 1.001 of its baseline value while holding all other parameters at their baseline values. Insensitive parameters, which have zero sensitivity for all characteristics, are not shown.

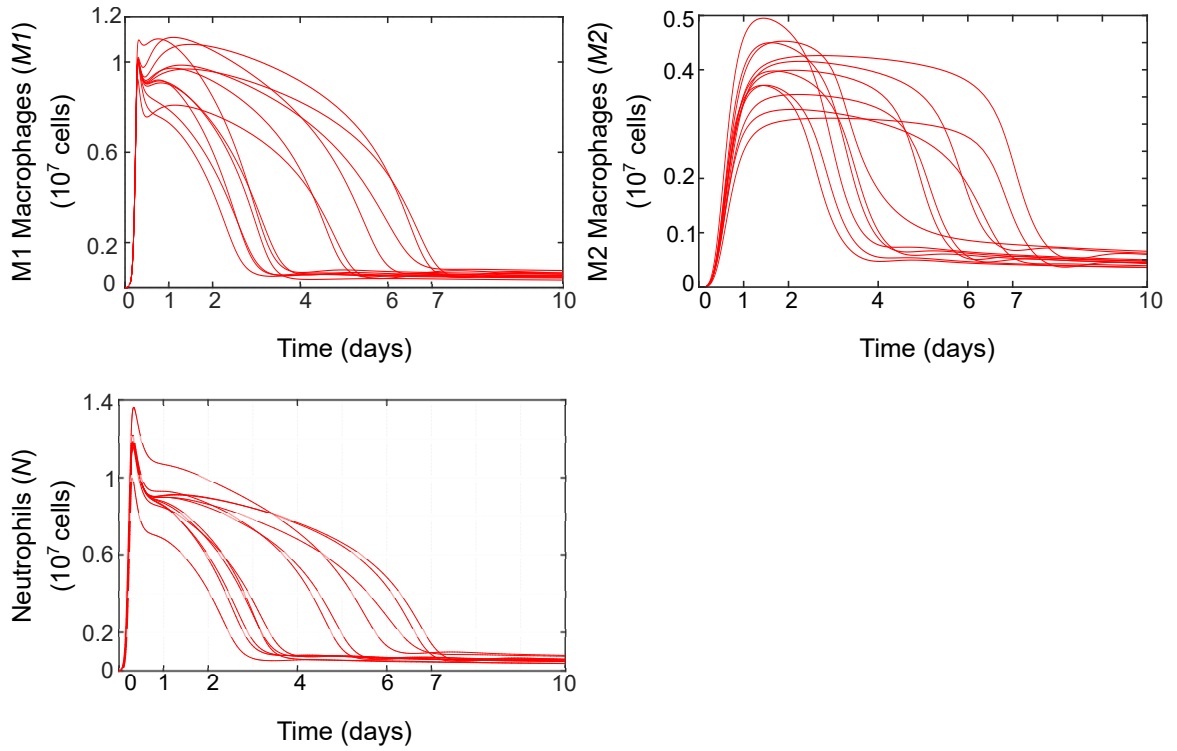


Fig. 34. **Extreme trajectories corresponding to pointwise 95% confidence interval.** The six identifiable parameters given in Table 11 were set one-at-a-time to values at either extreme of their 95% confidence intervals to explore variations in behavior within physiologically reasonable bounds given experimental data.

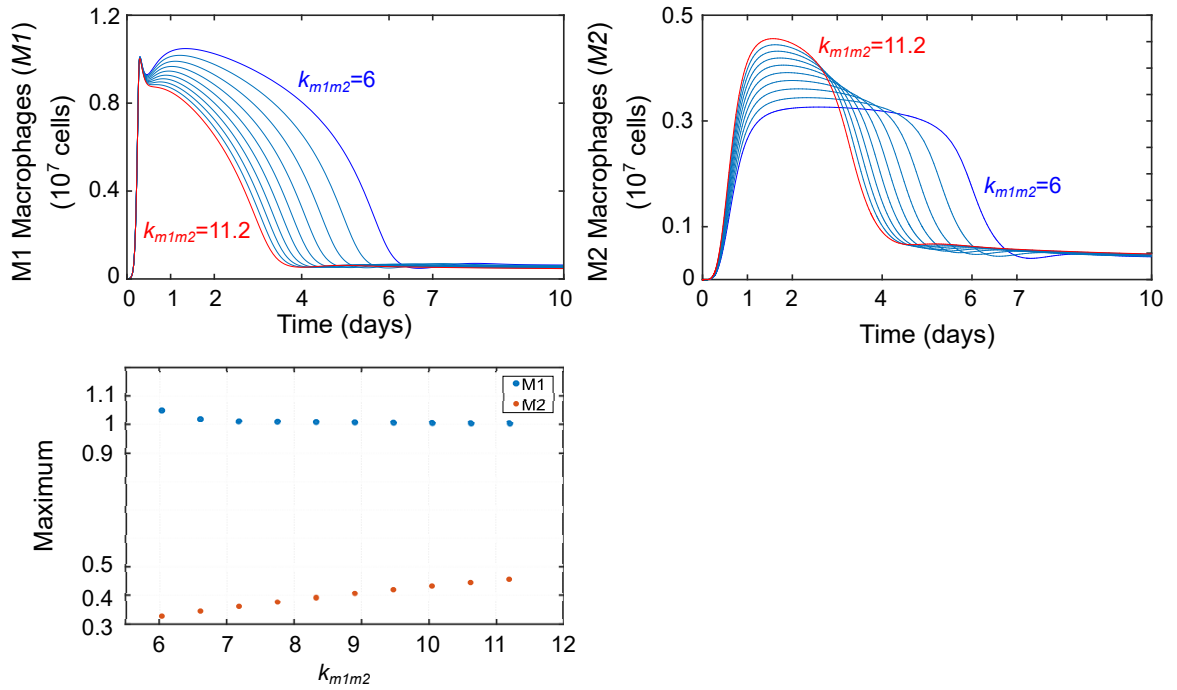


Fig. 35. **Results of perturbations in parameter k_{m1m2} .** Parameter k_{m1m2} , which models the transition rate of M1 to M2 macrophages, was varied within a factor of 1.3 of its baseline value of $k_{m1m2} = 8.62$. The effects of variations on M1, M2, and on the maximum values of each phenotype are shown. An increase in k_{m1m2} shortens the time course for both M1 and M2 and diminishes M1 peak magnitude slightly relative to the increasing in M2 peak magnitude. A decrease in k_{m1m2} extends the span of M1 and M2 activity and increases M1 peak magnitude slightly while decreasing M2 peak magnitude.

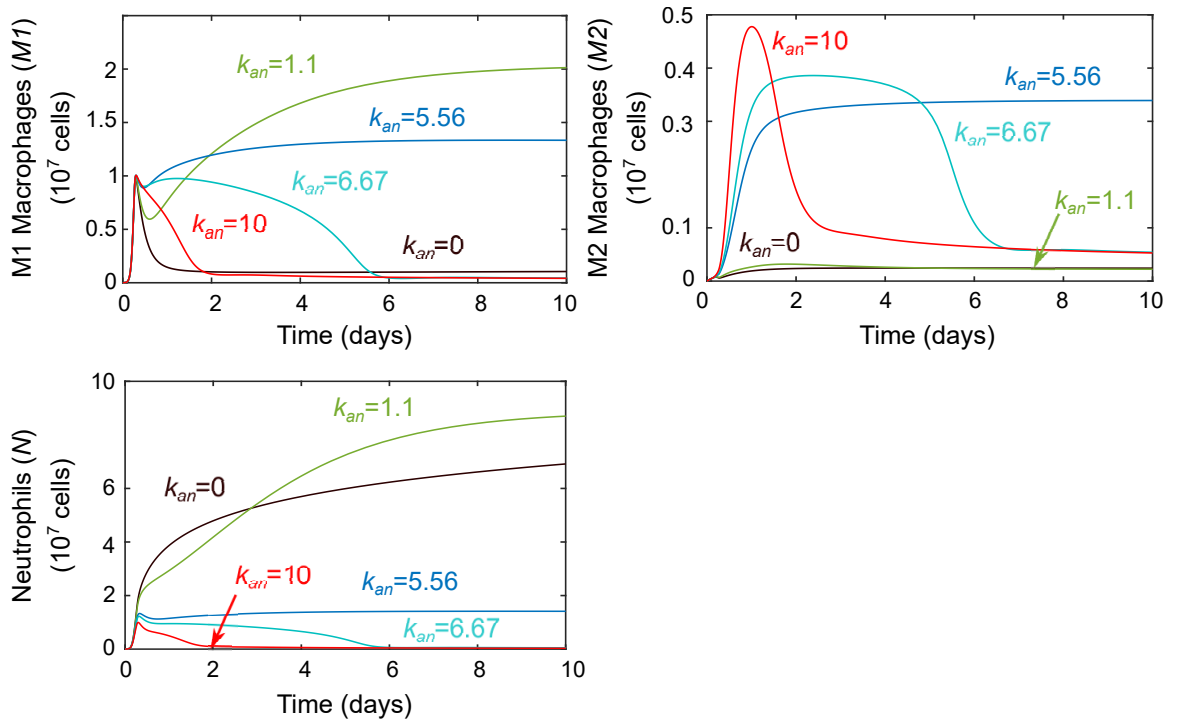


Fig. 36. **Results of perturbations in parameter k_{an} .** Parameter k_{an} , which models the rate of neutrophil apoptosis, was varied around its baseline value of $k_{an} = 7.108$. The effects of variations on M1, M2, and neutrophils are shown. If there is no neutrophil apoptosis, there is no M2 response. Values lower than baseline lead to a sustained inflammatory response from all immune cells while higher values shorten the time course of each.

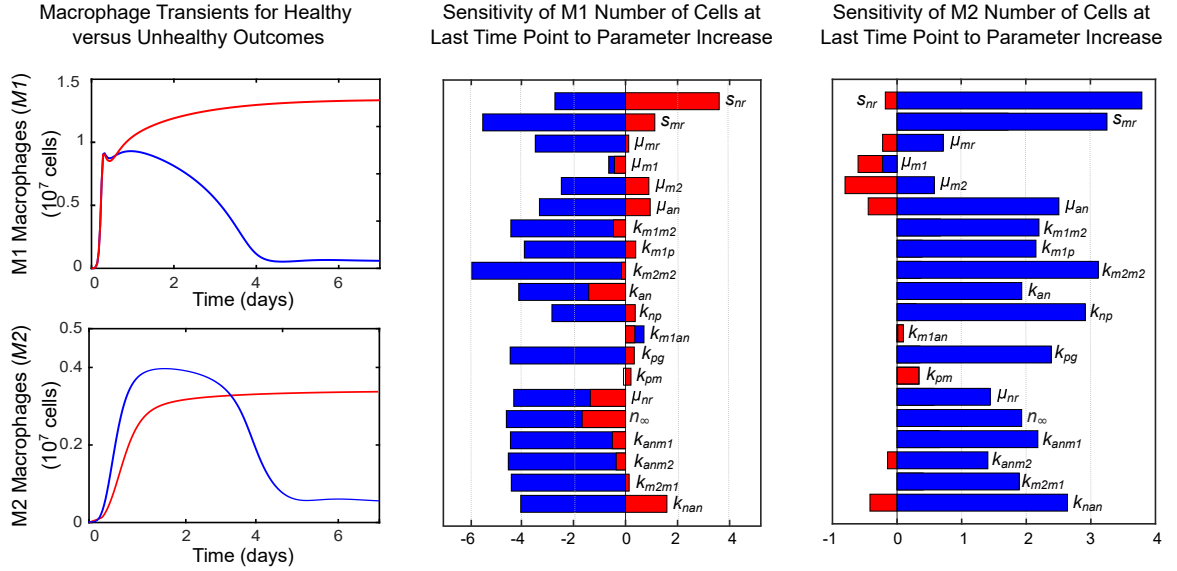


Fig. 37. **Sensitivity of M1 and M2 characteristics to parameter variations in the case of delayed neutrophil apoptosis (unhealthy response) versus a healthy response.** Predictions and sensitivities for a healthy response are plotted in blue, while predictions and sensitivities for an unhealthy response are plotted in red. A healthy M1 and M2 response that resolves, with all parameters at baseline values given in Tables 8 and 11 (including $k_{an} = 7.108$), is plotted versus an unhealthy, sustained M1 and M2 response resulting from reducing the value of parameter k_{an} to 5.56 while holding all other parameters constant. The bar charts compare the associated sensitivity of M1 and M2 characteristics to parameter variations in the healthy case versus the unhealthy case. Insensitive parameters, which have zero sensitivity for all characteristics, are not shown.

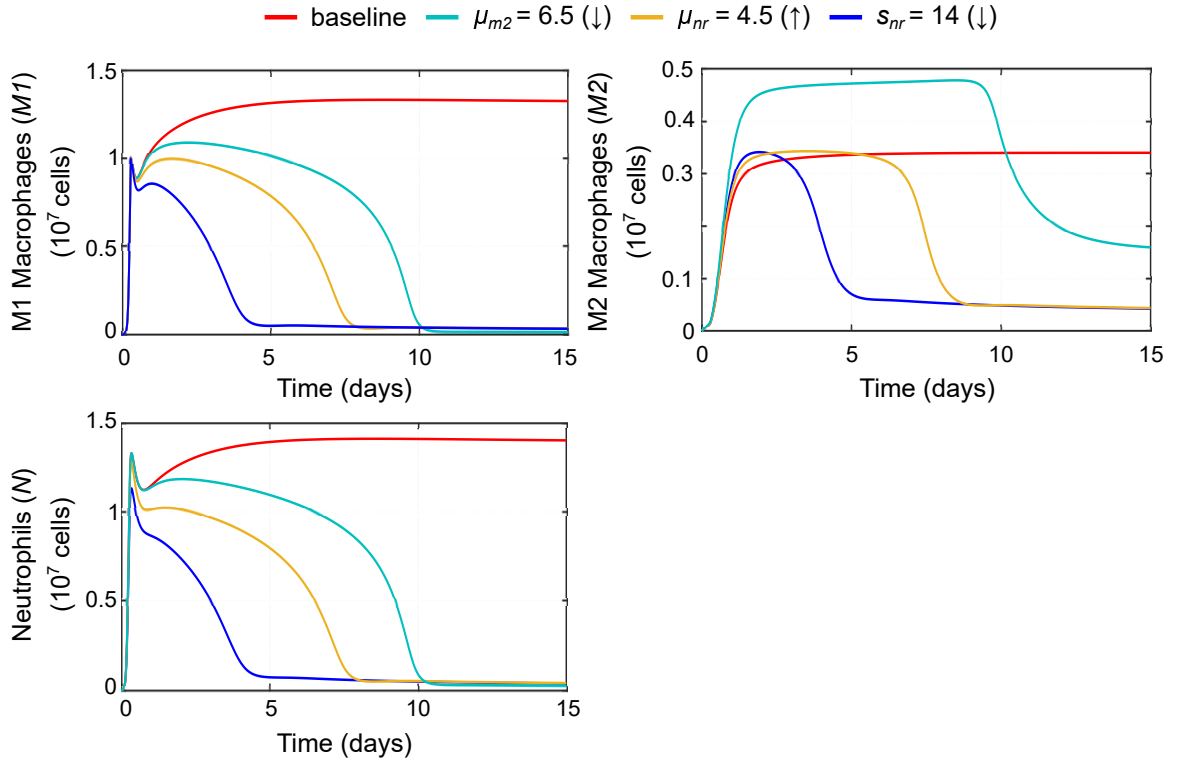


Fig. 38. **Parameter variations that resolve inflammation in the case of delayed neutrophil apoptosis.** Reducing the value of parameter k_{an} from baseline while holding all other parameters constant leads to sustained inflammation. We resolved inflammation in this case by varying each of three parameters separately: μ_{m2} , u_{nr} , or s_{nr} . All immune cells return to low levels if resting neutrophil influx or decay is modulated, while a population of M2 macrophages persists if M2s are directly targeted to resolve the inflammation.

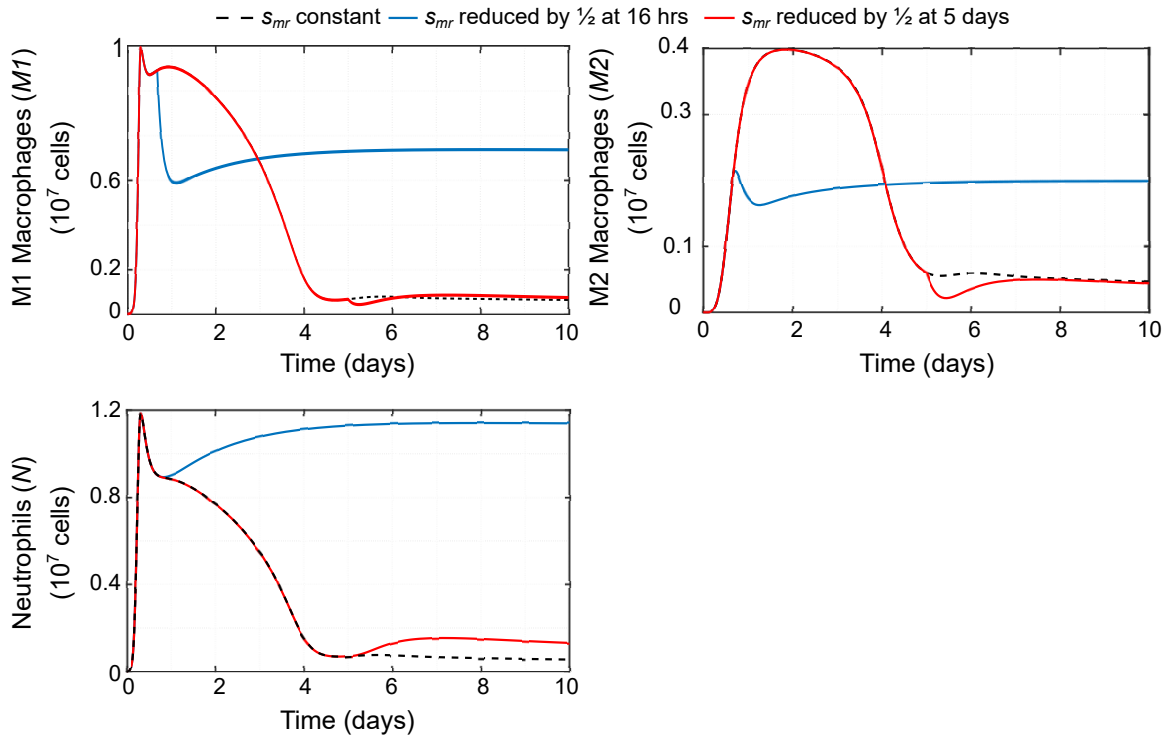


Fig. 39. **Predicted effects of reducing source of monocytes s_{mr} .** The effects of the baseline case of a constant influx of resting monocytes (that will differentiate into macrophages) is compared to the effects of reducing influx of monocytes at an early timepoint (16 hours) versus a late timepoint (5 days). Early intervention leads to sustained inflammation while late intervention leads to an increase in neutrophils.

CHAPTER 6

MACROPHAGE POLARIZATION IN ATHEROSCLEROSIS

6.1 Introduction

Atherosclerosis is the leading cause of death worldwide [147]. Adipose tissue can accumulate M1s which secrete pro-inflammatory cytokines that can in turn lead to insulin resistance and diabetes. These resident arterial plaque macrophages accumulate and adopt an inflammatory phenotype, which is why atherosclerosis is viewed as inflammatory [79, 80]. Chronic inflammatory diseases in general require timely peaks and ebbs in immune cell response in order for homeostasis to be restored. In the case of atherosclerosis, this macrophage phenotype switching is believed to be critical to a balanced response to excess cholesterol in the blood. Infiltrating macrophage-mediated removal of modified LDL from the intimal space should be followed by egress of lipid-loaded macrophages to prevent excessive accumulation and a transition of macrophages to pro-inflammatory foam cells. Our extended model will be able to provide hypothesis testing for points of intervention in early atherosclerosis that target macrophage phenotype, as has been proposed [131, 132, 133].

6.2 The Inflammatory Process in Early Atherosclerosis

6.2.1 The Blood

A high level of cholesterol associated with low density lipoprotein cholesterol particles (LDL-C) in plasma is a widely established risk factor of cardiovascular disease (CVD) risk [148]. LDL exists either in native or modified form such as oxidized (ox-

LDL) form. Native LDL-C does not contribute to ultimate foam cell formation, since LDL receptor expression on macrophages is downregulated in the presence of high levels of LDL-C [149]. However, when native LDL is modified to ox-LDL, the LDL receptors no longer function and uptake of LDL-C by macrophages occurs through scavenger receptors (SRs) and this process is not downregulated in the presence of high cholesterol levels [150]. Baseline circulating ox-LDL levels have thus been established as a predictor of atherosclerosis progression [151].

Toll-like receptor signaling in the presence of hyperlipidaemia promotes activation of circulating immune cells. About 80% of circulating monocytes recruited to plaques in mice are LY6C^{hi} (M1) and 20% are LY6C^{lo} (M2) [131].

6.2.2 The Gut

The high saturated fat and cholesterol content of the Western diet is strongly implicated in atherosclerosis. One factor that is receiving increasing consideration as a driver of disease progression is the increased gut permeability associated with this diet that, coupled with the associated unhealthy gut microbiome, allows a small amount of LPS (bacterial endotoxin lipopolysaccharide) to circulate in the bloodstream [152, 153, 154, 155, 156, 157]. This low grade inflammatory signal leads to chronic systemic inflammation that can become pro-atherogenic via a variety of pathways including (1) stimulation of macrophage influx in response to perceived pathogen, (2) downregulation of expression of transcription factor liver X receptor that suppresses cholesterol uptake, and (3) upregulation of cholesterol uptake by increasing expression of proatherogenic LDL receptor, very low density lipoprotein receptor, and adiponectin receptor 2 [158].

6.2.3 The Endothelium

In areas of the coronary artery wall that experience a large amount of shear due to blood flow, such as branches or bends, the endothelium becomes disrupted, and this activation promotes leukocyte and granulocyte [159, 160, 131] recruitment to the area. These cells then adhere to the luminal surface of the endothelial wall due to production of adhesion factors by activated endothelial cells [131, 161]. Low levels of circulating LPS may also activate the endothelium.

6.2.4 Foam cells

M1 macrophages uptake both normal and modified LDL; however, it is uptake of modified LDL that is largely unregulated and contributes most toward foam cell formation [148]. When macrophages take up LDL-C via scavenger receptors, macropinocytosis, and phagocytosis of aggregated LDL, they become foam cells. Cholesterol esters (CEs) associated with LDL are hydrolysed to free cholesterol within macrophages before migrating to the plasma membrane where any excess is re-esterified and stored as lipid droplets [162]. It is excessive cholesterol fatty acid accumulation which gives these macrophages a "foamy" appearance. Foam cells produce pro-inflammatory mediators (such as IL-1, IL-6, TNF, CCL2, CCL5, CXCL1) and macrophage retention factors (including netrin 1 and semaphorin 3E) [131] that promote inflammation in the developing plaque.

Cholesterol cannot efflux without first being released from stored CE by hydrolysis that is mediated by cholesterol ester hydrolase (CEH). So availability of CEH is considered a critical component of this process [163, 148]. In the absence of sufficient CEH and when other cholesterol trafficking pathways are overwhelmed, excess free cholesterol stored in foam cells can become toxic and induce endoplasmic reticulum

stress that leads to apoptosis [164]. Functioning foam cells are unable to effectively phagocytose these apoptotic foam cells due to their own dysregulated lipid metabolism pathways, and so secondary necrosis occurs, releasing lipids and other components that form the necrotic core in later stage plaques [131, 165].

6.2.5 The Role of Neutrophils

Neutrophils are also important in early atherosclerosis. Hypercholesterolemia alone has been shown to induce neutrophilia (high numbers of neutrophils in the blood), the degree of which is positively related to atherosclerotic lesion formation [159]. Neutrophils make up a small portion of the monocyte-dominated immune cell population of a plaque, however, the locations of highest neutrophil infiltration are also the areas with highest monocyte density [166]. In contrast, blocking neutrophil influx to the area of inflammation has been found to protect against plaque formation [167].

Release of pro-inflammatory products by neutrophils is considered a possible mechanism of monocyte recruitment to the area of a developing plaque [168, 169, 170, 171], and some additional mechanisms include:

- neutrophil products that promote differentiation of monocytes to an M1 phenotype [76, 77, 169, 172, 173, 174]
- neutrophil products that are chemotactic for monocytes and/or that cause monocyte adhesion to the endothelium [175, 176, 177, 178, 179, 180]
- neutrophil products that regulate foam cell development [181, 182]
- neutrophil extracellular trap (NET) formation that promotes pro-inflammatory cytokine production by macrophages [183, 184].

6.2.6 Treatments

In addition to established therapies such as statins and β -blockers, novel strategies to treat atherosclerosis are being tested in mouse models that target immune cells directly, some of which are outlined below.

Strategies that target neutrophils:

- blocking neutrophil influx with adoptive transfer of neutrophils with deficiency of chemokine receptor CXCR2 [167]
- induction of neutropenia (low numbers of neutrophils in the blood)[159, 169]
- antagonism of receptor for neutrophil chemokine [185]

Strategies that target macrophages:

- specific disruption of CD40 leukocyte signaling to skew immune response to an anti-inflammatory phenotype [186, 187]
- inhibition of pro-inflammatory macrophage migration inhibitory factor (MIF) [188, 189]
- interfering with pro-atherogenic chemokine receptors CCR5 and CCR2, which are used by M1s to enter plaques [190, 191, 192, 193, 194]

6.3 A Selection of ODE and PDE Models

An early model of lipoprotein oxidation *in vitro* was developed by Cobbold et al. [98] that tracks LDL, antioxidants, and free radicals and is also extended to include HDL.

Ougrinovskaia et al. [95] developed a model of early atherosclerosis that models local concentration of modified LDL (mLDL), capacity of active macrophages (foam

cells) to ingest mLDL, and internalized lipid content. The influx rate of LDL is set constant since it only varies in time with significant dietary changes. Uptake rate of modified LDL by foam cells is modeled with several different functions that saturate with increasing mLDL, and it is found that only saturating functions with one inflection point (exponent of 2) produce physiological results. In a later extension of their model [195] to include HDL, concentration of HDL is modeled with parameter h , and influx rate of LDL is modeled with a smooth, increasing, saturating function of h . Emigration rate of foam cells and modification rate of LDL are dependent on h , as is the influx rate of monocytes since HDL lowers the expression of adhesion molecules by endothelial cells.

The work of Bulelzai et al. [100] extends prior work by Zohdi et al. [196], that focuses on the effects of shear stress from blood flow. Here, the LDL oxidation process is not modeled, only LDL that is instantaneously oxidized as it enters the intima is included. The rate at which monocytes enter the intima changes with shear stress: for low shear it is considered linearly related to oxidized LDL, while higher shear stress gives rise to Michaelis-Menten type dynamics in the relationship [100]. However, while shear stress is an important factor in long-term evolution of plaques, and Bulelzai et al. predict dependence of lumen radius on shear stress once LDL uptake has passed a critical value, this importance is a factor in later stage plaque development rather than early atherosclerosis.

In McKay et al. [197], in addition to LDL oxidation, HDL, and radicals immune interactions including chemokines, proliferation factors, T-cells, smooth muscle cells, and macrophages. The model is built in stages, so that components can be examined analytically, and a third stage models spatial dynamics by tracking necrotic core buildup due to macrophage and smooth muscle cell death as well as collagen deposition.

The work of Zhang et al. [198] derives from both a prior PDE model [99] and lipid oxidation is modified from previous work [86, 98] to include foam cells and macrophages as separately tracked variables. Foam cell formation linearly depends only on phagocytosis of oxidized LDL by macrophages. Analysis of the model focuses on the effects of HDL between the two cases of constant influx over time versus time-varying influx. Chalmers et al. [96] developed a PDE model of early atherosclerosis including concentration of mLDL, concentration of chemoattractants and cytokines, density of monocytes and macrophages (tracked as a combined variable), and foam cells. They assume that the rate of macrophage conversion to foam cell is proportional to macrophage consumption of mLDL, and the resulting foam cells are assumed to be immobile. Model parameters are unknown, and given by relative order of magnitude.

Friedman et al. [97] developed a PDE model that includes M1, M2, and foam cell macrophages. In this model, only M1s influx to the area of the plaque, then transition to foam cell upon LDL-C uptake. Foam cells can transition to an M2 phenotype dependant on reverse cholesterol transport.

Finally, in Thon et al. [102], a complete ODE model is assembled from three submodels that are separately fit to *in vitro* experimental data. The first describes LDL modification and ingestion by macrophages. It had been determined experimentally that concentration of mLDL per macrophage saturates for increasing LDL, and this is reflected in the model. The modification of LDL is described as linear in the absence of any experimental information. The second submodel captures HDL and its inhibition of LDL modification. The third models the cholesterol cycle and reverse cholesterol transport based on *in vitro* experiments by Brown et al. [163].

In summary, existing models do not, to our knowledge, include systemic inflammation driven by circulating LPS and dietary cholesterol. Nor do they include neutrophils and macrophage polarization between phenotype, although in Friedman et al. [97]

foam cells can transition to M2. Only in the work of Zhang et al., Chalmers et al., and Friedman et al. [198, 96, 97] is a distinction made between macrophage and foam cell. Additionally, availability of cholesterol ester hydrolase (CEH), a rate limiting factor in reverse cholesterol transport, is not modeled in any previous work, to our knowledge.

6.4 Model Development

Here we extend our model of the interactions between neutrophils and M1 and M2 macrophages as described in 5 to the setting of atherosclerosis. Macrophage types now include both the foam cell state and the apoptotic foam cell state. As either M1 or M2 macrophages take up LDL-C, they transition to the foam cell state, and an excess of internalized lipids can lead to apoptosis. Apoptotic cells, composed of neutrophils and foam cells, contribute to accumulating debris that is also tracked as a first step in tracking necrotic core formation. In addition to immune cells, we include systemic inflammation driven by circulating LPS leaked from the gut and dietary cholesterol, both of which result from a Western diet. We distinguish between systemic and local inflammatory factors and immune cells as a first step in the development of a compartmentalized model that can be fit to measurements taken from the different compartments, as shown in Fig 40. The reverse cholesterol transport process is modeled with variables that track concentration of foam cell internalized free cholesterol and esterified cholesterol. HDL is currently included as a constant here although its functionality is highly variable and may change over the time course of plaque development. All variables appear with a description in Table 13. A schematic of the model shown in Fig 40. The model is described in Eqns 6.1-6.13, with model parameter descriptions and nominal values given in Table 14.

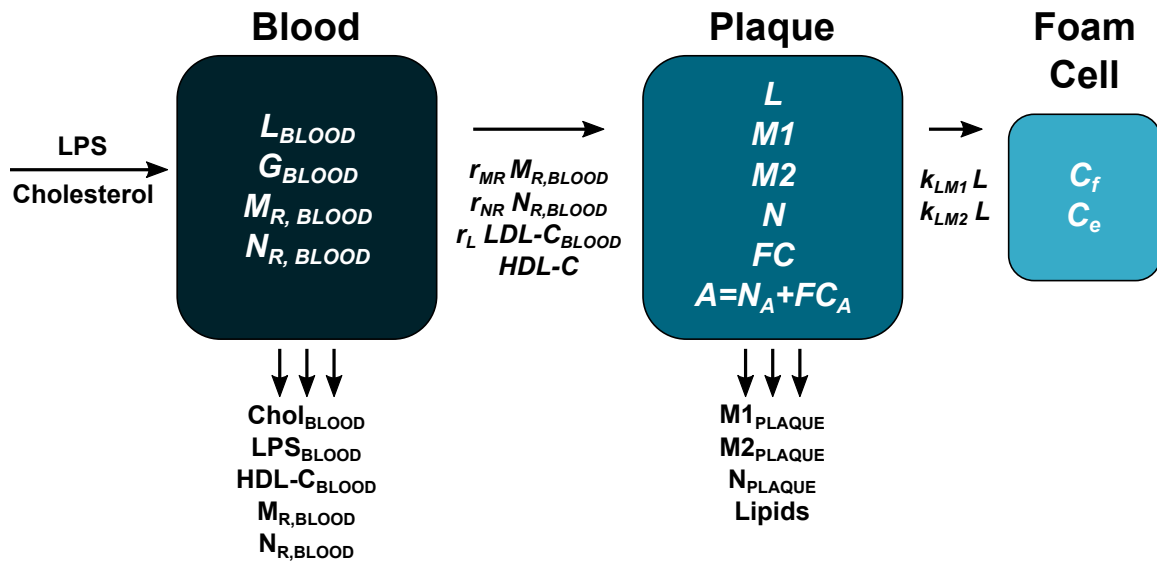


Fig. 40. **Diagram showing plan for model development.** Currently the model is built from the viewpoint of the plaque, with influxing macrophage and neutrophil precursors and cholesterol transported via high and low density lipoproteins. Reverse cholesterol transport occurs within the foam cells, modeled with variables C_f (free cholesterol) and C_e (cholesterol ester). For now we consider HDL-C influx constant.

Table 13. **Description of model variables.** Variables marked with (*) are currently set constant and appear as parameters in Table 14. However, circulating LDL-C will be modeled as a saturating function of dietary cholesterol and circulating LPS should also depend on dietary cholesterol.

Variable	Description
L_{blood}^*	circulating LDL-C
G_{blood}^*	circulating LPS
$M_{R,blood}$	circulating monocytes
$N_{R,blood}$	circulating granulocytes
L	LDL-C in plaque
$M1$	pro-inflammatory macrophages
$M2$	anti-inflammatory macrophages
N	neutrophils
N_A	apoptotic neutrophils
FC	foam cells
FC_A	apoptotic neutrophils
C_f	free (un-esterified) internalized cholesterol in foam cells
C_e	esterified internalized cholesterol in foam cells

LDL-C:

$$\begin{aligned}
 \frac{dL}{dt} = & \overbrace{r_L L_{blood}}^{\text{local influx of LDL-C}} - \overbrace{k_{LM1} M1 \frac{L^2}{a^2 + L^2}}^{\text{removal by M1 dep. on saturating function of ingested LDL-C}} \\
 & - \overbrace{k_{LM2} M2 \frac{L^2}{b^2 + L^2}}^{\text{removal by M2 dep. on saturating function of ingested LDL-C}} + \overbrace{\mu_{afc} C_F}_{\text{chol. spilled by necrotic FC}} \quad (6.1)
 \end{aligned}$$

Circulating macrophage and neutrophil precursors:

$$\begin{aligned} \frac{dM_{r,blood}}{dt} = & \underbrace{s_{mr}}_{\text{natural source}} - \underbrace{\mu_{nr}M_{r,blood}}_{\text{decay}} + \underbrace{k_{mrL}L_{blood}}_{\text{up-regulation of source rate from LDL-C}} \\ & + \underbrace{k_{mrg}G_{blood}}_{\text{up-regulation of source rate from LPS}} - \underbrace{R_{M1}M_{r,blood} - R_{M2}M_{r,blood}}_{\text{activation/influx}} \end{aligned} \quad (6.2)$$

$$\begin{aligned} \frac{dN_{r,blood}}{dt} = & \underbrace{s_{nr}}_{\text{natural source}} - \underbrace{\mu_{nr}N_{r,blood}}_{\text{decay}} + \underbrace{k_{nrL}L_{blood}}_{\text{up-regulation of source rate from LDL-C}} \\ & + \underbrace{k_{nrg}G_{blood}}_{\text{up-regulation of source rate from LPS}} - \underbrace{R_N N_{r,blood}}_{\text{activation/influx}} \end{aligned} \quad (6.3)$$

Macrophages:

$$\begin{aligned} \frac{dM1}{dt} = & \underbrace{R_{M1}M_{r,blood}}_{\text{activation/influx}} - \underbrace{k_{m1m2}k_{anm1}AN f_i(M1, N)}_{\text{transition to M2 per phagocytosed AN}} \\ & + \underbrace{k_{m2m1}M2}_{\text{transition to M1 from M2}} - \underbrace{\mu_{m1}M1}_{\text{efflux}} - \underbrace{k_{LM1}M1 \frac{L^2}{a^2 + L^2}}_{\text{transition to foam cell from LDL-C uptake}} \\ & - \underbrace{k_{m1fc}k_{afcm1}FC_A f_i(M1, N)}_{\text{transition to foam cell per phagocytosed } FC_A} \end{aligned} \quad (6.4)$$

$$\begin{aligned} \frac{dM2}{dt} = & \underbrace{R_{M2}M_{r,blood}}_{\text{activation/influx}} + \underbrace{k_{m1m2}k_{anm1}AN f_i(M1, N)}_{\text{transition from M1 per phagocytosed AN}} \\ & - \underbrace{k_{m2m1}M2}_{\text{transition to M1}} - \underbrace{\mu_{m2}M2}_{\text{efflux}} - \underbrace{k_{LM2}M2 \frac{L^2}{b^2 + L^2}}_{\text{transition to foam cell from LDL-C uptake}} \\ & - \underbrace{k_{m2fc}k_{afcm2}FC_A f_i(M2, N)}_{\text{transition to foam cell per phagocytosed } FC_A} + \underbrace{k_{fcm2}\mu_{cf} \frac{H^2}{d^2 + H^2} C_f FC}_{\text{transition from } FC \text{ from } C_f \text{ efflux [97]}} \end{aligned} \quad (6.5)$$

Macrophage activation rates:

$$\begin{aligned}
R_{M1} = & \overbrace{k_{m1L}L}^{\text{local LDL-C}} + \overbrace{k_{m1n}N}^{\text{neutrophil byproducts}} + \overbrace{k_{m1m1}M1}^{\text{M1s and their cytokines}} \\
& + \overbrace{k_{m1fc}FC}^{\text{foam cell products}} + \overbrace{k_{m1a}(\mu_{afc}FC_A + \mu_{an}N_A)}^{\text{necrotic cell byproducts}}
\end{aligned} \tag{6.6}$$

$$R_{M2} = \overbrace{k_{m2m2}M2}^{\text{M2s and their cytokines}} + \overbrace{k_c}^{\text{background anti-inflammatory cytokines}}$$

Neutrophils:

$$\frac{dN}{dt} = \overbrace{R_N N_{r,blood}}^{\text{activation}} - \overbrace{k_{an}N}^{\text{apoptosis}} \tag{6.7}$$

$$\begin{aligned}
\frac{dN_A}{dt} = & \overbrace{k_{an}N}^{\text{apoptosis}} - \overbrace{k_{anm1}N_A f_i(M1, N)}^{\text{removal by M1}} - \overbrace{k_{anm2}N_A f_i(M2, N)}^{\text{removal by M2}} - \overbrace{k_{ann}N}^{\text{removal by N}} \\
& - \overbrace{\mu_{an}N_A}^{\text{secondary necrosis}}
\end{aligned} \tag{6.8}$$

Neutrophil activation rate:

$$R_N = \overbrace{k_{nL}L}^{\text{local LDL-C}} + \overbrace{k_{na}((\mu_{afc}FC_A + \mu_{an}N_A))}^{\text{necrotic cell byproducts}}$$

Foam cells:

$$\begin{aligned}
\frac{dFC}{dt} &= \overbrace{k_{LM1}M1 \frac{L^2}{a^2 + L^2}}^{\text{transition from M1}} + \overbrace{k_{LM2}M2 \frac{L^2}{a^2 + L^2}}^{\text{transition from M2}} \\
&- \overbrace{k_{fcm2}\mu_{cf} \frac{H^2}{d^2 + H^2} C_f}_{\text{transition to M2 dep. on efflux [97]}} - \overbrace{k_{fca} \frac{C_f^2}{e^2 + C_f^2} FC}_{\text{apoptosis}} + \overbrace{k_{m1fc}k_{afcm1}FC_A f_i(M1, N)}^{\text{transition from M1 per phagocytosed } FC_A} \\
&+ \overbrace{k_{m2fc}k_{afcm2}FC_A f_i(M2, N)}^{\text{transition from M2 per phagocytosed } FC_A} \quad (6.9)
\end{aligned}$$

$$\begin{aligned}
\frac{dFC_A}{dt} &= \overbrace{k_{fca} \frac{C_f^2}{e^2 + C_f^2} FC}_{\text{apoptosis}} - \overbrace{k_{afcm1}FC_A f_i(M1, N)}^{\text{removal by M1}} - \overbrace{k_{afcm2}FC_A f_i(M2, N)}^{\text{removal by M2}} \\
&- \overbrace{\mu_{afc}FC_A}_{\text{secondary necrosis}} \quad (6.10)
\end{aligned}$$

Internalized lipids

Free cholesterol:

$$\begin{aligned}
\frac{dC_F}{dt} &= \overbrace{n_{cf}k_{LM1}M1 \frac{L^2}{a^2 + L^2}}^{\text{chol. assoc. w LDL taken up my M1}} + \overbrace{n_{cf}k_{LM2}M2 \frac{L^2}{b^2 + L^2}}^{\text{chol. assoc. w LDL taken up my M2}} \\
&- \overbrace{k_e C_f}_{\text{esterification [102, 163]}} + \overbrace{k_{ce} C_e CEH}_{\text{hydrolysis of chol, rate depends on CEH}} \\
&- \overbrace{\mu_{cf} \frac{H^2}{d^2 + H^2} C_f}_{\text{efflux sat. function of HDL, [102]}} + \overbrace{c_{m1}k_{LM1}M1 \frac{L^2}{a^2 + L^2}}^{\text{chol. in recruited M1s}} \\
&+ \overbrace{c_{m2}k_{LM2}M2 \frac{L^2}{a^2 + L^2}}^{\text{chol. in recruited M2s}} \quad (6.11)
\end{aligned}$$

Esterified cholesterol:

$$\frac{dC_e}{dt} = \overbrace{k_e C_f}^{\text{esterification [102, 163]}} - \overbrace{k_{ce} C_e C E H}^{\text{hydrolysis of chol, rate depends on CEH}} \quad (6.12)$$

Apoptotic cells (contribution to necrotic core):

$$f(FC_A, N_A) = \overbrace{\mu_{afc} FC_A}^{\text{secondary necrosis}} + \overbrace{\mu_{an} N_A}^{\text{secondary necrosis}} \quad (6.13)$$

Table 14.: Description of parameters and values.

Parameter	Description	Nominal Value
s_{mrb}	circulating monocytes in blood	$0.75/M$ -units/day
k_{mrrL}	activation rate of $M_{r,blood}$ by $LDL - C^{blood}$	$1.00/M$ -units/day
μ_{mrb}	decay of circulating monocytes	1.4 /day
k_{mrrg}	activation rate of M1 by LPS	$0.125/M$ -units/day
s_{nrB}	source of resting N	$1/N$ -units/day
μ_{nrB}	decay of resting N	16.402 /day
k_{m1n}	activation rate of M1 by N byproducts	$0.025/M$ -units/day
k_{m1m1}	activation rate of M1 by M1s and their cytokines	$0.001/M$ -units/day
k_{m2m1}	transition rate of M2 to M1	$0.117/M$ -units/day
u_{m1}	decay of M1 macrophages	6.826 /day
k_{m1m2*}	transition rate of M1 to M2	$8.617/M$ -units/day
k_{m2m2}	activation rate of M2 by M2s and their cytokines	$1.593/M$ -units/day
k_c	concentration of background anti-inflammatory	$0.125/M$ -units/day (fixed [3])
μ_{m2}	decay of M2 macrophages	8.271 /day

Continued on next page

Table 14 – Continued from previous page

Parameter	Description	Nominal Value
k_{na}	activation rate of N by apoptotic cells	0.608
n_{∞}	level of N for 50% inhibition of M activity	$0.156/N$ -units
k_{an}	transition rate of N to AN	$7.108/N$ -units/day
k_{ann}	destruction rate of AN by N	$0.001/N$ -units/day
k_{ann1}	destruction rate of AN by M1	$2.898/N$ -units/day
k_{ann2}	destruction rate of AN by M1	$90.958/N$ -units/day
μ_{an}	secondary necrosis of AN	1.309 /day
r_L	rate of circulating LDL-C influx to plaque	0.001
k_{mLm1}	rate of LDL-C uptake my M1	1
k_{mLm2}	rate of LDL-C uptake my M2	1
μ_{afc}	rate of FC apoptosis	$1 \text{ times } 10^{11}$
μ_{cf}	efflux rate of C_f	0.125
k_{fcm2}	transition rate of FC to M2	0.0125
a	Hill function constant for M1 uptake of L	1
b	Hill function constant for M2 uptake of L	1

Continued on next page

Table 14 – Continued from previous page

Parameter	Description	Nominal Value
d	Hill function constant for HDL-dependent FC transition to M2	1×10^4
e	Hill function constant for C_f -dependent FC apoptosis	1×10^4
H	constant HDL-C influx to plaque	1
k_e	C_f esterification rate	0.1
C_{fc}	free cholesterol in FC not from LDL-C uptake	0.0125
k_{ce}	hydrolysis rate of C_e	0.001
k_{nrL}	activation of circulating monocytes by circulating LDL-C	0.125
k_{nrg}	activation of circulating monocytes by circulating LPS	0.125
k_{nrg}	activation of circulating granulocytes by circulating LPS	0.125
G_b	constant influx of LPS to blood from leaky gut	1
L_b	circulating LDL-C dependent on dietary cholesterol	1
$k_{a,fcM1}$	removal of FC_A by M1s	10
$k_{a,fcM2}$	removal of FC_A by M2s	10
k_{m1L}	activation of M1s by $LDL - C_{blood}$	0.125
k_{m1a}	activation by necrotic cell byproducts	0.125

Continued on next page

Table 14 – Continued from previous page

Parameter	Description	Nominal Value
k_{nrL}	activation of circulating granulocytes by circulating LDL-C	0.125
k_{nL}	activation of N by $LDL - C_{blood}$	0.125
n_{cf}	cholesterol associated with LDL-C	1

Dietary cholesterol causes an increase in circulating LDL-C in the blood, which in turn influxes into the local environment of the plaque where it is taken up by M1 and M2 macrophages. If apoptotic foam cells have become too numerous for timely macrophage removal they undergo secondary necrosis, spilling their lipid burden and adding to LDL-C in the plaque, as modeled in Eq 6.1. Circulating LDL-C (L_{BLOOD}) and circulating LPS (G_{BLOOD}) are currently set constant and appear as parameters in Table 14. However, circulating LDL-C will be modeled as a saturating function of dietary cholesterol and circulating LPS should also depend on dietary cholesterol.

We no longer use the quasi-steady state assumption to model differentiation of circulating immune cells into macrophages and neutrophils, as in 5. Here we include dependence of circulating $M_{r,BLOOD}$ and $N_{r,BLOOD}$ on circulating LDL-C and LPS in Eqs 6.2-6.3 with the expectation that measurements for all of variables can be obtained from the blood in a future experiment (see projected outputs from the blood compartment in Fig 40).

Resting neutrophils influxing into the plaque become activated by local LDL-C and the debris formed by apoptotic cells at the rate $R_N(L, A)$. They undergo apoptosis at rate k_{an} . Apoptotic neutrophils are then removed by M1s at rate k_{anm1} , M2s at rate k_{anm2} , and by active neutrophils at rate k_{ann} . Apoptotic neutrophils that are not cleared undergo secondary necrosis at rate μ_{an} , contributing to the positive feedback described in the neutrophil activation term $R_N(L, A)$.

Resting monocytes (M_R) are next to arrive. The majority of these first monocytes differentiate to an inflammatory M1 phenotype in response to local LDL-C, byproducts of neutrophils, M1s and their cytokines, foam cells products, and cytokines spilled by necrotic apoptotic cells at rate $R_{M1}(L, N, M1, FC, A)$. Decay and polarization between M1 and M2 is modeled as described in 5.2. When M1 or M2 macrophages increase their lipid content above normal levels by taking up LDL-C or

apoptotic foam cells they transition to foam cells. Foam cells can transition to M2 macrophages dependent on HDL-C mediated cholesterol efflux [97].

Here we model esterification of free cholesterol within foam cells as a linear function, but in Thon et al. [102] buffer-like behavior of the cholesterol cycle is assumed based on *in vitro* experiments conducted by Brown et al. [163]. Also from Thon et al. is the idea of a maximum foam cell capacity for cholesterol $C_{f,max}$ and the “normal” load of cholesterol $C_{f,min}$ carried by macrophages that we have not yet incorporated for simplicity’s sake. Dependence of hydrolysis of free cholesterol on cholesterol ester hydrolase (CEH) is represented with a linear dependence on parameter CEH , currently set to a value of 1. This setup functions as a placeholder for later development: the parameter could be removed, with dependence on CEH rolled into cholesterol hydrolysis rate constant k_{ce} , or modeled with a more realistic functional dependence on CEH. We do not track plaque size directly, but we can track accumulation of necrotic foam cells and neutrophils, $f = \mu_{afc}FC_A + \mu_{an}N_A$, as a first step toward tracking plaque size in Eq 6.13.

Figs 41(a) and 42(a) show model predictions with parameters set at nominal values given in Table 14. Figs 41(b) and 42(b) show the predicted effects of removing dietary cholesterol on the basic model. In this example, for $t < 50$, there is some level of circulating LDL-C in the blood (i.e. $L_b = 1$) that is dependent on dietary cholesterol. For $t > 50$, we set the parameter $L_b=0.001$ to simulate a drastic reduction in circulating LDL-C that would result from the removal of cholesterol in the diet.

Immune cell levels decrease except for M1- and M2-derived active foam cells. This is due to reduced foam cell apoptosis since foam cell internalized lipid levels are decreased. Both free and esterified cholesterol per foam cell are substantially decreased, although esterified cholesterol is still increasing over time at a slower rate. Increasing availability of CEH (simulated by setting $CEH > 1$) is one approach to

modulate cholesterol esterification.

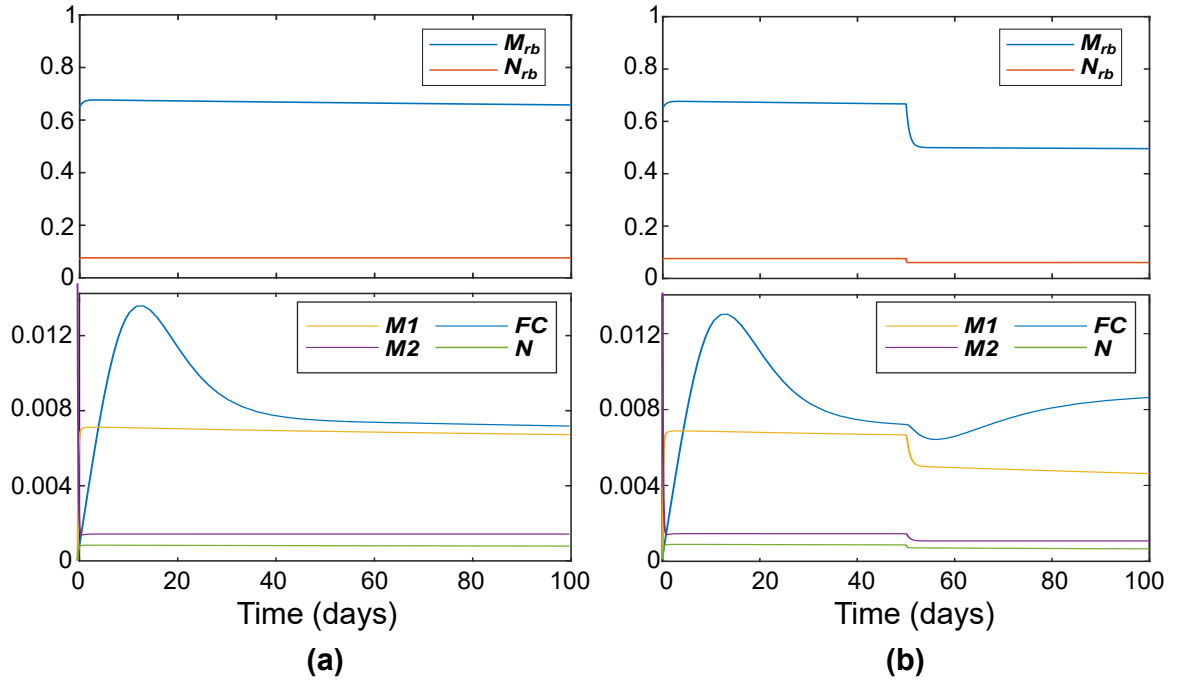


Fig. 41. **Predicted effects of removing dietary cholesterol on cells in the basic model.** (a) Parameters are set at the nominal values given in Table 14. (b) For $t < 50$, there is some level of circulating LDL-C in the blood (i.e. $L_b = 1$) that is dependent on dietary cholesterol. For $t > 50$, we set the parameter $L_b=0.001$ to simulate a drastic reduction in circulating LDL-C that would result from the removal of cholesterol in the diet. Immune cell levels decrease except for M1- and M2-derived foam cells due to reduced foam cell apoptosis.

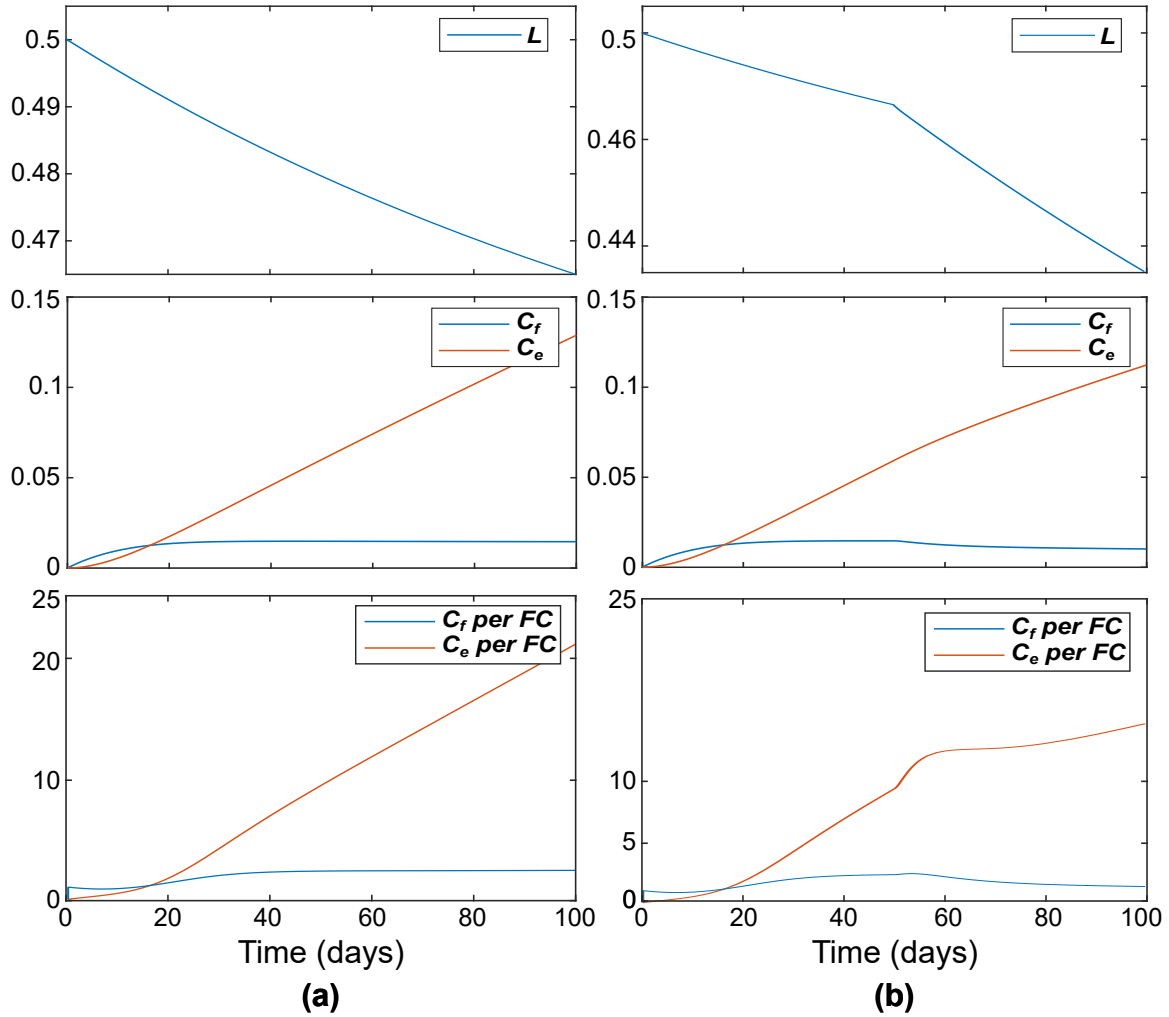


Fig. 42. **Predicted effects of removing dietary cholesterol on cholesterol in the basic model.** (a) Parameters are set at the nominal values given in Table 14. (b) For $t < 50$, there is some level of circulating LDL-C in the blood (i.e. $L_b = 1$) that is dependent on dietary cholesterol. For $t > 50$, we set the parameter $L_b=0.001$ to simulate a drastic reduction in circulating LDL-C that would result from the removal of cholesterol in the diet. Both free and esterified cholesterol per foam cell are substantially decreased, although esterified cholesterol is still increasing over time.

6.5 Discussion

Our work has extended the peritonitis model presented in Chapter 5 as well as the work of many others [98, 95, 100, 196, 197, 198, 96, 97] to include macrophage phenotype polarization in this system. Results from our numerical simulation of an intervention that removes dietary cholesterol demonstrates that in spite of a predicted modest impact on local LDL-C and an increase in foam cells, foam cell internalized lipids are significantly reduced. This model was built from the perspective of the plaque compartment, but the structure is in place to add greater levels of complexity, such as a more detailed blood compartment and variable components within.

In the future, a parameter estimation process similar to that presented in Chapter 5 can be performed to fit to experimental data. Sampling from each compartment may allow fitting in spite of the relative complexity of the model. Further, the model can be extended to include a spatial dimension with PDE modeling, to capture plaque size change.

CHAPTER 7

CONCLUSION

7.1 Summary

We have developed three mathematical models of biological systems with potential medical applications and analyzed each. For each application, once a model was developed a full exploration of model parameters was carried out. We applied Latin Hypercube Sampling methods to generate parameter sets that were then used in simulations to explore the limits of model behavior. The simulated data that results allows us to investigate parameter sensitivity and interactions and to set bounds on parameter space for later estimation. Once fitted to experimental data, the model parameters are the connection between the mathematical model and the biological reality. Understanding the limitations of model predictions as they relate to uncertainty in the parameter estimation process was a focus of our work.

Our model of human muscle hypertrophy in response to resistance exercise was created to investigate the effects of an increase in lean mass on long-term maintenance of a healthy body weight. Changes in body weight depend on changes in energy intake and energy expenditure and an imbalance can result in obesity. By 2030, over 50% of the US population is expected to be obese, and obesity-attributable disease is projected to rise precipitously [199]. Most dieters regain weight over time [6, 55, 7, 8], but a common attribute of successful dieters is continued physical activity [9]. Though resistance training carries many health benefits it is under-explored as a clinical intervention because the relationship between this type of exercise and energy expenditure is not as straightforward as for cardiovascular exercise. There is also a

great deal of individual variation in response to resistance exercise, making it harder to predict outcomes.

With our model, we tested our hypothesis that the incremental additional expenditure due to accumulation of lean mass could help maintain a healthy body composition following a diet. A simulated case study that compared the effects of a hypocaloric diet alone versus diet combined with cardiovascular or resistance exercise predicted that continued exercise could result in fat loss maintenance, even after a return to pre-diet energy intake levels. Using Latin Hypercube Sampling, we also simulated a cohort of hypothetical individuals with varied response to resistance exercise. In this way, our model could be used to predict clinical study outcomes for a population with varied response.

In our exploration of model parameters, we performed sensitivity analysis via PRCC calculations on simulated data, fit to data from a resistance exercise study, and trained decision trees on simulated data. When results from these varied approaches are considered together, the model is shown to produce biologically feasible predictions. For example, when fitted to male versus female data, parameters differ in a way that makes sense. The r value estimate for the female group is lower, which corresponds to a lower overall gain, the α value is also lower, which corresponds to slower response, the H_1 value is higher, (delayed response), and a lower H_2 value (lower potential increase given lower initial lean mass). With more group-specific data, population-level differences in response could be further explored. In addition, the important parameters that were discovered using sensitivity analysis and decision trees agreed across both methods.

In what is, to our knowledge, the first application of optimal control techniques to individual body mass change, we put body mass partitioning during a diet and exercise program into this framework and were able to explicitly characterize an

optimal quadratic control for the system. We performed numerical simulations under different goals: fat loss prioritization, equal weight given to fat loss and lean mass retention, and prioritization of maximization of lean mass at the final time. Overall, the model shows that the optimal strategy to retain or gain lean mass, which will help maintain results long-term given previous model predictions, is to diet moderately. The simulations also predict that even such a gradual and moderate implementation of dietary changes can result in fat loss.

We used this model of response to resistance exercise to demonstrate the qualitative analysis of biological model behavior with decision trees, a machine learning method. These methods can easily be implemented and can yet provide similar intuition on model parameters to other, more complicated techniques as demonstrated by our comparison to PRCC results. In addition to providing a visualization of parameter interactions that determine outcomes, the decision rules obtained can be used to find group-specific parameter sets and set bounds on parameter estimation.

Our model of macrophage polarization between the M1 and M2 phenotypes during inflammation was developed because the modulation of macrophage subpopulations has been proposed as an intervention strategy [131, 132, 133, 139]. However, mechanisms governing this polarization are not yet understood. With our model, insight can be gained about the key system components that drive the inflammatory process and shift macrophage populations. To our knowledge, it is also the first model of this type to be fit to *in vivo* experimental data.

Experimental data in the form of immune cell counts was obtained from the widely studied peritonitis mouse model of inflammation. The model fitting and parameter selection process that is developed here is shared in great detail. Identifiability of parameters is extremely important for the reliability of model predictions, and the limitations of the model with respect to parameters are clearly presented, with

confidence interval bounds placed on identifiable parameter estimates as well.

Our fitted model is used to test hypotheses about the factors that determine macrophage phenotype, such as clearance by macrophages of apoptotic cells (efferocytosis) [110, 74, 111, 112, 76]. Sensitivity analysis performed on the model suggests that neutrophils, and the resulting population of apoptotic neutrophils, are closely related to macrophage dynamics. In addition, we simulated a number of intervention scenarios such as targeting the macrophage phenotype transition rate directly or indirectly by targeting neutrophil apoptosis. We tested the blocking of the source of monocytes for recruitment to macrophages, and the results from our simulations showing the importance of timing of the intervention have been experimentally observed [131, 137, 138].

Our model of the inflammatory immune response in early atherosclerosis extends our previous model of inflammation and builds on the previous work of many others [98, 95, 100, 196, 197, 198, 96, 97]. There is a causal relationship between atherogenesis and increases in circulating monocytes and pro-inflammatory mediators and, further, positive relationships between plaque size, delayed clearance of macrophages, and reduced monocyte migration has been demonstrated [144, 145]. These results highlight the usefulness of a computational model of atherosclerosis that includes detailed immune cell interactions and activities to simulate targeted macrophage therapies [186, 187, 188, 189, 190, 191, 192, 193, 194] and targeted neutrophil therapies [159, 167, 169, 185]. With our model, we have simulated an intervention that removes or drastically reduces dietary cholesterol. Results show that even though the reduction in LDL-C local to the plaque is modest and there is an increase in foam cells, lipid burden per foam cell is significantly reduced. Inclusion of a framework for separate blood and local compartments, as well as circulating LPS from a leaky gut, allow this work to be extended to other disease systems featuring chronic inflammation.

7.2 Future directions

Since our model of body mass change is unique in its inclusion of response to resistance-type exercise, it can be used to further test different diet and exercise combination strategies as obesity interventions. One current limitation is a dearth of good quality longitudinal data from clinical studies where energy intake is controlled. Currently, such data only exists for starvation studies where exercise is not feasible, yet energy intake has a large impact on body mass. More data, preferably capturing a wide cross-section of the human population, is required to better define model parameters. Given data, population-specific submodels could be developed; for example, an elderly-specific model.

We can further test diet and exercise strategies with variations on the optimal control framework for such problems that we have developed. With the addition of a control for exercise, we may find an optimal combination strategy. A linear control is also yet to be characterized. Finding a reasonable time frame in which to reach weight loss goals can be a nontrivial problem, and usually a short time frame is arbitrarily set for a clinical intervention that is convenient in the short term but may be detrimental for long-term weight maintenance due to metabolic damage. Within this framework, we can solve for the goal time by fixing a fat mass target for the final time.

In modeling the inflammatory immune response, we used cellular feedback loops to approximate the effects of mediators for which we did not have experimental measurements. Explicit inclusion of these components would refine these models. For the current peritonitis model, additional data will also likely allow identification of more parameters. For our model of atherosclerosis, we hope to obtain experimental data for parameter estimation. The collection of data from the different compartments (blood, plaque, internalized lipids) will allow model refinement and we hope that this

will allow parameters to be estimated in spite of the high level of model complexity. Adding a spatial dimension to the model will allow a more detailed tracking of plaque size.

In conclusion, we will employ these models in gaining a deeper understanding of the underlying processes driving human disease such as obesity and those that feature chronic inflammation and we hope to apply these models to the testing of interventions.

Appendix A

CODE FOR THE RESISTANCE EXERCISE MODEL

A.1 SBML model file

This .xml file in Systems Biology Markup Language (SBML) can be imported into the Matlab Simbiology toolbox [200] or any other SBML-compatible software package.

```
1 <!--Model of body mass change in response to resistance ...  
   training -->  
2 <?xml version="1.0" encoding="UTF-8"?>  
3 <sbml xmlns="http://www.sbml.org/sbml/level2/version4" ...  
   level="2" version="4">  
4 <annotation>  
5   <SimBiology xmlns="http://www.mathworks.com">  
6     <Version Major="5" Minor="6" Point="0"/>  
7   </SimBiology>  
8 </annotation>  
9 <model id="mw17a63ba7_776d_4b73_ac96_564ca01b91df" ...  
   name="RT_12_18">  
10 <listOfCompartments>  
11   <compartment ...  
       id="mwb2ea0abf_52f0_4d92_b66c_0a37fa8ce2d1" ...  
       name="Schematic" size="1" constant="true"/>  
12 </listOfCompartments>  
13 <listOfSpecies>  
14   <species id="mw90c87dde_e0a8_4e05_afb2_29276061ec6c" ...  
       name="G" compartment=  
15 "mwb2ea0abf_52f0_4d92_b66c_0a37fa8ce2d1"  
16 initialConcentration="0.5"  
17 boundaryCondition="false" constant="false"/>  
18   <species id="mw11e3a509_3e54_42d4_9e04_8e8bf1141db5" ...  
       name="AT" compartment=  
19 "mwb2ea0abf_52f0_4d92_b66c_0a37fa8ce2d1"
```

```

20     initialConcentration="0" boundaryCondition="false" ...
        constant="false"/>
21 <species id="mwflc0663d_1a61_4564_90c7_be0412eab4d1" ...
        name="F" compartment=
22 "mwb2ea0abf_52f0_4d92_b66c_0a37fa8ce2d1"
23 initialConcentration="16.632" ...
        boundaryCondition="false" constant="false"/>
24 <species id="mwd216a905_5d4c_4f61_9571_9e3dcb45b108" ...
        name="L" compartment=
25 "mwb2ea0abf_52f0_4d92_b66c_0a37fa8ce2d1"
26 initialConcentration="27.82" ...
        boundaryCondition="false" constant="false"/>
27 <species id="mwba79cc5_8f27_4f2c_b2f7_3e62ae00c8b6" ...
        name="ECF" compartment=
28 "mwb2ea0abf_52f0_4d92_b66c_0a37fa8ce2d1"
29 initialConcentration="0" boundaryCondition="false" ...
        constant="false"/>
30 <species id="mw188ffe6b_491f_46b7_b33a_bbe49c5b175c" ...
        name="LBM" compartment=
31 "mwb2ea0abf_52f0_4d92_b66c_0a37fa8ce2d1"
32 initialConcentration="27.82" ...
        boundaryCondition="false" constant="false"/>
33 <species id="mwea9e5002_ae74_4804_8e16_0be189d41376" ...
        name="EI" compartment=
34 "mwb2ea0abf_52f0_4d92_b66c_0a37fa8ce2d1"
35 initialConcentration="1208" boundaryCondition="true" ...
        constant="false"/>
36 </listOfSpecies>
37 <listOfParameters>
38 <parameter ...
        id="mw735bcb0c_a7eb_4741_a7c7_68d451695bb2" ...
        name="r" value="0.01" constant="true"/>
39 <parameter ...
        id="mw0e5dd104_6c36_4d61_aaa0_304495f4958d" ...
        name="alpha" value="2" constant="true"/>
40 <parameter ...
        id="mw3e8ac7b4_c93c_46d1_afa3_0ffe81ac5fa9" ...
        name="beta" value="12" constant="true"/>
41 <parameter ...
        id="mw7d93fe54_abc0_4168_be20_b0c4cd50db7e" ...
        name="H_1" value="24" constant="true"/>
42 <parameter ...
        id="mwbcae1952_7942_4e93_baa0_602708e643ed" ...
        name="H_2" value="39.089204" constant="true"/>
43 <parameter ...

```

```

    id="mw6b754d96_d5ec_4c93_9c49_81a862fd99e3" ...
    name="kG" value="0" constant="false"/>
44 <parameter ...
    id="mwf757b81c_acf1_42fc_8c71_e8e8477f9c35" ...
    name="K" value="0" constant="true"/>
45 <parameter ...
    id="mwd655381f_5be7_40a6_9382_44a09fa2e4a9" ...
    name="EI0" value="1208" constant="true"/>
46 <parameter ...
    id="mwbefacf2e_0633_4509_b37a_67d3fb3abf08" ...
    name="CI" value="0" constant="false"/>
47 <parameter ...
    id="mwc3955de4_7ac4_4f85_9eb3_ecf3c9b28b9c" ...
    name="PAL" value="1.6" constant="true"/>
48 <parameter ...
    id="mwfac7025f_6dcc_4606_a379_4fefb55a4c9c" ...
    name="TEF" value="1" constant="false"/>
49 <parameter ...
    id="mw4dd84072_9c69_4ea2_b6d1_4b3f7d60e34c" ...
    name="EE" value="1" constant="false"/>
50 <parameter ...
    id="mw0dfa195b_9ad7_4855_8857_ff396398cab1" ...
    name="BW0" value="1" constant="true"/>
51 <parameter ...
    id="mw3f90ba7d_f81b_467e_a0a6_57941b3eb364" ...
    name="Δ_sodium" value="0" constant="true"/>
52 <parameter ...
    id="mwdab98099_f37d_420e_8aa3_5ff8cd6dad8" ...
    name="diet" value="1000" constant="false"/>
53 <parameter ...
    id="mw58e7a6e9_b243_49f7_8cd7_13efb5566da7" ...
    name="diet_time" value="40" constant="false"/>
54 </listOfParameters>
55 <listOfInitialAssignments>
56 <initialAssignment ...
    symbol="mw6b754d96_d5ec_4c93_9c49_81a862fd99e3">
57 <math xmlns="http://www.w3.org/1998/Math/MathML">
58 <apply>
59 <divide/>
60 <apply>
61 <times/>
62 <cn> 0.6 </cn>
63 <ci> mwea9e5002_ae74_4804_8e16_0be189d41376 </ci>
64 </apply>
65 <apply>

```

```

66         <power/>
67         <ci> mw90c87dde_e0a8_4e05_afb2_29276061ec6c </ci>
68         <cn type="integer"> 2 </cn>
69     </apply>
70 </apply>
71 </math>
72 </initialAssignment>
73 <initialAssignment ...
74     symbol="mwf757b81c_acf1_42fc_8c71_e8e8477f9c35">
75 <math xmlns="http://www.w3.org/1998/Math/MathML">
76     <apply>
77         <minus/>
78         <apply>
79             <minus/>
80             <apply>
81                 <minus/>
82                 <ci> ...
83                     mwd655381f_5be7_40a6_9382_44a09fa2e4a9 </ci>
84                 <apply>
85                     <times/>
86                     <cn> 3.107 </cn>
87                     <ci> ...
88                         mwf1c0663d_1a61_4564_90c7_be0412eab4d1 ..
89                         </ci>
90                 </apply>
91             </apply>
92         </apply>
93     </apply>
94 <apply>
95     <times/>
96     <cn> 21.989 </cn>
97     <ci> ...
98         mwd216a905_5d4c_4f61_9571_9e3dcb45b108 </ci>
99 </apply>
100 </apply>
101 <apply>
102     <times/>
103     <apply>
104         <minus/>
105         <apply>
106             <times/>
107             <cn> 0.9 </cn>
108             <ci> mwc3955de4_7ac4_4f85_9eb3_
109                 ecf3c9b28b9c </ci>
110         </apply>
111     </apply>
112     <cn type="integer"> 1 </cn>
113 </apply>

```



```

106         <apply>
107             <plus/>
108             <apply>
109                 <times/>
110                 <cn> 21.6 </cn>
111                 <ci> mwd216a905_5d4c_4f61_9571_
112                     9e3dcb45b108 </ci>
113             </apply>
114             <cn type="integer"> 370 </cn>
115         </apply>
116     </apply>
117 </math>
118 </initialAssignment>
119 <initialAssignment ...
120     symbol="mwbaef79cc5_8f27_4f2c_b2f7_3e62ae00c8b6">
121     <math xmlns="http://www.w3.org/1998/Math/MathML">
122         <apply>
123             <times/>
124             <cn> 0.2 </cn>
125             <apply>
126                 <plus/>
127                 <ci> mwf1c0663d_1a61_4564_90c7_be0412eab4d1 </ci>
128                 <ci> mwd216a905_5d4c_4f61_9571_9e3dcb45b108 </ci>
129             </apply>
130         </apply>
131     </math>
132 </initialAssignment>
133 <initialAssignment ...
134     symbol="mw0dfa195b_9ad7_4855_8857_ff396398cab1">
135     <math xmlns="http://www.w3.org/1998/Math/MathML">
136         <apply>
137             <plus/>
138             <ci> mwf1c0663d_1a61_4564_90c7_be0412eab4d1 </ci>
139             <ci> mwd216a905_5d4c_4f61_9571_9e3dcb45b108 </ci>
140         </apply>
141     </math>
142 </initialAssignment>
143 <initialAssignment ...
144     symbol="mw188ffe6b_491f_46b7_b33a_bbe49c5b175c">
145     <math xmlns="http://www.w3.org/1998/Math/MathML">
146         <ci> mwd216a905_5d4c_4f61_9571_9e3dcb45b108 </ci>
147     </math>
148 </initialAssignment>
149 <initialAssignment ...

```

```

148     symbol="mwea9e5002_ae74_4804_8e16_0be189d41376">
149     <math xmlns="http://www.w3.org/1998/Math/MathML">
150       <ci> mwd655381f_5be7_40a6_9382_44a09fa2e4a9 </ci>
151     </math>
152   </initialAssignment>
153 </listOfInitialAssignments>
154 <listOfRules>
155   <assignmentRule ...
156     variable="mwbefacf2e_0633_4509_b37a_67d3fb3abf08">
157     <math xmlns="http://www.w3.org/1998/Math/MathML">
158       <apply>
159         <times/>
160         <cn> 0.6 </cn>
161         <ci> mwea9e5002_ae74_4804_8e16_0be189d41376 </ci>
162       </apply>
163     </math>
164   </assignmentRule>
165   <assignmentRule ...
166     variable="mwfac7025f_6dcc_4606_a379_4fefb55a4c9c">
167     <math xmlns="http://www.w3.org/1998/Math/MathML">
168       <apply>
169         <times/>
170         <cn> 0.1 </cn>
171         <apply>
172           <minus/>
173           <ci> mwea9e5002_ae74_4804_8e16_0be189d41376 </ci>
174           <ci> mwd655381f_5be7_40a6_9382_44a09fa2e4a9 </ci>
175         </apply>
176       </apply>
177     </math>
178   </assignmentRule>
179   <assignmentRule ...
180     variable="mw4dd84072_9c69_4ea2_b6d1_4b3f7d60e34c">
181     <math xmlns="http://www.w3.org/1998/Math/MathML">
182       <apply>
183         <divide/>
184         <apply>
185           <plus/>
186           <ci> mwf757b81c_acf1_42fc_8c71_e8e8477f9c35 </ci>
187         </apply>
188       <times/>
189       <cn> 3.107 </cn>
190       <ci> ...
191         mwf1c0663d_1a61_4564_90c7_be0412eab4d1 </ci>
192     </apply>

```

```

188 <apply>
189   <times/>
190   <cn> 21.989 </cn>
191   <ci> ...
           mwd216a905_5d4c_4f61_9571_9e3dcb45b108 </ci>
192 </apply>
193 <apply>
194   <times/>
195   <apply>
196     <minus/>
197     <apply>
198       <times/>
199       <cn> 0.9 </cn>
200       <ci> mwc3955de4_7ac4_4f85_9eb3_
201         ecf3c9b28b9c </ci>
202     </apply>
203     <cn type="integer"> 1 </cn>
204   </apply>
205   <apply>
206     <plus/>
207     <apply>
208       <times/>
209       <cn> 21.6 </cn>
210       <ci> mwd216a905_5d4c_4f61_9571_
211         9e3dcb45b108 </ci>
212     </apply>
213     <cn type="integer"> 370 </cn>
214   </apply>
215 </apply>
216 <ci> mwfac7025f_6dcc_4606_a379_4fefb55a4c9c </ci>
217 <ci> mw11e3a509_3e54_42d4_9e04_8e8bf1141db5 </ci>
218 <apply>
219   <times/>
220   <apply>
221     <minus/>
222     <ci> ...
           mwea9e5002_ae74_4804_8e16_0be189d41376 ...
           </ci>
223   <apply>
224     <minus/>
225     <ci> mwbefacf2e_0633_4509_b37a_
226       67d3fb3abf08 </ci>
227   <apply>
228     <times/>
229     <ci> mw6b754d96_d5ec_4c93_9c49_

```

```

230         81a862fd99e3 </ci>
231     <apply>
232         <power/>
233         <ci> mw90c87dde_e0a8_4e05_afb2_
234             29276061ec6c </ci>
235         <cn type="integer"> 2 </cn>
236     </apply>
237 </apply>
238 </apply>
239 </apply>
240 <apply>
241     <plus/>
242     <apply>
243         <times/>
244         <cn> 0.1073 </cn>
245     <apply>
246         <divide/>
247         <cn type="integer"> 2 </cn>
248     <apply>
249         <plus/>
250         <cn type="integer"> 2 </cn>
251         <ci> mwf1c0663d_1a61_4564_90c7_
252             be0412eab4d1 </ci>
253     </apply>
254 </apply>
255 </apply>
256     <cn> 0.018987 </cn>
257 </apply>
258 </apply>
259 </apply>
260 <apply>
261     <plus/>
262     <cn type="integer"> 1 </cn>
263 <apply>
264     <times/>
265     <cn> 0.1073 </cn>
266 <apply>
267     <divide/>
268     <cn type="integer"> 2 </cn>
269 <apply>
270     <plus/>
271     <cn type="integer"> 2 </cn>
272     <ci> mwf1c0663d_1a61_4564_90c7_
273         be0412eab4d1 </ci>
274 </apply>

```

```

275         </apply>
276     </apply>
277     <cn> 0.018987 </cn>
278 </apply>
279 </apply>
280 </math>
281 </assignmentRule>
282 <rateRule ...
    variable="mw90c87dde_e0a8_4e05_afb2_29276061ec6c">
283 <math xmlns="http://www.w3.org/1998/Math/MathML">
284 <apply>
285 <divide/>
286 <apply>
287 <minus/>
288 <ci> mwbefacf2e_0633_4509_b37a_67d3fb3abf08 </ci>
289 <apply>
290 <times/>
291 <ci> ...
    mw6b754d96_d5ec_4c93_9c49_81a862fd99e3 </ci>
292 <apply>
293 <power/>
294 <ci> ...
    mw90c87dde_e0a8_4e05_afb2_29276061ec6c ...
    </ci>
295 <cn type="integer"> 2 </cn>
296 </apply>
297 </apply>
298 </apply>
299 <cn> 0.004 </cn>
300 </apply>
301 </math>
302 </rateRule>
303 <rateRule ...
    variable="mw11e3a509_3e54_42d4_9e04_8e8bf1141db5">
304 <math xmlns="http://www.w3.org/1998/Math/MathML">
305 <apply>
306 <divide/>
307 <apply>
308 <minus/>
309 <apply>
310 <times/>
311 <cn> 0.14 </cn>
312 <apply>
313 <minus/>
314 <ci> ...

```

```

315         mwea9e5002_ae74_4804_8e16_0be189d41376 ...
           </ci>
           <ci> ...
316             mwd655381f_5be7_40a6_9382_44a09fa2e4a9 ...
           </ci>
317         </apply>
318     </apply>
319     <ci> mw11e3a509_3e54_42d4_9e04_8e8bf1141db5 </ci>
320 </apply>
321 <cn type="integer"> 14 </cn>
322 </math>
323 </rateRule>
324 <rateRule ...
           variable="mwf1c0663d_1a61_4564_90c7_be0412eab4d1">
325 <math xmlns="http://www.w3.org/1998/Math/MathML">
326 <apply>
327 <minus/>
328 <apply>
329 <divide/>
330 <apply>
331 <times/>
332 <apply>
333 <minus/>
334 <cn type="integer"> 1 </cn>
335 <apply>
336 <divide/>
337 <cn type="integer"> 2 </cn>
338 <apply>
339 <plus/>
340 <cn type="integer"> 2 </cn>
341 <ci> mwf1c0663d_1a61_4564_90c7_
342     be0412eab4d1 </ci>
343 </apply>
344 </apply>
345 </apply>
346 <apply>
347 <minus/>
348 <apply>
349 <minus/>
350 <ci> mwea9e5002_ae74_4804_8e16_
351     0be189d41376 </ci>
352 <ci> mw4dd84072_9c69_4ea2_b6d1_
353     4b3f7d60e34c </ci>
354 </apply>

```

```

355         <apply>
356             <minus/>
357             <ci> mwbefacf2e_0633_4509_b37a_
358             67d3fb3abf08 </ci>
359         <apply>
360             <times/>
361             <ci> mw6b754d96_d5ec_4c93_9c49_
362             81a862fd99e3 </ci>
363         <apply>
364             <power/>
365             <ci> mw90c87dde_e0a8_4e05_afb2_
366             29276061ec6c </ci>
367             <cn type="integer"> 2 </cn>
368         </apply>
369     </apply>
370 </apply>
371 </apply>
372 </apply>
373 <cn> 9440.727 </cn>
374 </apply>
375 <apply>
376     <divide/>
377     <apply>
378         <times/>
379         <ci> ...
380             mw735bcb0c_a7eb_4741_a7c7_68d451695bb2 </ci>
381     <apply>
382         <divide/>
383         <apply>
384             <power/>
385             <ci> mwd216a905_5d4c_4f61_9571_
386             9e3dcb45b108 </ci>
387             <ci> mw0e5dd104_6c36_4d61_aaa0_
388             304495f4958d </ci>
389         </apply>
390     <apply>
391         <plus/>
392         <apply>
393             <power/>
394             <ci> mwd216a905_5d4c_4f61_9571_
395             9e3dcb45b108 </ci>
396             <ci> mw0e5dd104_6c36_4d61_aaa0_
397             304495f4958d </ci>
398         </apply>
399     </apply>

```

```

399         <power/>
400         <ci> mw7d93fe54_abc0_4168_be20_
401         b0c4cd50db7e </ci>
402         <ci> mw0e5dd104_6c36_4d61_aaa0_
403         304495f4958d </ci>
404     </apply>
405 </apply>
406 </apply>
407 <apply>
408     <divide/>
409     <cn type="integer"> 1 </cn>
410 <apply>
411     <plus/>
412     <cn type="integer"> 1 </cn>
413 <apply>
414     <power/>
415     <apply>
416         <divide/>
417         <ci> mwd216a905_5d4c_4f61_9571_
418         9e3dcb45b108 </ci>
419         <ci> mwbcae1952_7942_4e93_baa0_
420         602708e643ed </ci>
421     </apply>
422     <ci> mw3e8ac7b4_c93c_46d1_afa3_
423     0ffe81ac5fa9 </ci>
424 </apply>
425 </apply>
426 </apply>
427     <cn> 1816.444 </cn>
428 </apply>
429     <cn> 9440.727 </cn>
430 </apply>
431 </apply>
432 </math>
433 </rateRule>
434 <rateRule ...
      variable="mwd216a905_5d4c_4f61_9571_9e3dcb45b108">
435 <math xmlns="http://www.w3.org/1998/Math/MathML">
436     <apply>
437         <plus/>
438     <apply>
439         <divide/>
440     <apply>
441         <times/>
442     <apply>

```



```

443         <divide/>
444         <cn type="integer"> 2 </cn>
445         <apply>
446             <plus/>
447             <cn type="integer"> 2 </cn>
448             <ci> mwflc0663d_1a61_4564_90c7_
449                 be0412eab4d1 </ci>
450         </apply>
451     </apply>
452     <apply>
453         <minus/>
454         <apply>
455             <minus/>
456             <ci> mwea9e5002_ae74_4804_8e16_
457                 0be189d41376 </ci>
458             <ci> mw4dd84072_9c69_4ea2_b6d1_
459                 4b3f7d60e34c </ci>
460         </apply>
461         <apply>
462             <minus/>
463             <ci> mwbefacf2e_0633_4509_b37a_
464                 67d3fb3abf08 </ci>
465         <apply>
466             <times/>
467             <ci> mw6b754d96_d5ec_4c93_9c49_
468                 81a862fd99e3 </ci>
469         <apply>
470             <power/>
471             <ci> mw90c87dde_e0a8_4e05_afb2_
472                 29276061ec6c </ci>
473             <cn type="integer"> 2 </cn>
474         </apply>
475     </apply>
476 </apply>
477 </apply>
478 </apply>
479 <cn> 1816.444 </cn>
480 </apply>
481 <apply>
482     <times/>
483     <ci> mw735bcb0c_a7eb_4741_a7c7_68d451695bb2 </ci>
484 <apply>
485     <divide/>
486     <apply>
487         <power/>

```

```

488         <ci> mwd216a905_5d4c_4f61_9571_
489         9e3dcb45b108 </ci>
490         <ci> mw0e5dd104_6c36_4d61_aaa0_
491         304495f4958d </ci>
492     </apply>
493     <apply>
494         <plus/>
495         <apply>
496             <power/>
497             <ci> ...
498                 mwd216a905_5d4c_4f61_9571_9e3dcb45b108 ...
499                 </ci>
500             <ci> ...
501                 mw0e5dd104_6c36_4d61_aaa0_304495f4958d ...
502                 </ci>
503         </apply>
504     </apply>
505     <apply>
506         <power/>
507         <ci> mw7d93fe54_abc0_4168_be20_
508         b0c4cd50db7e </ci>
509         <ci> mw0e5dd104_6c36_4d61_aaa0_
510         304495f4958d </ci>
511     </apply>
512 </apply>
513 <apply>
514     <divide/>
515     <cn type="integer"> 1 </cn>
516     <apply>
517         <plus/>
518         <cn type="integer"> 1 </cn>
519     </apply>
520     <power/>
521     <apply>
522         <divide/>
523         <ci> mwd216a905_5d4c_4f61_9571_
524         9e3dcb45b108 </ci>
525         <ci> mwbcac1952_7942_4e93_baa0_
526         602708e643ed </ci>
527     </apply>
528     <ci> mw3e8ac7b4_c93c_46d1_afa3_
529     0ffe81ac5fa9 </ci>
530 </apply>
531 </apply>
532 </apply>

```

```

529         </apply>
530     </apply>
531 </math>
532 </rateRule>
533 <rateRule ...
    variable="mwba79cc5_8f27_4f2c_b2f7_3e62ae00c8b6">
534 <math xmlns="http://www.w3.org/1998/Math/MathML">
535     <apply>
536         <minus/>
537         <apply>
538             <times/>
539             <apply>
540                 <divide/>
541                 <cn type="integer"> 1 </cn>
542                 <cn> 3.22 </cn>
543             </apply>
544         <apply>
545             <minus/>
546             <ci> ...
                mw3f90ba7d_f81b_467e_a0a6_57941b3eb364 </ci>
547         <apply>
548             <times/>
549             <cn type="integer"> 3000 </cn>
550         <apply>
551             <minus/>
552             <ci> mwba79cc5_8f27_4f2c_b2f7_
553                 3e62ae00c8b6 </ci>
554             <apply>
555                 <times/>
556                 <cn> 0.2 </cn>
557                 <ci> mw0dfa195b_9ad7_4855_8857_
558                     ff396398cab1 </ci>
559             </apply>
560         </apply>
561     </apply>
562 </apply>
563 </math>
564 <math>
565     <times/>
566     <cn type="integer"> 4000 </cn>
567 <math>
568     <minus/>
569     <cn type="integer"> 1 </cn>
570 <math>
571     <divide/>

```

```

572         <ci> ...
           mwbefacf2e_0633_4509_b37a_67d3fb3abf08 ...
           </ci>
573     <apply>
574         <times/>
575         <cn> 0.6 </cn>
576         <ci> mwd655381f_5be7_40a6_9382_
577         44a09fa2e4a9 </ci>
578     </apply>
579 </apply>
580 </apply>
581 </apply>
582 </math>
583 </rateRule>
584 <rateRule ...
           variable="mw188ffe6b_491f_46b7_b33a_bbe49c5b175c">
585 <math xmlns="http://www.w3.org/1998/Math/MathML">
586     <apply>
587         <plus/>
588         <apply>
589             <minus/>
590             <apply>
591                 <times/>
592                 <apply>
593                     <divide/>
594                     <cn type="integer"> 1 </cn>
595                     <cn> 3.22 </cn>
596                 </apply>
597             </apply>
598             <apply>
599                 <minus/>
600                 <ci> ...
                   mw3f90ba7d_f81b_467e_a0a6_57941b3eb364 ...
                   </ci>
601             </apply>
602             <times/>
603             <cn type="integer"> 3000 </cn>
604         </apply>
605         <minus/>
606         <ci> mwba79cc5_8f27_4f2c_b2f7_
607         3e62ae00c8b6 </ci>
608     </apply>
609         <times/>
610         <cn> 0.2 </cn>
611         <ci> mw0dfa195b_9ad7_4855_8857_

```

```

612         ff396398cab1 </ci>
613     </apply>
614 </apply>
615 </apply>
616 </apply>
617 </apply>
618 <apply>
619     <times/>
620     <cn type="integer"> 4000 </cn>
621 </apply>
622     <minus/>
623     <cn type="integer"> 1 </cn>
624 </apply>
625     <divide/>
626     <ci> mwbefacf2e_0633_4509_b37a_
627     67d3fb3abf08 </ci>
628 </apply>
629     <times/>
630     <cn> 0.6 </cn>
631     <ci> mwd655381f_5be7_40a6_9382_
632     44a09fa2e4a9 </ci>
633 </apply>
634 </apply>
635 </apply>
636 </apply>
637 </apply>
638 <apply>
639     <divide/>
640 </apply>
641     <times/>
642 </apply>
643     <divide/>
644     <cn type="integer"> 2 </cn>
645 </apply>
646     <plus/>
647     <cn type="integer"> 2 </cn>
648     <ci> mwflc0663d_1a61_4564_90c7_
649     be0412eab4d1 </ci>
650 </apply>
651 </apply>
652 <apply>
653     <minus/>
654 </apply>
655     <minus/>
656     <ci> mwea9e5002_ae74_4804_8e16_

```

```

657         0be189d41376 </ci>
658         <ci> mw4dd84072_9c69_4ea2_b6d1_
659         4b3f7d60e34c </ci>
660     </apply>
661     <apply>
662         <minus/>
663         <ci> mwbefacf2e_0633_4509_b37a_
664         67d3fb3abf08 </ci>
665     <apply>
666         <times/>
667         <ci> mw6b754d96_d5ec_4c93_9c49_
668         81a862fd99e3 </ci>
669     <apply>
670         <power/>
671         <ci> mw90c87dde_e0a8_4e05_afb2_
672         29276061ec6c </ci>
673         <cn type="integer"> 2 </cn>
674     </apply>
675 </apply>
676 </apply>
677 </apply>
678 </apply>
679 <cn> 1816.444 </cn>
680 </apply>
681 <apply>
682     <times/>
683     <ci> mw735bcb0c_a7eb_4741_a7c7_68d451695bb2 </ci>
684 <apply>
685     <divide/>
686     <apply>
687         <power/>
688         <ci> ...
689             mwd216a905_5d4c_4f61_9571_9e3dcb45b108 ...
690         </ci>
691     <ci> ...
692             mw0e5dd104_6c36_4d61_aaa0_304495f4958d ...
693         </ci>
694 </apply>
695 <apply>
696     <plus/>
697     <apply>
698         <power/>
699         <ci> mwd216a905_5d4c_4f61_9571_
700         9e3dcb45b108 </ci>
701         <ci> mw0e5dd104_6c36_4d61_aaa0_

```

```

698         304495f4958d </ci>
699     </apply>
700     <apply>
701         <power/>
702         <ci> mw7d93fe54_abc0_4168_be20_
703         b0c4cd50db7e </ci>
704         <ci> mw0e5dd104_6c36_4d61_aaa0_
705         304495f4958d </ci>
706     </apply>
707 </apply>
708 </apply>
709 <apply>
710     <divide/>
711     <cn type="integer"> 1 </cn>
712 <apply>
713     <plus/>
714     <cn type="integer"> 1 </cn>
715 <apply>
716     <power/>
717     <apply>
718         <divide/>
719         <ci> mwd216a905_5d4c_4f61_9571_
720         9e3dcb45b108 </ci>
721         <ci> mwbae1952_7942_4e93_baa0_
722         602708e643ed </ci>
723     </apply>
724     <ci> mw3e8ac7b4_c93c_46d1_afa3_
725     0ffe81ac5fa9 </ci>
726 </apply>
727 </apply>
728 </apply>
729 </apply>
730 </math>
731 </rateRule>
732 </listOfRules>
733 <listOfEvents>
734     <event id="mw4a68a71c_d9aa_4767_818b_072f94eb6fe6" ...
735         name="event_1">
736     <trigger>
737         <math xmlns="http://www.w3.org/1998/Math/MathML">
738         <apply>
739             <geq/>
740             <csymbol encoding="text" definitionURL=
741             "http://www.sbml.org/sbml/symbols/time"> ...

```

```

742         time </csymbol>
743         <ci> mw58e7a6e9_b243_49f7_8cd7_13efb5566da7 </ci>
744     </apply>
745 </math>
746 </trigger>
747 <listOfEventAssignments>
748   <eventAssignment ...
749     variable="mwea9e5002_ae74_4804_8e16_0be189d41376">
750     <math xmlns="http://www.w3.org/1998/Math/MathML">
751       <apply>
752         <minus/>
753         <ci> ...
754           mwd655381f_5be7_40a6_9382_44a09fa2e4a9 </ci>
755         <ci> ...
756           mwdab98099_f37d_420e_8aa3_5ff8cd6dad8 </ci>
757       </apply>
758     </math>
759   </eventAssignment>
760 </listOfEventAssignments>
761 </event>
762 </listOfEvents>
763 </model>
764 </sbml>

```

A.2 Matlab code for Latin Hypercube Sampling

Code contained in this section is modified from code from Marino et al. [49]. Energy balance constants and initial conditions are those of the average NHANES male [41] given in Table 2.

A.2.1 ODE_LHS_NHANESmale.m (ODEs)

```

1 function du=ODE\_LHS\_NHANESmale(t,u,LHSmatrix,x,runs)
2 %% PARAMETERS %%
3
4 Parameter\_settings\_LHS\_NHANESmale;
5
6 PAL=LHSmatrix(x,1);

```



```

7 r=LHSmatrix(x,2);
8 a=LHSmatrix(x,3);
9 b=LHSmatrix(x,4);
10 c=LHSmatrix(x,5);
11 d=LHSmatrix(x,6);
12 dummy_LHS=LHSmatrix(x,7);
13
14 %%Input parameters%%
15 kG = 6960;
16 K = 778.0655;
17 EI0 = 2900;
18 Δ_sodium=0;
19 BW0=83.3;
20 diet = 800;
21 dietsteps = 8;
22
23 %example code to implement a weekly decrease in energy intake
24 %dietinc = diet/dietsteps;
25
26 % EI = NaN(size(t));
27 % % stopvar = floor(t./7);
28 % case1 = (t≤7*dietsteps);
29 % EI(case1) = EI0 - dietinc*floor(t(case1)/7);
30 % case2 = (7*dietsteps ≤t);
31 % EI(case2) = EI0-dietinc*floor((dietsteps*7)/7);
32
33 %constant energy intake
34 EI = EI0;
35 CI=0.6*EI;
36 RMR = 21.6*u(6)+370;
37
38 %thermic effect of feeding
39 TEF=.1*(EI-EI0);
40
41 %energy expenditure
42 EE=(K+3.107*u(3)+21.989*u(6)+(.9*PAL-1)*RMR+TEF+u(2)...
43 +(EI-(CI-kG*u(1)^2))*((.1073)*(2/(2+u(3)))...
44 +.018987))/(1+.1073*(2/(2+u(3)))+.018987);
45
46 %system of odes
47 %du(1) is dG/dt: glycogen storage
48 du(1)= (CI-kG*u(1)^2)/.004;
49 %du(2) is dAT/dt: adaptive thermogenesis);
50 du(2)=(.14*(EI-EI0)-u(2))/14;
51 %du(3) is dF/dt

```

```

52     du(3)=(1-2/(2+u(3)))*(EI-EE-(CI-kG*u(1)^2))/9440.727...
53     -r*((u(4)^a/(u(4)^(a+c^a)))*(1/(1+(u(4)/d)^b)));
54     %du(4) is dL/dt
55     du(4)=(2/(2+u(3)))*(EI-EE-(CI-kG*u(1)^2))/1816.444...
56     +r*((u(4)^a/(u(4)^(a+c^a)))*(1/(1+(u(4)/d)^b)));
57     %du(5) is dECF/dt
58     du(5) = (1/3.22)*(Δ_sodium-...
59     3000*(u(5)-0.2*BW0))-4000*(1-CI/(0.6*EI0));
60     %du(6) is dLBM/dt
61     du(6)=du(4)+du(5);
62     du=du';

```

A.2.2 Parameter_settings_LHS_NHANESmale.m (parameter baseline values and initial conditions)

```

1  % PARAMETER BASELINE VALUES
2
3  PAL=1.6;
4  r=0.01;
5  a=2;
6  b=10;
7  c=30;
8  d=65;
9  dummy_LHS=1;
10
11 % Parameter Labels
12 PRCC\_var={'PAL', 'r', ...
13           'a', 'b', 'c', 'd', 'dummy'}; %
14
15 %% TIME SPAN OF THE SIMULATION
16 t_end=365; % length of the simulations
17 tspan=(0:1:t_end); % time points where the output is ...
18           calculated
19           time_points=[84 730]; % time points of interest for the US ...
20           analysis
21
22 % INITIAL CONDITION FOR THE ODE MODEL
23 dG=0.5;
24 dAT=0;

```

```

23 dF=23.4;
24 dL=59.9-0.2*83.3;
25 dECF=0.2*83.3;
26 dLBM=59.9;

```

A.2.3 Model_LHS_NHANESmale.m (main file)

```

1
2 clear all;
3 close all;
4
5 %% Sample size N
6 runs=100;
7
8 %% LHS MATRIX %%
9 Parameter\_settings\_LHS\_NHANESmale;
10
11 PAL_LHS=LHS\_Call(1.6, PAL, 1.6, 0 ,runs,'unif'); % ...
    baseline = 10
12 r_LHS=LHS\_Call(1e-3, r,.1 , 0, runs,'unif'); % baseline = 3e-2
13 a_LHS=LHS\_Call(2,a,80, 0 ,runs,'unif'); % baseline = 2.4e-5
14 b_LHS=LHS\_Call(20, b,100, 0, runs,'unif'); % baseline = 3e-3
15 c_LHS= LHS\_Call(20 , c ,50 , 0 , runs , 'unif'); % ...
    baseline = 0.24
16 d_LHS=LHS\_Call(40,d,50, 0 ,runs,'unif'); % baseline = 1200
17 dummy_LHS=LHS\_Call(1,1,1e1, 0 ,runs,'unif'); % dummy parameter
18
19 %% LHS MATRIX and PARAMETER LABELS
20 LHSmatrix=[PAL_LHS r_LHS a_LHS b_LHS ...
21             c_LHS d_LHS dummy_LHS];
22
23 for x=1:runs %Run solution x times choosing different values
24     f=@ODE\_LHS\_NHANESmale;
25     x;
26     LHSmatrix(x,:);
27     [t,u]=ode15s(@(t,u) f(t,u,LHSmatrix,x,runs),tspan,u0,[]);
28     A=[t u]; % [time u]
29     %% Save the outputs at ALL time points [tspan]
30     T_RT(:,x)=A(:,1);
31     G_RT(:,x)=A(:,2);

```

```

32     AT_RT(:,x)=A(:,3);
33     F_RT(:,x)=A(:,4);
34     L_RT(:,x)=A(:,5);
35     ECF_RT(:,x)=A(:,6);
36     LBM_RT(:,x)=A(:,7);
37
38     %% Save only the outputs at the time points of ...
39     interest [time_points]:
40     %% MORE EFFICIENT
41     %     G(:,x)=A(time_points+1,1);
42     %     AT_lhs(:,x)=A(time_points+1,2);
43     %     F_lhs(:,x)=A(time_points+1,3);
44     %     L_lhs(:,x)=A(time_points+1,4);
45 end
46 %% Save the workspace
47 save Model_RT_PRCC.mat;
48 % CALCULATE PRCC
49 [prcc sign ...
    sign_label]=PRCC(LHSmatrix,L_RT,1:length(time_points),...
    PRCC_var,0.1);

```

A.2.4 LHS_Call.m (LHS algorithm file)

```

1 function ...
2     s=LHS\_Call(xmin,xmean,xmax,xsd,nsample,distrib,threshold)
3 % s=latin_hs(xmean,xsd,nsample,nvar)
4 % LHS from normal distribution, no correlation
5 % method of Stein
6 % Stein, M. 1987. Large Sample Properties of Simulations ...
7     Using Latin Hypercube Sampling.
8 %     Technometrics 29:143-151
9
10 if nsample==1
11     s=xmean;
12     return
13 end
14 if nargin<7
15     threshold=1e20;
16 end

```

```

16 [sample,nvar]=size(xmean);
17 if distrib == 'norm' % you only need to specify xmean & xsd
18     ran=rand(nsample,nvar);
19     s=zeros(nsample,nvar);
20     %method of Stein
21     for j=1: nvar
22         idx=randperm(nsample);
23         P=(idx'-ran(:,j))/nsample; % probability of ...
24         s(:,j) = xmean(j) + ltqnorm(P).* xsd(j); % this ...
25         % can be replaced by any inverse distribution function
26     end
27 end
28
29 if distrib == 'unif' % you only need to specify xmin & xmax
30     if xmin==0
31         xmin=1e-300;
32     end
33     nvar=length(xmin);
34     ran=rand(nsample,nvar);
35     s=zeros(nsample,nvar);
36     for j=1: nvar
37         idx=randperm(nsample);
38         P=(idx'-ran(:,j))/nsample;
39         xmax(j);
40         xmin(j);
41         xmax(j)/xmin(j);
42         if (xmax(j)<1 & xmin(j)<1) || (xmax(j)>1 & xmin(j)>1)
43             'SAME RANGE';
44             if (xmax(j)/xmin(j))<threshold %% It uses the ...
45                 log scale if the order of magnitude of ...
46                 [xmax-xmin] is bigger than threshold
47                 '<1e3: LINEAR SCALE';
48                 s(:,j) = xmin(j) + P.* (xmax(j)-xmin(j));
49             else
50                 '>1e3: LOG SCALE';
51                 s(:,j) = log(xmin(j)) + ...
52                     P.*abs(abs(log(xmax(j)))-abs(log(xmin(j))));
53                 s(:,j) = exp(s(:,j));
54             end
55         else
56             'e- to e+';
57             if (xmax(j)/xmin(j))<threshold %% It uses the ...
58                 log scale if the order of magnitude of ...

```

```

55         [xmax-xmin] is bigger than threshold
56         '<1e3: LINEAR SCALE';
57         s(:,j) = xmin(j) + P.* (xmax(j)-xmin(j));
58     else
59         '≥1e3: LOG SCALE';
60         s(:,j) = log(xmin(j)) + ...
61             P.*abs(log(xmax(j))-log(xmin(j)));
62         s(:,j) = exp(s(:,j));
63     end
64 end
65 %hist(s)    % plots the histogram of the pdf

```

Appendix B

MATLAB CODE FOR THE OPTIMAL CONTROL PROBLEM

```
1 function y = optdiet_payoff(params,init,T,A,B)
2 % example inputs:
3     %params=[1.5,0.25,9,77,66,74];
4     %init(initial conditions)=[27.2,72.8,3024];
5     %T(end time)=84;
6     %A(weight on fat loss in objective functional)=100;
7     %B(weight on lean mass maximization at final time in ...
8         objective functional)=100;
9
10 %constants
11 C=2;
12 beta_TEF=.1;
13 rho_L=1816.444;
14 rho_F=9440.727;
15 eta_L=229.4169;
16 eta_F=1028.903;
17 gamma_L=21.989;
18 gamma_F=3.107;
19
20 %params
21 PAL=params(1);
22 r = params(2);
23 a = params(3);
24 b = params(4);
25 c=params(5);
26 d=params(6);
27
28 %functions
29 F0 = init(1);
30 L0 = init(2);
31 EI0 = init(3);
32 K = EI0-3.107*F0-21.989*L0-(0.9*PAL-1)*(21.6*L0+370);
33
34 %optimality
```

```

34 test = -1;
35
36 Δ_test = 0.001;
37 N = 1000;
38 t = linspace(0,T,N+1);
39 h = T/N;
40 h2 = h/2;
41
42 F = zeros(1,N+1);
43 F(1) = init(1);
44 L = zeros(1,N+1);
45 L(1) = init(2);
46 EI = zeros(1,N+1);
47 EI(1) = init(3);
48
49 lambda1 = zeros(1,N+1);
50 lambda2 = zeros(1,N+1);
51 lambda2(N+1) = -B;
52 lambda3 = zeros(1,N+1);
53
54 u = zeros(1,N+1);
55 %%
56
57 while(test < 0)
58     oldu = u;
59     oldF= F;
60     oldL= L;
61     oldEI=EI;
62     oldlambda1 = lambda1;
63     oldlambda2 = lambda2;
64     oldlambda3 = lambda3;
65
66
67     for i = 1:N
68
69
70         k11 = (1-C/(C+F(i))) * (EI(i) - (K+gamma_F*F(i)+...
71         gamma_L*L(i) + ((1-beta_TEF)*PAL-1) * (21.6*L(i) ...
72         +370)+beta_TEF*(EI(i)-EI0) ...
73         +EI(i) * (C/(C+F(i)) * eta_L/rho_L+...
74         (1-C/(C+F(i))) * eta_F/rho_F)) / (1+C/(C+...
75         F(i)) * eta_L/rho_L + (1-C/(C+F(i))) * eta_F/rho_F)) / ...
76         9440.727-r * ((L(i)^a / (L(i)^a+c^a)) * (1/(1+...
77         (L(i)/d)^b))) * 1816.444/9440.727;
78

```



```

79      k12 = C/(C+F(i))* (EI(i)-(K+gamma_F*F(i)+...
80      gamma_L*L(i)+((1-beta_TEF)*PAL-1)*(21.6*L(i)...
81      +370)+beta_TEF*(EI(i)-EI0)+EI(i)*(C/(C+...
82      F(i))*eta_L/rho_L+(1-C/(C+F(i)))*eta_F/rho_F))/...
83      (1+C/(C+F(i))*eta_L/rho_L+(1-C/(C+F(i)))*...
84      eta_F/rho_F))/1816.444+r*((L(i)^a/(L(i)^a+...
85      c^a))*(1/(1+(L(i)/d)^b)));
86
87      k13=-u(i);
88
89      k21 = (1-C/(C+(F(i)+h2*k11)))*((EI(i)+h2*k13)-...
90      (K+gamma_F*(F(i)+h2*k11)+gamma_L*(L(i)+h2*k12)+...
91      ((1-beta_TEF)*PAL-1)*(21.6*(L(i)+h2*k12)+370)+...
92      beta_TEF*((EI(i)+h2*k13)-EI0)+(EI(i)+h2*k13)*...
93      (C/(C+(F(i)+h2*k11))*eta_L/rho_L+(1-C/(C+(F(i)+...
94      h2*k11))*eta_F/rho_F))/(1+C/(C+(F(i)+h2*k11))*...
95      eta_L/rho_L+(1-C/(C+(F(i)+h2*k11)))*...
96      eta_F/rho_F))/9440.727-r*((L(i)+h2*k12)^a/...
97      ((L(i)+h2*k12)^a+c^a))*(1/(1+((L(i)+h2*k12)/...
98      d)^b))*1816.444/9440.727;
99
100     k22 = (C/(C+(F(i)+h2*k11)))*((EI(i)+h2*k13)-...
101     (K+gamma_F*(F(i)+h2*k11)+gamma_L*(L(i)+h2*k12)+...
102     ((1-beta_TEF)*PAL-1)*(21.6*(L(i)+h2*k12)+370)+...
103     beta_TEF*((EI(i)+h2*k13)-EI0)+(EI(i)+h2*k13)*...
104     (C/(C+(F(i)+h2*k11))*eta_L/rho_L+(1-C/(C+(F(i)+...
105     h2*k11))*eta_F/rho_F))/(1+C/(C+(F(i)+h2*k11))*...
106     eta_L/rho_L+(1-C/(C+(F(i)+h2*k11)))*...
107     eta_F/rho_F))/1816.444+r*((L(i)+h2*k12)^a/...
108     ((L(i)+h2*k12)^a+c^a))*(1/(1+((L(i)+...
109     h2*k12)/d)^b)));
110
111     k23 = -0.5*(u(i)+u(i+1));
112
113     k31 = (1-C/(C+(F(i)+h2*k21)))*((EI(i)+h2*k23)-...
114     (K+gamma_F*(F(i)+h2*k21)+gamma_L*(L(i)+h2*k22)+...
115     ((1-beta_TEF)*PAL-1)*(21.6*(L(i)+h2*k22)+370)+...
116     beta_TEF*((EI(i)+h2*k23)-EI0)+(EI(i)+h2*k23)*...
117     (C/(C+(F(i)+h2*k21))*eta_L/rho_L+(1-C/(C+...
118     (F(i)+h2*k21))*eta_F/rho_F))/(1+C/(C+(F(i)+...
119     h2*k21))*eta_L/rho_L+(1-C/(C+(F(i)+h2*k21)))*...
120     eta_F/rho_F))/9440.727-r*((L(i)+h2*k22)^a/...
121     ((L(i)+h2*k22)^a+c^a))*(1/(1+((L(i)+h2*k22)/...
122     d)^b))*1816.444/9440.727;
123

```

```

124     k32 = (C/(C+(F(i)+h2*k21)))*(EI(i)+h2*k23)-...
125     (K+gamma_F*(F(i)+h2*k21)+gamma_L*(L(i)+...
126     h2*k22)+(1-beta_TEF)*PAL-1)*(21.6*(L(i)+...
127     h2*k22)+370)+beta_TEF*(EI(i)+h2*k23)-EI0)...
128     +(EI(i)+h2*k23)*(C/(C+(F(i)+h2*k21))*eta_L/...
129     rho_L+(1-C/(C+(F(i)+h2*k21))*eta_F/rho_F))/...
130     (1+C/(C+(F(i)+h2*k21))*eta_L/rho_L+(1-C/(C+...
131     (F(i)+h2*k21))*eta_F/rho_F))/1816.444+r*...
132     (((L(i)+h2*k22)^a/((L(i)+h2*k22)^a+c^a))*...
133     (1/(1+((L(i)+h2*k22)/d)^b)));
134
135     k33 = -0.5*(u(i)+u(i+1));
136
137     k41 = (1-C/(C+(F(i)+h2*k31)))*(EI(i)+h2*k33)-...
138     (K+gamma_F*(F(i)+h2*k31)+gamma_L*(L(i)+...
139     h2*k32)+(1-beta_TEF)*PAL-1)*(21.6*(L(i)+...
140     h2*k32)+370)+beta_TEF*(EI(i)+h2*k33)-EI0)...
141     +(EI(i)+h2*k33)*(C/(C+(F(i)+h2*k31))*eta_L/...
142     rho_L+(1-C/(C+(F(i)+h2*k31))*eta_F/rho_F))/...
143     (1+C/(C+(F(i)+h2*k31))*eta_L/rho_L+(1-C/(C+...
144     (F(i)+h2*k31))*eta_F/rho_F))/9440.727-r*...
145     (((L(i)+h2*k32)^a/((L(i)+h2*k32)^a+c^a))*...
146     (1/(1+((L(i)+h2*k32)/d)^b)))*1816.444/9440.727;
147
148     k42 = (C/(C+(F(i)+h2*k31)))*(EI(i)+h2*k33)-...
149     (K+gamma_F*(F(i)+h2*k31)+gamma_L*(L(i)+...
150     h2*k32)+(1-beta_TEF)*PAL-1)*(21.6*(L(i)+...
151     h2*k32)+370)+beta_TEF*(EI(i)+h2*k33)-EI0)...
152     +(EI(i)+h2*k33)*(C/(C+(F(i)+h2*k31))*eta_L/...
153     rho_L+(1-C/(C+(F(i)+h2*k31))*eta_F/rho_F))/...
154     (1+C/(C+(F(i)+h2*k31))*eta_L/rho_L+(1-C/(C+...
155     (F(i)+h2*k31))*eta_F/rho_F))/1816.444+...
156     r*(((L(i)+h2*k32)^a/((L(i)+h2*k32)^a+c^a))*...
157     (1/(1+((L(i)+h2*k32)/d)^b)));
158
159     k43 = -u(i+1);
160
161     F(i+1) = F(i) + (h/6)*(k11 + 2*k21 + 2*k31 + k41);
162     L(i+1) = L(i) + (h/6)*(k12 + 2*k22 + 2*k32 + k42);
163     EI(i+1) = EI(i) + (h/6)*(k13 + 2*k23 + 2*k33 + k43);
164 end
165 %%
166
167 for i = 1:N
168     j = N + 2 - i;

```

```

169 k11 = -A-lambda1(j)*C*(EI(j)-(K+gamma_F*F(j)+...
170 gamma_L*L(j)+((1-beta_TEF)*PAL-1)*(21.6*L(j)+...
171 370)+beta_TEF*(EI0-EI(j))+EI(j)*(C*eta_L/((C+...
172 F(j))*rho_L)+(1-C/(C+F(j)))*eta_F/rho_F))/ (1+...
173 C*eta_L/((C+F(j))*rho_L)+(1-C/(C+F(j)))*...
174 eta_F/rho_F))/(rho_F*(C+F(j))^2)-lambda1(j)*...
175 (1-C/(C+F(j)))*(-gamma_F+EI(j)*(-C*eta_L/...
176 ((C+F(j))^2*rho_L)+C*eta_F/((C+F(j))^2*...
177 rho_F))/ (1+C*eta_L/((C+F(j))*rho_L)+(1-C/(C+...
178 F(j))*eta_F/rho_F)+(K+gamma_F*F(j)+gamma_L*...
179 L(j)+((1-beta_TEF)*PAL-1)*(21.6*L(j)+370)+...
180 beta_TEF*(EI0-EI(j))+EI(j)*(C*eta_L/((C+...
181 F(j))*rho_L)+(1-C/(C+F(j)))*eta_F/rho_F))*...
182 (-C*eta_L/((C+F(j))^2*rho_L)+C*eta_F/((C+...
183 F(j))^2*rho_F))/ (1+C*eta_L/((C+F(j))*...
184 rho_L)+(1-C/(C+F(j)))*eta_F/rho_F)^2)/rho_F...
185 +lambda2(j)*C*(EI(j)-(K+gamma_F*F(j)+...
186 gamma_L*L(j)+((1-beta_TEF)*PAL-1)*(21.6*...
187 L(j)+370)+beta_TEF*(EI0-EI(j))+EI(j)*(C*...
188 eta_L/((C+F(j))*rho_L)+(1-C/(C+F(j)))*...
189 eta_F/rho_F))/ (1+C*eta_L/((C+F(j))*rho_L)+...
190 (1-C/(C+F(j)))*eta_F/rho_F))/(rho_L*(C+...
191 F(j))^2)-lambda2(j)*C*(-(gamma_F+EI(j))*...
192 (-C*eta_L/((C+F(j))^2*rho_L)+C*eta_F/((C+...
193 F(j))^2*rho_F))/ (1+C*eta_L/((C+F(j))*...
194 rho_L)+(1-C/(C+F(j)))*eta_F/rho_F)+(K+...
195 gamma_F*F(j)+gamma_L*L(j)+((1-beta_TEF)*...
196 PAL-1)*(21.6*L(j)+370)+beta_TEF*(EI0-...
197 EI(j))+EI(j)*(C*eta_L/((C+F(j))*rho_L)+...
198 (1-C/(C+F(j)))*eta_F/rho_F))*(-C*eta_L/...
199 ((C+F(j))^2*rho_L)+C*eta_F/((C+F(j))^2*...
200 rho_F))/ (1+C*eta_L/((C+F(j))*rho_L)+...
201 (1-C/(C+F(j)))*eta_F/rho_F)^2)/(rho_L*(C+F(j)));
202
203 k12 = B+lambda1(j)*(1-C/(C+F(j)))*(gamma_L+...
204 21.6*(1-beta_TEF)*PAL-21.6)/(rho_F*(1+C*...
205 eta_L/((C+F(j))*rho_L)+(1-C/(C+F(j)))*...
206 eta_F/rho_F))+lambda1(j)*r*L(j)^a*a/(rho_F*...
207 L(j)*(L(j)^a+c^a)*(1+(L(j)/d)^b))-...
208 lambda1(j)*r*(L(j)^a)^2*a/(rho_F*(L(j)^a+...
209 c^a)^2*(1+(L(j)/d)^b)*L(j))-lambda1(j)*r*...
210 L(j)^a*(L(j)/d)^b*b/(rho_F*(L(j)^a+c^a))*...
211 (1+(L(j)/d)^b)^2*L(j))+lambda2(j)*C*(gamma_L...
212 +21.6*(1-beta_TEF)*PAL-21.6)/(rho_L*(C+...
213 F(j))*(1+C*eta_L/((C+F(j))*rho_L)+(1-C/(C+...

```

```

214 F(j)) *eta_F/rho_F) -lambda2(j) *r*L(j)^a*a/...
215 (rho_L*L(j) * (L(j)^a+c^a) * (1+(L(j)/d)^b) +...
216 lambda2(j) *r* (L(j)^a)^2*a/(rho_L*(L(j)^a+...
217 c^a)^2*(1+(L(j)/d)^b)*L(j)) +lambda2(j) *r*...
218 L(j)^a*(L(j)/d)^b*b/(rho_L*(L(j)^a+c^a)*...
219 (1+(L(j)/d)^b)^2*L(j));
220
221 k13=-lambda1(j) * (1-C/(C+F(j))) * (1-(-beta_TEF+...
222 C*eta_L/((C+F(j))*rho_L) + (1-C/(C+F(j))) *eta_F/...
223 rho_F)/(1+C*eta_L/((C+F(j))*rho_L) + (1-C/(C+...
224 F(j)) *eta_F/rho_F))/rho_F -lambda2(j) *C*(1-...
225 (-beta_TEF+C*eta_L/((C+F(j))*rho_L) + (1-C/(C+...
226 F(j)) *eta_F/rho_F)/(1+C*eta_L/((C+F(j))*...
227 rho_L) + (1-C/(C+F(j))) *eta_F/rho_F))/(rho_L*...
228 (C+F(j)));
229
230 k21 = -A-(lambda1(j) -h2*k11) *C*((0.5*(EI(j)+...
231 EI(j-1)) - (K+gamma_F*(0.5*(F(j)+F(j-1)))) +...
232 gamma_L*(0.5*(L(j)+L(j-1)))) + ((1-beta_TEF)*...
233 PAL-1) * (21.6*(0.5*(L(j)+L(j-1)))+370) ...
234 +beta_TEF*(EI0-(0.5*(EI(j)+EI(j-1)))) + (0.5*...
235 (EI(j)+EI(j-1))) * (C*eta_L/((C+(0.5*(F(j)+...
236 F(j-1)))) *rho_L) + (1-C/(C+(0.5*(F(j)+...
237 F(j-1)))) *eta_F/rho_F))/(1+C*eta_L/((C+...
238 (0.5*(F(j)+F(j-1)))) *rho_L) + (1-C/(C+(0.5*...
239 (F(j)+F(j-1)))) *eta_F/rho_F))/(rho_F*(C+...
240 (0.5*(F(j)+F(j-1))))^2) - (lambda1(j) -...
241 h2*k11) * (1-C/(C+(0.5*(F(j)+F(j-1)))) *...
242 (-gamma_F+(0.5*(EI(j)+EI(j-1)))) *...
243 (-C*eta_L/((C+(0.5*(F(j)+F(j-1))))^2*rho_L) +...
244 C*eta_F/((C+(0.5*(F(j)+F(j-1))))^2*rho_F)))/...
245 (1+C*eta_L/((C+(0.5*(F(j)+F(j-1)))) *rho_L) +...
246 (1-C/(C+(0.5*(F(j)+F(j-1)))) *eta_F/rho_F) +...
247 (K+gamma_F*(0.5*(F(j)+F(j-1)))+gamma_L*(0.5*...
248 (L(j)+L(j-1)))) + ((1-beta_TEF)*PAL-1) * (21.6*...
249 (0.5*(L(j)+L(j-1)))+370) +beta_TEF*(EI0-(0.5*...
250 (EI(j)+EI(j-1)))) + (0.5*(EI(j)+EI(j-1))) *...
251 (C*eta_L/((C+(0.5*(F(j)+F(j-1)))) *rho_L) +...
252 (1-C/(C+(0.5*(F(j)+F(j-1)))) *eta_F/rho_F)) *...
253 (-C*eta_L/((C+(0.5*(F(j)+F(j-1))))^2*rho_L) +...
254 C*eta_F/((C+(0.5*(F(j)+F(j-1))))^2*rho_F)))/...
255 (1+C*eta_L/((C+(0.5*(F(j)+F(j-1)))) *rho_L) +...
256 (1-C/(C+(0.5*(F(j)+F(j-1)))) *eta_F/...
257 rho_F)^2)/rho_F + (lambda2(j) -h2*k12) *C*((0.5*...
258 (EI(j)+EI(j-1)) - (K+gamma_F*(0.5*(F(j)+...

```

```

259 F(j-1))+gamma_L*(0.5*(L(j)+L(j-1)))+...
260 ((1-beta_TEF)*PAL-1)*(21.6*(0.5*(L(j)+...
261 L(j-1))+370)+beta_TEF*(EI0-(0.5*(EI(j)+...
262 EI(j-1))))+(0.5*(EI(j)+EI(j-1)))*(C*eta_L/...
263 ((C+(0.5*(F(j)+F(j-1))))*rho_L)+(1-C/(C+...
264 (0.5*(F(j)+F(j-1))))*eta_F/rho_F)/(1+C*...
265 eta_L/((C+(0.5*(F(j)+F(j-1))))*rho_L)+(1-...
266 C/(C+(0.5*(F(j)+F(j-1))))*eta_F/rho_F)/...
267 (rho_L*(C+(0.5*(F(j)+F(j-1))))^2)-...
268 (lambda2(j)-h2*k12)*C*(-(gamma_F+(0.5*...
269 (EI(j)+EI(j-1)))*(-C*eta_L/((C+(0.5*(F(j)+...
270 F(j-1))))^2*rho_L)+C*eta_F/((C+(0.5*(F(j)+...
271 F(j-1))))^2*rho_F))/(1+C*eta_L/((C+(0.5*...
272 (F(j)+F(j-1))))*rho_L)+(1-C/(C+(0.5*(F(j)+...
273 F(j-1))))*eta_F/rho_F)+(K+gamma_F*(0.5*...
274 (F(j)+F(j-1))+gamma_L*(0.5*(L(j)+L(j-1)))+...
275 ((1-beta_TEF)*PAL-1)*(21.6*(0.5*(L(j)+...
276 L(j-1))+370)+beta_TEF*(EI0-(0.5*(EI(j)+...
277 EI(j-1))))+(0.5*(EI(j)+EI(j-1)))*(C*eta_L/...
278 ((C+(0.5*(F(j)+F(j-1))))*rho_L)+(1-C/(C+...
279 (0.5*(F(j)+F(j-1))))*eta_F/rho_F)*(-C*...
280 eta_L/((C+(0.5*(F(j)+F(j-1))))^2*rho_L)+...
281 C*eta_F/((C+(0.5*(F(j)+F(j-1))))^2*rho_F))...
282 /((1+C*eta_L/((C+(0.5*(F(j)+F(j-1))))*rho_L)+...
283 (1-C/(C+(0.5*(F(j)+F(j-1))))*eta_F/...
284 rho_F)^2)/(rho_L*(C+(0.5*(F(j)+F(j-1)))));
285
286 k22 = B+(lambda1(j)-h2*k11)*(1-C/(C+0.5*(F(j)+...
287 F(j-1)))*(gamma_L+21.6*(1-beta_TEF)*PAL-21.6)/...
288 (rho_F*(1+C*eta_L/((C+0.5*(F(j)+F(j-1))))*rho_L)...
289 +(1-C/(C+0.5*(F(j)+F(j-1))))*eta_F/rho_F))+...
290 (lambda1(j)-h2*k11)*r*0.5*(L(j)+L(j-1))^a*...
291 a/(rho_F*0.5*(L(j)+L(j-1))*(0.5*(L(j)+...
292 L(j-1))^a+c^a)*(1+(0.5*(L(j)+L(j-1))/d)^b)-...
293 (lambda1(j)-h2*k11)*r*(0.5*(L(j)+L(j-1))^a)^2*...
294 a/(rho_F*(0.5*(L(j)+L(j-1))^a+c^a)^2*(1+...
295 (0.5*(L(j)+L(j-1))/d)^b)*0.5*(L(j)+...
296 L(j-1))-(lambda1(j)-h2*k11)*r*0.5*(L(j)+...
297 L(j-1))^a*(0.5*(L(j)+L(j-1))/d)^b*b/...
298 (rho_F*(0.5*(L(j)+L(j-1))^a+...
299 c^a)*(1+(0.5*(L(j)+L(j-1))/d)^b)^2*0.5*(L(j)...
300 +L(j-1)))+(lambda2(j)-h2*k12)*C*(gamma_L+21.6*...
301 (1-beta_TEF)*PAL-21.6)/(rho_L*(C+0.5*(F(j)+...
302 F(j-1)))*(1+C*eta_L/((C+0.5*(F(j)+F(j-1))))*...
303 rho_L)+(1-C/(C+0.5*(F(j)+F(j-1))))*eta_F/...

```

```

304 rho_F))-(lambda2(j)-h2*k12)*r*0.5*(L(j)+...
305 L(j-1))^a*a/(rho_L*0.5*(L(j)+L(j-1))*(0.5*...
306 (L(j)+L(j-1))^a+c^a)*(1+(0.5*(L(j)+L(j-1))/...
307 d)^b)+(lambda2(j)-h2*k12)*r*(0.5*(L(j)+...
308 L(j-1))^a)^2*a/(rho_L*(0.5*(L(j)+L(j-1))^a+...
309 c^a)^2*(1+(0.5*(L(j)+L(j-1))/d)^b)*0.5*(L(j)...
310 +L(j-1)))+(lambda2(j)-h2*k12)*r*0.5*(L(j)+...
311 L(j-1))^a*(0.5*(L(j)+L(j-1))/d)^b*b/(rho_L*...
312 (0.5*(L(j)+L(j-1))^a+c^a)*(1+(0.5*(L(j)+...
313 L(j-1))/d)^b)^2*0.5*(L(j)+L(j-1)));
314
315 k23 = -(lambda1(j)-h2*k11)*(1-C/(C+0.5*(F(j)+...
316 F(j-1)))*(1-(-beta_TEF+C*eta_L/((C+0.5*(F(j)+...
317 F(j-1))*rho_L)+(1-C/(C+0.5*(F(j)+F(j-1))))*...
318 eta_F/rho_F)/(1+C*eta_L/((C+0.5*(F(j)+...
319 F(j-1))*rho_L)+(1-C/(C+0.5*(F(j)+F(j-1))))*...
320 eta_F/rho_F))/rho_F-(lambda2(j)-h2*k12)*C*...
321 (1-(-beta_TEF+C*eta_L/((C+0.5*(F(j)+F(j-1))*...
322 rho_L)+(1-C/(C+0.5*(F(j)+F(j-1))))*eta_F/...
323 rho_F)/(1+C*eta_L/((C+0.5*(F(j)+F(j-1))*...
324 rho_L)+(1-C/(C+0.5*(F(j)+F(j-1))))*eta_F/...
325 rho_F))/(rho_L*(C+0.5*(F(j)+F(j-1)))));
326
327
328 k31 =-A-(lambda1(j)-h2*k21)*C*((0.5*(EI(j)+...
329 EI(j-1)))-(K+gamma_F*(0.5*(F(j)+F(j-1)))+...
330 gamma_L*(0.5*(L(j)+L(j-1)))+(1-beta_TEF)*...
331 PAL-1)*(21.6*(0.5*(L(j)+L(j-1)))+370)...
332 +beta_TEF*(EI0-(0.5*(EI(j)+EI(j-1))))+...
333 (0.5*(EI(j)+EI(j-1)))*(C*eta_L/((C+(0.5*...
334 (F(j)+F(j-1))))*rho_L)+(1-C/(C+(0.5*(F(j)+...
335 F(j-1))))*eta_F/rho_F))/(1+C*eta_L/((C+...
336 (0.5*(F(j)+F(j-1))))*rho_L)+(1-C/(C+(0.5*...
337 (F(j)+F(j-1))))*eta_F/rho_F))/(rho_F*(C+...
338 (0.5*(F(j)+F(j-1))))^2)-(lambda1(j)-...
339 h2*k21)*(1-C/(C+(0.5*(F(j)+F(j-1)))))*...
340 (-gamma_F+(0.5*(EI(j)+EI(j-1)))*(-C*...
341 eta_L/((C+(0.5*(F(j)+F(j-1))))^2*rho_L)+...
342 C*eta_F/((C+(0.5*(F(j)+F(j-1))))^2*...
343 rho_F))/(1+C*eta_L/((C+(0.5*(F(j)...
344 +F(j-1))))*rho_L)+(1-C/(C+(0.5*(F(j)+...
345 F(j-1))))*eta_F/rho_F)+(K+gamma_F*...
346 (0.5*(F(j)+F(j-1)))+gamma_L*(0.5*(L(j)+...
347 L(j-1)))+(1-beta_TEF)*PAL-1)*(21.6*(0.5*...
348 (L(j)+L(j-1)))+370)+beta_TEF*(EI0-(0.5*...

```

```

349      (EI (j)+EI (j-1))) + (0.5*(EI (j)+EI (j-1))) *...
350      (C*eta_L/((C+(0.5*(F (j)+F (j-1))))*rho_L)+...
351      (1-C/(C+(0.5*(F (j)+F (j-1)))))*eta_F/rho_F))*...
352      (-C*eta_L/((C+(0.5*(F (j)+F (j-1))))^2*rho_L)+...
353      C*eta_F/((C+(0.5*(F (j)+F (j-1))))^2*rho_F))/...
354      (1+C*eta_L/((C+(0.5*(F (j)+F (j-1))))*rho_L)+...
355      (1-C/(C+(0.5*(F (j)+F (j-1)))))*eta_F/rho_F)^2)/...
356      rho_F+(lambda2 (j)-h2*k22)*C*((0.5*(EI (j)+...
357      EI (j-1)))-(K+gamma_F*(0.5*(F (j)+F (j-1)))+...
358      gamma_L*(0.5*(L (j)+L (j-1)))+(1-beta_TEF)*...
359      PAL-1)*(21.6*(0.5*(L (j)+L (j-1)))+370)+...
360      beta_TEF*(EI0-(0.5*(EI (j)+EI (j-1))))+(0.5*...
361      (EI (j)+EI (j-1)))*(C*eta_L/((C+(0.5*(F (j)+...
362      F (j-1))))*rho_L)+(1-C/(C+(0.5*(F (j)+...
363      F (j-1))))*eta_F/rho_F))/(1+C*eta_L/((C+...
364      (0.5*(F (j)+F (j-1))))*rho_L)+(1-C/(C+(0.5*...
365      (F (j)+F (j-1))))*eta_F/rho_F)/(rho_L*(C+...
366      (0.5*(F (j)+F (j-1))))^2)-(lambda2 (j)-h2*k22)*...
367      C*(-(gamma_F+(0.5*(EI (j)+EI (j-1))))*...
368      (-C*eta_L/((C+(0.5*(F (j)+F (j-1))))^2*rho_L)+...
369      C*eta_F/((C+(0.5*(F (j)+F (j-1))))^2*rho_F))/...
370      (1+C*eta_L/((C+(0.5*(F (j)+F (j-1))))*rho_L)+...
371      (1-C/(C+(0.5*(F (j)+F (j-1)))))*eta_F/rho_F)...
372      +(K+gamma_F*(0.5*(F (j)+F (j-1)))+gamma_L*...
373      (0.5*(L (j)+L (j-1)))+(1-beta_TEF)*PAL-1)*...
374      (21.6*(0.5*(L (j)+L (j-1)))+370)+beta_TEF*...
375      (EI0-(0.5*(EI (j)+EI (j-1))))+(0.5*(EI (j)+...
376      EI (j-1)))*(C*eta_L/((C+(0.5*(F (j)+...
377      F (j-1))))*rho_L)+(1-C/(C+(0.5*(F (j)+...
378      F (j-1))))*eta_F/rho_F))*(-C*eta_L/((C+...
379      (0.5*(F (j)+F (j-1))))^2*rho_L)+C*eta_F/...
380      ((C+(0.5*(F (j)+F (j-1))))^2*rho_F))...
381      /(1+C*eta_L/((C+(0.5*(F (j)+F (j-1))))*...
382      rho_L)+(1-C/(C+(0.5*(F (j)+F (j-1)))))*...
383      eta_F/rho_F)^2)/(rho_L*(C+(0.5*(F (j)+...
384      F (j-1)))));
385
386
387      k32 = B+(lambda1 (j)-h2*k21)*(1-C/(C+0.5*(F (j)+...
388      F (j-1))))*(gamma_L+21.6*(1-beta_TEF)*PAL-21.6)/...
389      (rho_F*(1+C*eta_L/((C+0.5*(F (j)+F (j-1))))*...
390      rho_L)+(1-C/(C+0.5*(F (j)+F (j-1))))*...
391      eta_F/rho_F)+(lambda1 (j)-h2*k21)*r*0.5*...
392      (L (j)+L (j-1))^a*a/(rho_F*0.5*(L (j)+...
393      L (j-1))*(0.5*(L (j)+L (j-1))^a+...

```

```

394      c^a) * (1 + (0.5 * (L(j) + L(j-1)) / d)^b)) - (lambda1(j) - ...
395      h2*k21) * r * (0.5 * (L(j) + L(j-1))^a)^2 * a / (rho_F * ...
396      (0.5 * (L(j) + L(j-1))^a + c^a)^2 * (1 + (0.5 * (L(j) + ...
397      L(j-1)) / d)^b) * 0.5 * (L(j) + L(j-1))) - (lambda1(j) - ...
398      h2*k21) * r * 0.5 * (L(j) + L(j-1))^a * (0.5 * (L(j) ...
399      + L(j-1)) / d)^b * b / (rho_F * (0.5 * (L(j) + L(j-1))^a + ...
400      c^a) * (1 + (0.5 * (L(j) + L(j-1)) / d)^b)^2 * 0.5 * (L(j) + ...
401      L(j-1))) + (lambda2(j) - h2*k22) * C * (gamma_L ...
402      + 21.6 * (1 - beta_TEF) * PAL - 21.6) / (rho_L * (C + 0.5 * ...
403      (F(j) + F(j-1))) * (1 + C * eta_L / ((C + 0.5 * (F(j) + ...
404      F(j-1))) * rho_L) + (1 - C / (C + 0.5 * (F(j) + F(j-1)))) * ...
405      eta_F / rho_F)) - (lambda2(j) - h2*k22) * ...
406      r * 0.5 * (L(j) + L(j-1))^a * a / (rho_L * 0.5 * (L(j) + ...
407      L(j-1)) * (0.5 * (L(j) + L(j-1))^a + c^a) * (1 + (0.5 * (L(j) ...
408      + L(j-1)) / d)^b)) + (lambda2(j) - h2*k22) * r * (0.5 * ...
409      (L(j) + L(j-1))^a)^2 * a / (rho_L * (0.5 * (L(j) + ...
410      L(j-1))^a + c^a)^2 * (1 + (0.5 * (L(j) ...
411      + L(j-1)) / d)^b) * 0.5 * (L(j) + L(j-1))) + (lambda2(j) ...
412      - h2*k22) * r * 0.5 * (L(j) + L(j-1))^a * (0.5 * (L(j) + ...
413      L(j-1)) / d)^b * b / (rho_L * (0.5 * (L(j) ...
414      + L(j-1))^a + c^a) * (1 + (0.5 * (L(j) + L(j-1)) / d)^b)^2 * ...
415      0.5 * (L(j) + L(j-1)));
416
417      k33 = -(lambda1(j) - h2*k21) * (1 - C / (C + 0.5 * (F(j) + ...
418      F(j-1)))) * (1 - (-beta_TEF + C * eta_L / ((C + 0.5 * ...
419      (F(j) + F(j-1))) * rho_L) + (1 - C / (C + 0.5 * (F(j) + ...
420      F(j-1)))) * eta_F / rho_F) / (1 + C * eta_L / ((C + 0.5 * ...
421      (F(j) + F(j-1))) * rho_L) + (1 - C / (C + 0.5 * (F(j) + ...
422      F(j-1)))) * eta_F / rho_F) / rho_F - (lambda2(j) - ...
423      h2*k22) * C * (1 - (-beta_TEF + C * eta_L / ((C + 0.5 * ...
424      (F(j) + F(j-1))) * rho_L) + (1 - C / (C + 0.5 * (F(j) + ...
425      F(j-1)))) * eta_F / rho_F) / (1 + C * eta_L / ((C + ...
426      0.5 * (F(j) + F(j-1))) * rho_L) + (1 - C / (C + 0.5 * ...
427      (F(j) + F(j-1)))) * eta_F / rho_F) / (rho_L * ...
428      (C + 0.5 * (F(j) + F(j-1)))));
429
430      k41 = -A - (lambda1(j) - h*k31) * C * (EI(j-1) - ...
431      (K + gamma_F * F(j-1) + gamma_L * L(j-1) + ((1 - ...
432      beta_TEF) * PAL - 1) * (21.6 * L(j-1) + 370) + ...
433      beta_TEF * (EI0 - EI(j-1)) + EI(j-1) * (C * eta_L / ...
434      ((C + F(j-1)) * rho_L) + (1 - C / (C + F(j-1)))) * ...
435      eta_F / rho_F) / (1 + C * eta_L / ((C + F(j-1)) * ...
436      rho_L) + (1 - C / (C + F(j-1))) * eta_F / rho_F) / ...
437      (rho_F * (C + F(j-1))^2 - (lambda1(j) - h*k31) * ...
438      (1 - C / (C + F(j-1)))) * (- (gamma_F + EI(j-1)) * ...

```



```

439      (-C*eta_L/((C+F(j-1))^2*rho_L)+C*eta_F/...
440      ((C+F(j-1))^2*rho_F))/ (1+C*eta_L/((C+...
441      F(j-1))*rho_L)+(1-C/(C+F(j-1)))*eta_F/...
442      rho_F)+(K+gamma_F*F(j-1)+gamma_L*L(j-1)+...
443      ((1-beta_TEF)*PAL-1)*(21.6*L(j-1)+370)+...
444      beta_TEF*(EI0-EI(j-1))+EI(j-1)*(C*eta_L/...
445      ((C+F(j-1))*rho_L)+(1-C/(C+F(j-1)))*eta_F/...
446      rho_F))*(-C*eta_L/((C+F(j-1))^2*rho_L)...
447      +C*eta_F/((C+F(j-1))^2*rho_F))/ (1+C*eta_L/...
448      ((C+F(j-1))*rho_L)+(1-C/(C+F(j-1)))*eta_F/...
449      rho_F)^2)/rho_F+(lambda2(j)-h*k32)*C*...
450      (EI(j-1)-(K+gamma_F*F(j-1)+gamma_L*L(j-1)...
451      +((1-beta_TEF)*PAL-1)*(21.6*L(j-1)+370)+...
452      beta_TEF*(EI0-EI(j-1))+EI(j-1)*(C*eta_L/...
453      ((C+F(j-1))*rho_L)+(1-C/(C+F(j-1)))*...
454      eta_F/rho_F))/ (1+C*eta_L/((C+F(j-1))*rho_L)...
455      +(1-C/(C+F(j-1)))*eta_F/rho_F))/ (rho_L*...
456      (C+F(j-1))^2)-(lambda2(j)-h*k32)*C*...
457      (-gamma_F+EI(j-1))*(-C*eta_L/((C+...
458      F(j-1))^2*rho_L)+C*eta_F/((C+F(j-1))^2*...
459      rho_F))/ (1+C*eta_L/((C+F(j-1))*rho_L)...
460      +(1-C/(C+F(j-1)))*eta_F/rho_F)+(K+gamma_F*...
461      F(j-1)+gamma_L*L(j-1)+((1-beta_TEF)*PAL-1)*...
462      (21.6*L(j-1)+370)+beta_TEF*(EI0-EI(j-1))+...
463      EI(j-1)*(C*eta_L/((C+F(j-1))*rho_L)...
464      +(1-C/(C+F(j-1)))*eta_F/rho_F))*(-C*eta_L/...
465      ((C+F(j-1))^2*rho_L)+C*eta_F/((C+F(j-1))^2*...
466      rho_F))/ (1+C*eta_L/((C+F(j-1))*rho_L)+...
467      (1-C/(C+F(j-1)))*eta_F/rho_F)^2)/ (rho_L*...
468      (C+F(j-1)));
469
470      k42 = B+(lambda1(j)-h*k31)*(1-C/(C+F(j-1)))*...
471      (gamma_L+21.6*(1-beta_TEF)*PAL-21.6)/(rho_F*...
472      (1+C*eta_L/((C+F(j-1))*rho_L)+(1-C/(C+...
473      F(j-1)))*eta_F/rho_F))+ (lambda1(j)-h*k31)*r*...
474      L(j-1)^a*a/(rho_F*L(j-1)*(L(j-1)^a+c^a)*(1+...
475      (L(j-1)/d)^b))- (lambda1(j)-h*k31)*r*...
476      (L(j-1)^a)^2*a/(rho_F*(L(j-1)^a+c^a)^2*(1+...
477      (L(j-1)/d)^b)*L(j-1))- (lambda1(j)-h*k31)*r*...
478      L(j-1)^a*(L(j-1)/d)^b*b/(rho_F*(L(j-1)^a+...
479      c^a)*(1+(L(j-1)/d)^b)^2*L(j-1))...
480      +(lambda2(j)-h*k32)*C*(gamma_L+21.6*(1-...
481      beta_TEF)*PAL-21.6)/(rho_L*(C+F(j-1))*(1+C*...
482      eta_L/((C+F(j-1))*rho_L)+(1-C/(C+F(j-1)))*...
483      eta_F/rho_F))- (lambda2(j)-h*k32)*r*L(j-1)^a*...

```

```

484     a/(rho_L*L(j-1)*(L(j-1)^a+c^a)*(1+(L(j-1)/...
485     d)^b)+(lambda2(j)-h*k32)*r*(L(j-1)^a)^2*a/...
486     (rho_L*(L(j-1)^a+c^a)^2*(1+(L(j-1)/d)^b)*...
487     L(j-1)+(lambda2(j)-h*k32)*r*L(j-1)^a*(L(j-1)/...
488     d)^b*b/(rho_L*(L(j-1)^a+c^a)*(1+(L(j-1)/...
489     d)^b)^2*L(j-1));
490
491     k43 = -(lambda1(j)-h*k31)*(1-C/(C+F(j-1)))*...
492     (1-(-beta_TEF+C*eta_L/((C+F(j-1))*rho_L)...
493     +(1-C/(C+F(j-1)))*eta_F/rho_F)/(1+C*eta_L/...
494     ((C+F(j-1))*rho_L)+(1-C/(C+F(j-1)))*...
495     eta_F/rho_F))/rho_F-(lambda2(j)-h*k32)*C*...
496     (1-(-beta_TEF+C*eta_L/((C+F(j-1))*rho_L)+...
497     (1-C/(C+F(j-1)))*eta_F/rho_F)/(1+C*...
498     eta_L/((C+F(j-1))*rho_L)+(1-C/(C+...
499     F(j-1)))*eta_F/rho_F))/(rho_L*(C+F(j-1)));
500
501     lambda1(j-1) = lambda1(j) - (h/6)*(k11 + 2*k21 + ...
502     2*k31 + k41);
503     lambda2(j-1) = lambda2(j) - (h/6)*(k12 + 2*k22 + ...
504     2*k32 + k42);
505     lambda3(j-1) = lambda3(j) - (h/6)*(k13 + 2*k23 + ...
506     2*k33 + k43);
507     end
508     %%
509
510     u1=3*lambda3;
511     u=0.5*(u1+oldu);
512
513     temp1=Δ_test*sum(abs(u))-sum(abs(oldu-u));
514     temp2=Δ_test*sum(abs(F))-sum(abs(oldF-F));
515     temp3=Δ_test*sum(abs(L))-sum(abs(oldL-L));
516     temp4=Δ_test*sum(abs(EI))-sum(abs(oldeI-EI));
517     temp5=Δ_test*sum(abs(lambda1))...
518     -sum(abs(olddlambd1-lambda1));
519     temp6=Δ_test*sum(abs(lambda2))...
520     -sum(abs(olddlambd2-lambda2));
521     temp7=Δ_test*sum(abs(lambda3))...
522     -sum(abs(olddlambd3-lambda3));
523     test=min(temp1,min(temp2,min(temp3,min(temp4,...
524     min(temp5,min(temp6,temp7))))));
525     end
526     y(1,:) = t;

```

```
526 y(2,:) = F;  
527 y(3,:) = L;  
528 y(4,:) = EI;  
529 y(5,:) = lambda1;  
530 y(6,:) = lambda2;  
531 y(7,:) = lambda3;  
532 y(8,:) = u;
```

Appendix C

PERITONITIS MODEL

C.1 Experimental data

Table 15. **Experimental data from mouse model of peritonitis.** At each time point, cells were harvested from a sample of n mice. Average cell counts for neutrophils (\bar{N}), M1 macrophages ($\bar{M1}$), and M2 macrophages ($\bar{M2}$) are given in units of (10^7) cells. Standard error of the mean for each cell type x is calculated as $\sigma_{\bar{x}} = \sigma_x/\sqrt{n}$.

Hours	n	\bar{N}	$\bar{M1}$	$\bar{M2}$	σ_N	$\sigma_{\bar{N}}$	σ_{M1}	$\sigma_{\bar{M1}}$	σ_{M2}	$\sigma_{\bar{M2}}$
16	8	0.868	0.835	0.214	0.316	0.112	0.311	0.110	0.063	0.022
20	8	0.798	0.834	0.266	0.302	0.107	0.322	0.114	0.136	0.048
24	8	1.034	1.106	0.380	0.363	0.128	0.388	0.137	0.145	0.051
40	5	0.653	0.816	0.349	0.378	0.169	0.499	0.223	0.244	0.109
48	8	0.800	0.890	0.457	0.350	0.124	0.396	0.140	0.245	0.087
72	4	0.600	0.625	0.409	0.425	0.213	0.396	0.180	0.106	0.053
96	8	0.185	0.083	0.174	0.109	0.039	0.033	0.012	0.112	0.040
120	8	0.076	0.035	0.081	0.055	0.019	0.022	0.008	0.067	0.024
144	8	0.146	0.0895	0.091	0.141	0.050	0.165	0.058	0.075	0.027
168	8	0.042	0.027	0.029	0.026	0.009	0.038	0.013	0.02	0.007

C.2 Code for the PottersWheel Matlab toolbox (model definition file)

Once this model is added to the PottersWheel toolbox in Matlab, it can also be exported in SBML format.

```

1 % PottersWheel model definition file
2
3 function m = m1m2_ode()
4
5 m = pwGetEmptyModel();
6
7 %% Meta information
8
9 m.name          = 'm1m2_ode';
10 m.description  = '';
11 m.authors      = {};
12 m.dates        = {'2019-03-17'};
13 m.modelFormat  = 3.0;
14
15 %% Default sampling time points
16 m.t = 0:0.01:10;
17
18 %% X - Dynamic variables
19 % m = pwAddX(m, *ID, *startValue, fitSetting, minValue, ...
20             maxValue, unit, compartment, name, description, ...
21             typeOfStartValue, designerProps, classname)
22 m = pwAddX(m, 'P' , 0.003, 'fix',    [],    [],    [],    ...
23             'comp_1', 'P' );
24 m = pwAddX(m, 'M1',    0, 'fix',    0,    [],    [],    ...
25             'comp_1', 'M1');
26 m = pwAddX(m, 'M2',    0, 'fix',    0,    [],    [],    ...
27             'comp_1', 'M2');
28 m = pwAddX(m, 'N' ,    0, 'fix',    0,    [],    [],    ...
29             'comp_1', 'N' );
30 m = pwAddX(m, 'AN',    0, 'fix',    0,    [],    [],    ...
31             'comp_1', 'AN');
32 m = pwAddX(m, 'B' , 1000, 'fix',    100, 10000,    [],    ...
33             'comp_1', 'B' );
34
35 %% K - Dynamic parameters
36 % m = pwAddK(m, *ID, *value, fitSetting, minValue, ...
37             maxValue, unit, name, description)
38 m = pwAddK(m, 'snr' , 16.4019920002305 , 'global', 10 ...
39             , 100 );
40 m = pwAddK(m, 'smr' , 21.4404 , 'fix' , 8 ...
41             , 100 );
42 m = pwAddK(m, 'umr' , 5.15642 , 'fix' , 5 ...
43             , 80 );
44 m = pwAddK(m, 'um1' , 6.82554344214172 , 'global', 1 ...

```

```

, 20 );
33 m = pwAddK(m, 'um2' , 8.27065197319285 , 'fix' , 1 ...
, 20 );
34 m = pwAddK(m, 'uan' , 1.30931317432207 , 'fix' , 1 ...
, 15 );
35 m = pwAddK(m, 'kmlm2', 8.61724199879709 , 'global', 0.1 ...
, 100 );
36 m = pwAddK(m, 'kmlp' , 1.00850022175004 , 'fix' , 1 ...
, 5 );
37 m = pwAddK(m, 'kmlm1', 0.000993236136020421, 'fix' , ...
0.0001, 5 );
38 m = pwAddK(m, 'km2m2', 1.59253772151022 , 'global', ...
0.001 , 5 );
39 m = pwAddK(m, 'kan' , 7.10822919836749 , 'fix' , 1 ...
, 30 );
40 m = pwAddK(m, 'knp' , 3.10009325649014 , 'global', ...
.001 , 50 );
41 m = pwAddK(m, 'kmlan', 0.997407471438622 , 'fix' , ...
0.001 , 5 );
42 m = pwAddK(m, 'kpg' , 35 , 'fix' , 10 ...
, 35 );
43 m = pwAddK(m, 'kpn' , 0.295024146368882 , 'fix' , ...
0.11 , 5 );
44 m = pwAddK(m, 'kpm' , 6.1103824249136 , 'fix' , 1 ...
, 10 );
45 m = pwAddK(m, 'unr' , 3.97753517990732 , 'fix' , 1 ...
, 10 );
46 m = pwAddK(m, 'n_inf', 0.156384088195465 , 'fix' , ...
0.01 , 5 );
47 m = pwAddK(m, 'kanm1', 2.89808017283302 , 'fix' , 0.1 ...
, 1000);
48 m = pwAddK(m, 'kanm2', 90.9575626487555 , 'global', 5 ...
, 1000);
49 m = pwAddK(m, 'km2m1', 0.117354199532277 , 'fix' , ...
0.01 , 1 );
50 m = pwAddK(m, 'kmln' , 0.025086814972565 , 'fix' , ...
0.01 , 5 );
51 m = pwAddK(m, 'p_inf', 0.003 , 'fix' , ...
1e-06 , 100 );
52 m = pwAddK(m, 'kb' , 10 , 'fix' , 0.5 ...
, 100 );
53 m = pwAddK(m, 'knan' , 0.607651029250834 , 'fix' , ...
0.0001, 5 );
54 m = pwAddK(m, 'kann' , 0.000600657675376788, 'fix' , ...
1e-06 , 0.01);

```

```

55 m = pwAddK(m, 'kc' , 0.0125, 'fix' , 1e-06 , 0.1);
56
57 %% O - Ordinary differential equations
58 % m = pwAddO(m, *ID, *rhs)
59 m = pwAddO(m, 'P' , ...
    'kpg*P*(1-P/(p_inf+B))-kpn*P*N-kpm*P*M1/(1+(N/n_inf)^2)...
60 -kpm*P*M2/(1+(N/n_inf)^2)');
61 m = pwAddO(m, 'M1' , ...
    'smr*(kmlp*P+kmln*N+kmlm1*M1+kmlan*uan*AN)/(umr...
62 +kmlp*P+kmln*N+kmlm1*M1+kmlan*uan*AN+km2m2*M2+sc)...
63 -um1*M1-kmlm2*kanm1*AN*M1/(1+(N/n_inf)^2)+km2m1*M2');
64 m = pwAddO(m, 'M2' , ...
    'smr*(km2m2*M2+kc)/(umr+kmlp*P+kmln*N+kmlm1*M1...
65 +kmlan*uan*AN+km2m2*M2+kc)-um2*M2+kmlm2*kanm1*AN*M1/(1...
66 +(N/n_inf)^2)-km2m1*M2');
67 m = pwAddO(m, 'N' , ...
    'snr*(knp*P+knan*uan*AN)/(unr+knp*P+knan*uan*AN)-kan*N');
68 m = pwAddO(m, 'AN' , 'kan*N-kanm1*AN*M1/(1+(N/n_inf)^2)...
69 -kanm2*AN*M2/(1+(N/n_inf)^2)-kann*N-uan*AN');
70 m = pwAddO(m, 'B' , '-kb*B*P');
71
72 %% C - Compartments
73 % m = pwAddC(m, *ID, *size, outside, spatialDim, name, ...
    unit, constant, designerProps, classname, description)
74 m = pwAddC(m, 'comp_1', 1);
75
76 %% Y - Observables
77 % m = pwAddY(m, *ID, *rhs, errorModelRhs, noiseType, unit, ...
    name, description, alternativeIDs, designerProps, classname)
78 m = pwAddY(m, 'N_obs' , 'N' );
79 m = pwAddY(m, 'M1_obs' , 'M1' );
80 m = pwAddY(m, 'M2_obs' , 'M2' );
81
82 %% Constraints
83 % m = pwAddCS(m, 'CS01', 'p_inf', '=', 'P(t==0)', 100);

```

C.3 XPP files

C.3.1 Simplified model used for numerical analysis of equilibria

,

```

1
2 #N as a function of AN
3 N=snr*knan*uan*AN/(kan*(unr+knan*uan*AN))
4
5 #Equations:
6 M1'=smr*km1m1*M1/(umr+km1m1*M1+km2m2*M2+kc)
7 -km1m2*kanm1*AN*M1/(1+(N/n_inf)^2)-um1*M1+km2m1*M2
8 M2'=smr*(km2m2*M2+kc)/(umr+km1m1*M1+km2m2*M2+kc)
9 +km1m2*kanm1*AN*M1/(1+(N/n_inf)^2)-um2*M2-km2m1*M2
10 AN'=kan*N-kanm1*AN*M1/(1+(N/n_inf)^2)
11 -kanm2*AN*M2/(1+(N/n_inf)^2)-kann*N-uan*AN
12
13 #Initial conditions
14 init M1=0, M2=0,AN=.5
15
16 #Parameters
17 par smr=21.4404,umr=5.15642,um1=6.83,um2=8.27065197319285
18 par km1m1=0.000993236136020421,km2m2=1.59
19 par km2m1=0.117354199532277,kc=0
20 par snr=16.4,knan=0.607,uan=1.309,unr=3.978,kan=7.108
21 par kanm1=2.898,kanm2=87.08,kann=0.001,n_inf=0.156,km1m2=8.281
22
23 #Numerics:
24 @ method=qrk, tol=0.0001, dt=0.01, total=45, bounds=10000000
25 @ xlo=0, xhi=12, ylo=0, yho=2
26 @ maxstore=10000000

```

C.3.2 Full model

```

1 #Parameters
2
3 par snr=15.88906,smr=21.4404,umr=5.156,um1=6.956,um2=8.27
4 par uan=1.309,km1m2=8.28,km1p=1.0085,km1m1=0.00099
5 par km2m2=1.624,kan=7.108,knp=3.703,km1an=0.997,kpg=35
6 par kpn=0.295,kpm=6.11,unr=3.9775,n_inf=0.156
7 par kanm1=2.898,kanm2=87.08,km2m1=0.117,km1n=0.025
8 par p_inf=0.003,kb=10,knan=0.608,kann=0.0006
9
10 # Inhibition functions
11 #f_i_M1 = M1/(1+(N/n_inf)^2)

```



```

12 #f_i_M2 = M2/(1+(N/n_inf)^2)
13
14 #Equations:
15 P'=kpg*P*(1-P/(p_inf+B))-kpn*P*N-kpm*P*M1/(1+(N/n_inf)^2)
16 -kpm*P*M2/(1+(N/n_inf)^2)
17 B'=-kb*B*P
18 M1'=(smr*(kmlp*P+kmln*N+kmlm1*M1+kmlan*uan*AN)/
19 (umr+kmlp*P+kmln*N+kmlm1*M1+kmlan*uan*AN
20 +km2m2*M2)-um1*M1-kmlm2*kanm1*AN*M1/(1+(N/n_inf)^2)+km2m1*M2
21 M2'=(smr*km2m2*M2/(umr+kmlp*P+kmln*N+kmlm1*M1+kmlan*uan*AN+
22 km2m2*M2)-um2*M2+kmlm2*kanm1*AN*M1/(1+(N/n_inf)^2)-km2m1*M2
23 N'=(knp*P+knan*uan*AN)/(unr+knp*P+knan*uan*AN)-kan*N
24 AN'=(kan*N-kanm1*AN*M1/(1+(N/n_inf)^2)
25 -kanm2*AN*M2/(1+(N/n_inf)^2)-kann*N-uan*AN
26 #Initial conditions
27 init P=0.003,B=1000,M1=0,M2=0,N=0,AN=0
28
29 #Numerics:
30 @ method=qrk, tol=0.0001, dt=0.01, total=100, bounds=10000000
31 @ xlo=0, xhi=12, ylo=0, yho=2
32 @ maxstore=10000000

```

Appendix D

SBML CODE FOR THE ATHEROSCLEROSIS MODEL

This .xml file in Systems Biology Markup Language (SBML) can be imported into the Matlab Simbiology toolbox [200] or any other SBML-compatible software package.

```
1 <?xml version="1.0" encoding="UTF-8"?>
2 <sbml xmlns="http://www.sbml.org/sbml/level2/version4" ...
   level="2" version="4">
3 <annotation>
4   <SimBiology xmlns="http://www.mathworks.com">
5     <Version Major="5" Minor="6" Point="0"/>
6   </SimBiology>
7 </annotation>
8 <model id="athero_1comp" name="athero_1comp">
9   <notes>
10    <body xmlns="http://www.w3.org/1999/xhtml">
11      <p>SBML model exported from PottersWheel on ...
        2019-03-26 09:07:01.</p>
12    <pre>
13      % PottersWheel model definition file
14
15      function m = athero_1comp()
16
17      m = pwGetEmptyModel();
18
19      %% Meta information
20
21      m.name          = &apos;athero_1comp&apos;;
22      m.description  = &apos;&apos;;
23      m.authors      = {};
24      m.dates        = {&apos;2018-11-21&apos;};
25      m.modelFormat = 3;
26
27      %% Default sampling time points
28      m.t = 0:0.01:80;
```

```

29
30 %% X - Dynamic variables
31 % m = pwAddX(m, *ID, *startValue, fitSetting, minValue, ...
    maxValue, unit, compartment, name, description, ...
    typeOfStartValue, designerProps, classname)
32 m = pwAddX(m, &apos;M_rb&apos;, 0.65, &apos;global&apos;, ...
    [], [], [], &apos;comp_1&apos;, ...
    &apos;M_rb&apos;, [] , [] , [] , ...
    &apos;protein.generic&apos;);
33 m = pwAddX(m, &apos;N_rb&apos;, 0.07, &apos;global&apos;, ...
    [], [], [], &apos;comp_1&apos;, ...
    &apos;N_rb&apos;, [] , [] , [] , ...
    &apos;protein.generic&apos;);
34 m = pwAddX(m, &apos;M1&apos;, 0, &apos;fix&apos;, ...
    0, [], [], &apos;comp_1&apos;, ...
    &apos;M1&apos;, [] , [] , [] , ...
    &apos;protein.generic&apos;);
35 m = pwAddX(m, &apos;M2&apos;, 0, &apos;fix&apos;, ...
    0, [], [], &apos;comp_1&apos;, ...
    &apos;M2&apos;, [] , [] , [] , ...
    &apos;protein.generic&apos;);
36 m = pwAddX(m, &apos;N&apos;, 0, &apos;fix&apos;, ...
    0, [], [], &apos;comp_1&apos;, &apos;N&apos;, ...
    , [] , [] , [] , ...
    &apos;protein.generic&apos;);
37 m = pwAddX(m, &apos;AN&apos;, 0, &apos;fix&apos;, ...
    0, [], [], &apos;comp_1&apos;, ...
    &apos;AN&apos;, [] , [] , [] , ...
    &apos;protein.generic&apos;);
38 m = pwAddX(m, &apos;L&apos;, 1, &apos;global&apos;, ...
    0, 1000, [], &apos;comp_1&apos;, &apos;L&apos;, ...
    , [] , [] , [] , ...
    &apos;protein.generic&apos;);
39 m = pwAddX(m, &apos;FC&apos;, 1e-06, &apos;fix&apos;, ...
    0, [], [], &apos;comp_1&apos;, ...
    &apos;FC&apos;, [] , [] , [] , ...
    &apos;protein.generic&apos;);
40 m = pwAddX(m, &apos;FC_A&apos;, 0, &apos;fix&apos;, ...
    0, [], [], &apos;comp_1&apos;, ...
    &apos;FC_A&apos;, [] , [] , [] , ...
    &apos;protein.generic&apos;);
41 m = pwAddX(m, &apos;C_f&apos;, 0, &apos;global&apos;, ...
    0, [], [], &apos;comp_1&apos;, ...
    &apos;C_f&apos;, [] , [] , [] , ...
    &apos;protein.generic&apos;);

```

```

42 m = pwAddX(m, &apos;C_e&apos; , 0, &apos;global&apos;, ...
    0, [], [], &apos;comp_1&apos;, ...
    &apos;C_e&apos; , [] , [] , [] , ...
    &apos;protein.generic&apos;);
43 m = pwAddX(m, &apos;A&apos; , 0, &apos;fix&apos; , ...
    0, [], [], &apos;comp_1&apos;, &apos;A&apos; ...
    , [] , [] , [] , ...
    &apos;protein.generic&apos;);
44
45
46 %% K - Dynamic parameters
47 % m = pwAddK(m, *ID, *value, fitSetting, minValue, ...
    maxValue, unit, name, description)
48 m = pwAddK(m, &apos;snrb&apos; , 1 , ...
    &apos;global&apos;, 10 , 100 );
49 m = pwAddK(m, &apos;smrb&apos; , 0.75 , ...
    &apos;global&apos;, 8 , 100 );
50 m = pwAddK(m, &apos;umrb&apos; , 1.4 , ...
    &apos;global&apos;, 5 , 80 );
51 m = pwAddK(m, &apos;um1&apos; , 6.82554 , ...
    &apos;global&apos;, 1 , 20 );
52 m = pwAddK(m, &apos;um2&apos; , 8.27065 , ...
    &apos;global&apos;, 1 , 20 );
53 m = pwAddK(m, &apos;uan&apos; , 1.30931 , ...
    &apos;global&apos;, 1 , 15 );
54 m = pwAddK(m, &apos;km1m2&apos; , 8.61724 , ...
    &apos;global&apos;, 0.1 , 100 );
55 m = pwAddK(m, &apos;km1m1&apos; , 0.000993236 , ...
    &apos;global&apos;, 0.0001, 5 );
56 m = pwAddK(m, &apos;km2m2&apos; , 1.59254 , ...
    &apos;global&apos;, 0.001 , 5 );
57 m = pwAddK(m, &apos;kan&apos; , 7.10822919836749 , ...
    &apos;fix&apos; , 1 , 30 );
58 m = pwAddK(m, &apos;km1an&apos; , 0.997407471438622 , ...
    &apos;fix&apos; , 0.001 , 5 );
59 m = pwAddK(m, &apos;unrb&apos; , 16.402 , ...
    &apos;global&apos;, 1 , 10 );
60 m = pwAddK(m, &apos;n_inf&apos; , 0.156384088195465 , ...
    &apos;fix&apos; , 0.01 , 5 );
61 m = pwAddK(m, &apos;kanm1&apos; , 2.89808017283302 , ...
    &apos;fix&apos; , 0.1 , 1000 );
62 m = pwAddK(m, &apos;kanm2&apos; , 90.9575626487555 , ...
    &apos;global&apos;, 5 , 1000 );
63 m = pwAddK(m, &apos;km2m1&apos; , 0.117354199532277 , ...
    &apos;fix&apos; , 0.01 , 1 );

```

```

64 m = pwAddK(m, &apos;km1n&apos; , 0.025086814972565 , ...
    &apos;fix&apos; , 0.01 , 5 );
65 m = pwAddK(m, &apos;knan&apos; , 0.607651029250834 , ...
    &apos;fix&apos; , 0.0001, 5 );
66 m = pwAddK(m, &apos;kann&apos; , 0.000600657675376788, ...
    &apos;fix&apos; , 1e-06 , 0.01 );
67 m = pwAddK(m, &apos;sc&apos; , 0.0125 , ...
    &apos;fix&apos; , 1e-06 , 0.1 );
68 m = pwAddK(m, &apos;rL&apos; , 0.001 , ...
    &apos;global&apos;, 1e-06 , 0.1 );
69 m = pwAddK(m, &apos;klm1&apos; , 1 , ...
    &apos;global&apos;, 1e-06 , 0.1 );
70 m = pwAddK(m, &apos;klm2&apos; , 1 , ...
    &apos;global&apos;, 1e-06 , 0.1 );
71 m = pwAddK(m, &apos;kafc&apos; , 100000000000 , ...
    &apos;global&apos;, 1e-06 , 0.1 );
72 m = pwAddK(m, &apos;ucf&apos; , 0.125 , ...
    &apos;global&apos;, 1e-06 , 0.1 );
73 m = pwAddK(m, &apos;a&apos; , 1 , ...
    &apos;global&apos;, 1e-06 , 100 );
74 m = pwAddK(m, &apos;km1fc&apos; , 0.0125 , ...
    &apos;global&apos;, 1e-06 , 0.1 );
75 m = pwAddK(m, &apos;km2fc&apos; , 0.0125 , ...
    &apos;global&apos;, 1e-06 , 0.1 );
76 m = pwAddK(m, &apos;kfcm2&apos; , 0.0125 , ...
    &apos;global&apos;, 1e-06 , 0.1 );
77 m = pwAddK(m, &apos;uafc&apos; , 0.000125 , ...
    &apos;global&apos;, 1e-06 , 0.1 );
78 m = pwAddK(m, &apos;L_b&apos; , 1 , ...
    &apos;global&apos;, 1e-06 , 0.5 );
79 m = pwAddK(m, &apos;b&apos; , 1 , ...
    &apos;global&apos;, 1e-06 , 100 );
80 m = pwAddK(m, &apos;d&apos; , 10000 , ...
    &apos;global&apos;, 1e-06 , 100 );
81 m = pwAddK(m, &apos;e&apos; , 10000 , ...
    &apos;global&apos;, 1e-06 , 100 );
82 m = pwAddK(m, &apos;H&apos; , 0 , ...
    &apos;global&apos;, 1e-06 , 100 );
83 m = pwAddK(m, &apos;ke&apos; , 0.1 , ...
    &apos;global&apos;, 1e-06 , 5 );
84 m = pwAddK(m, &apos;cfc&apos; , 0.0125 , ...
    &apos;global&apos;, 1e-06 , 5 );
85 m = pwAddK(m, &apos;kce&apos; , 0.001 , ...
    &apos;global&apos;, 1e-06 , 5 );
86 m = pwAddK(m, &apos;kmr1&apos; , 0.125 , ...

```

```

    &apos;global&apos;;, 1e-06 , 5      );
87 m = pwAddK(m, &apos;kmr&apos; , 0.125      , ...
    &apos;global&apos;;, 1e-06 , 5      );
88 m = pwAddK(m, &apos;knrg&apos; , 0.125      , ...
    &apos;global&apos;;, 1e-06 , 5      );
89 m = pwAddK(m, &apos;G_b&apos; , 1      , ...
    &apos;global&apos;;, 1e-06 , 5      );
90 m = pwAddK(m, &apos;kafc1&apos;;, 10      , ...
    &apos;global&apos;;, 1e-06 , 5      );
91 m = pwAddK(m, &apos;kafc2&apos;;, 10      , ...
    &apos;global&apos;;, 1e-06 , 5      );
92 m = pwAddK(m, &apos;km11&apos; , 0.125      , ...
    &apos;global&apos;;, 1e-06 , 5      );
93 m = pwAddK(m, &apos;km1a&apos; , 0.125      , ...
    &apos;global&apos;;, 1e-06 , 5      );
94 m = pwAddK(m, &apos;knrl&apos; , 0.125      , ...
    &apos;global&apos;;, 1e-06 , 5      );
95 m = pwAddK(m, &apos;kn1&apos; , 0.125      , ...
    &apos;global&apos;;, 1e-06 , 5      );
96 m = pwAddK(m, &apos;n_cf&apos; , 1      , ...
    &apos;global&apos;;, 1e-06 );
97
98
99 %% 0 - Ordinary differential equations
100 % m = pwAddO(m, *ID, *rhs)
101 m = pwAddO(m, &apos;M_rb&apos;;, &apos;smrb...
102 +kmrl*L_b+kmrg*G_b-umrb*M_rb-(km11*L...
103 +km1n*N+km1m1*M1+km1fc*FC+km1a*A)*M_rb...
104 -(km2m2*M2+sc)*M_rb&apos;);
105 m = pwAddO(m, &apos;N_rb&apos;;, &apos;...
106 snrb+knrl*L_b+knrg*G_b-unrb*N_rb...
107 -(knan*uan*AN+kn1*L)*N_rb&apos;);
108 m = pwAddO(m, &apos;M1&apos; , &apos;...
109 (km11*L+km1n*N+km1m1*M1+km1fc*FC...
110 +km1a*A)*M_rb-um1*M1-km1m2*kanm1*AN*M1/...
111 (1+(N/n_inf)^2)+km2m1*M2-klm1*M1*L^2/...
112 (a^2+L^2)-km1fc*kafc1*FC_A*M1/(1+...
113 (N/n_inf)^2)&apos;; );
114 m = pwAddO(m, &apos;M2&apos; , &apos;...
115 (km2m2*M2+sc)*M_rb-um2*M2...
116 +km1m2*kanm1*AN*M1/(1+(N/n_inf)^2)...
117 -km2m1*M2-klm2*M2*L^2/(b^2+L^2)...
118 -km2fc*kafc2*FC_A*M2/(1+(N/n_inf)^2)...
119 +kfc2*ucf*H^2/(d^2+H^2)*C_f*FC&apos; );
120 m = pwAddO(m, &apos;N&apos; , &apos;...

```

```

121 (knan*uan*AN+kn1*L)*N_rb-kan*N&apos; );
122 m = pwAddO(m, &apos;AN&apos; , &apos;...
123 kan*N-kanm1*AN*M1/(1+(N/n_inf)^2)...
124 -kanm2*AN*M2/(1+(N/n_inf)^2)-kann*N...
125 -uan*AN&apos;);
126 m = pwAddO(m, &apos;L&apos;&apos;...
127 rL*L_b-klm1*M1*L^2/(a^2+L^2)...
128 -klm2*M2*L^2/(b^2+L^2)+uafc*C_f&apos;);
129 m = pwAddO(m, &apos;FC&apos;&apos;...
130 klm1*M1*L^2/(a^2+L^2)+klm2*M2*L^2/...
131 (b^2+L^2)-kafc*C_f^2/(e^2+C_f^2)*FC...
132 -kfc2*ucf*H^2/(d^2+H^2)*FC...
133 +km1fc*kafc1*FC_A*M1/(1+(N/n_inf)^2)...
134 +km2fc*kafc2*FC_A*M2/(1+(N/n_inf)^2)&apos;);
135 m = pwAddO(m, &apos;FC_A&apos;, &apos;...
136 kafc*C_f^2/(e^2+C_f^2)*FC...
137 -kafc1*FC_A*M1/(1+(N/n_inf)^2)...
138 -kafc2*FC_A*M2/(1+(N/n_inf)^2)&apos;);
139 m = pwAddO(m, &apos;C_f&apos; , &apos;...
140 n_cf*klm1*M1*L^2/(a^2+L^2)...
141 +n_cf*klm2*M2*L^2/(b^2+L^2)-ke*C_f...
142 +kce*C_e-ucf*H^2/(d^2+H^2)*FC+cfc*FC&apos;);
143 m = pwAddO(m, &apos;C_e&apos; ,...
144 &apos;ke*C_f-kce*C_e&apos;);
145 m = pwAddO(m, &apos;A&apos; ,...
146 &apos;uan*AN+uafc*FC_A&apos;);
147
148 %% C - Compartments
149 % m = pwAddC(m, *ID, *size, outside, spatialDim, name, ...
    unit, constant, designerProps, classname, description)
150 m = pwAddC(m, &apos;comp_1&apos;, 1);
151
152 %% CS - Constraints
153 % m = pwAddCS(m, *ID, *lhs, *operator, *rhs, lambda)
154 m = pwAddCS(m, &apos;CS01&apos;, &apos;M_rb(t==0)&apos;, ...
    &apos;=&apos;, &apos;0&apos;, 100);
155
156 %% Y - Observables
157 % m = pwAddY(m, *ID, *rhs, errorModelRhs, noiseType, unit, ...
    name, description, alternativeIDs, designerProps, classname)
158 m = pwAddY(m, &apos;N_obs&apos; , &apos;N&apos; );
159 m = pwAddY(m, &apos;M1_obs&apos;, &apos;M1&apos;);
160 m = pwAddY(m, &apos;M2_obs&apos;, &apos;M2&apos;);
161
162

```

```

163 </pre>
164     </body>
165 </notes>
166 <listOfCompartments>
167     <compartment id="mw85534cb3_656e_4ae6_853a_...
168     b669adddf273" name="comp_1" size="1" constant="true"/>
169 </listOfCompartments>
170 <listOfSpecies>
171     <species id="M_rb" name="M_rb" ...
172         compartment="mw85534cb3_656e_4ae6_853a_b669adddf273" ...
173         initialConcentration="0.65" ...
174         boundaryCondition="false" constant="false"/>
175     <species id="N_rb" name="N_rb" ...
176         compartment="mw85534cb3_656e_4ae6_853a_...
177         _b669adddf273" initialConcentration="0.07" ...
178         boundaryCondition="false" constant="false"/>
179     <species id="M1" name="M1" ...
180         compartment="mw85534cb3_656e_4ae6_853a_...
181         b669adddf273" initialConcentration="0" ...
182         boundaryCondition="false" constant="false"/>
183     <species id="M2" name="M2" ...
184         compartment="mw85534cb3_656e_4ae6_853a_...
185         b669adddf273" initialConcentration="0" ...
186         boundaryCondition="false" constant="false"/>
187     <species id="N" name="N" ...
188         compartment="mw85534cb3_656e_4ae6_853a_...
189         b669adddf273" initialConcentration="0" ...
190         boundaryCondition="false" constant="false"/>
191     <species id="AN" name="AN" ...
192         compartment="mw85534cb3_656e_4ae6_853a_...
193         b669adddf273" initialConcentration="0" ...
194         boundaryCondition="false" constant="false"/>
195     <species id="L" name="L" ...
196         compartment="mw85534cb3_656e_4ae6_853a_...
197         b669adddf273" initialConcentration="0.5" ...
198         boundaryCondition="false" constant="false"/>
199     <species id="FC" name="FC" ...
200         compartment="mw85534cb3_656e_4ae6_853a_...
201         b669adddf273" initialConcentration="1e-06" ...
202         boundaryCondition="false" constant="false"/>
203     <species id="FC_A" name="FC_A" ...
204         compartment="mw85534cb3_656e_4ae6_853a_...
205         b669adddf273" initialConcentration="0" ...
206         boundaryCondition="false" constant="false"/>
207     <species id="C_f" name="C_f" ...

```



```

189     compartment="mw85534cb3_656e_4ae6_853a_...
b669adddf273" initialConcentration="0" ...
    boundaryCondition="false" constant="false"/>
190 <species id="C_e" name="C_e" ...
    compartment="mw85534cb3_656e_4ae6_853a_...
191 b669adddf273" initialConcentration="0" ...
    boundaryCondition="false" constant="false"/>
192 <species id="A" name="A" ...
    compartment="mw85534cb3_656e_4ae6_853a_...
193 b669adddf273" initialConcentration="0" ...
    boundaryCondition="false" constant="false"/>
194 <species id="N_obs" name="N_obs" ...
    compartment="mw85534cb3_656e_4ae6_853a_...
195 b669adddf273" initialConcentration="0" ...
    boundaryCondition="false" constant="false"/>
196 <species id="M1_obs" name="M1_obs" ...
    compartment="mw85534cb3_656e_4ae6_853a_...
197 b669adddf273" initialConcentration="0" ...
    boundaryCondition="false" constant="false"/>
198 <species id="M2_obs" name="M2_obs" ...
    compartment="mw85534cb3_656e_4ae6_853a_...
199 b669adddf273" initialConcentration="0" ...
    boundaryCondition="false" constant="false"/>
200 <species id="mwdddccd99_fb4a_48c0_b494_4e1laf1d6dc3" ...
    name="Cf_per_FC" ...
    compartment="mw85534cb3_656e_4ae6_853a_...
201 b669adddf273" initialConcentration="0" ...
    boundaryCondition="false" constant="false"/>
202 <species id="mw3f564d8f_5efe_4e65_8b69_5a225f077cef" ...
    name="C_e_per_FC" ...
    compartment="mw85534cb3_656e_4ae6_853a_...
203 b669adddf273" initialConcentration="0" ...
    boundaryCondition="false" constant="false"/>
204 </listOfSpecies>
205 <listOfParameters>
206 <parameter id="snrb" name="snrb" value="1" ...
    constant="true"/>
207 <parameter id="smrb" name="smrb" value="0.75" ...
    constant="true"/>
208 <parameter id="umrb" name="umrb" value="1.4" ...
    constant="true"/>
209 <parameter id="um1" name="um1" value="6.82554" ...
    constant="true"/>
210 <parameter id="um2" name="um2" value="8.27065" ...
    constant="true"/>

```

```

211 <parameter id="uan" name="uan" value="1.30931" ...
      constant="true"/>
212 <parameter id="k1m2" name="k1m2" value="8.61724" ...
      constant="true"/>
213 <parameter id="k1m1" name="k1m1" ...
      value="0.000993236" constant="true"/>
214 <parameter id="k2m2" name="k2m2" value="1.59254" ...
      constant="true"/>
215 <parameter id="kan" name="kan" ...
      value="7.10822919836749" constant="true"/>
216 <parameter id="unrb" name="unrb" value="16.402" ...
      constant="true"/>
217 <parameter id="n_inf" name="n_inf" ...
      value="0.156384088195465" constant="true"/>
218 <parameter id="kanm1" name="kanm1" ...
      value="2.89808017283302" constant="true"/>
219 <parameter id="kanm2" name="kanm2" ...
      value="90.9575626487555" constant="true"/>
220 <parameter id="k2m1" name="k2m1" ...
      value="0.117354199532277" constant="true"/>
221 <parameter id="k1n" name="k1n" ...
      value="0.025086814972565" constant="true"/>
222 <parameter id="knan" name="knan" ...
      value="0.607651029250834" constant="true"/>
223 <parameter id="kann" name="kann" ...
      value="0.000600657675376788" constant="true"/>
224 <parameter id="sc" name="sc" value="0.0125" ...
      constant="true"/>
225 <parameter id="rL" name="rL" value="0.001" ...
      constant="true"/>
226 <parameter id="k1m1" name="k1m1" value="1" ...
      constant="true"/>
227 <parameter id="k1m2" name="k1m2" value="1" ...
      constant="true"/>
228 <parameter id="kafc" name="kafc" ...
      value="100000000000" constant="true"/>
229 <parameter id="ucf" name="ucf" value="0.125" ...
      constant="true"/>
230 <parameter id="a" name="a" value="1" constant="true"/>
231 <parameter id="k1fc" name="k1fc" value="0.0125" ...
      constant="true"/>
232 <parameter id="k2fc" name="k2fc" value="0.0125" ...
      constant="true"/>
233 <parameter id="k2fc2" name="k2fc2" value="0.0125" ...
      constant="true"/>

```

```

234 <parameter id="uafc" name="uafc" value="0.000125" ...
      constant="true"/>
235 <parameter id="L_b" name="L_b" value="1" ...
      constant="false"/>
236 <parameter id="b" name="b" value="1" constant="true"/>
237 <parameter id="d" name="d" value="10000" ...
      constant="true"/>
238 <parameter id="e" name="e" value="10000" ...
      constant="true"/>
239 <parameter id="H" name="H" value="1" constant="true"/>
240 <parameter id="ke" name="ke" value="0.1" ...
      constant="true"/>
241 <parameter id="kce" name="kce" value="0.001" ...
      constant="true"/>
242 <parameter id="kmrl" name="kmrl" value="0.125" ...
      constant="true"/>
243 <parameter id="kmrg" name="kmrg" value="0.125" ...
      constant="true"/>
244 <parameter id="knrg" name="knrg" value="0.125" ...
      constant="true"/>
245 <parameter id="G_b" name="G_b" value="1" ...
      constant="false"/>
246 <parameter id="kafcm1" name="kafcm1" value="10" ...
      constant="true"/>
247 <parameter id="kafcm2" name="kafcm2" value="10" ...
      constant="true"/>
248 <parameter id="km1l" name="km1l" value="0.125" ...
      constant="true"/>
249 <parameter id="km1a" name="km1a" value="0.125" ...
      constant="true"/>
250 <parameter id="knrl" name="knrl" value="0.125" ...
      constant="true"/>
251 <parameter id="knl" name="knl" value="0.125" ...
      constant="true"/>
252 <parameter id="n_cf" name="n_cf" value="1" ...
      constant="true"/>
253 <parameter ...
      id="mw6c599f7d_e448_4ea2_b9ed_835769597483" ...
      name="cm1" value="0.0125" constant="true"/>
254 <parameter ...
      id="mw834ed067_5f95_40fe_b737_c027a32d22f0" ...
      name="cm2" value="0.0125" constant="true"/>
255 </listOfParameters>
256 <listOfRules>
257 <rateRule variable="M_rb">

```

```

258 <math xmlns="http://www.w3.org/1998/Math/MathML">
259   <apply>
260     <minus/>
261     <apply>
262       <minus/>
263       <apply>
264         <minus/>
265         <apply>
266           <plus/>
267           <ci> smrb </ci>
268           <apply>
269             <times/>
270             <ci> kmrl </ci>
271             <ci> L_b </ci>
272           </apply>
273         <apply>
274           <times/>
275           <ci> kmrg </ci>
276           <ci> G_b </ci>
277         </apply>
278       </apply>
279     <apply>
280       <times/>
281       <ci> umrb </ci>
282       <ci> M_rb </ci>
283     </apply>
284   </apply>
285   <apply>
286     <times/>
287     <apply>
288       <plus/>
289       <apply>
290         <times/>
291         <ci> kmll </ci>
292         <ci> L </ci>
293       </apply>
294       <apply>
295         <times/>
296         <ci> km1n </ci>
297         <ci> N </ci>
298       </apply>
299     <apply>
300       <times/>
301       <ci> km1m1 </ci>
302       <ci> M1 </ci>

```

```

303         </apply>
304         <apply>
305             <times/>
306             <ci> kmlfc </ci>
307             <ci> FC </ci>
308         </apply>
309         <apply>
310             <times/>
311             <ci> kmla </ci>
312             <ci> A </ci>
313         </apply>
314     </apply>
315     <ci> M_rb </ci>
316 </apply>
317 </apply>
318 <apply>
319     <times/>
320 <apply>
321     <plus/>
322 <apply>
323     <times/>
324     <ci> km2m2 </ci>
325     <ci> M2 </ci>
326 </apply>
327     <ci> sc </ci>
328 </apply>
329     <ci> M_rb </ci>
330 </apply>
331 </apply>
332 </math>
333 </rateRule>
334 <rateRule variable="N_rb">
335     <math xmlns="http://www.w3.org/1998/Math/MathML">
336     <apply>
337         <minus/>
338     <apply>
339         <minus/>
340     <apply>
341         <plus/>
342         <ci> snrb </ci>
343     <apply>
344         <times/>
345         <ci> knrl </ci>
346         <ci> L_b </ci>
347     </apply>

```

```

348         <apply>
349             <times/>
350             <ci> knrg </ci>
351             <ci> G_b </ci>
352         </apply>
353     </apply>
354     <apply>
355         <times/>
356         <ci> unrb </ci>
357         <ci> N_rb </ci>
358     </apply>
359 </apply>
360 <apply>
361     <times/>
362     <apply>
363         <plus/>
364         <apply>
365             <times/>
366             <ci> knan </ci>
367             <ci> uan </ci>
368             <ci> AN </ci>
369         </apply>
370     <apply>
371         <times/>
372         <ci> knl </ci>
373         <ci> L </ci>
374     </apply>
375 </apply>
376     <ci> N_rb </ci>
377 </apply>
378 </math>
379 </rateRule>
380 <rateRule variable="M1">
381     <math xmlns="http://www.w3.org/1998/Math/MathML">
382         <apply>
383             <minus/>
384             <apply>
385                 <minus/>
386                 <apply>
387                     <plus/>
388                     <apply>
389                         <minus/>
390                         <apply>
391                             <minus/>

```

```

393 <apply>
394 <times/>
395 <apply>
396 <plus/>
397 <apply>
398 <times/>
399 <ci> km1l </ci>
400 <ci> L </ci>
401 </apply>
402 <apply>
403 <times/>
404 <ci> km1n </ci>
405 <ci> N </ci>
406 </apply>
407 <apply>
408 <times/>
409 <ci> km1m1 </ci>
410 <ci> M1 </ci>
411 </apply>
412 <apply>
413 <times/>
414 <ci> km1fc </ci>
415 <ci> FC </ci>
416 </apply>
417 <apply>
418 <times/>
419 <ci> km1a </ci>
420 <ci> A </ci>
421 </apply>
422 </apply>
423 <ci> M_rb </ci>
424 </apply>
425 <apply>
426 <times/>
427 <ci> um1 </ci>
428 <ci> M1 </ci>
429 </apply>
430 </apply>
431 <apply>
432 <divide/>
433 <apply>
434 <times/>
435 <ci> km1m2 </ci>
436 <ci> kanm1 </ci>
437 <ci> AN </ci>

```

```

438         <ci> M1 </ci>
439     </apply>
440 <apply>
441     <plus/>
442     <cn type="integer"> 1 </cn>
443     <apply>
444         <power/>
445         <apply>
446             <divide/>
447             <ci> N </ci>
448             <ci> n_inf </ci>
449         </apply>
450         <cn type="integer"> 2 </cn>
451     </apply>
452 </apply>
453 </apply>
454 </apply>
455 <apply>
456     <times/>
457     <ci> km2m1 </ci>
458     <ci> M2 </ci>
459 </apply>
460 </apply>
461 <apply>
462     <divide/>
463     <apply>
464         <times/>
465         <ci> klm1 </ci>
466         <ci> M1 </ci>
467     <apply>
468         <power/>
469         <ci> L </ci>
470         <cn type="integer"> 2 </cn>
471     </apply>
472 </apply>
473 <apply>
474     <plus/>
475     <apply>
476         <power/>
477         <ci> a </ci>
478         <cn type="integer"> 2 </cn>
479     </apply>
480 <apply>
481     <power/>
482     <ci> L </ci>

```



```

483         <cn type="integer"> 2 </cn>
484     </apply>
485 </apply>
486 </apply>
487 </apply>
488 <apply>
489     <divide/>
490     <apply>
491         <times/>
492         <ci> km1fc </ci>
493         <ci> kafcm1 </ci>
494         <ci> FC_A </ci>
495         <ci> M1 </ci>
496     </apply>
497     <apply>
498         <plus/>
499         <cn type="integer"> 1 </cn>
500     </apply>
501         <power/>
502         <apply>
503             <divide/>
504             <ci> N </ci>
505             <ci> n_inf </ci>
506         </apply>
507         <cn type="integer"> 2 </cn>
508     </apply>
509 </apply>
510 </apply>
511 </math>
512 </rateRule>
513 <rateRule variable="M2">
514     <math xmlns="http://www.w3.org/1998/Math/MathML">
515     <apply>
516     <plus/>
517     <apply>
518     <minus/>
519     <apply>
520     <minus/>
521     <apply>
522     <minus/>
523     <apply>
524     <plus/>
525     <apply>
526     <minus/>
527

```

```

528     <apply>
529         <times/>
530         <apply>
531             <plus/>
532             <apply>
533                 <times/>
534                 <ci> km2m2 </ci>
535                 <ci> M2 </ci>
536             </apply>
537             <ci> sc </ci>
538         </apply>
539         <ci> M_rb </ci>
540     </apply>
541     <apply>
542         <times/>
543         <ci> um2 </ci>
544         <ci> M2 </ci>
545     </apply>
546 </apply>
547 <apply>
548     <divide/>
549     <apply>
550         <times/>
551         <ci> kmlm2 </ci>
552         <ci> kanm1 </ci>
553         <ci> AN </ci>
554         <ci> M1 </ci>
555     </apply>
556     <apply>
557         <plus/>
558         <cn type="integer"> 1 </cn>
559     </apply>
560         <power/>
561         <apply>
562             <divide/>
563             <ci> N </ci>
564             <ci> n_inf </ci>
565         </apply>
566         <cn type="integer"> 2 </cn>
567     </apply>
568 </apply>
569 </apply>
570 </apply>
571 <apply>
572     <times/>

```

```

573         <ci> km2m1 </ci>
574         <ci> M2 </ci>
575     </apply>
576 </apply>
577 <apply>
578     <divide/>
579     <apply>
580         <times/>
581         <ci> klm2 </ci>
582         <ci> M2 </ci>
583     <apply>
584         <power/>
585         <ci> L </ci>
586         <cn type="integer"> 2 </cn>
587     </apply>
588 </apply>
589 <apply>
590     <plus/>
591     <apply>
592         <power/>
593         <ci> b </ci>
594         <cn type="integer"> 2 </cn>
595     </apply>
596 <apply>
597     <power/>
598     <ci> L </ci>
599     <cn type="integer"> 2 </cn>
600 </apply>
601 </apply>
602 </apply>
603 </apply>
604 <apply>
605     <divide/>
606     <apply>
607         <times/>
608         <ci> km2fc </ci>
609         <ci> kafcm2 </ci>
610         <ci> FC_A </ci>
611         <ci> M2 </ci>
612     </apply>
613 <apply>
614     <plus/>
615     <cn type="integer"> 1 </cn>
616 <apply>
617     <power/>

```

```

618         <apply>
619             <divide/>
620             <ci> N </ci>
621             <ci> n_inf </ci>
622         </apply>
623         <cn type="integer"> 2 </cn>
624     </apply>
625 </apply>
626 </apply>
627 </apply>
628 <apply>
629     <times/>
630     <apply>
631         <divide/>
632         <apply>
633             <times/>
634             <ci> kfc2 </ci>
635             <ci> ucf </ci>
636         </apply>
637         <power/>
638         <ci> H </ci>
639         <cn type="integer"> 2 </cn>
640     </apply>
641 </apply>
642 <apply>
643     <plus/>
644     <apply>
645         <power/>
646         <ci> d </ci>
647         <cn type="integer"> 2 </cn>
648     </apply>
649     <apply>
650         <power/>
651         <ci> H </ci>
652         <cn type="integer"> 2 </cn>
653     </apply>
654 </apply>
655 </apply>
656 <ci> C_f </ci>
657 <ci> FC </ci>
658 </apply>
659 </apply>
660 </math>
661 </rateRule>
662 <rateRule variable="N">

```

```

663 <math xmlns="http://www.w3.org/1998/Math/MathML">
664   <apply>
665     <minus/>
666     <apply>
667       <times/>
668       <apply>
669         <plus/>
670         <apply>
671           <times/>
672           <ci> knan </ci>
673           <ci> uan </ci>
674           <ci> AN </ci>
675         </apply>
676       <apply>
677         <times/>
678         <ci> knl </ci>
679         <ci> L </ci>
680       </apply>
681     </apply>
682     <ci> Nrb </ci>
683   </apply>
684   <apply>
685     <times/>
686     <ci> kan </ci>
687     <ci> N </ci>
688   </apply>
689 </math>
690 </rateRule>
691 <rateRule variable="AN">
692   <math xmlns="http://www.w3.org/1998/Math/MathML">
693     <apply>
694       <minus/>
695       <apply>
696         <minus/>
697         <apply>
698           <minus/>
699           <apply>
700             <minus/>
701             <apply>
702               <times/>
703               <ci> kan </ci>
704               <ci> N </ci>
705             </apply>
706           </apply>
707         <apply>

```

```

708         <divide/>
709     <apply>
710         <times/>
711         <ci> kanm1 </ci>
712         <ci> AN </ci>
713         <ci> M1 </ci>
714     </apply>
715 <apply>
716     <plus/>
717     <cn type="integer"> 1 </cn>
718     <apply>
719         <power/>
720         <apply>
721             <divide/>
722             <ci> N </ci>
723             <ci> n_inf </ci>
724         </apply>
725         <cn type="integer"> 2 </cn>
726     </apply>
727 </apply>
728 </apply>
729 </apply>
730 <apply>
731     <divide/>
732     <apply>
733         <times/>
734         <ci> kanm2 </ci>
735         <ci> AN </ci>
736         <ci> M2 </ci>
737     </apply>
738     <apply>
739         <plus/>
740         <cn type="integer"> 1 </cn>
741         <apply>
742             <power/>
743             <apply>
744                 <divide/>
745                 <ci> N </ci>
746                 <ci> n_inf </ci>
747             </apply>
748             <cn type="integer"> 2 </cn>
749         </apply>
750     </apply>
751 </apply>
752 </apply>

```

```

753         <apply>
754             <times/>
755             <ci> kann </ci>
756             <ci> N </ci>
757         </apply>
758     </apply>
759     <apply>
760         <times/>
761         <ci> uan </ci>
762         <ci> AN </ci>
763     </apply>
764 </math>
765 </rateRule>
766 <rateRule variable="L">
767     <math xmlns="http://www.w3.org/1998/Math/MathML">
768         <apply>
769             <plus/>
770             <apply>
771                 <minus/>
772                 <apply>
773                     <minus/>
774                     <apply>
775                         <times/>
776                         <ci> rL </ci>
777                         <ci> L_b </ci>
778                     </apply>
779                 </apply>
780             <apply>
781                 <divide/>
782                 <apply>
783                     <times/>
784                     <ci> klm1 </ci>
785                     <ci> M1 </ci>
786                 </apply>
787                 <power/>
788                 <ci> L </ci>
789                 <cn type="integer"> 2 </cn>
790             </apply>
791         </apply>
792         <apply>
793             <plus/>
794             <apply>
795                 <power/>
796                 <ci> a </ci>
797                 <cn type="integer"> 2 </cn>

```

```

798         </apply>
799         <apply>
800             <power/>
801             <ci> L </ci>
802             <cn type="integer"> 2 </cn>
803         </apply>
804     </apply>
805 </apply>
806 </apply>
807 <apply>
808     <divide/>
809     <apply>
810         <times/>
811         <ci> klm2 </ci>
812         <ci> M2 </ci>
813     </apply>
814     <power/>
815     <ci> L </ci>
816     <cn type="integer"> 2 </cn>
817 </apply>
818 </apply>
819 <apply>
820     <plus/>
821     <apply>
822         <power/>
823         <ci> b </ci>
824         <cn type="integer"> 2 </cn>
825     </apply>
826     <apply>
827         <power/>
828         <ci> L </ci>
829         <cn type="integer"> 2 </cn>
830     </apply>
831 </apply>
832 </apply>
833 </apply>
834 <apply>
835     <times/>
836     <ci> uafc </ci>
837     <ci> C_f </ci>
838 </apply>
839 </apply>
840 </math>
841 </rateRule>
842 <rateRule variable="FC">

```



```

843 <math xmlns="http://www.w3.org/1998/Math/MathML">
844   <apply>
845     <plus/>
846     <apply>
847       <minus/>
848       <apply>
849         <minus/>
850         <apply>
851           <plus/>
852           <apply>
853             <divide/>
854             <apply>
855               <times/>
856               <ci> klm1 </ci>
857               <ci> M1 </ci>
858               <apply>
859                 <power/>
860                 <ci> L </ci>
861                 <cn type="integer"> 2 </cn>
862               </apply>
863             </apply>
864             <apply>
865               <plus/>
866               <apply>
867                 <power/>
868                 <ci> a </ci>
869                 <cn type="integer"> 2 </cn>
870               </apply>
871               <apply>
872                 <power/>
873                 <ci> L </ci>
874                 <cn type="integer"> 2 </cn>
875               </apply>
876             </apply>
877           </apply>
878           <apply>
879             <divide/>
880             <apply>
881               <times/>
882               <ci> klm2 </ci>
883               <ci> M2 </ci>
884               <apply>
885                 <power/>
886                 <ci> L </ci>
887                 <cn type="integer"> 2 </cn>

```

```

888         </apply>
889     </apply>
890     <apply>
891         <plus/>
892         <apply>
893             <power/>
894             <ci> b </ci>
895             <cn type="integer"> 2 </cn>
896         </apply>
897         <apply>
898             <power/>
899             <ci> L </ci>
900             <cn type="integer"> 2 </cn>
901         </apply>
902     </apply>
903 </apply>
904 </apply>
905 <apply>
906     <times/>
907     <apply>
908         <divide/>
909         <apply>
910             <times/>
911             <ci> kafc </ci>
912             <apply>
913                 <power/>
914                 <ci> Cf </ci>
915                 <cn type="integer"> 2 </cn>
916             </apply>
917         </apply>
918         <apply>
919             <plus/>
920             <apply>
921                 <power/>
922                 <ci> e </ci>
923                 <cn type="integer"> 2 </cn>
924             </apply>
925             <apply>
926                 <power/>
927                 <ci> Cf </ci>
928                 <cn type="integer"> 2 </cn>
929             </apply>
930         </apply>
931     </apply>
932 <ci> FC </ci>

```

```

933     </apply>
934 </apply>
935 <apply>
936   <times/>
937   <apply>
938     <divide/>
939     <apply>
940       <times/>
941       <ci> kfc2 </ci>
942       <ci> ucf </ci>
943       <apply>
944         <power/>
945         <ci> H </ci>
946         <cn type="integer"> 2 </cn>
947       </apply>
948     </apply>
949   <apply>
950     <plus/>
951     <apply>
952       <power/>
953       <ci> d </ci>
954       <cn type="integer"> 2 </cn>
955     </apply>
956   <apply>
957     <power/>
958     <ci> H </ci>
959     <cn type="integer"> 2 </cn>
960   </apply>
961 </apply>
962 </apply>
963 <ci> FC </ci>
964 </apply>
965 </apply>
966 <apply>
967   <divide/>
968   <apply>
969     <times/>
970     <ci> kmlfc </ci>
971     <ci> kafcm1 </ci>
972     <ci> FC_A </ci>
973     <ci> M1 </ci>
974   </apply>
975 <apply>
976   <plus/>
977   <cn type="integer"> 1 </cn>

```

```

978         <apply>
979             <power/>
980             <apply>
981                 <divide/>
982                 <ci> N </ci>
983                 <ci> n_inf </ci>
984             </apply>
985             <cn type="integer"> 2 </cn>
986         </apply>
987     </apply>
988 </apply>
989 <apply>
990     <divide/>
991     <apply>
992         <times/>
993         <ci> km2fc </ci>
994         <ci> kafcm2 </ci>
995         <ci> FC_A </ci>
996         <ci> M2 </ci>
997     </apply>
998     <apply>
999         <plus/>
1000         <cn type="integer"> 1 </cn>
1001     </apply>
1002         <power/>
1003         <apply>
1004             <divide/>
1005             <ci> N </ci>
1006             <ci> n_inf </ci>
1007         </apply>
1008         <cn type="integer"> 2 </cn>
1009     </apply>
1010 </apply>
1011 </apply>
1012 </math>
1013 </rateRule>
1014 <rateRule variable="FC_A">
1015     <math xmlns="http://www.w3.org/1998/Math/MathML">
1016         <apply>
1017             <minus/>
1018             <apply>
1019                 <minus/>
1020                 <apply>
1021                     <times/>

```

```

1023     <apply>
1024         <divide/>
1025         <apply>
1026             <times/>
1027             <ci> kafc </ci>
1028             <apply>
1029                 <power/>
1030                 <ci> C_f </ci>
1031                 <cn type="integer"> 2 </cn>
1032             </apply>
1033         </apply>
1034     <apply>
1035         <plus/>
1036         <apply>
1037             <power/>
1038             <ci> e </ci>
1039             <cn type="integer"> 2 </cn>
1040         </apply>
1041         <apply>
1042             <power/>
1043             <ci> C_f </ci>
1044             <cn type="integer"> 2 </cn>
1045         </apply>
1046     </apply>
1047 </apply>
1048 <ci> FC </ci>
1049 </apply>
1050 <apply>
1051     <divide/>
1052     <apply>
1053         <times/>
1054         <ci> kafcm1 </ci>
1055         <ci> FC_A </ci>
1056         <ci> M1 </ci>
1057     </apply>
1058     <apply>
1059         <plus/>
1060         <cn type="integer"> 1 </cn>
1061     </apply>
1062     <power/>
1063     <apply>
1064         <divide/>
1065         <ci> N </ci>
1066         <ci> n_inf </ci>
1067     </apply>

```

```

1068         <cn type="integer"> 2 </cn>
1069     </apply>
1070 </apply>
1071 </apply>
1072 </apply>
1073 <apply>
1074     <divide/>
1075 <apply>
1076     <times/>
1077     <ci> kafcm2 </ci>
1078     <ci> FC_A </ci>
1079     <ci> M2 </ci>
1080 </apply>
1081 <apply>
1082     <plus/>
1083     <cn type="integer"> 1 </cn>
1084 <apply>
1085     <power/>
1086 <apply>
1087     <divide/>
1088     <ci> N </ci>
1089     <ci> n_inf </ci>
1090 </apply>
1091     <cn type="integer"> 2 </cn>
1092 </apply>
1093 </apply>
1094 </apply>
1095 </apply>
1096 </math>
1097 </rateRule>
1098 <rateRule variable="C_f">
1099     <math xmlns="http://www.w3.org/1998/Math/MathML">
1100     <apply>
1101     <minus/>
1102     <apply>
1103     <plus/>
1104     <apply>
1105     <minus/>
1106     <apply>
1107     <plus/>
1108     <apply>
1109     <divide/>
1110     <apply>
1111     <times/>
1112     <apply>

```

```

1113         <plus/>
1114         <ci> n_cf </ci>
1115         <ci> mw6c599f7d_e448_4ea2_b9ed_...
1116         835769597483 </ci>
1117     </apply>
1118     <ci> klm1 </ci>
1119     <ci> M1 </ci>
1120     <apply>
1121         <power/>
1122         <ci> L </ci>
1123         <cn type="integer"> 2 </cn>
1124     </apply>
1125 </apply>
1126 <apply>
1127     <plus/>
1128     <apply>
1129         <power/>
1130         <ci> a </ci>
1131         <cn type="integer"> 2 </cn>
1132     </apply>
1133     <apply>
1134         <power/>
1135         <ci> L </ci>
1136         <cn type="integer"> 2 </cn>
1137     </apply>
1138 </apply>
1139 </apply>
1140 <apply>
1141     <divide/>
1142     <apply>
1143         <times/>
1144         <apply>
1145             <plus/>
1146             <ci> n_cf </ci>
1147             <ci> mw834ed067_5f95_40fe_b737_...
1148             c027a32d22f0 </ci>
1149         </apply>
1150         <ci> klm2 </ci>
1151         <ci> M2 </ci>
1152     <apply>
1153         <power/>
1154         <ci> L </ci>
1155         <cn type="integer"> 2 </cn>
1156     </apply>
1157 </apply>

```

```

1158         <apply>
1159             <plus/>
1160             <apply>
1161                 <power/>
1162                 <ci> b </ci>
1163                 <cn type="integer"> 2 </cn>
1164             </apply>
1165             <apply>
1166                 <power/>
1167                 <ci> L </ci>
1168                 <cn type="integer"> 2 </cn>
1169             </apply>
1170         </apply>
1171     </apply>
1172 </apply>
1173 <apply>
1174     <times/>
1175     <ci> ke </ci>
1176     <ci> C_f </ci>
1177 </apply>
1178 </apply>
1179 <apply>
1180     <times/>
1181     <ci> kce </ci>
1182     <ci> C_e </ci>
1183 </apply>
1184 </apply>
1185 <apply>
1186     <times/>
1187     <apply>
1188         <divide/>
1189         <apply>
1190             <times/>
1191             <ci> ucf </ci>
1192             <apply>
1193                 <power/>
1194                 <ci> H </ci>
1195                 <cn type="integer"> 2 </cn>
1196             </apply>
1197         </apply>
1198     <apply>
1199         <plus/>
1200         <apply>
1201             <power/>
1202             <ci> d </ci>

```



```

1203         <cn type="integer"> 2 </cn>
1204     </apply>
1205     <apply>
1206         <power/>
1207         <ci> H </ci>
1208         <cn type="integer"> 2 </cn>
1209     </apply>
1210 </apply>
1211 </apply>
1212 <ci> FC </ci>
1213 </apply>
1214 </apply>
1215 </math>
1216 </rateRule>
1217 <rateRule variable="C_e">
1218     <math xmlns="http://www.w3.org/1998/Math/MathML">
1219         <apply>
1220             <minus/>
1221             <apply>
1222                 <times/>
1223                 <ci> ke </ci>
1224                 <ci> C_f </ci>
1225             </apply>
1226             <apply>
1227                 <times/>
1228                 <ci> kce </ci>
1229                 <ci> C_e </ci>
1230             </apply>
1231         </apply>
1232     </math>
1233 </rateRule>
1234 <rateRule variable="A">
1235     <math xmlns="http://www.w3.org/1998/Math/MathML">
1236         <apply>
1237             <plus/>
1238             <apply>
1239                 <times/>
1240                 <ci> uan </ci>
1241                 <ci> AN </ci>
1242             </apply>
1243             <apply>
1244                 <times/>
1245                 <ci> uafc </ci>
1246                 <ci> FC_A </ci>
1247             </apply>

```

```

1248         </apply>
1249     </math>
1250 </rateRule>
1251 <assignmentRule variable="N_obs">
1252     <math xmlns="http://www.w3.org/1998/Math/MathML">
1253         <ci> N </ci>
1254     </math>
1255 </assignmentRule>
1256 <assignmentRule variable="M1_obs">
1257     <math xmlns="http://www.w3.org/1998/Math/MathML">
1258         <ci> M1 </ci>
1259     </math>
1260 </assignmentRule>
1261 <assignmentRule variable="M2_obs">
1262     <math xmlns="http://www.w3.org/1998/Math/MathML">
1263         <ci> M2 </ci>
1264     </math>
1265 </assignmentRule>
1266 <assignmentRule ...
1267     variable="mwdddccd99_fb4a_48c0_b494_4e11af1d6dc3">
1268     <math xmlns="http://www.w3.org/1998/Math/MathML">
1269         <apply>
1270             <divide/>
1271             <ci> C_f </ci>
1272             <ci> FC </ci>
1273         </apply>
1274     </math>
1275 </assignmentRule>
1276 <assignmentRule ...
1277     variable="mw3f564d8f_5efe_4e65_8b69_5a225f077cef">
1278     <math xmlns="http://www.w3.org/1998/Math/MathML">
1279         <apply>
1280             <divide/>
1281             <ci> C_e </ci>
1282             <ci> FC </ci>
1283         </apply>
1284     </math>
1285 </assignmentRule>
1286 </listOfRules>
1287 </model>
1288 </sbml>

```

REFERENCES

- [1] Kevin D Hall et al. “Quantification of the effect of energy imbalance on body-weight”. In: *The Lancet* 378.9793 (2011), pp. 826–837.
- [2] Marika Leenders et al. “Elderly men and women benefit equally from prolonged resistance-type exercise training”. In: *Journals of Gerontology - Series A Biological Sciences and Medical Sciences* 68.7 (2013), pp. 769–779. ISSN: 10795006. DOI: 10.1093/gerona/gls241.
- [3] Angela Reynolds et al. “A reduced mathematical model of the acute inflammatory response: I. Derivation of model and analysis of anti-inflammation”. In: *Journal of theoretical biology* 242.1 (2006), pp. 220–236.
- [4] Rebecca A Segal et al. “A Differential Equation Model of Collagen Accumulation in a Healing Wound”. en. In: *Bulletin of Mathematical Biology* 74.9 (Sept. 2012), pp. 2165–2182. ISSN: 0092-8240, 1522-9602. DOI: 10.1007/s11538-012-9751-z.
- [5] Nathan B Menke et al. “An in silico approach to the analysis of acute wound healing”. In: *Wound repair and regeneration* 18.1 (2010), pp. 105–113.
- [6] Pedro Corral et al. “Dietary adherence during weight loss predicts weight regain”. In: *Obesity* 19.6 (2011), pp. 1177–1181.
- [7] Iris Shai and Meir J Stampfer. “Weight-loss diets—can you keep it off?” In: *The American journal of clinical nutrition* 88.5 (2008), pp. 1185–1186.
- [8] Christina Garcia Ulen et al. “Weight regain prevention”. In: *Clinical Diabetes* 26.3 (2008), pp. 100–113.

- [9] Rena R Wing and Suzanne Phelan. “Long-term weight loss maintenance”. In: *The American journal of clinical nutrition* 82.1 (2005), 222S–225S.
- [10] D Scott and V Hirani. “Sarcopenic obesity”. In: *European Geriatric Medicine* 7.3 (2016), pp. 214–219.
- [11] Preethi Srikanthan and Arun S Karlamangla. “Relative muscle mass is inversely associated with insulin resistance and prediabetes. Findings from the third National Health and Nutrition Examination Survey”. In: *The Journal of Clinical Endocrinology & Metabolism* 96.9 (2011), pp. 2898–2903.
- [12] Leslie H Willis et al. “Effects of aerobic and/or resistance training on body mass and fat mass in overweight or obese adults”. In: *Journal of Applied Physiology* 113.12 (2012), pp. 1831–1837.
- [13] E Sanal, F Ardic, and S Kirac. “Effects of aerobic or combined aerobic resistance exercise on body composition in overweight and obese adults: gender differences. A randomized intervention study.” In: *European journal of physical and rehabilitation medicine* 49.1 (2013), pp. 1–11.
- [14] Suleen S Ho et al. “The effect of 12 weeks of aerobic, resistance or combination exercise training on cardiovascular risk factors in the overweight and obese in a randomized trial”. In: *BMC public health* 12.1 (2012), p. 704.
- [15] Konstantin N Pavlou et al. “Effects of dieting and exercise on lean body mass, oxygen uptake, and strength.” In: *Medicine and Science in Sports and Exercise* 17.4 (1985), pp. 466–471.
- [16] Allan Geliebter et al. “Effects of strength or aerobic training on body composition, resting metabolic rate, and peak oxygen consumption in obese dieting

- subjects.” In: *The American journal of clinical nutrition* 66.3 (1997), pp. 557–563.
- [17] Randy W Bryner et al. “Effects of resistance vs. aerobic training combined with an 800 calorie liquid diet on lean body mass and resting metabolic rate”. In: *Journal of the American College of Nutrition* 18.2 (1999), pp. 115–121.
- [18] Joshua J Avila et al. “Effect of moderate intensity resistance training during weight loss on body composition and physical performance in overweight older adults”. In: *European journal of applied physiology* 109.3 (2010), pp. 517–525.
- [19] Seymour S Alpert. “A two-reservoir energy model of the human body.” In: *The American journal of clinical nutrition* 32.8 (1979), pp. 1710–1718.
- [20] Seymour S Alpert. “Growth, thermogenesis, and hyperphagia.” In: *The American journal of clinical nutrition* 52.5 (1990), pp. 784–792.
- [21] Seymour S Alpert. “A limit on the energy transfer rate from the human fat store in hypophagia”. In: *Journal of theoretical biology* 233.1 (2005), pp. 1–13.
- [22] Edward H Livingston et al. “Biexponential model for predicting weight loss after gastric surgery for obesity”. In: *Journal of Surgical Research* 101.2 (2001), pp. 216–224.
- [23] Kevin D Hall, Heather L Bain, and Carson C Chow. “How adaptations of substrate utilization regulate body composition”. In: *International journal of obesity* 31.9 (2007), pp. 1378–1383.
- [24] Kevin D Hall and Peter N Jordan. “Dynamic coordination of macronutrient balance during infant growth: Insights from a mathematical model”. In: *The FASEB Journal* 22.1 Supplement (2008), pp. 305–1.

- [25] Vincent W Antonetti. “The equations governing weight change in human beings”. In: *The American journal of clinical nutrition* 26.1 (1973), pp. 64–71.
- [26] Philip R Payne and Alan E Dugdale. “A model for the prediction of energy balance and body weight”. In: *Annals of human biology* 4.6 (1977), pp. 525–535.
- [27] Klaas R Westerterp, Jeroen HHLM Donkers, Elisabeth WHM Fredrix, et al. “Energy intake, physical activity and body weight: a simulation model”. In: *British Journal of Nutrition* 73.03 (1995), pp. 337–347.
- [28] Jean-Pierre Flatt. “Carbohydrate—Fat Interactions and Obesity Examined by a Two-Compartment Computer Model”. In: *Obesity research* 12.12 (2004), pp. 2013–2022.
- [29] Baojun Song and Diana M Thomas. “Dynamics of starvation in humans”. In: *Journal of mathematical biology* 54.1 (2007), pp. 27–43.
- [30] Kevin D Hall. “Predicting metabolic adaptation, body weight change, and energy intake in humans”. In: *American Journal of Physiology-Endocrinology and Metabolism* 298.3 (2010), E449–E466.
- [31] J-Emeterio Navarro-Barrientos, Daniel E Rivera, and Linda M Collins. “A dynamical model for describing behavioural interventions for weight loss and body composition change”. In: *Mathematical and computer modelling of dynamical systems* 17.2 (2011), pp. 183–203.
- [32] Diana M Thomas et al. “A simple model predicting individual weight change in humans”. In: *Journal of biological dynamics* 5.6 (2011), pp. 579–599.
- [33] Frank P Kozusko. “Body weight setpoint, metabolic adaption and human starvation”. In: *Bulletin of mathematical biology* 63.2 (2001), pp. 393–403.

- [34] Edmund Christiansen and Lars Garby. “Prediction of body weight changes caused by changes in energy balance”. In: *European journal of clinical investigation* 32.11 (2002), pp. 826–830.
- [35] Carson C Chow and Kevin D Hall. “The dynamics of human body weight change”. In: *PLoS Comput Biol* 4.3 (2008), e1000045.
- [36] Kevin D Hall. “Mechanisms of metabolic fuel selection: modeling human metabolism and body-weight change”. In: *Engineering in Medicine and Biology Magazine, IEEE* 29.1 (2010), pp. 36–41.
- [37] Karl M Nelson et al. “Prediction of resting energy expenditure from fat-free mass and fat mass.” In: *The American journal of clinical nutrition* 56.5 (1992), pp. 848–856.
- [38] MONICA J Hubal et al. “Variability in muscle size and strength gain after unilateral resistance training”. In: *Med Sci Sports Exerc* 37.6 (2005), pp. 964–72.
- [39] John K Petrella et al. “Potent myofiber hypertrophy during resistance training in humans is associated with satellite cell-mediated myonuclear addition: a cluster analysis”. In: *Journal of applied physiology* 104.6 (2008), pp. 1736–1742.
- [40] Mathias Wernbom, Jesper Augustsson, and Roland Thomeé. “The influence of frequency, intensity, volume and mode of strength training on whole muscle cross-sectional area in humans”. In: *Sports Medicine* 37.3 (2007), pp. 225–264.
- [41] LG Borrud et al. “Body composition data for individuals 8 years of age and older: US population, 1999-2004.” In: *Vital and health statistics. Series 11, Data from the national health survey* 250 (2010), pp. 1–87.

- [42] Danielle R Bouchard et al. “Impact of resistance training with or without caloric restriction on physical capacity in obese older women”. In: *Menopause* 16.1 (2009), pp. 66–72.
- [43] Douglas L Ballor et al. “Resistance weight training during caloric restriction enhances lean body weight maintenance.” In: *The American journal of clinical nutrition* 47.1 (1988), pp. 19–25.
- [44] Barbara J Nicklas et al. “Effects of resistance training with and without caloric restriction on physical function and mobility in overweight and obese older adults: a randomized controlled trial”. In: *The American journal of clinical nutrition* 101.5 (2015), pp. 991–999.
- [45] Mark D Mifflin et al. “A new predictive equation for resting energy expenditure in healthy individuals.” In: *The American journal of clinical nutrition* 51.2 (1990), pp. 241–247.
- [46] John J Cunningham. “Body composition as a determinant of energy expenditure: a synthetic review and a proposed general prediction equation.” In: *The American journal of clinical nutrition* 54.6 (1991), pp. 963–969.
- [47] Alexandra M Johnstone et al. “Factors influencing variation in basal metabolic rate include fat-free mass, fat mass, age, and circulating thyroxine but not sex, circulating leptin, or triiodothyronine”. In: *The American journal of clinical nutrition* 82.5 (2005), pp. 941–948.
- [48] Michael McKay. “Latin hypercube sampling as a tool in uncertainty analysis of computer models”. In: *Proceedings of the 1992 Winter Simulation Conference* (1992). DOI: 10.1145/167293.167637.

- [49] Simeone Marino et al. “A methodology for performing global uncertainty and sensitivity analysis in systems biology”. In: *Journal of Theoretical Biology* 254.1 (2008), pp. 178–196. ISSN: 00225193. DOI: 10.1016/j.jtbi.2008.04.011.
- [50] Brett A Dolezal and Jeffrey A Potteiger. “Concurrent resistance and endurance training influence basal metabolic rate in nondieting individuals”. In: *Journal of applied physiology* 85.2 (1998), pp. 695–700.
- [51] Michael S Lo et al. “Training and detraining effects of the resistance vs. endurance program on body composition, body size, and physical performance in young men”. In: *The Journal of Strength & Conditioning Research* 25.8 (2011), pp. 2246–2254.
- [52] Jacob M Wilson et al. “The effects of 12 weeks of beta-hydroxy-beta-methylbutyrate free acid supplementation on muscle mass, strength, and power in resistance-trained individuals: a randomized, double-blind, placebo-controlled study”. In: *European journal of applied physiology* 114.6 (2014), pp. 1217–1227.
- [53] Jeffrey R Stout et al. “Effect of calcium β -hydroxy- β -methylbutyrate (CaHMB) with and without resistance training in men and women 65+ yrs: a randomized, double-blind pilot trial”. In: *Experimental gerontology* 48.11 (2013), pp. 1303–1310.
- [54] Tyler A Churchward-Venne et al. “There are no nonresponders to resistance-type exercise training in older men and women”. In: *Journal of the American Medical Directors Association* 16.5 (2015), pp. 400–411.
- [55] Wim HM Saris. “Very-low-calorie diets and sustained weight loss”. In: *Obesity* 9.S11 (2001).

- [56] Mark D Peterson, Ananda Sen, and Paul M Gordon. “Influence of resistance exercise on lean body mass in aging adults: a meta-analysis”. In: *Medicine and science in sports and exercise* 43.2 (2011), p. 249.
- [57] Eric T Trexler, Abbie E Smith-Ryan, and Layne E Norton. “Metabolic adaptation to weight loss: implications for the athlete”. In: *Journal of the International Society of Sports Nutrition* 11.1 (2014), p. 1.
- [58] Lisette G De Pillis and Ami Radunskaya. “A mathematical tumor model with immune resistance and drug therapy: an optimal control approach”. In: *Computational and Mathematical Methods in Medicine* 3.2 (2001), pp. 79–100.
- [59] Mehmet Itik, Metin U Salamci, and Stephen P Banks. “Optimal control of drug therapy in cancer treatment”. In: *Nonlinear Analysis: Theory, Methods & Applications* 71.12 (2009), e1473–e1486.
- [60] Yazdan Batmani and Hamid Khaloozadeh. “Optimal chemotherapy in cancer treatment: state dependent Riccati equation control and extended Kalman filter”. In: *Optimal Control Applications and Methods* 34.5 (2013), pp. 562–577.
- [61] Robert F Stengel et al. “Optimal control of innate immune response”. In: *Optimal control applications and methods* 23.2 (2002), pp. 91–104.
- [62] Denise Kirschner, Suzanne Lenhart, and Steve Serbin. “Optimal control of the chemotherapy of HIV”. In: *Journal of mathematical biology* 35.7 (1997), pp. 775–792.

- [63] Gul Zaman, Yong Han Kang, and Il Hyo Jung. “Stability analysis and optimal vaccination of an SIR epidemic model”. In: *BioSystems* 93.3 (2008), pp. 240–249.
- [64] Omar Balatif, Mostafa Rachik, J Bouyaghroumni, et al. “Application of optimal control theory to an SEIR model with immigration of infectives”. In: *International Journal of Computer Science Issues (IJCSI)* 10.2 Part 2 (2013), p. 230.
- [65] Dipo Aldila et al. “Optimal control problem of treatment for obesity in a closed population”. In: *International Journal of Mathematics and Mathematical Sciences* 2014 (2014).
- [66] Amnon Levy. “Rational eating: can it lead to overweightness or underweightness?” In: *Journal of health economics* 21.5 (2002), pp. 887–899.
- [67] Lev Semenovich Pontryagin. *Mathematical theory of optimal processes*. Routledge, 2018.
- [68] Lamberto Cesari. *Optimization—theory and applications: problems with ordinary differential equations*. Vol. 17. Springer Science & Business Media, 2012.
- [69] Gangaram S Ladde, Vangipuram Lakshmikantham, and Aghalaya S Vatsala. *Monotone iterative techniques for nonlinear differential equations*. Vol. 27. Pitman Publishing, 1985.
- [70] Wendell H Fleming and Raymond W Rishel. *Deterministic and stochastic optimal control*. Vol. 1. Springer Science & Business Media, 1975.
- [71] Suzanne Lenhart and John T Workman. *Optimal control applied to biological models*. Crc Press, 2007.

- [72] MATLAB. *version 9.2.0 (R2017a)*. Natick, Massachusetts: The MathWorks Inc., 2017.
- [73] L. Breiman. *Classification and regression trees*. Wadsworth statistics/probability series. Wadsworth International Group, 1984. ISBN: 9780534980535. URL: <https://books.google.com/books?id=uxPvAAAAAAAJ>.
- [74] Jeremy S Duffield. “The inflammatory macrophage: a story of Jekyll and Hyde”. In: *Clinical science* 104.1 (2003), pp. 27–38.
- [75] Siamon Gordon. “Alternative activation of macrophages”. en. In: *Nature Reviews Immunology* 3.1 (June 2003), pp. 23–35. ISSN: 1474-1733. DOI: 10.1038/nri978.
- [76] Samielle K Brancato and Jorge E Albina. “Wound Macrophages as Key Regulators of Repair”. en. In: *The American Journal of Pathology* 178.1 (June 2011), pp. 19–25. ISSN: 00029440. DOI: 10.1016/j.ajpath.2010.08.003.
- [77] Babak Mahdavian Delavary et al. “Macrophages in skin injury and repair”. In: *Immunobiology* 216.7 (2011), pp. 753–762.
- [78] Charles D. Mills and Klaus Ley. “M1 and M2 macrophages: The chicken and the egg of immunity”. In: *Journal of Innate Immunity* 6.6 (2014), pp. 716–726. ISSN: 16628128. DOI: 10.1159/000364945.
- [79] Jinghua Bie et al. “Improved insulin sensitivity in high-fat high-cholesterol fed LDLR^{-/-} mice with macrophage-specific transgenic expression of cholesteryl ester hydrolase: Role of macrophage inflammation and infiltration into adipose tissue”. In: *Journal of Biological Chemistry* (2010), jbc-M109.

- [80] David M Mosser and Justin P Edwards. “Exploring the full spectrum of macrophage activation”. In: *Nature Reviews Immunology* 8.12 (June 2008), pp. 958–969. ISSN: 14741733. DOI: 10.1038/nri2448.
- [81] Antonio Sica et al. “Tumour-associated macrophages are a distinct M2 polarised population promoting tumour progression: potential targets of anti-cancer therapy”. In: *European journal of cancer* 42.6 (2006), pp. 717–727.
- [82] Wenchao Zhou et al. “Periostin secreted by glioblastoma stem cells recruits M2 tumour-associated macrophages and promotes malignant growth”. In: *Nature cell biology* 17.2 (2015), p. 170.
- [83] G Broughton 2nd, Jeffrey E Janis, and Christopher E Attinger. “The basic science of wound healing.” In: *Plastic and reconstructive surgery* 117.7 Suppl (2006), 12S–34S.
- [84] Giulia Chinetti-Gbaguidi, Sophie Colin, and Bart Staels. “Macrophage subsets in atherosclerosis”. In: *Nature Reviews Cardiology* 12.1 (2015), p. 10.
- [85] Adam D Kennedy and Frank R DeLeo. “Neutrophil apoptosis and the resolution of infection”. In: *Immunologic research* 43.1-3 (2009), pp. 25–61.
- [86] Jonathan A Sherratt and JD Murray. “Models of epidermal wound healing”. In: *Proceedings of the Royal Society of London B: Biological Sciences* 241.1300 (1990), pp. 29–36.
- [87] Qi Mi et al. “Agent-based model of inflammation and wound healing: insights into diabetic foot ulcer pathology and the role of transforming growth factor- β 1”. In: *Wound Repair and Regeneration* 15.5 (2007), pp. 671–682.

- [88] Richard C Schugart et al. “Wound angiogenesis as a function of tissue oxygen tension: a mathematical model”. In: *Proceedings of the National Academy of Sciences* 105.7 (2008), pp. 2628–2633.
- [89] Vissagan Gopalakrishnan, Moses Kim, and Gary An. “Using an agent-based model to examine the role of dynamic bacterial virulence potential in the pathogenesis of surgical site infection”. In: *Advances in wound care* 2.9 (2013), pp. 510–526.
- [90] Andrew D Rouillard and Jeffrey W Holmes. “Mechanical regulation of fibroblast migration and collagen remodelling in healing myocardial infarcts”. In: *The Journal of physiology* 590.18 (2012), pp. 4585–4602.
- [91] Yunji Wang et al. “Mathematical modeling and stability analysis of macrophage activation in left ventricular remodeling post-myocardial infarction”. In: *BMC genomics* 13.6 (2012), p. 1.
- [92] J L Dunster, H M Byrne, and J R King. “The Resolution of Inflammation: A Mathematical Model of Neutrophil and Macrophage Interactions”. en. In: *Bulletin of Mathematical Biology* 76.8 (July 2014), pp. 1953–1980. ISSN: 0092-8240, 1522-9602. DOI: 10.1007/s11538-014-9987-x.
- [93] Racheal L. Cooper et al. “Modeling the effects of systemic mediators on the inflammatory phase of wound healing”. In: *Journal of Theoretical Biology* 367 (2015), pp. 86–99. ISSN: 10958541. DOI: 10.1016/j.jtbi.2014.11.008.
- [94] Katherine Wendelsdorf et al. “Model of colonic inflammation: immune modulatory mechanisms in inflammatory bowel disease”. In: *Journal of theoretical biology* 264.4 (2010), pp. 1225–1239.

- [95] Anna Ougrinovskaia, Rosemary S Thompson, and Mary R Myerscough. “An ODE model of early stages of atherosclerosis: mechanisms of the inflammatory response”. In: *Bulletin of mathematical biology* 72.6 (2010), pp. 1534–1561.
- [96] Alexander D Chalmers et al. “Bifurcation and dynamics in a mathematical model of early atherosclerosis”. In: *Journal of mathematical biology* 71.6-7 (2015), pp. 1451–1480.
- [97] Avner Friedman and Wenrui Hao. “A mathematical model of atherosclerosis with reverse cholesterol transport and associated risk factors”. In: *Bulletin of mathematical biology* 77.5 (2015), pp. 758–781.
- [98] CA Cobbold, JA Sherratt, and SRJ Maxwell. “Lipoprotein oxidation and its significance for atherosclerosis: a mathematical approach”. In: *Bulletin of mathematical biology* 64.1 (2002), pp. 65–95.
- [99] AI Ibragimov et al. “A mathematical model of atherogenesis as an inflammatory response”. In: *Mathematical Medicine and Biology* 22.4 (2005), pp. 305–333.
- [100] Muhammad AK Bulelzai and Johan LA Dubbeldam. “Long time evolution of atherosclerotic plaques”. In: *Journal of theoretical biology* 297 (2012), pp. 1–10.
- [101] Vincent Calvez et al. “Mathematical and numerical modeling of early atherosclerotic lesions”. In: *ESAIM: Proceedings*. Vol. 30. EDP Sciences. 2010, pp. 1–14.
- [102] Moritz P Thon et al. “A Quantitative Model of Early Atherosclerotic Plaques Parameterized Using In Vitro Experiments”. In: *Bulletin of mathematical biology* 80.1 (2018), pp. 175–214.

- [103] Junehyuk Lee, Frederick R Adler, and Peter S Kim. “A mathematical model for the macrophage response to respiratory viral infection in normal and asthmatic conditions”. In: *Bulletin of mathematical biology* 79.9 (2017), pp. 1979–1998.
- [104] Roland Brun, Peter Reichert, and Hans R Künsch. “Practical identifiability analysis of large environmental simulation models”. In: *Water Resources Research* 37.4 (2001), pp. 1015–1030.
- [105] Attila Gábor, Alejandro F Villaverde, and Julio R Banga. “Parameter identifiability analysis and visualization in large-scale kinetic models of biosystems”. In: *BMC systems biology* 11.1 (2017), p. 54.
- [106] Mette S Olufsen and Johnny T Ottesen. “A practical approach to parameter estimation applied to model predicting heart rate regulation”. In: *Journal of mathematical biology* 67.1 (2013), pp. 39–68.
- [107] Marisa C Eisenberg and Michael AL Hayashi. “Determining identifiable parameter combinations using subset profiling”. In: *Mathematical biosciences* 256 (2014), pp. 116–126.
- [108] Laura M Ellwein et al. “Sensitivity analysis and model assessment: mathematical models for arterial blood flow and blood pressure”. In: *Cardiovascular Engineering* 8.2 (2008), pp. 94–108.
- [109] Scott R Pope et al. “Estimation and identification of parameters in a lumped cerebrovascular model”. In: *Math Biosci Eng* 6.1 (2009), pp. 93–115.
- [110] David G Greenhalgh. “The role of apoptosis in wound healing”. In: *The international journal of biochemistry & cell biology* 30.9 (July 1998), pp. 1019–1030.

- [111] R D Stout. “Functional plasticity of macrophages: reversible adaptation to changing microenvironments”. en. In: *Journal of Leukocyte Biology* 76.3 (July 2004), pp. 509–513. ISSN: 0741-5400. DOI: 10.1189/jlb.0504272.
- [112] Margaret L Novak and Timothy J Koh. “Macrophage phenotypes during tissue repair”. In: *Journal of leukocyte biology* 93.6 (2013), pp. 875–881.
- [113] Jinghua Bie, Bin Zhao, and Shobha Ghosh. “Atherosclerotic lesion progression is attenuated by reconstitution with bone marrow from macrophage-specific cholesteryl ester hydrolase transgenic mice”. In: *American Journal of Physiology-Regulatory, Integrative and Comparative Physiology* 301.4 (2011), R967–R974.
- [114] Lars Esmann et al. “Phagocytosis of apoptotic cells by neutrophil granulocytes: diminished proinflammatory neutrophil functions in the presence of apoptotic cells”. In: *The journal of immunology* 184.1 (2010), pp. 391–400.
- [115] Kristina Rydell-Törmänen, Lena Uller, and Jonas S Erjefält. “Neutrophil cannibalism—a back up when the macrophage clearance system is insufficient”. In: *Respiratory research* 7.1 (2006), p. 143.
- [116] R D Stout. “Editorial: Macrophage functional phenotypes: no alternatives in dermal wound healing?” en. In: *Journal of Leukocyte Biology* 87.1 (June 2010), pp. 19–21. ISSN: 0741-5400. DOI: 10.1189/jlb.0509311.
- [117] Bard Ermentrout. *Simulating, analyzing, and animating dynamical systems: a guide to XPPAUT for researchers and students*. Vol. 14. Siam, 2002.
- [118] Thomas Maiwald and Jens Timmer. “Dynamical modeling and multi-experiment fitting with PottersWheel”. In: *Bioinformatics* 24.18 (2008), pp. 2037–2043.

- [119] Hirotogu Akaike. “Information theory and an extension of the maximum likelihood principle”. In: *Proceedings of the 2nd International Symposium on Information Theory*. 1973, pp. 267–281.
- [120] Alejandro F Villaverde, Antonio Barreiro, and Antonis Papachristodoulou. “Structural identifiability of dynamic systems biology models”. In: *PLoS computational biology* 12.10 (2016), e1005153.
- [121] Yunfei Chu and Juergen Hahn. “Parameter set selection via clustering of parameters into pairwise indistinguishable groups of parameters”. In: *Industrial & Engineering Chemistry Research* 48.13 (2008), pp. 6000–6009.
- [122] Yonathan Bard. “Nonlinear parameter estimation”. In: (1974).
- [123] A Raue et al. “Addressing parameter identifiability by model-based experimentation”. In: *IET systems biology* 5.2 (2011), pp. 120–130.
- [124] Susan A Murphy and Aad W Van der Vaart. “On profile likelihood”. In: *Journal of the American Statistical Association* 95.450 (2000), pp. 449–465.
- [125] T Magnus et al. “Microglial phagocytosis of apoptotic inflammatory T cells leads to down-regulation of microglial immune activation.” In: *Journal of immunology (Baltimore, Md. : 1950)* 167.9 (2001), pp. 5004–5010. ISSN: 0022-1767. DOI: 10.4049/jimmunol.167.9.5004.
- [126] P L van Lent et al. “Uptake of apoptotic leukocytes by synovial lining macrophages inhibits immune complex-mediated arthritis.” In: *Journal of leukocyte biology* 70.5 (2001), pp. 708–14. ISSN: 0741-5400.
- [127] Ludovic Arnold et al. “Inflammatory monocytes recruited after skeletal muscle injury switch into antiinflammatory macrophages to support myogenesis”. In:

- J Exp Med* 204.5 (2007), pp. 1057–1069. ISSN: 0022-1007. DOI: 10.1084/jem.20070075.
- [128] R E Voll et al. “Immunosuppressive effects of apoptotic cells.” In: *Nature* 390.6658 (1997), pp. 350–1. ISSN: 0028-0836. DOI: 10.1038/37022.
- [129] Valerie A Fadok et al. “Macrophages that have ingested apoptotic cells in vitro inhibit proinflammatory cytokine production through autocrine/paracrine mechanisms involving TGF-beta, PGE2, and PAF.” In: *Journal of Clinical Investigation* 101.4 (July 1998), p. 890.
- [130] Mai-Lan N Huynh, Valerie A Fadok, and Peter M Henson. “Phosphatidylserine-dependent ingestion of apoptotic cells promotes TGF- β 1 secretion and the resolution of inflammation”. en. In: *Journal of Clinical Investigation* 109.1 (July 2002), pp. 41–50. ISSN: 0021-9738. DOI: 10.1172/JCI11638.
- [131] Kathryn J Moore, Frederick J Sheedy, and Edward A Fisher. “Macrophages in atherosclerosis: a dynamic balance”. In: *Nature Reviews Immunology* 13.10 (2013), p. 709.
- [132] Andrew C Li and Christopher K Glass. “The macrophage foam cell as a target for therapeutic intervention”. In: *Nature medicine* 8.11 (2002), p. 1235.
- [133] RL Tiwari, V Singh, and MK Barthwal. “Macrophages: an elusive yet emerging therapeutic target of atherosclerosis”. In: *Medicinal research reviews* 28.4 (2008), pp. 483–544.
- [134] Jenna M McCracken and Lee-Ann H Allen. “Regulation of human neutrophil apoptosis and lifespan in health and disease”. In: *Journal of cell death* 7 (2014), JCD–S11038.

- [135] SW Crooks and RA Stockley. “Leukotriene B4”. In: *The international journal of biochemistry & cell biology* 30.2 (1998), pp. 173–178.
- [136] Oliver Soehnlein et al. “Neutrophils as protagonists and targets in chronic inflammation”. In: *Nature Reviews Immunology* 17.4 (2017), p. 248.
- [137] Mayumi Egawa et al. “Inflammatory monocytes recruited to allergic skin acquire an anti-inflammatory M2 phenotype via basophil-derived interleukin-4”. In: *Immunity* 38.3 (2013), pp. 570–580.
- [138] Laura Denney et al. “Activation of invariant NKT cells in early phase of experimental autoimmune encephalomyelitis results in differentiation of Ly6Chi inflammatory monocyte to M2 macrophages and improved outcome”. In: *The Journal of Immunology* (2012), p. 1103608.
- [139] Prakash Saha et al. “The monocyte/macrophage as a therapeutic target in atherosclerosis”. In: *Current opinion in pharmacology* 9.2 (2009), pp. 109–118.
- [140] Katherine R Martin et al. “Transgenic mice expressing human proteinase 3 exhibit sustained neutrophil-associated peritonitis”. In: *The Journal of Immunology* (2017), ji1601522.
- [141] Sesquile Ramon et al. “The protectin PCTR1 is produced by human M2 macrophages and enhances resolution of infectious inflammation”. In: *The American journal of pathology* 186.4 (2016), pp. 962–973.
- [142] Stefan Juhas et al. “RX-207, a small molecule inhibitor of protein interaction with glycosaminoglycans (SMIGs), reduces experimentally induced inflammation and increases survival rate in cecal ligation and puncture (CLP)-induced sepsis”. In: *Inflammation* 41.1 (2018), pp. 307–314.

- [143] Jacques Deguine et al. “Local TNFR1 signaling licenses murine neutrophils for increased TLR-dependent cytokine and eicosanoid production”. In: *The Journal of Immunology* (2017), p. 1601465.
- [144] Julianty Angsana et al. “Syndecan-1 modulates the motility and resolution responses of macrophages”. In: *Arteriosclerosis, thrombosis, and vascular biology* 35.2 (2015), pp. 332–340.
- [145] Erez Feige et al. “Inhibition of monocyte chemotaxis by VB-201, a small molecule lecinoxoid, hinders atherosclerosis development in ApoE^{-/-} mice”. In: *Atherosclerosis* 229.2 (2013), pp. 430–439.
- [146] Thais A Jacinto et al. “Increased ROS production and DNA damage in monocytes are biomarkers of aging and atherosclerosis”. In: *Biological research* 51.1 (2018), p. 33.
- [147] Simon Barquera et al. “Global overview of the epidemiology of atherosclerotic cardiovascular disease”. In: *Archives of medical research* 46.5 (2015), pp. 328–338.
- [148] Shobha Ghosh. “Macrophage cholesterol homeostasis and metabolic diseases: critical role of cholesteryl ester mobilization”. In: *Expert review of cardiovascular therapy* 9.3 (2011), pp. 329–340.
- [149] Joseph L Goldstein et al. “Binding site on macrophages that mediates uptake and degradation of acetylated low density lipoprotein, producing massive cholesterol deposition”. In: *Proceedings of the National Academy of Sciences* 76.1 (1979), pp. 333–337.

- [150] Shen Gao and Jing Liu. “Association between circulating oxidized low-density lipoprotein and atherosclerotic cardiovascular disease”. In: *Chronic diseases and translational medicine* 3.2 (2017), pp. 89–94.
- [151] Shen Gao et al. “Circulating Oxidized Low-Density Lipoprotein Levels Independently Predict 10-Year Progression of Subclinical Carotid Atherosclerosis: A Community-Based Cohort Study”. In: *Journal of atherosclerosis and thrombosis* (2018), p. 43299.
- [152] Siddhartha S Ghosh et al. “Oral supplementation with non-absorbable antibiotics or curcumin attenuates western diet-induced atherosclerosis and glucose intolerance in LDLR^{-/-} mice—role of intestinal permeability and macrophage activation”. In: *PloS one* 9.9 (2014), e108577.
- [153] Robert A Koeth et al. “Intestinal microbiota metabolism of L-carnitine, a nutrient in red meat, promotes atherosclerosis”. In: *Nature medicine* 19.5 (2013), p. 576.
- [154] Margarita Martinez-Medina et al. “Western diet induces dysbiosis with increased E coli in CEABAC10 mice, alters host barrier function favouring AIEC colonisation”. In: *Gut* (2013), gutjnl–2012.
- [155] Swaroop Pendyala, Jeanne M Walker, and Peter R Holt. “A high-fat diet is associated with endotoxemia that originates from the gut”. In: *Gastroenterology* 142.5 (2012), pp. 1100–1101.
- [156] Annika Lindskog Jonsson and Fredrik Bäckhed. “Role of gut microbiota in atherosclerosis”. In: *Nature Reviews Cardiology* 14.2 (2017), p. 79.

- [157] Jacques Amar et al. “Energy intake is associated with endotoxemia in apparently healthy men—”. In: *The American journal of clinical nutrition* 87.5 (2008), pp. 1219–1223.
- [158] Dmitry A Chistiakov et al. “Role of gut microbiota in the modulation of atherosclerosis-associated immune response”. In: *Frontiers in microbiology* 6 (2015), p. 671.
- [159] Maik Drechsler et al. “Hyperlipidemia-Triggered Neutrophilia Promotes Early AtherosclerosisClinical Perspective”. In: *Circulation* 122.18 (2010), pp. 1837–1845.
- [160] Zei-Shung Huang et al. “Peripheral differential leukocyte counts in humans vary with hyperlipidemia, smoking, and body mass index”. In: *Lipids* 36.3 (2001), pp. 237–245.
- [161] Eric P Schmidt et al. “On, around, and through: neutrophil-endothelial interactions in innate immunity”. In: *Physiology* 26.5 (2011), pp. 334–347.
- [162] Bin Zhao et al. “Macrophage-specific transgenic expression of cholesteryl ester hydrolase significantly reduces atherosclerosis and lesion necrosis in *Ldlr*^{-/-} mice”. In: *The Journal of clinical investigation* 117.10 (2007), pp. 2983–2992.
- [163] Michael S Brown, YK Ho, and JL Goldstein. “The cholesteryl ester cycle in macrophage foam cells. Continual hydrolysis and re-esterification of cytoplasmic cholesteryl esters.” In: *Journal of Biological Chemistry* 255.19 (1980), pp. 9344–9352.
- [164] Bo Feng et al. “The endoplasmic reticulum is the site of cholesterol-induced cytotoxicity in macrophages”. In: *Nature cell biology* 5.9 (2003), p. 781.

- [165] Ira Tabas. “Consequences and therapeutic implications of macrophage apoptosis in atherosclerosis: the importance of lesion stage and phagocytic efficiency”. In: *Arteriosclerosis, thrombosis, and vascular biology* 25.11 (2005), pp. 2255–2264.
- [166] Pierre Rotzius et al. “Distinct infiltration of neutrophils in lesion shoulders in ApoE^{-/-} mice”. In: *The American journal of pathology* 177.1 (2010), pp. 493–500.
- [167] Alma Zerneck et al. “Protective role of CXC receptor 4/CXC ligand 12 unveils the importance of neutrophils in atherosclerosis”. In: *Circulation research* 102.2 (2008), pp. 209–217.
- [168] Oliver Soehnlein et al. “Neutrophil-derived heparin-binding protein (HBP/-CAP37) deposited on endothelium enhances monocyte arrest under flow conditions”. In: *The Journal of Immunology* 174.10 (2005), pp. 6399–6405.
- [169] Oliver Soehnlein et al. “Neutrophil secretion products pave the way for inflammatory monocytes”. In: *Blood* 112.4 (2008), pp. 1461–1471.
- [170] Cristina D Ciornei et al. “Human antimicrobial peptide LL-37 is present in atherosclerotic plaques and induces death of vascular smooth muscle cells: a laboratory study”. In: *BMC cardiovascular disorders* 6.1 (2006), p. 49.
- [171] Liliana Legedz et al. “Cathepsin G is associated with atheroma formation in human carotid artery”. In: *Journal of hypertension* 22.1 (2004), pp. 157–166.
- [172] V Kumar and A Sharma. “Neutrophils: Cinderella of innate immune system”. In: *International immunopharmacology* 10.11 (2010), pp. 1325–1334.

- [173] Sarah Fox et al. “Neutrophil apoptosis: relevance to the innate immune response and inflammatory disease”. In: *Journal of innate immunity* 2.3 (2010), pp. 216–227.
- [174] Susu M Zughaier, William M Shafer, and David S Stephens. “Antimicrobial peptides and endotoxin inhibit cytokine and nitric oxide release but amplify respiratory burst response in human and murine macrophages”. In: *Cellular microbiology* 7.9 (2005), pp. 1251–1262.
- [175] Birgitta Agerberth et al. “The human antimicrobial and chemotactic peptides LL-37 and α -defensins are expressed by specific lymphocyte and monocyte populations”. In: *Blood* 96.9 (2000), pp. 3086–3093.
- [176] Oleg Chertov et al. “Identification of human neutrophil-derived cathepsin G and azurocidin/CAP37 as chemoattractants for mononuclear cells and neutrophils”. In: *Journal of Experimental Medicine* 186.5 (1997), pp. 739–747.
- [177] Oliver Soehnlein, Alma Zerneck, and Christian Weber. “Neutrophils launch monocyte extravasation by release of granule proteins”. In: *Thrombosis and haemostasis* 101.02 (2009), pp. 198–205.
- [178] De Yang et al. “LL-37, the neutrophil granule- and epithelial cell-derived cathelicidin, utilizes formyl peptide receptor-like 1 (FPRL1) as a receptor to chemoattract human peripheral blood neutrophils, monocytes, and T cells”. In: *Journal of Experimental Medicine* 192.7 (2000), pp. 1069–1074.
- [179] Elliot S Barnathan et al. “Immunohistochemical localization of defensin in human coronary vessels.” In: *The American journal of pathology* 150.3 (1997), p. 1009.

- [180] Taunia D Lee et al. “CAP37, a novel inflammatory mediator: its expression in endothelial cells and localization to atherosclerotic lesions”. In: *The American journal of pathology* 160.3 (2002), pp. 841–848.
- [181] Ha Young Lee et al. “Role of formyl peptide receptor 2 on the serum amyloid A-induced macrophage foam cell formation”. In: *Biochemical and biophysical research communications* 433.2 (2013), pp. 255–259.
- [182] Ha Young Lee et al. “Oxidized low-density lipoprotein-induced foam cell formation is mediated by formyl peptide receptor 2”. In: *Biochemical and biophysical research communications* 443.3 (2014), pp. 1003–1007.
- [183] Jason S Knight et al. “Peptidylarginine deiminase inhibition reduces vascular damage and modulates innate immune responses in murine models of atherosclerosis”. In: *Circulation research* 114.6 (2014), pp. 947–956.
- [184] Annika Warnatsch et al. “Neutrophil extracellular traps license macrophages for cytokine production in atherosclerosis”. In: *Science* 349.6245 (2015), pp. 316–320.
- [185] YuanHua Qin et al. “Recombinant human CXCL8 (3-72) K11R/G31P regulates smooth muscle cell proliferation and migration through blockage of interleukin-8 receptor”. In: *IUBMB life* 65.1 (2013), pp. 67–75.
- [186] Dirk Lievens et al. “The multi-functionality of CD40L and its receptor CD40 in atherosclerosis”. In: *Thrombosis and haemostasis* 101.02 (2009), pp. 206–214.
- [187] Esther Lutgens et al. “Deficient CD40-TRAF6 signaling in leukocytes prevents atherosclerosis by skewing the immune response toward an antiinflammatory profile”. In: *Journal of Experimental Medicine* 207.2 (2010), pp. 391–404.

- [188] Christian Weber and Heidi Noels. “Atherosclerosis: current pathogenesis and therapeutic options”. In: *Nature medicine* 17.11 (2011), p. 1410.
- [189] Jürgen Bernhagen et al. “MIF is a noncognate ligand of CXC chemokine receptors in inflammatory and atherogenic cell recruitment”. In: *Nature medicine* 13.5 (2007), p. 587.
- [190] Rory R Koenen and Christian Weber. “Therapeutic targeting of chemokine interactions in atherosclerosis”. In: *Nature reviews Drug discovery* 9.2 (2010), p. 141.
- [191] Rory R Koenen et al. “Disrupting functional interactions between platelet chemokines inhibits atherosclerosis in hyperlipidemic mice”. In: *Nature medicine* 15.1 (2009), p. 97.
- [192] Jim Gilbert et al. “Effect of CC chemokine receptor 2 CCR2 blockade on serum C-reactive protein in individuals at atherosclerotic risk and with a single nucleotide polymorphism of the monocyte chemoattractant protein-1 promoter region”. In: *The American journal of cardiology* 107.6 (2011), pp. 906–911.
- [193] Elisa A Liehn et al. “A new monocyte chemotactic protein-1/chemokine CC motif ligand-2 competitor limiting neointima formation and myocardial ischemia/reperfusion injury in mice”. In: *Journal of the American College of Cardiology* 56.22 (2010), pp. 1847–1857.
- [194] Vincent Braunersreuther et al. “A novel RANTES antagonist prevents progression of established atherosclerotic lesions in mice”. In: *Arteriosclerosis, thrombosis, and vascular biology* 28.6 (2008), pp. 1090–1096.

- [195] Anna Cohen, Mary R Myerscough, and Rosemary S Thompson. “Athero-protective effects of High Density Lipoproteins (HDL): An ODE model of the early stages of atherosclerosis”. In: *Bulletin of mathematical biology* 76.5 (2014), pp. 1117–1142.
- [196] TI Zohdi. “A simple model for shear stress mediated lumen reduction in blood vessels”. In: *Biomechanics and modeling in mechanobiology* 4.1 (2005), pp. 57–61.
- [197] Cameron McKay et al. “Towards a model of atherosclerosis”. In: *University of Strathclyde* (2005), pp. 1–29.
- [198] Shuai Zhang, LR Ritter, and AI Ibragimov. “Foam cell formation in atherosclerosis: HDL and macrophage reverse cholesterol transport”. In: *Discrete Contin Dyn Syst Supplements* (2013), pp. 825–835.
- [199] Y Claire Wang et al. “Health and economic burden of the projected obesity trends in the USA and the UK”. In: *The Lancet* 378.9793 (2011), pp. 815–825.
- [200] *Simbiology User’s Guide*. Natick, Massachusetts: The MathWorks Inc., 2019.

VITA

Marcella Torres was born on October 27, 1981 on an air force base in Omaha, Nebraska to her mother, an Argentinean-born American soldier newly returned from Germany. She is married to Derek Tresize, with whom she has two children, Miles and Maxine. With him, she co-owns a personal training studio in Richmond, Virginia and has co-authored several popular guides to nutrition and fitness training for bodybuilding competitions.

In her K-12 years, Marcella attended a magnet school for the visual arts. She served as first chair violist in school and state orchestras, without ever knowing that the music her strings produced was governed by ratios of whole numbers. At age 11, Marcella was one of 50 students in the state of Virginia to score higher than the average college-bound twelfth-grader on the SATs in a John Hopkins talent search, due entirely to the verbal score. She spent hours of her time outside of class writing philosophical essays and verbally deconstructing the arguments of others without knowing that she was playing with proofs and mathematical logic. In her final two years of high school, Marcella attended a vocational school program in fashion design, happily drafting flat patterns to deform into three-dimensional wearable shapes without ever realizing she was doing topology. There was not yet any sign of an interest in the quantitative subjects as traditionally taught: she earned a C in her sole high school mathematics course: pre-algebra. Marcella went on to spectacularly fail the community college entrance exam after several years of work in textile factories and apartment cleaning. Nevertheless, she persisted and with borrowed textbooks and late nights after work made up 4 years of missed high school mathematics in two months.

After transferring from Pierce Community College in Fort Steilacoom, Washington, Marcella earned a Bachelor of Science in Mathematical Sciences with a concentration in Applied Mathematics and a minor in Physics from Virginia Commonwealth University in 2007, magna cum laude. While an undergraduate, Marcella was a member of the University Honors program, served as president of the Society of Physics Students, was a member of Sigma Pi Sigma Physics Honor Society, and earned a number of scholarships and fellowships including two National Science Foundation Scholarships and a summer research fellowship in medical physics at the Medical College of Virginia Massey Cancer Center. She also worked as a math tutor and teaching assistant throughout this period, and as a research assistant in the solid state physics laboratory of Dr. Alison Baski from 2005 to 2007.

Following her undergraduate degree, Marcella worked full time as an actuarial associate for three years, passing three actuarial examinations in probability theory, financial mathematics, and mathematical economics before leaving the field to start a business and enter graduate school. While pursuing her Master of Science degree in Applied Mathematics and doctorate from Virginia Commonwealth University, Marcella worked as a graduate assistant, teaching and assistant teaching 12 courses in mathematics and statistics from undergraduate to graduate level. In her final year, she earned a SREB Dissertation Fellowship aimed at increasing minority representation among faculty. With this support, she has worked to improve her teaching skills and make her approach to the teaching of mathematics and systems biology more inclusive by participating in the Preparing Future Faculty program.